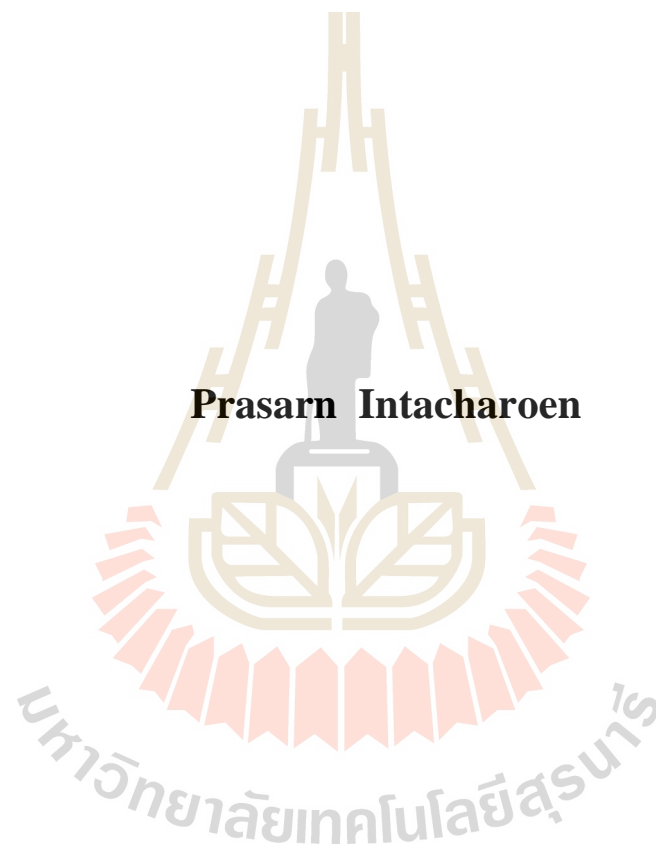


**GEOINFORMATICS APPLICATIONS TO MARINE
WATER QUALITY AND RED TIDE PHENOMENON
ASSESSMENT IN THE UPPER GULF OF THAILAND**



Prasarn Intacharoen

**A Thesis Submitted in Partial Fulfillment of the Requirements for the
Degree of Doctor of Philosophy in Geoinformatics**

Suranaree University of Technology

Academic Year 2016

การประยุกต์ภูมิสารสนเทศในการประเมินคุณภาพน้ำทะเลและปรากฏการณ์
น้ำทะเลเปลี่ยนสีในอ่าวไทยตอนบน



วิทยานิพนธ์นี้เป็นส่วนหนึ่งของการศึกษาตามหลักสูตรปริญญาวิทยาศาสตรดุษฎีบัณฑิต

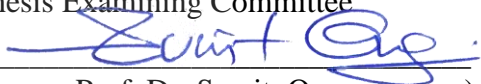
สาขาวิชาภูมิสารสนเทศ
มหาวิทยาลัยเทคโนโลยีสุรนารี

ปีการศึกษา 2559

**GEOINFORMATICS APPLICATIONS TO MARINE WATER
QUALITY AND RED TIDE PHENOMENON ASSESSMENT
IN THE UPPER GULF OF THAILAND**

Suranaree University of Technology has approved this thesis submitted in partial fulfillment of the requirements for the Degree of Doctor of Philosophy.

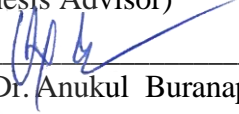
Thesis Examining Committee


(Assoc. Prof. Dr. Suwit Ongsomwang)

Chairperson


(Assoc. Prof. Dr. Songkot Dasananda)

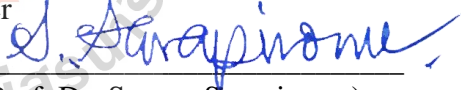
Member (Thesis Advisor)


(Asst. Prof. Dr. Anukul Buranapratheprat)

Member


(Assoc. Prof. Dr. Sura Pattanakiat)

Member


(Asst. Prof. Dr. Sunya Sarapirome)

Member


(Dr. Pantip Piyatadsananon)

Member


(Prof. Dr. Santi Maensiri)


(Prof. Dr. Sukit Limpijumnong)

Vice Rector for Academic Affairs
and Innovation

Dean of Institute of Science

ประสาร อินทเจริญ : การประยุกต์ภูมิสารสนเทศในการประเมินคุณภาพน้ำทะเลและ
ปรากฏการณ์น้ำทะเลเปลี่ยนสีในอ่าวไทยตอนบน (GEOINFORMATICS
APPLICATIONS TO MARINE WATER QUALITY AND RED TIDE PHENOMENON
ASSESSMENT IN THE UPPER GULF OF THAILAND) อาจารย์ที่ปรึกษา :
รองศาสตราจารย์ ดร.ทรงกต ทศานนท์ 274 หน้า.

ปัจจุบันการรายงานผลความเสื่อมโทรมของคุณภาพน้ำและการเกิดปรากฏการณ์น้ำทะเลเปลี่ยนสีบริเวณอ่าวไทยตอนบนมีมากขึ้น ดังนั้นระบบการสำรวจข้อมูลที่มีประสิทธิภาพ ให้ผลการทำงานที่ถูกต้อง แม่นยำ และทันสมัย (เพื่อรองรับการติดตามและการแจ้งเตือนล่วงหน้า) จึงถือได้ว่ามีความสำคัญยิ่ง การประยุกต์เทคโนโลยีภูมิสารสนเทศในการศึกษาวิจัยนี้มีวัตถุประสงค์ 3 ประการคือ (1) เพื่อระบุแบบจำลองที่เหมาะสมสำหรับการประมาณค่าระดับความเข้มข้นของปริมาณคลอโรฟิลล์-เอ ตะกอนสารแขวนลอยและสารอินทรีย์ละลายน้ำ จากข้อมูลภาพถ่ายจากดาวเทียมโมดิส (2) เพื่อศึกษาการเปลี่ยนแปลงความเข้มข้นขององค์ประกอบทั้ง 3 ประเภทข้างต้นและสถานภาพของสารอาหารในเขตอ่าวไทยตอนบน ระหว่างปี พ.ศ. 2553 ถึง 2555 และ (3) เพื่อสร้างแผนที่ความเปราะบางต่อการเกิดปรากฏการณ์น้ำทะเลเปลี่ยนสีในบริเวณอ่าวไทยตอนบน โดยใช้แบบจำลองอัตราส่วนความถี่และวิธีการรวมหลักเกณฑ์ค่าล่วงหน้าอย่างง่าย

ผลการศึกษาพบว่า แบบจำลองที่เหมาะสมสำหรับการประมาณค่าความเข้มข้นของคลอโรฟิลล์-เอ ตะกอนสารแขวนลอยและสารอินทรีย์ละลายน้ำ จากข้อมูลภาพถ่ายจากดาวเทียมโมดิส คือ แบบจำลอง OC3M ($R^2 = 0.60$) แบบจำลอง TSM ($R^2 = 0.72$) และแบบจำลอง Chula ($R^2 = 0.78$) ตามลำดับ สำหรับการวิเคราะห์แบบจำลองโครงข่ายประสาทเทียมโดยใช้ทฤษฎีแบบหลายชั้น พบว่าลักษณะโครงสร้างของชั้นข้อมูลการวิเคราะห์ที่เหมาะสมคือ 10:30:10:1 ซึ่งสามารถให้ผลลัพธ์ได้ในระดับที่ดีทั้ง 3 องค์ประกอบ ส่วนผลการวิเคราะห์การเปลี่ยนแปลงสถานะแวดล้อมทางทะเลในอ่าวไทยตอนบนระหว่างปี พ.ศ. 2553 ถึง 2555 พบว่าระดับความเข้มข้นของทั้ง 3 องค์ประกอบมีค่าอยู่ในระดับค่อนข้างต่ำในฤดูแล้งและเพิ่มสูงขึ้นอย่างต่อเนื่องจนถึงค่าสูงสุดในช่วงฤดูฝน สำหรับพื้นที่ที่มีค่าความเข้มข้นสูงสุดที่สุดของคลอโรฟิลล์-เอ (คือสถานภาพสารอาหารในช่วงขั้นของ eutrophic state/hyper-eutrophic state) และตะกอนสารแขวนลอย มักจะพบมีค่าสูงอยู่ในบริเวณใกล้ชายฝั่งและใกล้ปากแม่น้ำสายหลัก แต่สารอินทรีย์ละลายน้ำพบว่ามีค่าสูงที่สุดจะมีการแพร่กระจายจากบริเวณชายฝั่งไปสู่เขตนน้ำลึก สำหรับการวิเคราะห์ผลกระทบของเหตุการณ์น้ำท่วมใหญ่เมื่อปี พ.ศ. 2554 นั้น พบว่าความเข้มข้นของคลอโรฟิลล์-เอ มีการลดลงเป็นอย่างมาก (ค่าสูงสุด/ค่าเฉลี่ย) นอกจากนี้ยังพบว่าค่าความสัมพันธ์ขององค์ประกอบทั้ง 3 ประเภท

ในช่วงฤดูแล้งอยู่ในระดับปานกลาง (ค่า R ประมาณ 0.4-0.6) ส่วนช่วงฤดูฝนมีการผันแปรตามกันในระดับต่ำ

ผลการศึกษการสร้างแผนที่ความแปรปรวนต่อการเกิดปรากฏการณ์น้ำทะเลเปลี่ยนสีสำหรับอ่าวไทยตอนบนที่สร้างโดยแบบจำลองอัตราส่วนความถี่และวิธีการรวมหลักเกณฑ์ค่าถ่วงน้ำหนักอย่างง่าย พบว่าพื้นที่เสี่ยงต่อการเกิดปรากฏการณ์น้ำทะเลเปลี่ยนสีสูงที่สุดคือในเขตน้ำตื้นใกล้ชายฝั่ง ใกล้ปากแม่น้ำสายหลัก โดยเฉพาะแม่น้ำท่าจีนและแม่น้ำบางปะกง โดยผลของการวิเคราะห์แบบรวมหลักเกณฑ์ค่าถ่วงน้ำหนักอย่างง่าย มีผลการประเมินความถูกต้องดีที่สุดคือกรณีศึกษาที่ 6 (ประกอบด้วย 2 ตัวแปรคือ ตะกอนสารแขวนลอย และสารอินทรีย์ละลายน้ำ) โดยมีความถูกต้องของพื้นที่ได้กราฟ เท่ากับ 0.94 เช่นเดียวกับกรณีของการวิเคราะห์ที่ใช้แบบจำลองอัตราส่วนความถี่ซึ่งมีค่าเท่ากับ 0.75 อย่างไรก็ตาม นอกเหนือจากการประเมินผลค่าความถูกต้องของพื้นที่ได้กราฟแล้ว ควรมีการพิจารณาความสมจริงของเหตุการณ์ที่เกิดขึ้นกับผลที่ได้จากการประเมินความแปรปรวนของการวิเคราะห์เชิงพื้นที่ประกอบด้วยเช่นกัน



สาขาวิชาการรับรู้จากระยะไกล

ปีการศึกษา 2559

ลายมือชื่อนักศึกษา _____

ลายมือชื่ออาจารย์ที่ปรึกษา _____

ลายมือชื่ออาจารย์ที่ปรึกษาร่วม _____

(Handwritten signature)

(Handwritten signature)

(Handwritten signature)

PRASARN INTACHAROEN : GEOINFORMATICS APPLICATIONS TO
MARINE WATER QUALITY AND RED TIDE PHENOMENON
ASSESSMENT IN THE UPPER GULF OF THAILAND. THESIS ADVISOR
: ASSOC. PROF. SONGKOT DASANANDA, Ph.D. 274 PP.

UGoT/CDOM/CHLOROPHYLL-A/MODIS/TSS/ANN ANALYSIS/FREQUENCY
RATIO / SIMPLE ADDITIVE WEIGHTS

Deterioration of water quality and occurrences of red tide events were reported more often in recent years within UGoT zone. Hence, effective data observation system (for monitoring and warning purposes) with high accuracy and up-to-date information product is greatly essential. This need can be achieved through application of advanced geoinformatics technology which became main aim of this research from which three specific objectives were proposed; (1) to identify optimal model for the determination of concentration level for three important marine water constituents, i.e., chlorophyll-a, total suspended solids, and color dissolved organic matter, from the satellite-based MODIS data, (2) to observe variation in mapped concentration of the referred constituents and trophic state of water quality in the UGoT during years 2010 to 2012 and (3) to formulate credible red-tide susceptibility maps for the UGoT through the frequency ratio and simple additive weighting methods.

First, the optimal models for concentration extraction of the Chl-a, TSS, and CDOM from MODIS-based reflectance data were identified as OC3M ($R^2 = 0.60$), TSM ($R^2 = 0.72$) and Chula ($R^2 = 0.78$), respectively. In addition, the primary ANN analysis (MLP type with optimal structure of 10:30:10:1) also demonstrated promising

outcome for the prediction of those constituents. Derived concentration maps for each constituent (through their respective optimal models) from years 2010 to 2012 showed that concentration levels of these concerned constituents were relatively low in dry season and gradually rising towards their peak values in wet season. Top concentration areas for Chl-a (and also for the critical trophic states- eutrophic/hyper-eutrophic) and TSS were often located close to shore and to some major river mouths, but those of CDOM were appeared more widespread into deep-water zone. Effects of year 2011, mega flood over central Thailand were also apparent, especially, great drop of Chl-a (maximum/ mean) during wet season of 2011. Moreover, moderate correlation among studied constituents was found during dry season ($R \approx 0.4-0.6$) while low correlation often evidenced in wet season.

Finally, analysis of the red tide susceptibility maps formulated by SAW and FR methods indicated that, in general, highly prone areas to red tide occurred in shallow water zone. Thus displayed close to main river mouths, especially the Thachin and the Bang Pakong Rivers. For SAW case, Type 6 scenario (two factors: TSS and CDOM) gained best validation accuracy (AUC = 0.94), as well as that of the FR case (AUC = 0.75). However, apart from the AUC assessed outcome, the realistic outlook of the assessed map should be taken into consideration for its prediction ability also.

School of Remote Sensing

Academic Year 2016

Student's Signature _____

Advisor's Signature _____

Co-advisor's Signature _____



ACKNOWLEDGEMENTS

This is my great pleasure to express my profound gratitude and appreciation to my thesis advisor, Assoc. Prof. Dr. Songkot Dasananda and co-advisor, Asst. Prof. Dr. Anukul Buranapratheprat for their guidance, kind assistance and informative discussion on many concerned problems. My thesis would never be completed without their help.

I am also very grateful to all thesis examining committee; Asst. Prof. Dr. Sunya Sarapirome, Assoc. Prof. Dr. Suwit Ongsomwang, Assoc. Prof. Dr. Sura Pattanakiat and Dr. Pantip Piyatadsananon for their critical comments and valuable suggestions on this thesis. Profound thanks are also due to Prof. Dr. Satsuki Matsumura for providing the necessary data and to all the corresponding experts for their questionnaire responses. In addition, I would like to greatly thank Mr. Tinn Tirakultomorn, for crucial helps and recommendations on necessary RS and GIS techniques for this thesis.

On this occasion, I would also like to express my grateful acknowledgement to the Department of Aquatic Science, Faculty of Science, Burapha University (my current work place) for providing financial support for my Ph.D. study at Suranaree University of Technology.

Finally, the wholehearted appreciation is devoted to my family for giving me inspiration and long-lasting love, best wishes, and support.

Prasarn Intacharoen

CONTENTS

	Page
ABSTRACT IN THAI.....	I
ABSTRACT IN ENGLISH	III
ACKNOWLEDGEMENTS.....	V
CONTENTS	VI
LIST OF TABLES.....	XI
LIST OF FIGURES	XVI
LIST OF ABBREVIATIONS.....	XXI
CHAPTER	
I INTRODUCTION.....	1
1.1 Problem background and significance of the study.....	1
1.2 Research objectives	3
1.3 Scope and limitations of the study	4
1.4 Study area.....	5
1.5 Expected results.....	5
II LITERATURE REVIEWS	7
2.1 Eutrophication phenomenon.....	7
2.1.1 Environmental factors and eutrophication	8
2.1.2 State of trophic for coastal marine eutrophication	11
2.2 Remote sensing for coastal eutrophication assessment.....	12

CONTENTS (Continued)

	Page
2.3 Ocean color of case II water and optical properties	18
2.3.1 Chlorophyll-a models	21
2.3.2 Total suspended solids models	23
2.3.3 Color dissolved organic matter models	26
2.4 Relevant researches on eutrophication	28
2.4.1 Remote sensing for water constituents	28
2.4.2 Applications of artificial neural networks	34
2.4.3 Spatial assessment of eutrophication.....	39
2.5 Red tide and Chlorophyll-a studies in the Gulf of Thailand	42
2.5.1 Red tide phenomena	42
2.5.2 Chlorophyll-a studies.....	44
2.6 Concepts of the relevant used methods	46
2.6.1 Local maximum fitting analysis (LMF)	46
2.6.2 Frequency ratio analysis (FR)	47
2.6.3 Simple additive weighting (SAW)	48
2.6.4 Area under the curve method (AUC)	49
III EQUIPMENT, DATA AND METHODOLOGY.....	52
3.1 Equipment	52
3.2 Data requirement	52
3.3 Research methodology	53

CONTENTS (Continued)

	Page
3.3.1 Data collection and preparation.....	57
3.3.2 Evaluation for optimal retrieval models	61
3.4 Applications of the optimal method	67
3.5 Formulation of the red tide susceptibility maps	69
IV MODIS-BASED EMPIRICAL MODEL DEVELOPMENT FOR MARINE CONSTITUENT CONCENTRATION ASSESSMENT OVER UGoT	73
4.1 In situ data collection and preparation	73
4.1.1 Data from field observation in UGoT.....	74
4.1.2 Profiling reflectance radiometer (PRR) measurement.....	77
4.2 MODIS satellite dataset.....	84
4.3 Modeling assessment.....	85
4.3.1 Chl-a model modification.....	88
4.3.2 TSS model modification.....	90
4.3.3 CDOM model modification.....	91
4.4 Artificial neural network (ANN) model	104
4.5 Conclusion.....	118
V MODIS-BASED MONITORING OF COASTAL ENVIRONMENT IN THE UPPER GULF OF THAILAND.....	120
5.1 Main river discharges into the UGoT.....	120

CONTENTS (Continued)

	Page
5.2 MODIS-based observations of target constituents in 2010 to 2012	124
5.2.1 Spatial/temporal variations of Chl-a concentration	124
5.2.2 Spatial/temporal variations of TSS concentration	132
5.2.3 Spatial/temporal variations of CDOM concentration	139
5.3 Relationships of Chl-a, TSS and CDOM concentration data	145
5.4 Trophic states over the UGoT area from years 2010 to 2012	151
5.5 Conclusions	159
VI RESULTS OF RED TIDE SUSCEPTIBILITY INDEX	
FORMULATION	162
6.1 Preparation of necessary factors for model's analysis	163
6.1.1 Reference red tide occurrence maps	163
6.1.2 Total suspended solids	169
6.1.3 Color dissolved organic matter	175
6.1.4 Sea water depth and distance from river mouths	180
6.1.5 Velocity of surface current	182
6.2 Red tide susceptibility mapping by SAW method	186
6.3 Red tide susceptibility mapping by FR method	197
6.4 Conclusion	209
VII CONCLUSIONS AND RECOMMENDATIONS	212
7.1 Model development for marine constituent determination	212

CONTENTS (Continued)

	Page
7.2 MODIS-based monitoring of coastal environment in the UGoT	214
7.3 Red tide susceptibility analysis and mapping	216
7.4 Recommendations	218
REFERENCES	220
APPENDICES	238
APPENDIX A THE MAIN OF MARINE WATER CONSTITUENT PARAMETERS	239
APPENDIX B ANCILLARY DATA OF OCEANIC PARAMETERS	242
APPENDIX C THE PRR MEASUREMENT AND MODIS DATA FOR MODELING	247
APPENDIX D THE EMPIRICAL METHOD FOR THREE WATER CONSTITUENTS.....	252
APPENDIX E THE HISTORICAL DATA OF RED TIDE PHENOMENA IN UGOT	256
APPENDIX F SAW-QUESTIONNAIRE	268
CURRICULUM VITAE.....	274

LIST OF TABLES

Table	Page
2.1 Simple trophic state classification for marine systems	12
2.2 Current ocean-color sensors	16
2.3 Spectral bands of sensors in visible region.	16
2.4 Extended MODIS band suitable for ocean environmental studies.....	17
2.5 Science datasets included in a standard MODIS Level-2 ocean color file	18
2.6 Visible remote sensing over land, open ocean and case II waters.	21
2.7 Comparison between variables and class limits of the general classification system of OECD.....	41
2.8 OECD Fixed Boundary System	41
2.9 Reported of the red tide phenomena in the Gulf of Thailand (1957-2001).....	43
2.10 Examples of the frequency ratio values for the used causative factors.....	50
3.1 Details of the principal data needed for the research	53
3.2 Geographic coordinate system of sampling sites in UGoT.....	58
3.3 Spectral measurements of the PRR-2600 and 2610 instruments compared with those of the MODIS instruments at optical region.....	59
3.4 The empirical models applied for the retrieval of Chl-a data in this research ...	64
3.5 The empirical models applied for the retrieval of TSS data in this research	65
3.6 The empirical models applied for the retrieval CDOM data in this research.....	66
3.7 Modified of OECD Fixed Boundary System for UGoT performance.	68

LIST OF TABLES (Continued)

Table	Page
3.8 Influencing parameters for red tide phenomena evaluation in UGoT.....	72
4.1 Five cruises surveys in UGoT	74
4.2 Coefficient determination (R^2) of PRR reflectance and MODIS Level 2.....	89
4.3 Modified empirical models for Chl-a estimation based on in situ and PRR dataset	92
4.4 The performance of Chl-a models based on PRR data for Chl-a prediction	94
4.5 The optimal model for Chl-a extraction from MODIS data (OC3M).....	94
4.6 Modified empirical models for TSS predictions based on in situ and PRR dataset	96
4.7 The performance of TSS models based on PRR data for TSS prediction.....	98
4.8 The optimal model for TSS extraction from MODIS data (TSM).....	98
4.9 Modified empirical models for CDOM predictions based on in situ and PRR dataset	100
4.10 The performance of CDOM models based on PRR data for CDOM prediction.....	102
4.11 The optimal model for CDOM extraction from MODIS data (Chula model) .	102
4.12 Detail of input parameters for the applied ANN model	107
4.13 Details of the parameter and performance data of the applied ANN model.....	107
4.14 Weights information of neurons across layers of first step	108
4.15 Weights information of neurons across layers of second step	109

LIST OF TABLES (Continued)

Table	Page
4.16 Weights information of neurons across layers of third step	110
4.17 Sensitivity of model to forcing independent variables to be constant (1)	110
4.18 Sensitivity of model to forcing independent variables to be constant (2)	111
4.19 Sensitivity of model to forcing independent variables to be constant (3)	111
4.20 Summary of coefficient and wavebands influence results of ANN model based on Chl-a assessment.....	112
4.21 Summary of coefficient and wavebands influence results of ANN model based on TSS assessment.....	112
4.22 Summary of coefficient and wavebands influence results of ANN model based on CDOM assessment.....	113
4.23 Comparison of ANN and empirical models performance.	117
5.1 Monsoonal seasons in Thailand	121
5.2 Main rivers discharges into UGoT in year 1997	121
5.3 Statistical of annual rainfall of four river basin from years 1985 to 2014.	122
5.4 Annual river discharges into UGoT from years 2010 to 2012	122
5.5 Standard statistics of Chl-a concentration in year 2010	130
5.6 Standard statistics of Chl-a concentration in year 2011	130
5.7 Standard statistics of Chl-a concentration in year 2012	130
5.8 Standard statistics of TSS concentration in year 2010.....	137

LIST OF TABLES (Continued)

Table	Page
5.9 Standard statistics of TSS concentration in year 2011	137
5.10 Standard statistics of TSS concentration in year 2012	137
5.11 Standard statistics of CDOM concentraion in year 2010	143
5.12 Standard statistics of CDOM concentraion in year 2011	143
5.13 Standard statistics of CDOM concentraion in year 2012	143
5.14 Previous researches concerned the relationship of Chl-a, TSS and CDOM	148
5.15 Correlation matrix of Chl-a, TSS and CDOM from years 2010 to 2012	149
5.16 The results of trophic state classification in the year 2010	154
5.17 The results of trophic state classification in the year 2011	156
5.18 The results of trophic state classification in the year 2012	158
6.1 Classified area for the TSS-based tendency maps in Figure 6.3	174
6.2 Standard statistics of original TSS data of the classified maps in Figure 6.3. .	174
6.3 Classified area for the CDOM-based tendency maps in Figure 6.4.....	179
6.4 Standard statistics of original CDOM data of classified maps in Figure 6.4 ...	179
6.5 Classified area for the tendency maps in Figures 6.5 and 6.6.....	182
6.6 Classified area for the tendency maps seen in Figure 6.7.	186
6.7 Standard statistics of the derived monthly surface current velocity data.	186
6.8 Seven examined scenarios for red-tide susceptibly mapping (Type 1-7).....	188
6.9 Evaluation of preference score by the multiple comparison analysis	188
6.10 Total preference score and final normalized weight in each listed scenario....	189

LIST OF TABLES (Continued)

Table	Page
6.11 Associated class weights for input factors in SAW model.....	189
6.12 Classified area for red-tide susceptibility category based on SAW model.	196
6.13 The results of accuracy assessment based on SAW model.....	197
6.14 Derivation of the associated FR attribute weights.....	199
6.15 Summary of FR class weights for all reference red tide maps and the average FR for each specific attribute.....	202
6.16 Classified area for red-tide susceptibility category based on FR method.	208
6.17 The results of accuracy assessment base on FR model.	209

LIST OF FIGURES

Figure	Page
1.1 Map of the study area	6
2.1 Conceptual model of eutrophication	10
2.2 Secchi disk depth for different types of water and of RS reflectance from the sea bottom.	14
2.3 An illustration of the triangular diagram in use to classify waters.....	20
2.4 Variation of remote sensing reflectance with TSM according to the model for various red and near infrared wavelengths	25
2.5 CDOM power law empirical algorithm equations between three evaluated reflectance band ratios versus CDOM a_{g412}	28
2.6 Linear regression fit between the in situ suspended sediment concentrations and remote sensing reflectance measurements used for the development of the regional algorithm	33
2.7 Average CDOM and chlorophyll-a specific absorption at different wavelength for Narragansett Bay	34
2.8 Three layer neural network with only one hidden layer.....	35
2.9 Architecture of neural network	37
2.10 ANN construction after training.....	38
2.11 Local maximum fitting method.....	46
2.12 Basic procedure of Simple Additive Weighting Method analysis	51

LIST OF FIGURES (Continued)

Figure	Page
2.13 Computed accuracies of the susceptibility in terms of the AUC.....	51
3.1 Work flowchart of the empirical method based on objective 1.....	54
3.2 Work flowchart of the ANN method based on objective 1	55
3.3 Work flowchart of the research based on objective 2	56
3.4 Work flowchart of the research based on objective 3	56
3.5 Sampling locations during the cruise surveys in 2003 to 2004.....	58
3.6 Examples of past red tide locations in UGoT area	61
4.1 Seasonal circulation in UGoT	75
4.2 Chlorophyll-a distribution maps of in-situ data in UGoT from October 2003 to October 2004	79
4.3 Total suspended solid distribution maps of in situ data in UGoT from October 2003 to October 2004	80
4.4 Color dissolved organic matter distribution maps of in situ data in UGoT from October 2003 to October 2004	81
4.5 Spectral variations based on PRR measurement from cruise 1	82
4.6 Spectral variations based on PRR measurement from cruise 2.....	83
4.7 Spectral variations based on PRR measurement from cruise 3.....	83
4.8 Spectral variations based on PRR measurement from cruise 4.....	83
4.9 Spectral variations based on PRR measurement from cruise 5.....	84
4.10 Spectral variations based on MODIS L2 reflectance in cruise 1.....	86

LIST OF FIGURES (Continued)

Figure	Page
4.11 Spectral variations based on MODIS L2 reflectance in cruise 2.....	86
4.12 Spectral variations based on MODIS L2 reflectance in cruise 3.....	87
4.13 Spectral variations based on MODIS L2 reflectance in cruise 4.....	87
4.14 Spectral variations based on MODIS L2 reflectance in cruise 5.....	87
4.15 MODIS-based OC3M model performance for Chl-a prediction/mapping.....	94
4.16 MODIS-based Chl-a concentration map derived by the OC3M model..	95
4.17 MODIS-based TSM model performance for TSS prediction/mapping	98
4.18 MODIS-based TSS concentration map derived by the TSM model	99
4.19 MODIS-based Chula model performance for CDOM prediction/mapping	102
4.20 MODIS-based CDOM concentration map derived by the Chula model.....	103
4.21 ANN structure for the prediction of Chl-a/TSS/CDOM from MODIS data ...	107
4.22 Example of Chl-a concentration map derived by the applied ANN model.....	114
4.23 Example of TSS concentration map derived by the applied ANN model.....	115
4.24 Example of CDOM concentration map built by the applied ANN model	116
5.1 Four main river discharge for years 2010 to 2012	123
5.2 Spatial distributions of monthly Chl-a in year 2010	127
5.3 Spatial distributions of monthly Chl-a in year 2011	128
5.4 Spatial distributions of monthly Chl-a in year 2012	129
5.5 Maximum/mean of Chl-a concentration in 2010 to 2012 (OC3M model).....	131
5.6 Spatial distributions of monthly TSS in year 2010	134

LIST OF FIGURES (Continued)

Figure	Page
5.7 Spatial distributions of monthly TSS in year 2011	135
5.8 Spatial distributions of monthly TSS in year 2012	136
5.9 Maximum/mean TSS concentration from years 2010 to 2012 (TSM model).	138
5.10 Spatial distributions of monthly CDOM in year 2010	140
5.11 Spatial distributions of monthly CDOM in year 2011	141
5.12 Spatial distributions of monthly CDOM in year 2012	142
5.13 Maximum/mean of CDOM concentration from years 2010 to 2012 (Chula model).....	144
5.14 Correlation data of three water constituents from years 2010 to 2012.....	150
5.15 Trophic state maps of Chl-a based on OC3M model in year 2010.	153
5.16 Area percentage of classified trophic state in year 2010.....	154
5.17 Trophic state maps of Chl-a based on OC3M model in year 2011.	155
5.18 Area percentage of classified trophic state in year 2011.....	156
5.19 Trophic state maps of Chl-a based on OC3M model in year 2012.	157
5.20 Area percentage of classified trophic state in year 2012.....	158
5.21 Summary trophic state of ET and HT from years 2010 to 2012	159
6.1 Reference red-tide maps for model's application process.....	164
6.2 Reference red-tide maps for susceptibility map's validation process.	167
6.3 Classified TSS-based red-tide tendency of occurrence maps.....	171
6.4 Classified CDOM-based red-tide tendency of occurrence maps	176

LIST OF FIGURES (Continued)

Figure	Page
6.5 Classified red-tide tendency of occurrence map based on water depth	181
6.6 Classified red-tide tendency of occurrence map based on distance away from four main river mouths.	181
6.7 Surface current maps of UGoT	183
6.8 Red-tide susceptibility maps by SAW method.....	194
6.9 An accuracy assessment result based on AUC method of SAW model.....	196
6.10 Red-tide susceptibility maps by FR method.....	206
6.11 An accuracy assessment result based on AUC method of FR model.....	208

LIST OF ABBREVIATIONS

ANN	=	Artificial neural network
AUC	=	Area under the curve method
BP	=	Back propagation algorithm
CDOM	=	Color dissolved organic matter
Chl-a	=	Chlorophyll-a
CTD	=	Conductivity-temperature-depth sensor
DMCR	=	Department of Marine and Coastal Resources
IMS	=	Institute of Marine Science, Burapha University
EI	=	Eutrophication Index
ET	=	Eutrophic
FR	=	Frequency Ratio
HT	=	Hyper-eutrophic
IOPs	=	Inherent Optical Properties
LMF	=	Local maximum fitting algorithm method
MAPE	=	Mean absolute percent error
MLP	=	Multilayer perceptron
MODIS	=	MODerate resolution Imaging Spectroradiometer
MT	=	Mesotrophic
NE	=	Northeast monsoon
OC3M	=	Ocean color algorithm that using three wavebands

LIST OF ABBREVIATIONS (Continued)

OECD	=	Organization for economic Co-operation and development
OT	=	Oligotrophic
PRR	=	Profiling reflectance radiometer
PS	=	Preference score
RTSI	=	Red tide susceptibility index
SAW	=	Simple additive weights
SW	=	South-west monsoon
TSS	=	Total suspended solids
UGoT	=	Upper Gulf of Thailand
UT	=	Ultra-oligotrophic
WLC	=	Weighted linear combination

CHAPTER I

INTRODUCTION

1.1 Problem background and significance of the study

Marine environments consist of nature and resources of ocean, sea and coastal zone that cover more than 70% of the earth surface. They contain huge amount of living species and several important natural resources which are very crucial for mankind. However, in recent decades, marine ecosystem was considerably deteriorated due mostly to huge discharges of waste from both land-based sources and ocean-based sources. The origins of these pollutants are mainly from human activities and their impacts are evidenced globally nowadays especially along the coastal zones of mega cities. These activities comprise of both land-based, e.g., coastal urbanization, industrial development, agriculture intensification, tourism, and ocean-based activities, e.g., seabed exploration, oil refinery, and risk of petroleum and other toxic chemical transportation (Ramsey, 2005; Smith and Schindler, 2009; Subramanian, n.d).

One of highly concerned marine pollutions is eutrophic phenomenon. Typically, eutrophication is defined as a substantial increase of some chemical nutrients, especially those containing nitrogen or phosphorus, in an ecosystem that cause adverse impact to environment as a whole. The direct result of eutrophication is a sharp increase in the amount of small plants like phytoplankton or algae in the polluted water body (called plankton bloom or algae bloom). Subsequent impacts include the depletions of

dissolved oxygen in water and critical reductions of the water quality and animal populations, like fish. The problem of eutrophication has risen dramatically with the population growth, excessive use of fertilizers, and increase in industrialization (Khan and Aliansari, 2005; Helsinki Commission, 2009).

Water qualities in the Upper Gulf of Thailand (UGoT) are notably deteriorated in recent years especially at the mouths of the four major rivers (i.e. the Bang Pakong, the Chao Phraya, the Mae Klong and the Tha Chin Rivers). This degradation is due mainly to the increase of nutrient inputs from agriculture activities, mariculture industry, and household sewage. One of the effects from water quality degradation in the area is the occurrence of red tide phenomenon, which has become more common incidence in recent years (Menasveta, n.d.). According to reports by the Institute of Marine Science and DMCR, there are more than 220 cases of the red tide phenomena were occurred in the UGoT from years 1957 to 2016.

In general, the assessment of marine water quality and eutrophication intensity are carried out through the evaluation of water samples collected from some specific locations close to coastal areas or from the ship-based surveys. Such traditional methods are relatively expensive and insufficient to provide comprehensive information over the large area. To overcome these limitations, geoinformatics technology has been implemented to quantify water qualities of the interested area through the use of satellite-based monitoring and assessment. Water constituents including chlorophyll-a (Chl-a), total suspended solids (TSS), and color dissolved organic matter (CDOM) can be estimated. However such satellite-based water quality assessment in UGoT was rarely reported so far, e.g., Phoomwongpitak (2003); Bhatrasataponkul (2004); and Buranapratheprat, Niemann, Matsumura, and Yanagi (2009).

This thesis will systematically explore apparent capability of satellite technology on the quantification of three crucial seawater constituents (Chl-a, TSS, CDOM) for assessing water quality, within UGoT. The daily MODIS data in visible and NIR bands, along with the concurrent in-situ data from field surveys, will be implemented to build effective algorithm for the extraction of all stated constituents. Knowledge of this kind is necessary for the up-to-date evaluation of water quality on daily basis as well as the monitoring of the eutrophication incidence in this area. The MODIS-based susceptibility maps of red-tide occurrence will be established by two different methods: WLC (weighted linear combination) and FR (frequency ratio). These obtained maps will be applied to identify areas with high tendency for red-tide formation based on the relationships between a group of chosen parameters and the observed occurrences of the incidence in the past. The results yielded from these stated works can contribute comprehensive knowledge on capability of the developed algorithms in the mapping and monitoring of Chl-a, TSS, and CDOM distribution over UGoT well as the main influencing factors and susceptible areas for critical eutrophication development, which has not been thoroughly investigated so far.

1.2 Research objectives

Principal objectives of the thesis are as follows:

(1) To identify optimal models for the determination of concentration of three key marine water constituents: chlorophyll-a, total suspended solids, and color dissolved organic matter, from the satellite-based on MODIS data.

(2) To observe variation in mapped concentration of the referred constituents and trophic state of water quality in UGoT during years 2010-2012.

(3) To formulate credible red-tide susceptibility maps for UGoT through the frequency ratio and simple additive weighting methods.

1.3 Scope and limitations of the study

Scope and limitations of this study can be summarized as follows:

(1) Study area is UGoT covering the area of about 10,360 km² incorporating the continuous coastal zone from the Chonburi province to Petchaburi province (Figure 1). The reference location is 12°35'45" N, 99°57'30" E and 12°35'45" N, 100°57'45" E (พระราชบัญญัติกำหนดเขตจังหวัดในอ่าวไทยตอนใน, 2502).

(2) The retrieval models for Chl-a, TSS, and CDOM are developed empirically from the found relationship of the MODIS reflectance data and associated field data for each stated constituent.

(3) Red tide data are mainly collected from records of the responsible agencies and through the observation of MODIS sensors during process of marine environment condition observation and assessment (in Objective 2). In this case, only MODIS cloud-free images are used for the analysis.

(4) Only surface concentration of the listed constituents gained from the satellite imagery is used in the water quality analysis and the red tide investigation is based only on amount of the surface Chl-a data (not on causative plankton species).

(5) All empirical algorithms are built based on observed in situ water constituent data obtained during field surveys in years 2003 to 2004 from the PRR instrument along with the concurrent MODIS data during that time.

(6) Classification of trophic level is based on amount of the observed Chl-a data as explained in the “OECD Fixed Boundary System index” detailed in Table 2.8.

(7) All spatial distribution maps in this study are analyzed based on 1 km².

1.4 Study area

The Upper Gulf of Thailand incorporates continuous coastal zone from Chonburi province to Petchaburi province (Figure 1.1) with four major rivers attached along its northern boundary, namely; the Maeklong, the Thachin, the Chao Phraya and the Bang Pakong Rivers. Its average depth is 20 m, a slope in average is 0.2 m/km and total surface area of about 10,360 km². It is also an important resource for the fishing industry, tourism and port operations.

1.5 Expected results

(1) Effective methods for the determination of the referred marine constituents (Chl-a, TSS, and CDOM) data from the MODIS reflectance data in the UGoT area.

(2) Knowledge on the variation of mapped concentration of the aforementioned marine constituents in the UGoT during the examined period.

(3) Credible red tide susceptibility maps for the UGoT to enhance knowledge on formation mechanism and occurrence chances of red tide incidence in the area.

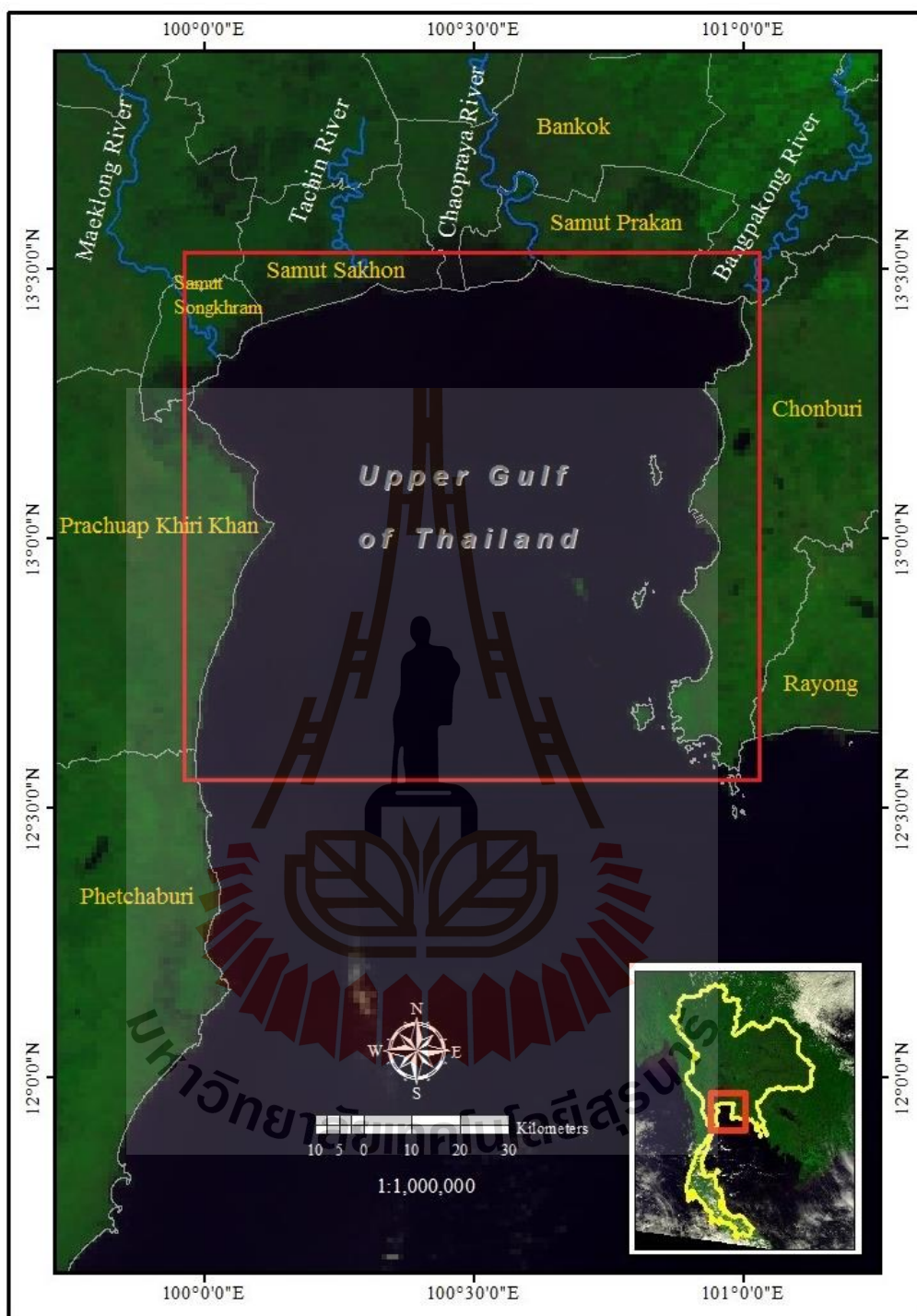


Figure 1.1 Map of the study area (UGoT).

CHAPTER II

LITERATURE REVIEWS

This chapter contains basic concepts of relevant issues in this work including following topics: (1) eutrophication phenomenon characteristics (ecosystem variables to environment in eutrophication phenomenon and trophic states for the coastal marine eutrophication), (2) satellite-based coastal water quality and eutrophication assessment, (3) optical properties of case II ocean water in relation to the Chl-a, TSS and CDOM, (4) applications of remote sensing and artificial neural networks (ANN) on sea water constituents and eutrophication assessment, (5) red tide and Chl-a studies in the Gulf of Thailand, and (6) concepts of the relevant used methods, i.e., frequency ratio (FR), simple additive weighting (SAW) and area under the curve method (AUC).

2.1 Eutrophication phenomenon

Eutrophication is a deterioration of water quality resulted from the combination effects of excessive growth of phytoplankton leading to the imbalance of primary and secondary productivity and faster rate of succession from existing to higher serial stage caused by nutrient enrichment through runoffs that carry down over used fertilizers from agro-ecosystems and/or discharged human waste from the settlements (Khan and Aliansari, 2005). This process is driven by the enrichment of water by essential nutrients, especially those of nitrogen and/or phosphorus, leading to the increased

growth, primary production and biomass of algae; changes in balance of the organisms; and water quality degradation (Ferreira et al., 2011).

Naumann was the first to define “Lake Eutrophication” in 1919 as the increase of nutritive substances in lake, especially phosphorus and nitrogen (Hutchinson, 1967). Several definitions of the eutrophication were defined and used so far; for examples, according to Steele (1974), eutrophication is the increase of the growth rate of algae, following a faster rate of nutrients in marine environment as well as consequences or by Nixon (1995), eutrophication is an increase in rate of supply of organic matter to an ecosystem. Also, the European Environmental Agency introduced this definition for its research program, eutrophication means enhanced primary production due to excess supply of nutrients from human activities, independent of natural productivity level for the area (EEA, 2001).

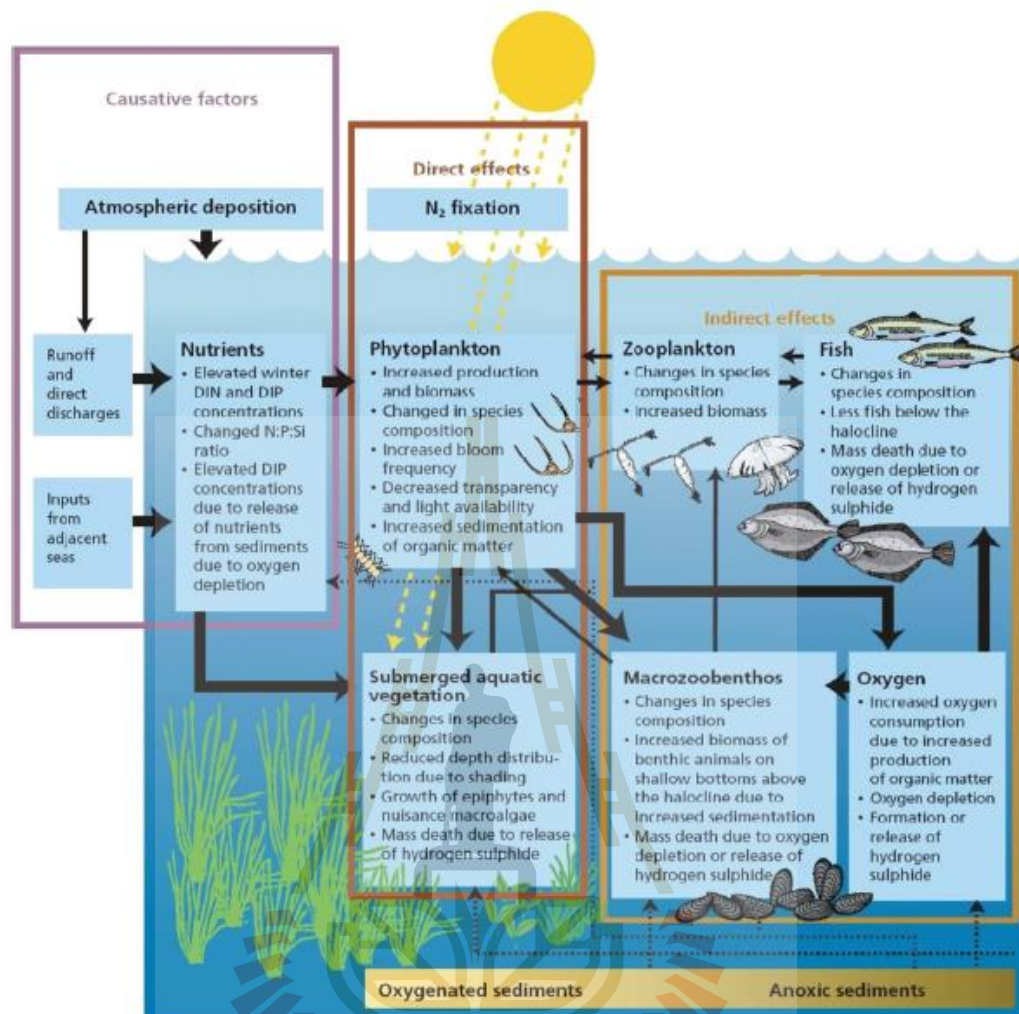
2.1.1 Environmental factors and eutrophication

Major nutrients causing eutrophication are nitrogen and phosphorus. For monitoring eutrophication in marine environment, a large number of variables beyond nitrogen and phosphorus are needed. Measurements on nutrients from riverine inputs are considered crucial for the enrichment assessment of marine environment. Traditionally, several variables are needed for the eutrophication assessment. Those are inorganic nitrogen (e.g. nitrate, nitrite, ammonia), inorganic phosphorus (orthophosphates), and production of organic matter (Chl-a, phytoplankton density, and macrophyte biomass) (Kitsiou and Karydis, 2011).

Eutrophication is therefore a worldwide environmental issue detrimental to the environmental sustainability. Distribution patterns of phytoplankton organisms are closely related to both the physical states (e.g. salinity, water temperature, turbidity,

and sunlight) and biological processes (e. g. coastal food web and habitat locations) (Chang, Xuan, and Yang, 2013). Nitrogen and phosphorus nutrients have accelerated the fluxes of these elements to coastal waters, and fertilization of coastal ecosystems is now a serious environmental problem because it can stimulate plant growth and disrupt the balance between the production and metabolism of organic matter in coastal zone. In the coastal ecosystems with low N or P density, rate of plant biomass production and accumulation is limited (Cloern, 2001). Change in rate of primary production indicates the trophic status of aquatic ecosystems and their health (Khan and Aliansari, 2005).

Figure 2.1 details a balanced marine ecosystem characterized by: (1) a pelagic food chain (phytoplankton < zooplankton/zoobenthos < fish), which effectively couples production to consumption and minimizes potential for excess decomposition, (2) natural species composition of plankton and benthic organisms, (3) if appropriate, a natural distribution of the submerged aquatic vegetation. Nutrient enrichment results in changes in the structure and function of the marine ecosystems, as indicated with bold lines. Dashed lines indicate release of hydrogen sulphide (H_2S) and phosphorus, under anoxic conditions at the sediment water interface, which is positively related to the oxygen depletion. In addition, nitrogen is eliminated by denitrification in anoxic sediment (Ferreira et al., 2011).



Source: Ferreira et al., 2011.

Figure 2.1 Conceptual model of eutrophication. The arrows indicate the interactions between different ecological compartments.

2.1.2 State of trophic levels for coastal marine eutrophication

Indices and models for evaluating eutrophic levels are very important tools for assessing degree of the anthropogenic influences on eutrophication in estuaries and coastal environments (Alves, Flores-Montes, Gaspar, Gomes, and Feitosa, 2013). Knowledge on the variation of available nutrients in the ecosystem is important to identify eutrophic states over water of interest. According to Nixon (1995), this simple scheme (as seen in Table 2.1) is useful for estuarine and coastal ocean ecosystems.

The term “indicator” is often introduced in the marine environment to describe ecological status, to assess water quality and to provide practical information for the coastal management practices. A definition of an indicator in a broader sense has been initiated by Burger (2006) as follows: “Indicator: Index or measurement end point to evaluate health of a system; physical, biological, economic”. The multimetric index proposed by Primpas et al. (2010) was found efficient in discriminating the water types. Four nutrient variables and Chl-a concentrations were used for identifying eutrophic, mesotrophic and oligotrophic water types. The Eutrophication Index (EI) proposed is shown as follow:

$$EI = 0.297C_{PO4} + 0.261C_{NO3} + 0.296C_{NO2} + 0.275C_{NH3} + 0.214C_{Chl-a}, \quad (2.1)$$

where C is nutrient and Chl-a concentrations.

This index was adapted to a five level scale compatible with the criteria required by the European Water Framework Directive: (a) < 0.04: High quality, (b) 0.04 - 0.38: Good, (c) 0.38 - 0.85: Moderate, (d) 0.85 - 1.51: Poor and (e) > 1.51: Bad (Kitsiou and Karydis, 2011).

Daily productivity based on ^{14}C method (d_{pc} in unit of $\text{mgCm}^{-3}\text{d}^{-1}$) may be estimated using average Chl-a concentration (C_k in unit of Chl. m^{-3}) by Equation 2.2 (a and b are constants) as follows (Fallkowski et al., 1998):

$$\log_{10}(d_{pc}) = a + b \cdot \log_{10}(C_k) \quad (2.2)$$

Equations 2.1 and 2.2 can be used for trophic state retrieval in the water bank (i. e. nutrient components and Chl-a). As Chl-a is more observable than the related nutrients, it has been widely used as a primary indicator for the categorize of trophic state (e.g. in Koponen, Pulliainen, Kallio, and Hallikainen, 2002).

Table 2.1 Simple trophic state classification for marine systems.

Trophic state	Organic Carbon Supply ($\text{gC}/\text{m}^2/\text{y}$)
Oligotrophic	< 100
Mesotrophic	100-300
Eutrophic	301-500
Hypertrophic	> 500

Source: Nixon, 1995.

2.2 Remote sensing for coastal eutrophication assessment

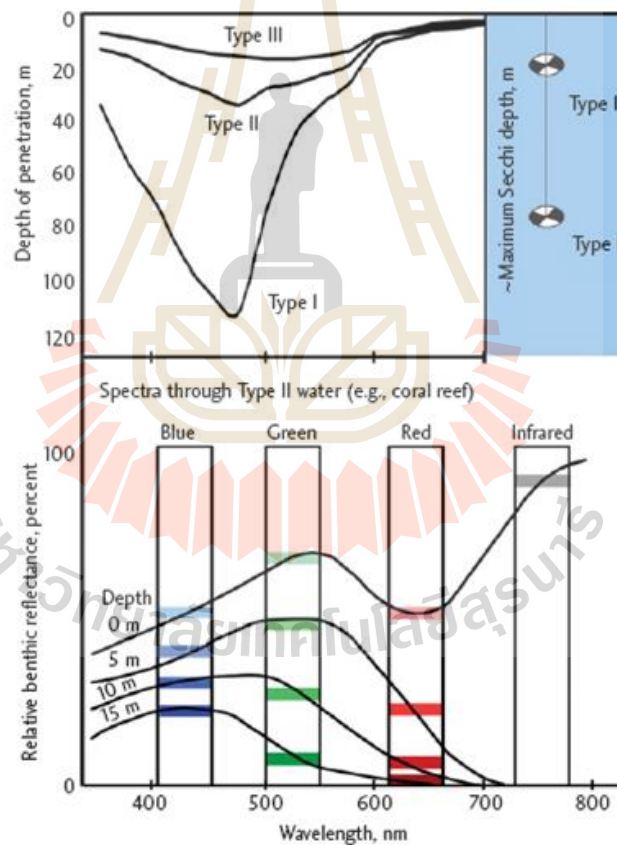
Pioneer studies of coastal eutrophication were done through the use of conceptual model, with emphasis on measuring signal nutrient concentrations or fluxes and the responses (phytoplankton biomass, primary production, oxygen concentrations or consumption rates). How the signal of changing nutrients is related to phytoplankton biomass or primary production in estuaries is a major approach. Certainly, there is a fundamental linkage between the processes of N delivery and the algal-based

expressions of eutrophication (Cloern, 2001). A great abundance of primary producers distributing in large area of the marine ecosystem can be monitored by using the remote sensing technique which plays a key role in measuring ocean productivity. Multiple in water variables involved in the remote sensing system can have large effects on the amount of light radiance moving toward the sensor (Horning, Robinson, Sterling, Turner, and Spector, 2010).

Most natural waters contain several components like planktons, sediments and colored matter that affect three prominent related parameters including photic zone depth, secchi disk depth, and spectral attenuation coefficient. Different wavelengths of the light penetrate clear water to different depths proportional to the inverse of attenuation coefficient of the water. In general, wavelengths shorter than 500 or 580 nm (blue/green) penetrate deep into water body and can easily reflect off the bottom then come back to the observer. Longer wavelengths (yellow/red) are not penetrate very deep and infrared does not penetrate water column at all (Figure 2.2). As a rule of thumb for clear coastal waters such as over coral reef (Type II), blue light shall penetrate to a maximum of about 25-30 m, green light penetrates to a maximum of about 15 m, while red/near-infrared penetrates about 5 and 0.5 m, respectively, and mid to far infrared light is fully absorbed (Horning et al., 2010).

For eutrophication assessment, it typically requires not only large number of variables, but also the spatial distribution of eutrophic levels based on each of the variables. The final thematic maps illustrate spatial distribution of eutrophic conditions. These need appropriate methodologies tools and various parameters. Fortunately, this can easily be performed through the use of a geographic information system (GIS) (Xu, Tao, Dason, and Li, 2001).

Water properties are key indicators of how effective the remote sensing sensors can be used to monitor marine environment. Formal classification of the ocean waters is as follows: Type I, for extremely clear oceanic waters of low productivity, Type II, for clear coastal waters, like those over coral reef, typically having more attenuation, and Type III, for the turbid waters, as with many estuarine waters. To imagine these classification schemes in ecological terms, if the secchi disk depth is less than 2 m, optical remote sensing will observe only top meter of the water column.



Source: Horning et al., 2010.

Figure 2.2 Secchi disk depth for different types of water (top) and RS reflectance from the sea bottom.

The measurement of water properties is most developed for remote sensing of open ocean (Type I) beginning with ocean color sensors such as the NASA's Coastal Zone Color Scanner (CZCS) in 1978 followed by the SeaWiFS and MODIS sensors. These sensors provide continuous standard ocean color products applied for the regional and local understanding of aquatic ecosystems (Behrenfeld and Falkowski, 1997; Horning et al., 2010).

Ocean satellite sensors

A variety of sensors for ocean color measurement are at work at present (as listed in Table 2.2) with many more whose services were already ended, e.g. OCTS, MODIS, OCM-2 and VIIRS sensors (Table 2.3). However, the most prominent one nowadays is MODIS sensor (MODerate resolution Imaging Spectroradiometer), which is the main instrument aboard NASA's Terra and Aqua satellites. Both MODIS instruments can view entire Earth's surface every 1 to 2 days, acquiring data in 36 spectral bands at spatial resolutions of 250 m (band 1-2), 500 m (band 3-7) and 1,000 m (band 8-36) (as detailed in Table 2.4). These data can improve understanding of global dynamics and processes occurring on the ocean bio-optical properties based on knowledge of the water-leaving radiance information on daily basis (at 1- km spatial resolution) and the productivity product on weekly basis (at 4.6 km, 36 km and 1° resolution).

The available MODIS products at present are as follows (as described in Table 2.5): water-leaving radiance, Chl-a concentration from 0.01-50 mg/m³, Chl-a fluorescence and fluorescence efficiency, coccolithophore pigment concentration and calcite concentration, suspended sediment concentration, phytoplankton spectral

absorption, dissolved organic matter (DOM) absorption, and the primary productivity (PP) weekly indices (NASA-Ocean Color, 2012).

Table 2.2 Current ocean-color sensors.

Sensor	Agency	Satellite	Launch Date	Swath (km)	Spatial resolution (m)	Band	Spectral Coverage (nm)
OCTS/ CZI	SOA (China)	HY-1B	11 Apr. 2007	3000 500	1100 250	10 4	402-885 433-695
GOCI	KARI/KIOST (South Korea)	COMS	26 Jun 2010	2500	500	8	400 - 865
MODIS- Aqua	NASA (USA)	Aqua (EOS-M1)	4 May. 2002	2330	250/500/1000	36	405-14,385
MODIS- Terra	NASA (USA)	Terra (EOS-M1)	18 Dec. 1999	2330	250/500/1000	36	405-14,385
OCM-2	ISRO (India)	Oceansat-2 (India)	23 Sep. 2009	1420	360/4000	8	400 - 900
OLCI	ESA/ EUMETSAT	Sentinel 3A	16 Feb. 2016	1270	300/1200	21	400-1020
VIIRS	NOAA (USA)	Suomi NPP	28 Oct. 2011	3000	370/740	22	402-11,800

Source: IOCCG, 2000.

Table 2.3 Spectral bands of some ocean sensors in visible region (400 to 760 nm).

OCTS													
BC	412	443	-	490	520	-	565	-	670	-	-	750	865
BW	10	10	-	10	10	-	10	-	10	-	-	20	40
MODIS													
BC	412.5	443	-	488	531	-	551	-	667	678	-	748	
BW	20	20	-	10	10	-	10	-	10	10	-	10	
OCM-2													
BC	412	443	-	490	510	-	555	620				740	865
BW	20	20	-	20	20	-	20	20				30	40
VIIRS													
BC	412	445	488				555			672			865
BW	20	18	20				20			20			39

(Note: BC = Band center in nm, BW = Bandwidth in nm)

Source: IOCCG, 2000.

Table 2.4 Extended MODIS band suitable for ocean environmental studies.

Band Number	Wavelength (nm)	Band Width (nm)	Spatial Resolution (m)	SNR at L_{typ}	L_{typ} $mWcm^{-2} \mu m^{-1}sr^{-1}$	L_{max} $mWcm^{-2} \mu m^{-1}sr^{-1}$	Notes
8	412	15	1000	1773	7.84	26.9	1
9	443	10	1000	2253	6.99	19.0	1
3	469	20	500	556	6.52	59.1	
10	488	10	1000	2270	5.38	14.0	1
11	531	10	1000	2183	3.87	11.1	1
12	551	10	1000	2200	3.50	8.8	1
4	555	20	500	349	3.28	53.2	
1	645	50	250	140	1.65	51.2	3
13	667	10	1000	1962	1.47	4.2	1
14	678	10	1000	2175	1.38	4.2	1
15	748	10	1000	1371	0.889	3.5	1
2	859	35	250	103	0.481	24.0	
16	869	15	1000	1112	0.460	2.5	1
5	1240	20	500	25	0.089	12.3	
6	1640	35	500	19	0.028	4.9	2
7	2130	50	500	12	0.008	1.7	

1: Standard bands for ocean color, 2: 1640 channel not function on MODIS/Aqua, 3: Never saturated.

Source: Franz et al., 2006.

The information of the ocean color MODIS level-2 products was illustrated in Table 2.5. The water-leaving radiance (nL_w) fields have been replaced with remote sensing reflectance (R_{rs}) MODIS products also include R_{rs} for land channels at 469, 555, and 645 nm, aggregated to nominal 1-km resolution of the ocean color channels. The MODIS data at 551 nm is reported at 547 nm, as this is more consistent with true center of the band-pass and thus reduces the need for model-based band-pass corrections (NASA-Ocean Color, 2012).

Table 2.5 Science datasets included in a standard MODIS Level-2 ocean color file.

Products	Description
aot_869	aerosol optical thickness at 869-nm
angstrom	aerosol Angstrom exponent at 443-nm relative to 869-nm
Rrs_412	remote sensing reflectance at 412-nm
Rrs_443	remote sensing reflectance at 443-nm
Rrs_469	remote sensing reflectance at 469-nm
Rrs_488	remote sensing reflectance at 488-nm
Rrs_531	remote sensing reflectance at 531-nm
Rrs_547	remote sensing reflectance at 547-nm
Rrs_555	remote sensing reflectance at 555-nm
Rrs_645	remote sensing reflectance at 645-nm
Rrs_667	remote sensing reflectance at 667-nm
Rrs_678	remote sensing reflectance at 678-nm
chlor_a	chlorophyll-a (OC3v5 algorithm)
Kd_490	diffuse attenuation at 490-nm (KD2 algorithm)
pic	particulate inorganic carbon (Gordon and Balch algorithm)
poc	particulate organic carbon (Stramski algorithm)
cdom_index	colored dissolved organic matter index (Morel algorithm)
par	daily mean photosynthetically available radiation (Frouin algorithm)
ipar	instantaneous photosynthetically available radiation
nflh	fluorescence line height (normalized)

Source: NASA-Ocean Color, 2012.

2.3 Ocean color of case II water and optical properties

In principle, coastal region and lake are often classified as Case II water which is more complex than Case I water in terms of compositions and optical properties. Thus, interpretation of optical signals from Case II water can therefore be rather difficult. In addition, Case II waters are influenced not just by phytoplankton and related particles as in Case I, but also by other substances that vary independently of phytoplankton, notably inorganic particles and yellow substances. However, with more advanced sensors coming, prospect of having better algorithms for Case II waters has

improved vastly (IOCCG, 2000). These stated technological advances are matched by scientific endeavors to improve interpretation of the ocean color in Case II water.

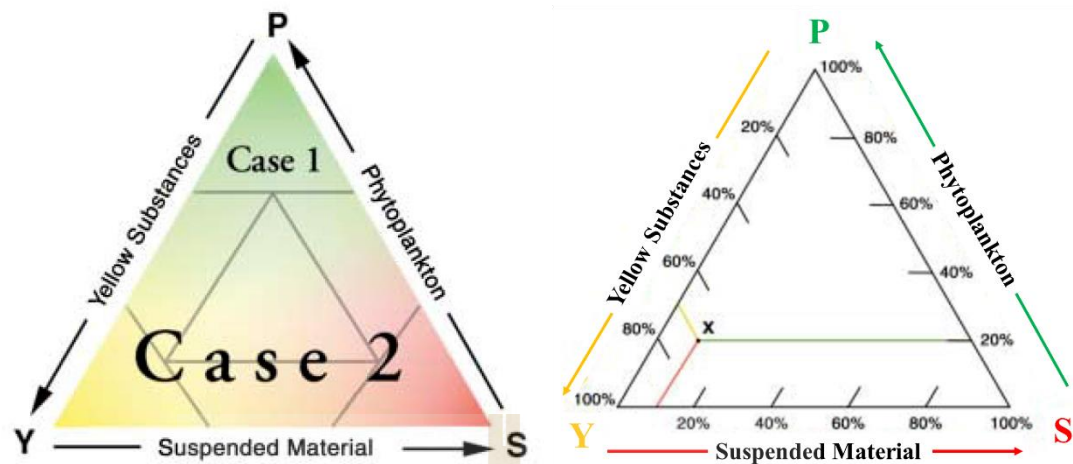
When analyzing optical properties of seawater, we need to distinguish effect of water itself on light property apart from effects of the dissolved and suspended matter presented in the water (Ambarwulan, 2010). In theory, optical perspective is governed by three main components which are as follows:

(1) Phytoplankton. This term includes phytoplankton as well as other microscopic organisms. These are major influence on optical properties.

(2) Suspended material (inorganic). This term refers mainly to the suspended material of inorganic nature, like the sediment. However, microscopic organisms are also “suspended” material in nature but are not included in the study in general.

(3) Yellow substance. This term is usually referred to the colored dissolved, organic substances but it also includes “detrital” particulate material, which generally has absorption characteristics similar to the yellow substances. In theory, the yellow substances, in names of “gelbstoff” or “colored dissolved organic matter (CDOM)”, are a group of organic, dissolved substances, consisting of the humic and fulvic acids.

These substances have been heavily examined in recent decades to determine their origin and chemical composition. The studies are normally restricted to the UV component of the EM spectrum, where absorption is much higher than in visible part. However, yellow substance in addition to pigments (e.g. Chl-a) and nonliving material (e.g. suspended sediment) has become one of the key factors determining characteristics of total light absorption spectrum evidenced in the visible portion (Figure 2.3).



Source: IOCCG, 2000.

Figure 2.3 An illustration of the triangular diagram (also known as the trilinear graph) in use to classify waters. The classification is based on the relative contributions to an optical property from 3 components: phytoplankton, yellow substances and suspended material at 440 nm.

The relationship between concentrations of aquatic constituents is non-linear and small changes in the reflected signal are often used to retrieve needed information. This implies the necessity of measuring instruments with a high signal-to-noise ratio. Also, the proximity to land and the possibility of encountering highly-reflective waters call for sensors with a high dynamic range. The remotely sensed data for Case II waters requires the use of suitable sensors with ground resolutions and repeat cycles that are compatible with the scales of the features to be monitored, as well as complementary in situ experiments that are carefully designed. Typical time and space scales of features to be monitored in coastal/inland water bodies differ from those of other environments, and the applications are more varied, as detailed in Table 2.6 (IOCCG, 2000).

Table 2.6 Visible remote sensing over land, open ocean and case II waters.

Land	Open Ocean Waters (Case I waters)	Coastal and Inland Waters (Case II waters)
Sensor Requirements		
Broad spectral bands	Narrow spectra bands	Narrow spectra bands
Wide dynamic range	Narrow dynamic rang	Wide dynamic rang
Low signal-to-noise	High signal-to-noise	High signal-to-noise
Techniques		
Clustering; classification	Atmospheric correction; pigment algorithm	Radiative transfer; multivariate techniques
Characteristics of Feature to be Monitored		
Spatial scales ≈ 10 m	Spatial scales ≈ 1 km	Spatial scales ≈ 30 m
Time scales $\approx 10 - 100$ d	Time scales ≈ 1 d	Time scales ≈ 0.2 d
Many spectral signatures	One spectral signature	Many spectral signature
Application Envisaged		
Land use/Land cover	Pigment concentration	Concentrations of three components
Change over time	Bloom dynamics, productivity	Bloom dynamics, produc- tivity, sediment transport, coastal dynamics
Disturbance/disease	Carbon cycle, harmful algal blooms	Carbon cycle, harmful algal blooms, water quality, aqua- culture, fisheries, leisure activities

Source: IOCCG, 2000.

2.3.1 Chlorophyll-a models

Estimation of Chl-a concentration by remote sensing is based on effect of Chl-a on the optical properties of water which define the way water reacts to incident light, and is done by the direct or indirect measurement of the optical properties. The Chl-a algorithms usually combine the ground-based observation data and the remotely sensed data to explain pattern of spatial variability and combined another information together in developing models to address questions of ecological interest (Horning et al., 2010). These relationships are generally accounted for by developing empirical, semi-analytical or the radiation transfer models among these the empirical modeling, or experimental algorithm, is the simplest and most implemented approach (Shen, Xu,

and Guo, 2012). This involves establishment of statistical relationship (e.g. regression) between the measured data obtained during field observations with those gained by the satellite. If a strong relationship exists between satellite-measured radiance and field parameter of interest, the prediction algorithm could be established. However, it might be not appropriate to use a relationship derived from one area in place with different environment. Usually, single/multiple band ratios and different formulation, e.g. power function, multiple regression, hyperbolic, second/ third order polynomials, or log-transformed data are applied for such task (O'Reilly et al., 1998).

According to O'Reilly et al. (1998), most empirical equations are derived by the statistical regression of radiance data versus chlorophyll. An optical reflectance (R_{rs}) models can be converted to derive chlorophyll data and absorption coefficients of other optically active components in the water, such as backscattering coefficient (b_b). Then, magnitude of each one from the measurements of water-leaving radiance [$L_w(\lambda)$] and down-welling irradiance [$E_d(0^+, \lambda)$] can be determined, given some assumptions about angular distribution of light in the water. The key is to accurately model spectral behavior of absorption factor [$a(\lambda)$] for each component while spectral behavior of backscatter [$b_b(\lambda)$] is not as dynamic. The R_{rs} model is given by the following equation:

$$R_{rs}(\lambda) \approx \frac{b_b(\lambda)}{a(\lambda)} \quad (2.3)$$

where the “constant” is unchanging with respect to λ and θ_0 .

As sunlight penetrates in the water column, its magnitude and spectral quality is altered by water molecule (w) and relevant constituents, e. g. phytoplankton (p), non-algal particles (np) (detritus and minerals) and a colored fraction of the total

dissolved organic matter (cdom). Absorption [$a(\lambda)$] and scattering [$b(\lambda)$] coefficients of the water are then represented by sum of the optical properties inherent to each of these constituents as follows (Mélin and Hoepffner, 2011):

$$a(\lambda) = a_w(\lambda) + a_p(\lambda) + a_{np}(\lambda) + a_{cdom}(\lambda) \quad (2.4)$$

$$b(\lambda) = b_w(\lambda) + b_p(\lambda) + b_{np}(\lambda) \quad (2.5)$$

To calculate normalized water-leaving radiance, radiance signal gained through the satellite is corrected for atmospheric light-scattering and solar zenith angle effects. Remote sensing reflectance calculated for each band is the fundamental measure for use in optical remote sensing of ocean color. In parallel to its calculation from satellite data, reflectance can also be measured in the field by shipboard and in-water methods for use in calibration, model development and validation. Phytoplankton is the major source of color seen in deep ocean where chlorophyll-a is its primary photosynthetic pigment. As green is less absorbed by chlorophyll-a than blue and red light, thus, the greener in color of ocean water (or greener in spectrum of backscattered sunlight) indicates higher concentration of phytoplankton. As a consequence, there are several standard algorithms being developed and validated for using satellite-based multi-spectral data to estimate chlorophyll-a data effectively (Horning et al., 2010).

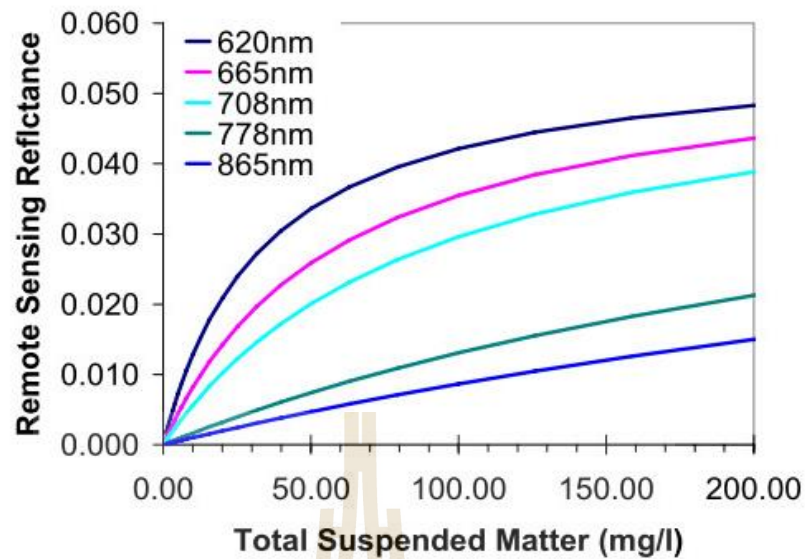
2.3.2 Total suspended solids (TSS) models

Suspended matter is made up of fine particles whose some are present naturally in river water, like plankton, fine plant debris and minerals, while others might come from human activity (organic/inorganic matter). Suspended matter can make water more turbid, giving a negative impact on river and stream biology (EEA, 2001).

Suspended solids refers to mass of the suspended matter and is measured in the unit of mg/l. Interest in the remote sensing of suspended matter is motivated by the environmental and economic importance of sediment transport in coastal waters. Applications include the optimization of dredging/dumping operations, assessing the environmental impact of offshore building activities, understanding geomorphological change, evaluating fluxes of the particulate organic carbon from rivers to the sea, etc. In RS studies, TSS can be estimated via the optical properties of suspended particles assuming, either directly or indirectly, a constant relationship between particle mass and particulate scattering or absorption. TSS may be a more relevant parameter for certain water quality applications where optical properties, like water transparency, are directly important (Ruddick et al., 2008).

The TSS quantification algorithms from the water-leaving reflectance data are often operated in a single band, band ratio, and multispectral. The linear regression performance of single-band algorithm is usually best for low to moderate reflectance and their accuracy depends on the validity of the underlying assumptions, particularly that the total backscatter is proportional to the TSS concentration and that space-time variability of non-particulate absorption can be neglected. The mathematical methods in use are normally relied on a forward model based on radiative transfer simulations and a neural network inversion procedure (Ruddick et al., 2008).

Figure 2.4 demonstrates relationship of various spectral reflectance and difference of total suspended matter. For low reflectance (< 0.01), the relationship is approximately linear, then becoming more non-linear but still monotonic for moderate reflectance (0.01 to 0.03) before reaching an asymptotic value (near 0.05) (Ruddick et al., 2008).



Source: Ruddick et al., 2008.

Figure 2.4 Variation of remote sensing reflectance with TSM according to the model for various red and near infrared wavelengths.

The methods of calculus can be used to derive theoretical relations of diffuse light fluxes into and out of a turbid and light-scattering medium. Small errors found in estimating the atmospheric contribution can cause significant bias in the estimation of water constituents. For this reason, information about the sensor spectral profile and the atmospheric properties at the acquisition time is required to estimate atmospheric scattering and/or absorption effects. According to Ambarwulan (2010), there are three main steps to be carried out to estimate of TSM concentration from the satellite-based data (MERIS). The first step is extraction of TSM concentration from in situ data set, second step is the retrieval of the TSM concentration from satellite data, and the last step is data analysis and accuracy assessment.

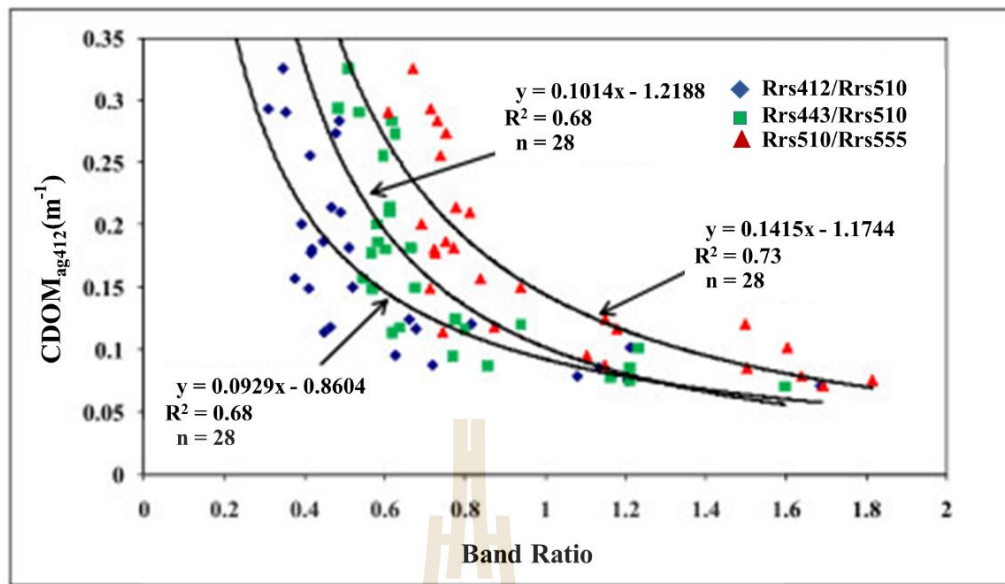
2.3.3 Color dissolved organic matter (CDOM) models

CDOM is regarded as a major determinant of the optical properties of natural waters and as it directly affects both the availability and spectral quality of light in water column. Quantitative and qualitative assessments of CDOM optics are crucial through the remote sensing use (Kowalczyk, Stedmon, and Markager, 2006). In surface water, CDOM is usually involved in chemical, photochemical and microbial processes. Principally, CDOM can protect organisms from UV damage and provides primary barrier photon absorption that drives abiotic photochemistry in the oceans. In natural water, CDOM absorbs UV and visible light according to energy of the electronic states of molecule as well as to its intermediate vibrational or the rotational levels (Ferrari, Dowell, Grossi, and Targa, 1996).

Coastal water where land discharge is important, yellow substance can be predominant factor in shifting water color. In oceanic water, though absorption by yellow substance is weak and often hardly measurable in the visible domain, its influence cannot be considered negligible. At the 440 nm, this is a useful wavelength in the remote sensing studies because it corresponds to the maximal absorption by algal pigments (Keith, Yoder, and Freeman, 2002). The CDOM can effect on accuracy of RS algorithms to predict chlorophyll-a data and phytoplankton biomass estimates in coastal areas. Sources of CDOM include rivers and groundwater which primarily carry it from soils, but coastal waters can also contain plankton and vascular aquatic plant derived CDOM produced in river and estuaries (Corbett, 2007).

CDOM can have different spectral properties depending on its origin. Spectral slope of CDOM is often utilized to characterize its composition and is an exponential function of the absorption coefficient versus wavelength. Differences in

spectral slope can indicate the origin of CDOM. In general, lower spectral slopes indicate an origin of freshwater and coastal environments, and longer slopes indicate an origin within the marine environment. In addition, the absorbance spectrum of CDOM overlaps that of chlorophyll and can account for over 50% of the total absorption at 443 nm, the wavelength at which chlorophyll concentrations are most often measured and CDOM absorption can be several times that of chlorophyll. From these reasons, CDOM has been linked to chlorophyll or other biomass amount, particulate material, nutrients, rainfall and land use. CDOM is an important element of multi-sensor detection and analysis systems due to various reasons. CDOM thresholds can be applied to generate a warning/indicator flag, and it is an optical indicator of salinity fronts. In situ CDOM data can be combined with bio-optical measurements not only to improve estimates of optical properties and the light field, but also used in the algorithms classifying waters with harmful algal blooms. In addition, CDOM data can help constrain harmful algal blooms (HABs) and can improve the accuracy of in situ fluorometric chlorophyll-a estimates in high CDOM water (Corbett, 2007). Figure 2.5 shows the CDOM algorithm evaluation for coastal regime (Reyes-Pesaresi, 2010).



Source: Reyes-Pesaresi, 2010.

Figure 2.5 CDOM power law empirical algorithm equations between three evaluated reflectance band ratios versus CDOM_{ag412}.

2.4 Relevant researches on eutrophication

2.4.1 Remote sensing for water constituents

In Ambarwulan (2010), optical properties in water were calculated by the process of hydro-optical model. The output results would indicate the different signal characteristics from the water constituents. Sub-surface irradiance reflectance was seen highest at short wavelength (400 nm) in clear water (offshore) and decreased with increasing wavelength. In contrast, near-shore turbid water had peak wavelength at about 580 nm and the second highest peak at 685 nm. In addition, water constituent reflectance was measured and put into the IOP model for coefficient calculation of TSM and Chl-a to create the distribution maps.

In O'Reilly et al. (1998), standard chlorophyll-a product provided from the SeaWiFS sensor was derived from the ocean chlorophyll-4 algorithm (OC4) using band ratios of the remotely sensed reflectance (R_{rs}) of four bands (443, 490, 510, and 555 nm) as follows (coefficients were derived based ground observations):

$$C_a = 10^{(0.366 - 3.067 R + 1.930 R^2 + 0.649 R^3 - 1.532 R^4)} \quad (2.6a)$$

where

$$R = \log_{10} \left\{ \max \left[\frac{R_{rs(433)}}{R_{rs(555)}}, \frac{R_{rs(490)}}{R_{rs(555)}}, \frac{R_{rs(510)}}{R_{rs(555)}} \right] \right\} \quad (2.6b)$$

Aiken et al. (1995) concluded that the $L_w(488)/L_w(551)$ ratio is most effective for empirical determination of the Chl-a using the following formula (c_0 , c_1 , c_2 , and c_3 are empirically-derived constants):

$$\log[chla]_{emp} = c_0 + c_1 \log(r_{35}) + c_2 [\log(r_{35})]^2 + c_3 [\log(r_{35})]^2 \quad (2.7a)$$

where

$$r_{35} = \frac{R_{rs(488)}}{R_{rs(551)}} \quad (2.7b)$$

In work of Marghany and Hashim (2010), MODIS data were applied to map chlorophyll-a spatial variations along eastern coast of Malaysia. The study aimed to find proper algorithm that can be used to accurately estimate Chl-a concentrations from four applied algorithms: (1) Aiken's, (2) Clark-3-bands, (3) Gordon, and (4) the Normalized Difference Chlorophyll Index (NDCI). These algorithms are based on nonlinear relationship between electromagnetic spectra of blue and green portions with in situ measurements of chlorophyll-a concentrations. The selected band wavelengths

(input data) were at 443, 448, 531 and 551 nm. It was found that Aiken's algorithm is most appropriate for mapping chlorophyll distribution as it shows lowest error (RMSE) of $\pm 0.10 \text{ mg/m}^3$ in the study.

In Pan, Tang and Weng (2010), the obtained Chl-a concentrations from the in situ measurement in the Northern South China Sea (NSCS) were used to compare with those derived from the standard algorithms used by NASA (OC2v4, OC4v4, and OC3M) for global Chl-a extraction from MODIS and SeaWiFS radiance data. Comparison between satellite and in situ Chl-a data for time and spatial differences were done at ± 48 hours and 3×3 pixels, respectively. Gained results reveal a systematic overestimation of Chl-a data by the used algorithms. Therefore, the OC2 and OC4 algorithms (for SeaWiFS) and OC3M algorithm (for MODIS) were adapted to NSCS by fitting the satellite data set to in situ Chl-a data in NSCS. With new coefficients from field data, the regional version of three algorithms showed rather good performance with RMSE values of 0.245, 0.245, and 0.288 respectively.

Gitelson, Gurlin, Moses, and Barrow (2009) had applied two-band model of the MODIS and three-band model of the MERIS data to estimate Chl-a data in the turbid productive water. These equations are as follows:

$$\text{MODIS}_{2\text{band}} = R_{(748)}/R_{(667)}, \quad (2.8a)$$

$$\text{MERIS}_{3\text{band}} = (R_{(665)}^{-1} - R_{(708.5)}^{-1}) R_{(753.75)} \quad (2.8b)$$

This work revealed that the MERIS three-band model for the Chl-a data retrieval was better than the MODIS two-band model with RMSE of $< 5.1 \text{ mg/m}^3$ and $< 7.5 \text{ mg/m}^3$ for Chl-a ranging from 2 to 50 mg/m^3 , respectively. However, the MODIS two-band model can be applied for estimating moderate-to-high Chl-a concentrations exceeding

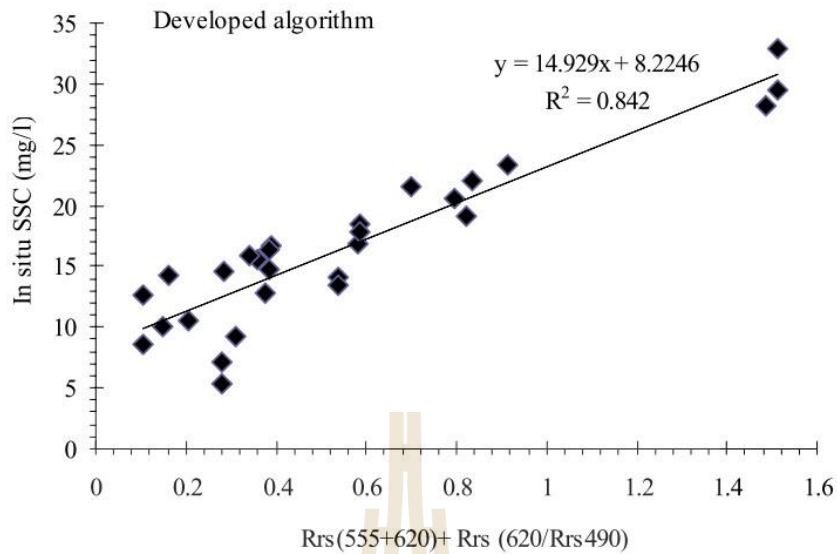
20 mg/m³, typically in phytoplankton bloom condition. Benefit from higher spectral resolution of the MERIS data, both two-band and three-band models can be reliably used for estimating wide ranging of Chl-a concentrations including Chl-a < 20 mg/m³, especially for coastal and estuarine waters.

Giardino, Bresciani, Pilkaityt, Bartoli, and Razinkovas (2010) reported result of the estimation and validation MERIS data for CDOM and Chl-a mapping by using different atmospheric correction techniques in Curonian Lagoon. It was found that the neural network-based Case II Regional processor was suitable for mapping of CDOM. For Chl-a, the band-ratio algorithm applied to the image data corrected with the 6S code was found more appropriate. This work demonstrated the usefulness of MERIS in investigating eutrophic aquatic ecosystems. Aqua-MODIS products in near-infrared (NIR) and the shortwave infrared (SWIR) bands were used in Son and Wang (2012) to identify their mutual correlations with the in-situ normalized water-leaving radiances, $nL_w(\lambda)$, Chl-a and TSS at the Chesapeake Bay. Results showed that, there was a good relationship in the TSS and water diffuse attenuation coefficient (k_d 490) but they had some variation in the Chl-a and $nL_w(\lambda)$.

Amin and Abdullah (2010) applied MODIS L1B land/atmosphere channels (band 1 to 7) to derive algorithm for the detections of turbid and shallow coastal water areas. In order to improve chlorophyll retrieving algorithm over ocean, an algorithm to mask out the turbid coastal water area needs to be developed. In performance, they used a simple algorithm of log₁₀ ratio of two MODIS channels at 0.47 and 0.55 μ m (bands 3 and 4, respectively) to identify and mark shallow coastal water and high amount of the suspended sediment area in the Gulf of Martaban. Lately, Sravanthi, Ramana, Yunus, Ashraf, Ali, and Narayana (2013) had developed regional

algorithm from the conventional methods (Tassan's algorithm) based on the found empirical relationship of the suspended sediment concentrations (SSCs) to radiometer RS reflectance values (R_{rs}) and satellite data in the coastal waters of Kerala. Their results revealed different wavelengths from band combinations as 490, 555, 620 nm indicated good correlation ($R^2 = 0.84$; linear regression) as shown in Figure 2.6. This regional algorithm was then implemented for the retrieval of SSCs from Oceansat-2 OCM sensor data and these results were validated. Results yielded from this work could help in understanding the amounts and dispersal patterns of the suspended sediments in the coastal waters of India, which in turn would be very helpful in the coastal zone management and maintenance of navigational channels.

Recently, Ha, Koike, and Nhuan (2014) had developed technique for estimating Chl-a concentrations in tropical coastal waters by using remotely sensed data of Terra-MODIS imagery in specific sites of found abundant phytoplankton and using geostatistics to improve the spatial resolution from 1 km to 100 m. Two traditional models, the blue-green band ratio and the red-near infrared band ratio were evaluated and comparison with the ratio of green and blue band reflectance (rGBr) concerning the bio-optical property of Chl-a, based-on 40 sites with corresponding in situ data. In this case, the rGBr model was found to have highest correlation to reference Chl-a density which makes it useful for the eutrophic monitoring condition of tropical coastal site. In addition, to improve the spatial resolution of MODIS image data, geostatistics has been adopted. Finally, the authors were suggested DOS model for suitability of atmospheric correction in tropical waters.



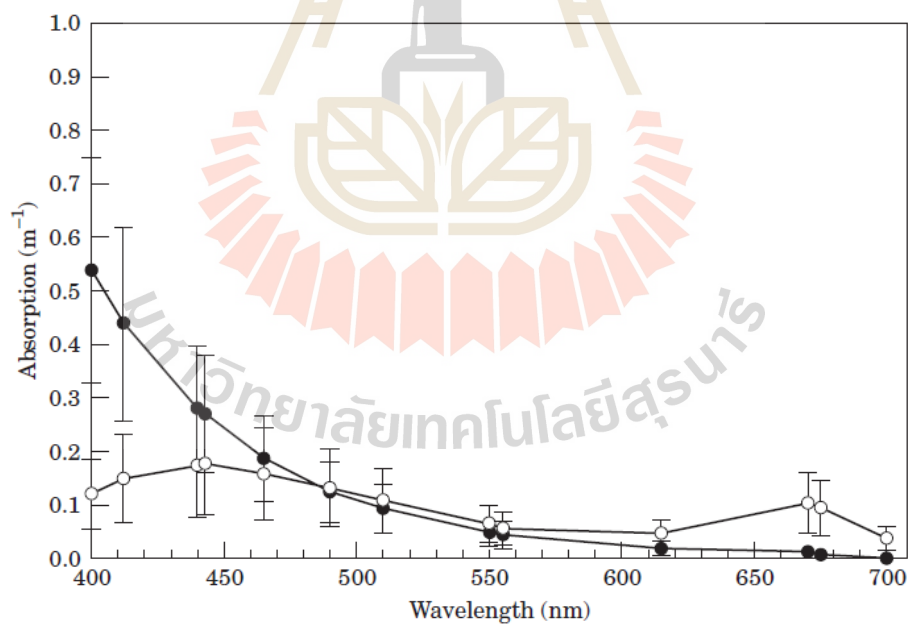
Source: Sravanthi et al., 2013.

Figure 2.6 Linear regression fit between the in situ suspended sediment concentration (SSC) and remote sensing reflectance (Rrs) used for development of regional algorithm.

Keith, Yoder, and Freeman (2002) reported characteristics of temporal and spatial variability of CDOM absorption over an annual cycle in the Narragansett Bay and Block Island Sound (Rhode Island) based on the collected water samples for the measurements of CDOM absorption coefficients and Chl-a concentrations. The yields of spectral absorption curve were plotted in range of 400 to 700 nm. The total downwelling irradiance (E_d) was collected from the upper 0.5 m of the water column at 412, 443, 490, 510, 555, and 665 nm by using PRR 600 Series profiling reflectance radiometer instruments. The difficulty in developing ocean color algorithms to predict Chl-a concentrations data was underscored by the influence that CDOM often has as a major absorber of light over the same wavelengths favored by phytoplankton. The data showed that average CDOM absorption coefficient at 412 nm was 0.45 m^{-1} and the average spectral slope was 0.02 nm^{-1} (Figure 2.7).

2.4.2 Applications of artificial neural networks (ANN)

Characteristics of most ecological data are often bulky, non-linear and highly complicated, usually showing noise, redundancy, internal relations and outliers. Traditionally, multivariate analyses of ecological data are utilized using conventional methods based on the linear principles, such as the multiple regression or discriminant analysis. Nowadays, an artificial neural networks (ANNs) was also applied in decision process to the analysis. Formerly, ANNs were regarded as “black boxes” because they always give an answer (output) when being fed with the data (input), although the internal processes taking place within the network were not clearly understood. The most popular ANNs in ecological applications are multilayer perceptron (MLP) with

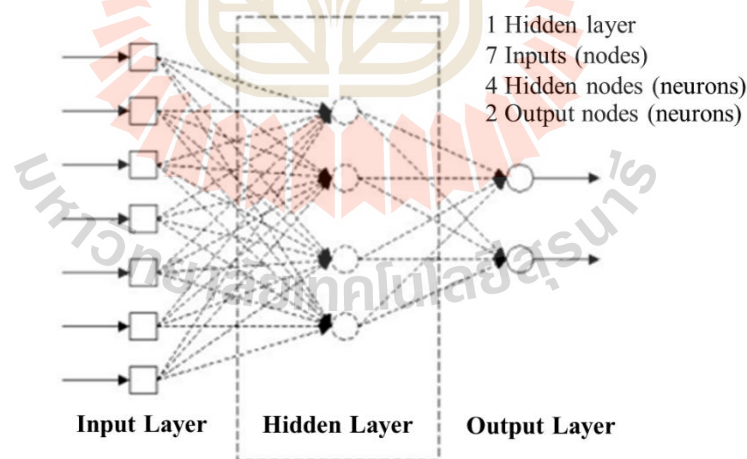


Source: Keith, Yoder, and Freeman, 2002.

Figure 2.7 Average CDOM (●) and chlorophyll-a (○) specific absorption at different wavelength for Narragansett Bay.

back-propagation algorithm and the Kohonen network or the self-organizing map (SOM). In supervised learning, the known target values are fed to the ANNs during training stage, after which the network is tested using exclusively the input values. For unsupervised learning, target values are not given to the network, which usually performs some kind of dimensionality reduction or clustering (Baruah, 2002).

Basically, all ANN models, which are sometimes called computational neural networks (CNNs) (Smith, Goodchild, and Longley, 2007), have similar structure of topology representing by system of the interconnected nodes in three layers designed to solve a certain problem. There is an input layer consisting of nodes that receive the inputs from external environment (Figure 2.8). The process continues until the output layer is completed and fires their output to the external environment (Baruah, 2002; Quetglas, Ordines, and Guijarro, 2011).



Source: Baruah, 2002.

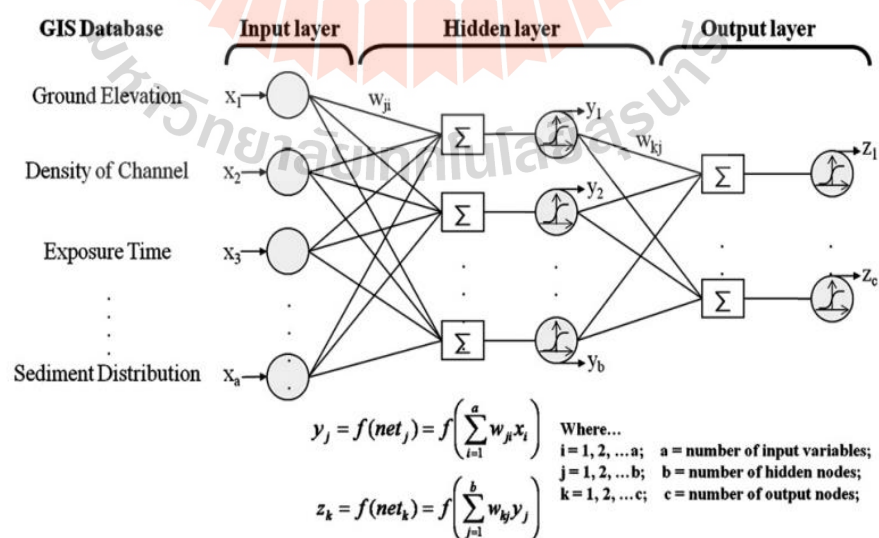
Figure 2.8 Three layer neural network with one hidden layer.

The main advantages of neural networks are their capability to evaluate extremely complex functions which is useful for the modeling of various geo-physical transfer function of the non-linear functions model with large numbers of variables. Typically, the system is able to combine detailed physical description of remote sensing process in terms of a forward model and faster to implement for mass processing of satellite data and is particularly useful in the real-time processing. Moreover, it is a powerful implementation for the retrieval of water constituents within coastal regime. In contrast, the procedure needed extensive experience on both design and training. Neural network is relatively expensive to prepare, especially when sophisticated model is used for computing the training and test data set (Baruah, 2002).

The ability of neural networks to identify pattern and reduce dimensions in the data could be utilized in the areas that were once used for multivariate statistical analysis, neural networks are recently considered as a new alternative to overcome statistical analysis problems. Neural network methods are nonparametric in the sense that a functional form need not be specified a priori. Initially, arbitrary values can be assigned to the weights of the network. Each case from a sample can be “loaded” onto the input layer of the network, and the input nodes simply send these values to the output nodes. Each output node calculates weighted sum of the inputs using weights assigned to the connections. The output or activation value of a neuron is determined by a transfer function. The weight values are adjusted by the specified learning rule (Jang and Yang, 2001). The multilayer perceptron (MLP) is supervised ANNs whose architecture is defined by highly interconnected neurons (units or nodes) that process information in parallel along three successive layers. This system uses training dataset to adjust connection weights in order to minimize the error between the observed and

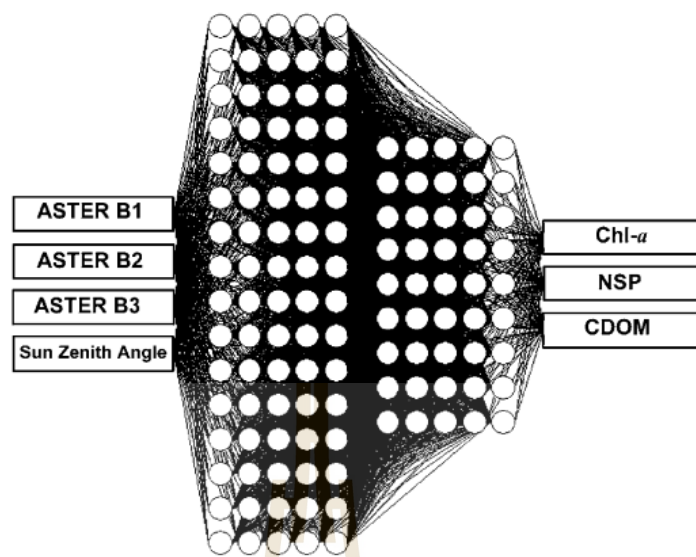
predicted values. For the SOMs (or the Kohonen network), they are the unsupervised ANNs that approximate probability density function (PDF) of the input data to display datasets in a more comprehensible representation form (Baruah, 2002). The MLP was found to function well in modeling non-linear phenomena, e. g. in works of Lee et al., (2013) (Figure 2.9) and Kishino, Tanaka, and Ishizaka (2005) (Figure 2.10).

MODIS data were used in work of Wang, Zhou, Xu, Song, and Wang (2009) to derive suspended sediment concentration (SSC) in surface water of estuary based on ANN and regression model. The used ANN was a multilayer/feed-forward type with a back-propagation (BP) model for correcting error. The results demonstrated significant correlations between in situ measurements and band 1-2 reflectance values of MODIS images. Typically, ANN outputs had provided the higher performance of correlation ($R^2 = 0.98$; $n = 25$) and RMSE ($<10\%$). Finally, this study showed that the MODIS 250 m daily products and the used ANN model are useful for the monitoring of surface SSC dynamic within high-energy coastal water environments.



Source: Lee et al., 2013.

Figure 2.9 Architecture of neural network.



Source: Kishino, Tanaka, and Ishizaka, 2005.

Figure 2.10 ANN construction after training, which consists of two hidden layers; units are 80 and 45 in each layers, respectively.

It was found in work of Huo, He, Su, Xi, and Zhu (2013) that artificial neural network (ANN) model could be satisfactorily used to determine water quality indicators through eutrophication state in lake. In this work, they had created four water quality model related to key factors that influence a number of water quality indicators where input layer for eutrophication indicators were dissolved oxygen (DO), total nitrogen (TN), chlorophyll-a (Chl-a) and sechi disk depth (SD). The results indicated that the used ANN model performed well in the prediction of these indicators with reasonable accuracy. The models can preserve nonlinear characteristics between input and output variables, which are superior to the traditional statistical models. Finally, this study suggested that the neural network is a valuable tool for lake management.

Recently, Lee, Park, Koo, Ryu, Choi, and Woo (2013) have reported the application of ANN and remote sensing data for mapping areas of macro-benthos habitat potential in tidal flats, Korea. There, eight variable data set extracted from remotely-sensed data were employed in the analysis and the result revealed strong correlations between the formulated potential maps and species locations. It was discovered that exposure time, DEM, and NIR band were the most important factors for each species.

2.4.3 Spatial assessment of eutrophication

Spatial assessment of eutrophication incidence was reported in several works based on the obtained in situ data and/or remotely-sensed data (mostly from the satellite-based operation). For examples, Kitsiou and Karydis (1998) have developed categorical mapping for the quantitative assessment of eutrophication in the Gulf of Saronicos, Greece, based principally on a thematic map generated from the synthesis of four variables causing eutrophication. The categorical map for each variable was made by kriging interpolation method and four trophic levels were identified (eutrophic, upper-mesotrophic, lower-mesotrophic and oligotrophic) based on the nutrient and phytoplankton concentration scaling. Multi-criteria methods were applied to create a final categorical map showing four trophic levels within the area. Critical values for discriminating between these four eutrophic levels were drawn from the eutrophication scale. The highest priority was given to the phytoplankton amount as the most crucial parameter for characterizing eutrophication, the second highest weight was assigned to nitrate data as it represents a significant limiting factor in the phytoplankton's growth, and the third to phosphate concentration and the last to ammonia concentration.

Smith, Tilman, and Nekola (1999) reported about the impacts of nutrients in eutrophication phenomenon which are concerned by interaction between fresh water, marine and the terrestrial ecosystems. Those effected to the ecosystem structure and function were changed. These more successful of researches were applied to prediction and monitoring in lake and reservoirs while could be applied to the estuarine and coastal marine environments. This report was indicated several task of researcher are successful implemented by OECD (1982) to the coastal or marine eutrophication. Investigated and model (OECD) implementation were developed by Vollenweider (1992) which applied to the Northern Adriatic Sea (1992), Baltic Sea (1992), and Norwegian marine water (1992 and 1997).

In 2002, Koponen et al. reported application of airborne and simulated satellite remote sensing data for classification of three water quality variables: secchi depth, turbidity, and chlorophyll-a. Class limits for the water quality variables were obtained from two operational classification standards. When RS data (MERIS) was used, a combination of them proved to be the most suitable. The feasibility of the system for operational use was tested by training and testing the retrieval algorithms with separated data sets. In this case, the classification accuracy is 90% for 3 secchi depth classes, 79% for 5 turbidity classes, and 78% for 5 chlorophyll classes. Details of classified category scale are as shown in Table 2.7.

Stednick and Hall (2003) had analyzed nutrients discharge from various sources through the stream to quantify the trophic status, algae growth and primary production. To identify the trophic state of water, the OECD Fixed Boundary System (Table 2.8) is found useful whose criteria are based on data of mean chl-a, total

phosphorous and secchi disk depth, along with the peak chlorophyll-a and the minimum secchi disk depth to classify a lake/reservoir from ultra-oligotrophic to hyper-eutroph.

Table 2.7 Comparison between variables and class limits of the general classification system developed for lakes in Finland and OECD lake water classification presented in Koponen et al. (2002). (Note: N/A = not applicable).

Variable	Class				
	Ultraoligo-trophic (excellent)	Oligo-trophic (good)	Meso-trophic (satisfactory)	Eutro-phic (poor)	Hyper-trophic (bad)
Secchi depth (m), Finnish	>2.5	1-2.5	<1	-	-
Secchi depth (m), OECD	>12	>6	6-3	3-1.5	<1.5
Turbidity(FNU), Finnish	<1.5	>1.5	-	-	-
Turbidity(FNU), OECD	N/A	N/A	N/A	N/A	N/A
Total phosphorus ($\mu\text{g/l}$), Finnish	<12	<30	<50	50-100	>100
Total phosphorus ($\mu\text{g/l}$), OECD	<4	<10	10-35	35-100	>100
Mean Chl-a ($\mu\text{g/l}$), Finnish	<4	<10	<20	20-50	>50
Max. Chl ($\mu\text{g/l}$), OECD	<2.5	<8	8-25	25-75	>75

Table 2.8 OECD Fixed Boundary System.

	Annual mean TP	Annual mean Chlorophyll-a	Annual peak Chlorophyll-a	Annual mean secchi disk depth	Annual minimum secchi disk depth
	$\mu\text{g/l}$			meter	
Ultra-oligotrophic	≤ 4.0	≤ 1.0	≤ 2.5	≥ 12.0	≥ 6.0
Oligotrophic	≤ 10.0	≤ 2.5	≤ 8.0	≥ 6.0	≥ 3.0
Mesotrophic	10 – 35	2.5 – 8.0	8.0 – 25.0	6.0 – 3.0	3.0 – 1.5
Eutrophic	35 – 100	8.0 – 25.0	25.0 – 75.0	3.0 – 1.5	1.5 – 0.7
Hyper-eutrophic	≥ 100.0	≥ 25.0	≥ 75.0	≤ 1.5	≤ 0.7

Source: OECD, 1982.

2.5 Red tide and Chlorophyll-a studies in the Gulf of Thailand

2.5.1 Red tide phenomena

Eutrophication is also frequently evidenced in the Gulf of Thailand (GoT) indicated by the occurrence of the harmful algal blooms (HABs), or red tide, phenomenon, during which the algae become so numerous and discolor coastal waters (hence the name “red tide”). Major factors influencing red tide events are including warm sea surface temperatures, low salinity, high nutrient content, calm sea, and rain followed by sunny days during summer months. In addition, the algae related to red tide can spread or be carried away at rather long distances by winds, currents, storms, or ships (Bruckner, 2013). The first scientific record on red tide phenomenon in Thai waters was by Charernphol (1958). Since then red tide incidences and their impacts on the fisheries industry have been observed more frequently and continuously. Red tides often occur in the Gulf of Thailand especially during the rainy season (May-October) around four major river mouths (Bang Pakong, Chao Phraya, Tha Chin, Mae Klong) due to rather high amount of key nutrients in river discharge (Lirdwitayaprasit, nd.).

The major factors for transportation of red tides are tidal current, wind driven current and dispersion (Harn, 1991). Thus, distribution of the surface Chl-a in shallow water area depends on water column condition and blooming of phytoplankton is required rather stable state of water. Phytoplankton population intensifies near sea surface and then blooms when vertical diffusivity is low, related to the weak wind, or upwelling. But high vertical diffusivity from strong wind and down-welling shall cause plankton cells to disperse throughout water column, thereby, inhibiting plankton cells to accumulate near sea surface (Buranapratheprat, Yanagi, and Matsumura, 2008).

The predominant phytoplankton of the red tide phenomena seen in the Upper Gulf of Thailand (2003 to 2004) were reported in Chumnantana (2006). It was found that the water discolorations had occurred throughout the year and the crucial red tide phytoplankton were diatoms and dinoflagellate in which the major observed species is dinoflagellate (*Noctiluca scintillans*). This work measured ten parameters namely; temperature, pH, salinity, dissolved oxygen, chlorophyll-a, total suspended solids, nitrite, nitrate, ammonia, and orthophosphate. Water quality parameter of temperature, pH and DO were positively related to red tide phytoplankton density and negatively related to total suspended solids. However, highly frequent occurrence of phenomena indicated that the estuary could be identified as highly eutrophic area.

Table 2.9 Report of the red tide phenomena seen in the Gulf of Thailand (1957-2001).

Place	Year																							
	'57	'58	'59	'60	'61	'62	'63	'64	'65	'66	'67	'68	'69	'70	'71	'72	'73	'74	'75	'76	'77	'78	'79	
Chumporn - Surat Thani	■																							
Hua Hin - Prachuab Kiri Khan											■	■												
Phetchaburi																								
Mae Klong River Mouth - Samut Songkram																								
The Chin River Mouth - Samut Sakorn																						■	■	■
Chao Phraya River Mouth - Samut Prakarn																						■	■	■
Bang Pakon River Mouth - Chachoengsao																								
Coastline of Chon Buri and Rayong																								

Place	Year																							
	'80	'81	'82	'83	'84	'85	'86	'87	'88	'89	'90	'91	'92	'93	'94	'95	'96	'97	'98	'99	'00	'01	'02	
Chumporn - Surat Thani		■	■																					
Hua Hin - Prachuab Kiri Khan		■	■									■	■	■										
Phetchaburi						■	■	■				■	■	■										
Mae Klong River Mouth - Samut Songkram												■	■	■										
The Chin River Mouth - Samut Sakorn	■	■	■									■	■	■								■	■	■
Chao Phraya River Mouth - Samut Prakarn	■	■	■																			■	■	■
Bang Pakon River Mouth - Chachoengsao		■	■																					
Coastline of Chon Buri and Rayong		■	■			■	■	■	■	■	■	■	■	■	■	■	■	■	■	■	■	■	■	■

Source: Wongsupap, 2008.

In work of Wongsupap (2008), the hydrodynamic model, water quality and nutrient transport model and eutrophication model were used to process eutrophic condition in the UGoT by using observed data in 1999 to 2005. Results indicated that the high freshwater discharges with high nutrient loadings from the four main river mouths as mentioned earlier have contributed to the nutrient enrichment of UGoT. Especially, the Chao Phraya and the Tha Chin Rivers were most dominant loading of nutrient by the fresh water being discharged into UGoT while the flow circulation has played great role for seasonal and spatial variation of eutrophication occurrence. In this work, water quality condition was evaluated using amount of water quality parameters (DO, ammonia, nitrate, and phosphate) and eutrophication parameter (chlorophyll-a) compared with their threshold value. The numerical model was also used to explain relations between hydrodynamic, water quality, and eutrophication conditions through policies implement based on water quality management in UGoT's coastal area.

2.5.2 Chlorophyll-a studies

In the past decade, several studies were made on the estimation of Chl-a concentration from their associated sunlight reflectance data in the GoT region. For examples, optical environment of the underwater was examined in Matsumura, Siripong, and Lirdwitayaprasit (2006) for identifying the relationship of the seasonal underwater optical energy and the primary productivity (PP). Consequently, the local algorithms were derived and applied to estimate concentration data of Chl-a, CDOM and suspended substances (SS). In this method, field data of water properties were used to validate gained satellite-based data (ADEOS-2/GLI). Finally, the best fit correlation for the estimated Chl-a, CDOM and SS data called "Chula-algorithms", were proposed as follows:

$$\text{CDOM } k(412) = -0.1981 \ln(R) + 0.067, \quad (2.9a)$$

$$R = R_{rs}(412,0-) / R_{rs}(565, 0-) \quad (2.9b)$$

$$\text{Chl-a } (\mu\text{g/l}) = 181.4 \exp(-4.74R), \quad (2.10a)$$

$$R = R_{rs}(520) / R_{rs}(565) \quad (2.10b)$$

$$\text{Total SS (mg/l)} = 1.16 \ln[R_{rs}(670,0-)] + 10.23 \quad (2.11)$$

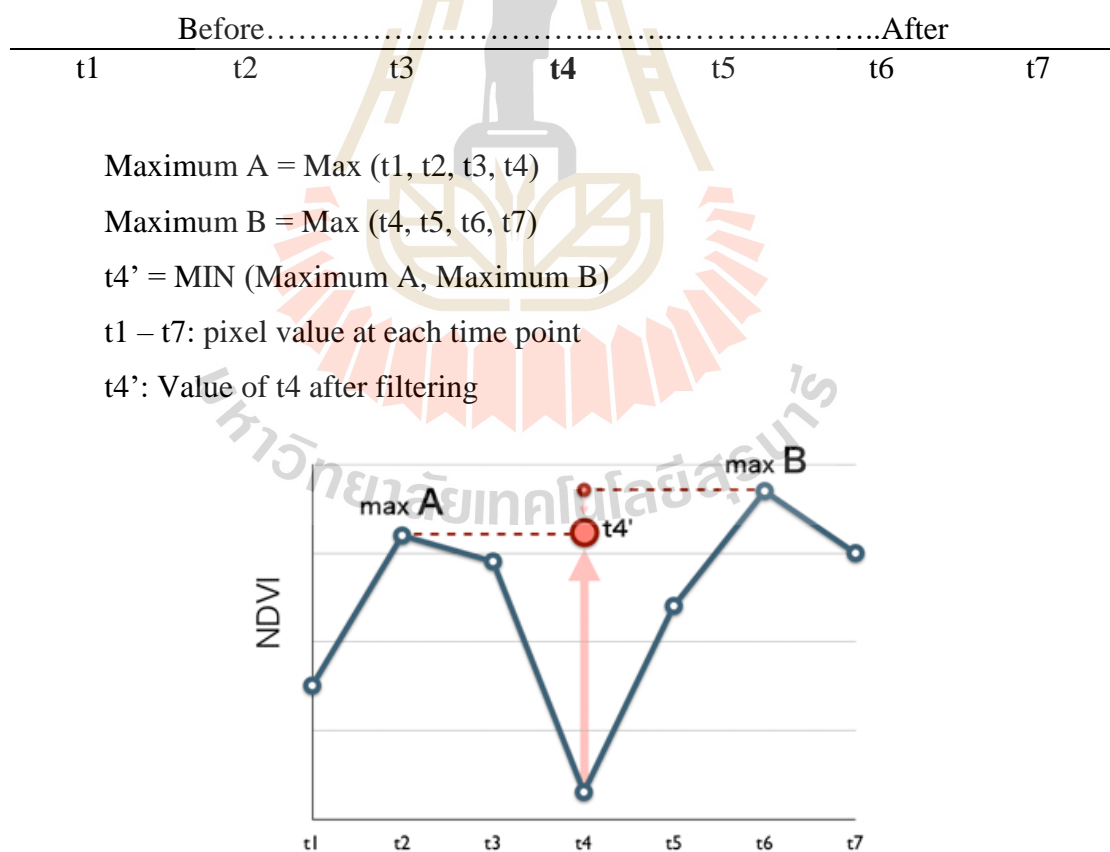
Similarly, Buranapratheprat (2007), the empirical algorithms was built based on found relationship between field Chl-a data and corresponding reflectance ratios measurement. The method was straightforward by using developed regression-based analysis to convert reflectance to Chl-a concentration. In most published works, blue-green ratios are often used to formulate empirical algorithms for Chl-a estimation because the blue zone is notably sensitive to chlorophyll absorption while the green one is quite stable to chlorophyll variations. Among these, ratios of 443/560, 490/560 and 520/560 nm are widely used for algorithm development.

In addition, Kobayashi et al. (2010) reported influence of the optical properties of inorganic suspended solids (ISS) on coastal ocean color by using the satellite data. An in-water algorithm approach was evaluated using optical model for highly turbid coastal water in the upper Gulf of Thailand. The backscattering coefficient of ISS was calculated using Lorenz-Mie scattering theory. Two in-water algorithms were used. The first was SeaWiFS OC4v4 (OC4) algorithm and the second was the empirical algorithm (Chula-algorithms) for UGoT used by the Global Imager (GLI) (Matsumura et al., 2006). It was found that, for the ISS concentrations of 10 g/m^3 , an estimation of chlorophyll-a (Chl-a) concentration within a factor of 2 on a logarithmic scale is possible in Chl-a range of 4-30 mg/m^3 .

2.6 Concepts of the relevant used methods

2.6.1 Local maximum fitting analysis (LMF)

Satellite images require improvement of observed data being degraded in quality by cloud and haze. On this issue, the local maximum fitting (LMF) algorithm can be applied to eliminate the influence of cloud and haze and then increase quality of original satellite images. LMF method is always applied to seasonal vegetation changes and using min-max filtering to eliminate cloud contamination (Kungvalchokechai and Sawada, 2013) (Figure 2.11). This process can eliminate abnormal data and generate smooth data with low influence of cloud and noise (Wada and Ohira, 2004).



Sources: Wada and Ohira, 2004.

Figure 2.11 Local Maximum Fitting method.

As seen in Figure 2.11, the maximum value A of four points before continuous time-series data (pixel t4) and the maximum value B of four points after continuous time-series data at that point were identified and compared. The lesser value of both is then assigned to be new value of the considered point (pixel t4). The process shall be applied to all relevant pixels (Wada and Ohira, 2004; Thirakultomorn, 2010).

2.6.2 Frequency ratio analysis

Frequency ratio (FR) is a well-known probabilistic model often used in landslides evaluation approach to find correlation level between the applied causative factors and past landslide incidences over a specific area. Basic process is to identify ratio of the landslide percentage (for each class of the input factor) and percentage of the area occupied by that class called the frequency ratio (Yilmaz, 2009), or,

$$FR = \frac{(CLP/TLP)}{(CA/TA)} \quad (2.12)$$

where CLP is number of landslide pixels seen in a specific class (of a certain factor), TLP is total number of the observed landslide pixels, CA is the associated class/attribute area and TA is total study area. FR value of each attributing class of each factor (type or range) indicates correlation level of that class to past occurrences of landslide events within the area starting from 0 (no correlation) to 1 (average correlation) and more than 1 (very high correlation) (see Table 2.10 for examples). Finally, landslide susceptibility index (LSI) for a defined unit area (e.g. a pixel) can be calculated by the summarization of the frequency ratio values of all relevant factor attributes:

$$LSI = FR_1 + FR_2 + \dots + FR_n \quad (2.13)$$

where n is the number of all input factors in use. The landslide susceptibility score represents the relative chances to have landslide occurrence over an area of interest. The greater of LSI value means the higher probability to have landslide incidence and the lower the value means the lower chance to have it.

2.6.3 Simple additive weighting (SAW)

For spatial analysis, a number of criterion weighting procedures are most importance for the judgments of relevant decision makers. Four method performance approaches include the ranking, rating, pairwise comparison, and trade-off analysis. (Malczewski, 1999). The rating methods require decision maker to estimate weights on the basis of a predetermined scale; for example, a scale of 0 to 100 can be used. One of the simplest methods is the “point allocation approach” which requires decision maker to allocate 100 points across the criteria of interest. Specifically, it is based on allocating point ranging from 0 to 100, where 0 indicates that the criterion can be ignored and 100 represents situation where only one criterion is needed to be considered in a considered decision situation. The more point that a criterion receives, the greater is relative more importance. The rating method can be criticized for its still lack of theoretical or formal foundations (Malczewski, 1999).

Various multi-criteria decision making (MCDM) methods were invented to solve diverse applications of the decision problems. One of the MCDM methods is additive weighting-based method. However, the method is not explicitly disseminated and its applications are not-well received by many MCDM (Abdullah and Adawiyah, 2014). Simple additive weighting (SAW) method is the most often used techniques for tackling spatial multi-attribute decision making. It works based on basic concept of weighted average. A total score is then obtained for each alternative by multiplying the

importance weighted assigning for each attribute by the scaled value provided to the alternative on attributes, and summing the products of overall attributes.

Then the overall scores is chosen. Formally, the decision rule evaluates each alternative, A_i , by following formula:

$$A_i = \sum w_i x_{ij}, \quad (2.14)$$

where x_{ij} is the score of i^{th} alternative with respect to j^{th} attribute, and the weight w^{ij} is a normalized weight, so that $\sum w_i = 1$. The weights represent the relative importance of the alternatives (Malczewski, 1999). The SAW procedure is shown in Figure 2.12.

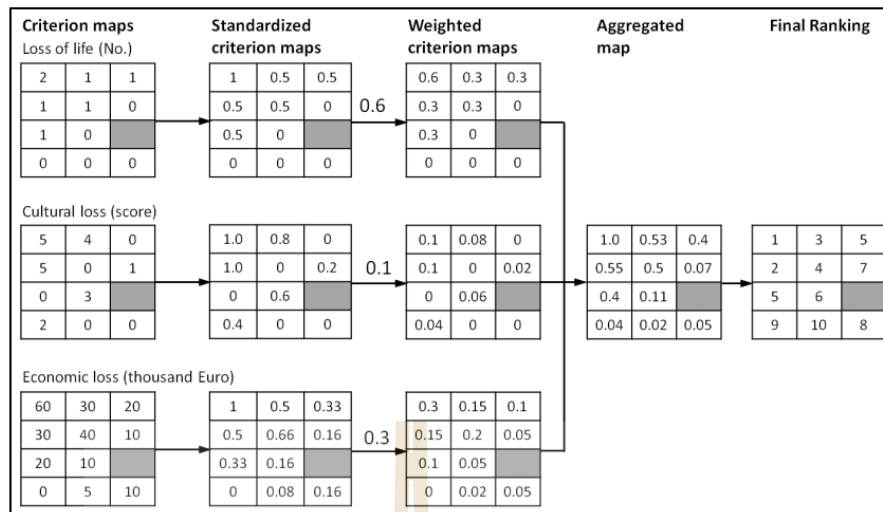
2.6.4 Area under the curve method

Area under the curve (AUC) method is mostly used for validation of the susceptibility map in the spatial analysis approaches. Therefore, the AUC can be used to assess prediction accuracy qualitatively like in work of Poudyal, Chang, Oh, and Lee (2010); Intarawichian and Dasananda (2010). The AUC represents ideal variation from zero to a maximum of 1.0, the higher values mean higher accuracy of the map under consideration. In this method, the derived LSI data of all cells within the study area are sorted in descending order (from high to low) before divided to 100 respective classes, with accumulated 1% intervals. The ranking orders (from 1 to 100) are then given to each defined LSI class beginning at the very high susceptibility ones towards the very low ones, respectively. To assess the predictive capability of the map, the total LSI ranking orders (1-100) are plotted against accumulative amount of landslide incidences for each specific class (in term of percentage of the total number). This shall appear as a line and the AUC can be assessed afterwards (Figure 2.13).

Table 2.10 Examples of the frequency ratio (FR) values for the used causative factors.

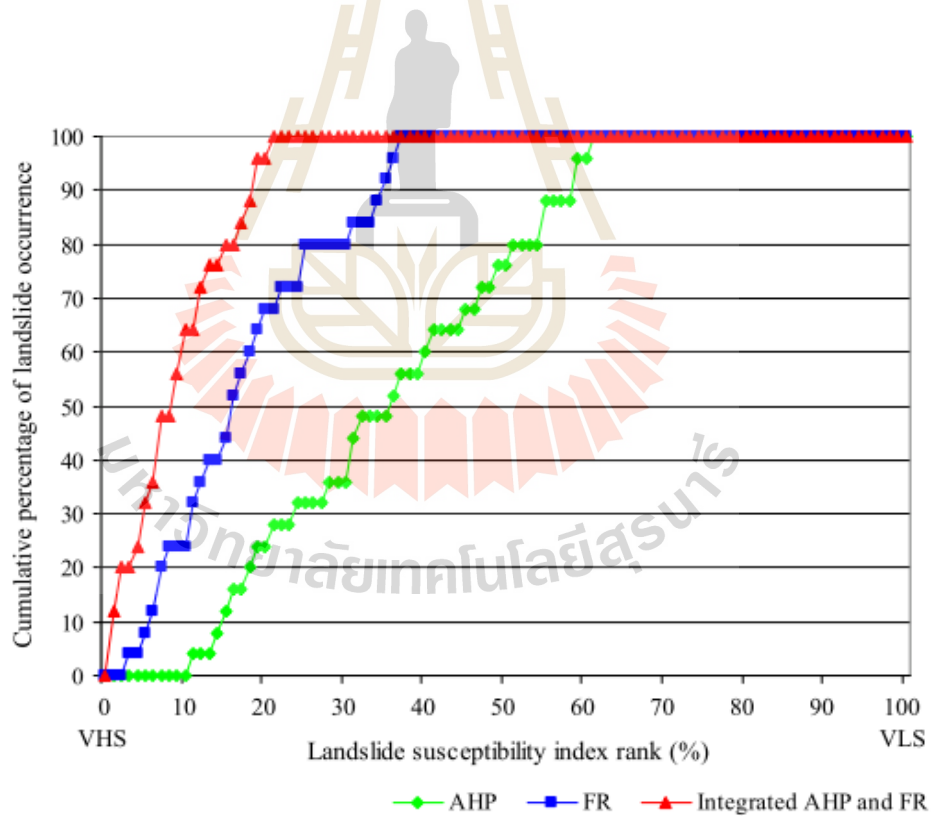
Layer	Class	Number of total cell	Percentage of pixels	Number of landslide	Percentage of landslide	Frequency ratio	
Slope angle (o)	0-15	169,976	10.09	5	4.50	0.45	
	16-20	210,201	12.48	7	6.31	0.51	
	21-23	182,713	10.85	6	5.41	0.50	
	24-26	196,628	11.67	8	7.21	0.62	
	27-29	192,573	11.43	10	9.01	0.79	
	30-32	170,472	10.12	21	18.92	1.87	
	33-35	143,411	8.51	7	6.31	0.74	
	36-39	148,012	8.79	14	12.61	1.44	
	40-45	143,186	8.50	16	14.41	1.70	
	46-82	127,099	7.54	17	15.32	2.03	
	No data	345	0.02	0	0.00	0.00	
	Slope aspect	Flat	27,822	1.65	4	3.60	2.18
		N	226,897	13.47	7	6.31	0.47
		NE	134,583	7.99	8	7.21	0.90
E		107,987	6.41	19	17.12	2.67	
SE		195,300	11.59	27	24.32	2.10	
S		283,526	16.83	25	22.52	1.34	
SW		252,148	14.97	13	11.71	0.78	
W		192,970	11.45	8	7.21	0.63	
NW		263,238	15.62	0	0.00	0.00	
No data		345	0.02	0	0.00	0.00	
Slope curvature		1 (-)	738,395	43.83	59	53.15	1.21
	2 (0)	175,435	10.41	6	5.41	0.52	
	3 (+)	770,642	45.74	46	41.44	0.91	
	No data	344	0.02	0	0.00	0.00	
Distance from Drainage (m)	0-14	182,928	10.86	4	5.56	0.51	
	20-36	185,378	11.00	25	34.72	3.16	
	40-58	169,234	10.04	14	19.44	1.94	
	60-80	168,125	9.98	3	4.17	0.42	
	82-110	172,871	10.26	7	9.72	0.95	
	111-142	162,653	9.65	10	13.89	1.44	
	143-183	164,644	9.77	3	4.17	0.43	
	184-244	160,561	9.53	1	1.39	0.15	
	245-350	160,074	9.50	2	2.78	0.29	
	351-870	158,003	9.38	3	4.17	0.44	
	No data	345	0.02	0	0.00	0.00	
	Land use	Cutting	1,301	0.08	5	4.50	58.33
		Cultivation	990,828	58.81	36	32.43	0.55
		Forest	625,547	37.13	57	51.35	1.38
Grassland		40,932	2.43	11	9.91	4.08	
Bush		15,277	0.91	2	1.80	1.99	
Sand		7,217	0.43	0	0.00	0.00	
Riverstream		3,324	0.20	0	0.00	0.00	
Lake		45	0.00	0	0.00	0.00	
Nodata		345	0.02	0	0.00	0.00	

Poudyal et al., 2010.



Source: Burzel, Dassanayake, and Oumeraci, 2012.

Figure 2.12 Basic procedure of Simple Additive Weighting Method (SAW) analysis.



Source: Intarawichian and Dasananda, 2010.

Figure 2.13 Computed accuracies of the susceptibility in terms of the AUC.

CHAPTER III

EQUIPMENT, DATA AND METHODOLOGY

This chapter describes details of the applied equipment, required input data and relevant research methodology including optimal retrieval models identification for Chl-a, TSS and CDOM in the UGoT area from MODIS data and the formulation of red tide susceptibility maps using SAW and FR methods.

3.1 Equipment

Equipment including hardware and software are summarized as below:

- 1) Desktop Computer, Notebook,
- 2) SeaDas Version 7.3 (image pre-processing of AQUA/TERRA MODIS),
- 3) ERDAS Imagine (image processing and analysis),
- 4) ESRI ArcMap (spatial analysis, SAW and FR analysis),
- 5) IDRISI (ANN analysis and correlation analysis),
- 6) TNTmips (local maximum fitting analysis)

3.2 Data requirement

Details of the needed principal input data, including remotely sensed data and GIS dataset, are presented in Table 3.1.

Table 3.1 Details of the principal data needed for the research.

Data category	Data description	Format	Source	Objective
PRR reflectance data	From field surveys (at 6 spectral bands as listed in Table 3.3)	Point	Matsumura et al. (2006)	1
MODIS reflectance data	From space-based observation (at 10 spectral bands as listed in Table 3.3)	Raster	MODIS website	1, 2, 3
In situ marine constituents data	From field surveys and lab analysis of Chl-a, TSS and CDOM concentration (Appendix A)	Point	Matsumura et al. (2006)	1
Red tide occurrence data	From official records and the MODIS observations (Appendix E)	Point/raster	DMCR/IMS/MODIS	3
Ancillary data	Bathymetry and surface current	Vector	Aquatic science, BUU	3

DMCR: Department of Marine and Coastal Resources,
 IMS: Institutes of Marine Science, Burapha University (BUU).

3.3 Research methodology

The work in this thesis is divided into three principal parts in accordance with three objectives stated earlier. Details of work procedure for each part are as follows (see Figures 3.1-3.4 for detailed work flowchart).

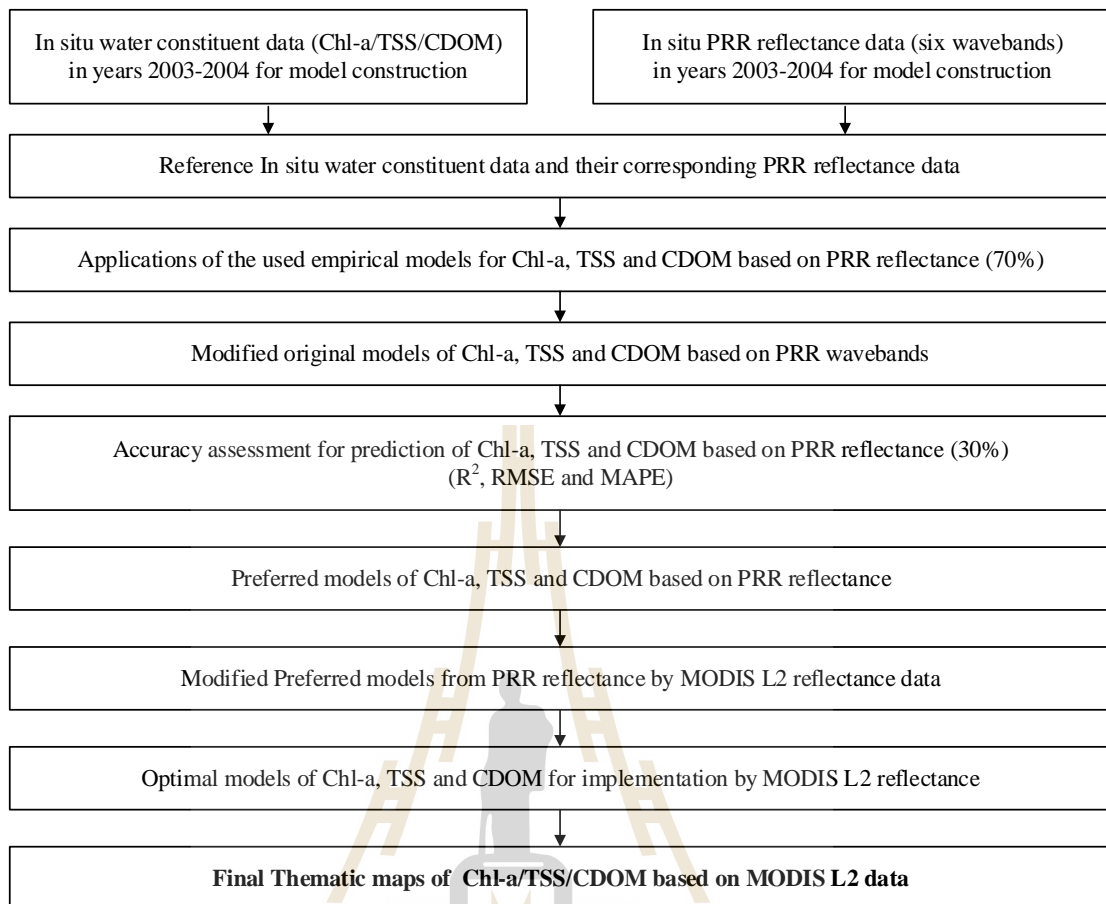


Figure 3.1 Work flowchart of the empirical method based on objective 1.

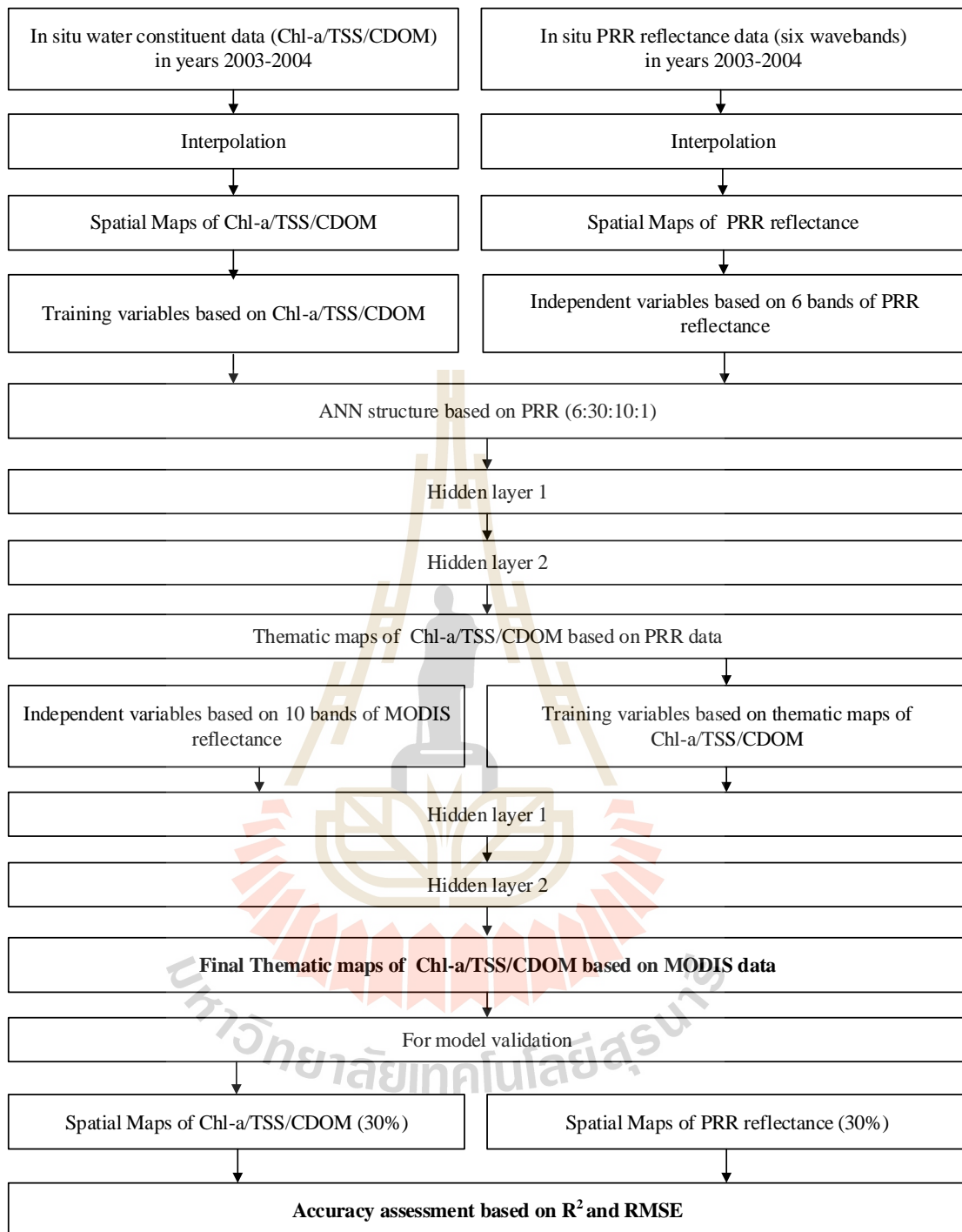


Figure 3.2 Work flowchart of the ANN method based on objective 1.

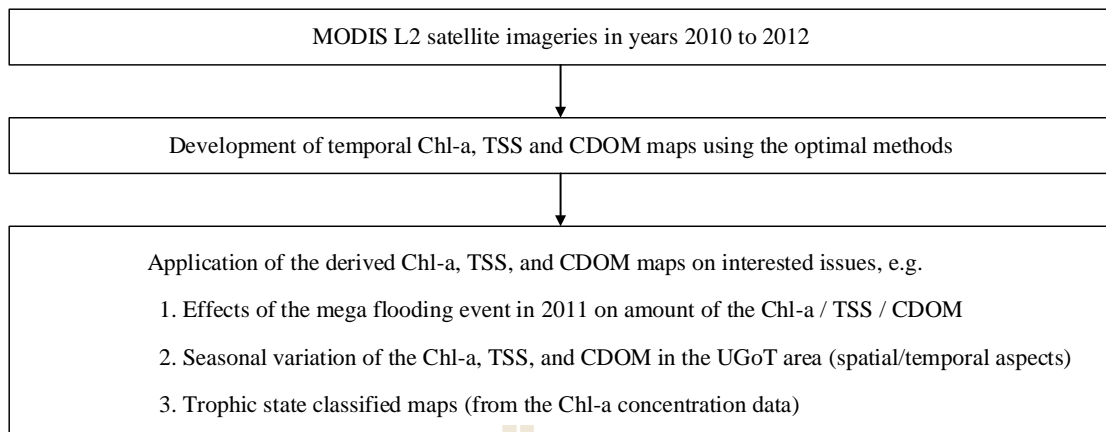


Figure 3.3 Work flowchart of the research based on objective 2.

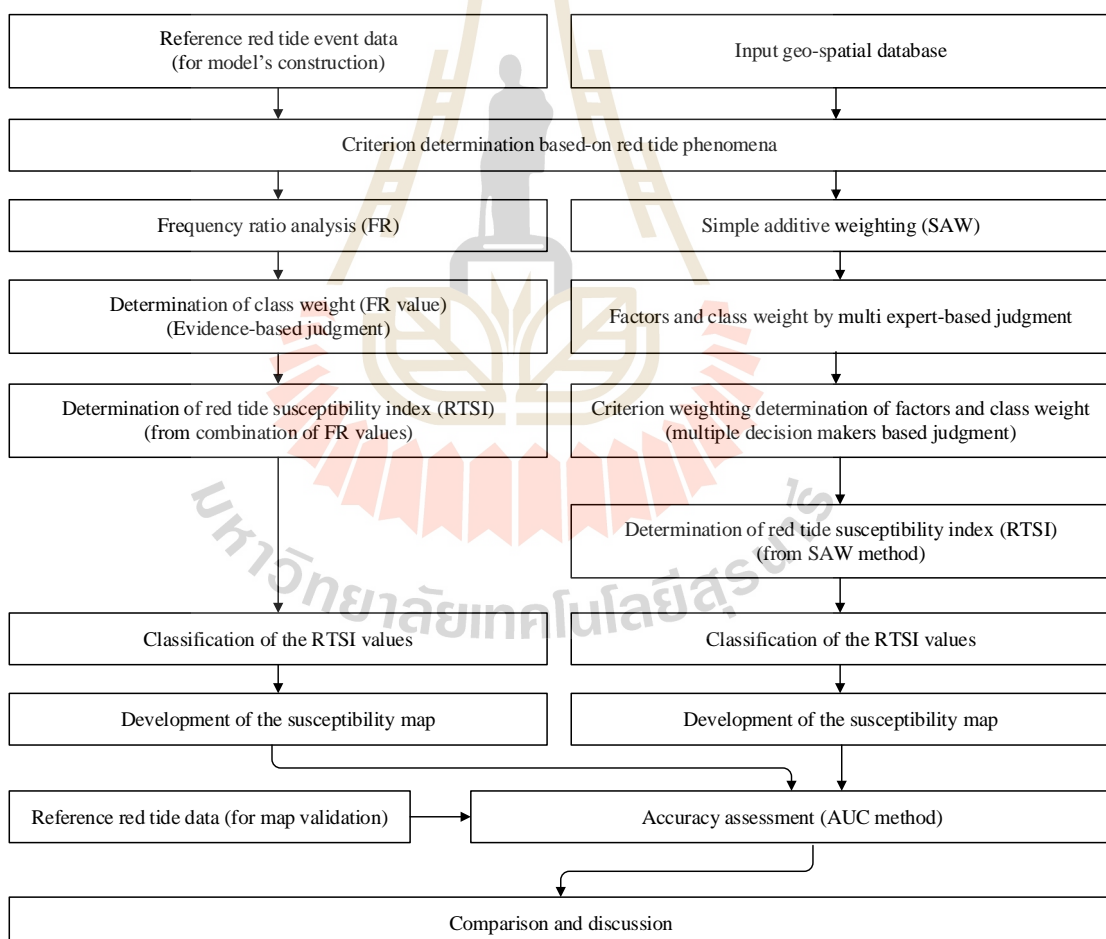


Figure 3.4 Work flowchart of the research based on objective 3.

3.3.1 Data collection and preparation

Main objective of work in this part is to accumulate all essential data from the responsible agencies and from field surveys of the UGOT area (to examine optical properties of sea surface and collect samples of sea water for further laboratory analysis) (as listed in Table 3.1). Main tasks to be achieved in this part are as follows.

(1) Obtaining optical properties (sunlight reflectance) of the sea surface within the UGoT area using the profiling reflectance radiometer (PRR) instrument (Biospherical Instruments Inc., 2002) during the organized cruise surveys in 2003 and 2004 whose sampling locations are as shown in Figure 3.5 and Table 3.2. The PRR is an optical instrument that measures both downwelling irradiance and upwelling nadir radiance. Among several types of the PRR instrument, the PRR-2600 sensor is designed for measuring of radiance data underwater while the PRR-2610 is used for the measuring of radiance data at surface. These sensors can measure solar radiance data (downwelling and upwelling) at broad spectral range of 340-900 nm with 6 standard channels available centered at 412, 443, 490, 520, 565, 670 nm and PAR (Photosynthetically Available Radiation) at 400-700 nm range (see Table 3.3 for more details). The PRR instruments also have specific sensors for measuring temperature, pressure, or depth of water also (Horning et al., 2010).

(2) Collecting in situ data of each examined marine constituent (Chl-a, TSS, CDOM) through the analysis of water samples (from cruise surveys in years 2003 to 2004) in laboratory based on standard guidelines illustrated in Strickland and Parsons (1972). Here, the total suspended solids in mg/l is measured as dry weight of residue and filter while chlorophyll-a and colored dissolved organic matter (CDOM) concentration data were measured spectrophotometrically.

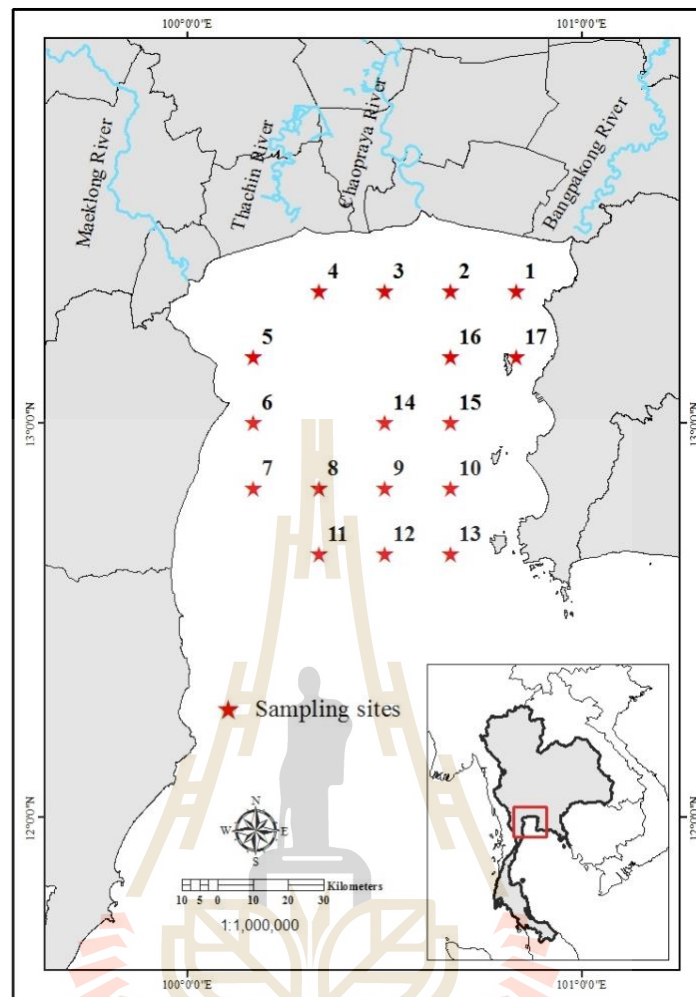


Figure 3.5 Sampling locations during the cruise surveys in 2003 to 2004.

Table 3.2 Geographic coordinate system of sampling sites in UGoT.

Station	Latitude (N)	Longitude (E)	Bottom Depth (m)
1	13 20.03	100 49.97	13.0
2	13 20.00	100 39.99	15.7
3	13 20.02	100 29.99	10.6
4	13 20.00	100 19.99	9.0
5	13 10.00	100 09.99	16.8
6	15 59.96	100 10.01	17.8
7	12 49.76	100 10.10	18.8
8	12 50.01	100 20.00	24.9
9	12 49.98	100 30.03	22.1
10	12 50.03	100 40.00	28.2
11	12 39.99	100 20.01	27.7
12	12 40.04	100 30.02	24.6
13	12 40.01	100 40.01	37.2
14	13 00.00	100 29.99	19.7
15	13 00.02	100 40.02	16.0
16	13 10.02	100 40.00	20.5
17	13 09.99	100 50.51	27.0

Table 3.3 Spectral measurements of the PRR-2600 and 2610 instruments compared with those of the MODIS instruments at optical region.

PRR-2600, 2610		MODIS		
Band center (nm)	Bandwidth (nm)	Band no./ Band center (nm)	Wavebands products of Level 2 (nm)	Bandwidth (nm)
412*	10	8 / 412	412	15
443*	10	9 / 443	443	10
			469**	10
		10 / 488	488	10
490*	10			
520*	10	11 / 531	531	10
			547	10
		12 / 551		10
			555**	10
565*	10			
			645**	10
		13 / 667	667	10
670*	10			
		14 / 678	678	10
		15 / 748		10
		16 / 869		10

* Spectral measurements of the PRR used in this study.

** Generated from MODIS 250 m or 500 m data aggregated to 1 km.

Source: Horning et al., 2010.

(3) Accumulating MODIS reflectance data (from sensors onboard the Terra and Aqua satellites) in 10 spectral bands as described in Table 3.3. Three main groups of the MODIS data are implemented in this work. The first one is for the measurements during years 2003 and 2004 in accordance with the period of cruise surveys stated earlier (for further comparison to evaluate optimal retrieval model for each constituent). The second group is for the measurements during years 2010 to 2012 (or the observation and assessment of marine environmental situation and variation) while the last group is for the measurements from years 2005 to 20015 (for the establishment and evaluate red tide susceptibility map). According to information given in Table 3.3, three spectral ranges of the MODIS observing bands are available for

further use in this study: blue bands (at 412, 443, 469, and 488 nm), green bands (at 531, 547, and 555 nm) and red bands (at 645, 667, and 678 nm).

(4) Gathering the red tide occurrence data in the UGoT area from the available sources, e. g. the Aquatic Science Departments and the Institute of Marine Science of Burapha University, the Marine Science Department of Chulalongkorn University, Department of Fishery, the Department of Marine and Coastal Resources, the Pollution Control Department. These are shown in Appendix F. In addition, the identified information of red tide incidences extracted from the MODIS data is also included in the analysis. Initial information of interest is time, location and spatial extent of the occurrences. Examples of the past red tide locations are displayed in Figure 3.6 (mostly concentrated close to some major river mouths).

(5) Preparing relevant input data or their proxy parameters (in proper format) which are required for formation of red tide susceptibility map (as listed in Table 3.6). Some proxy parameters are applied as potential indicators for the actual nutrient data: distance from river mouth, distance from coastal urban/industrial area, and distance from coast line/local drainage. Supporting marine conditions are bathymetry and circulation pattern of sea surface current. Prior assumption is that red tide incidence should occur more effectively in calm sea close to shore (shallow water) and close to the major river mouths (with high amount of nutrient discharge).

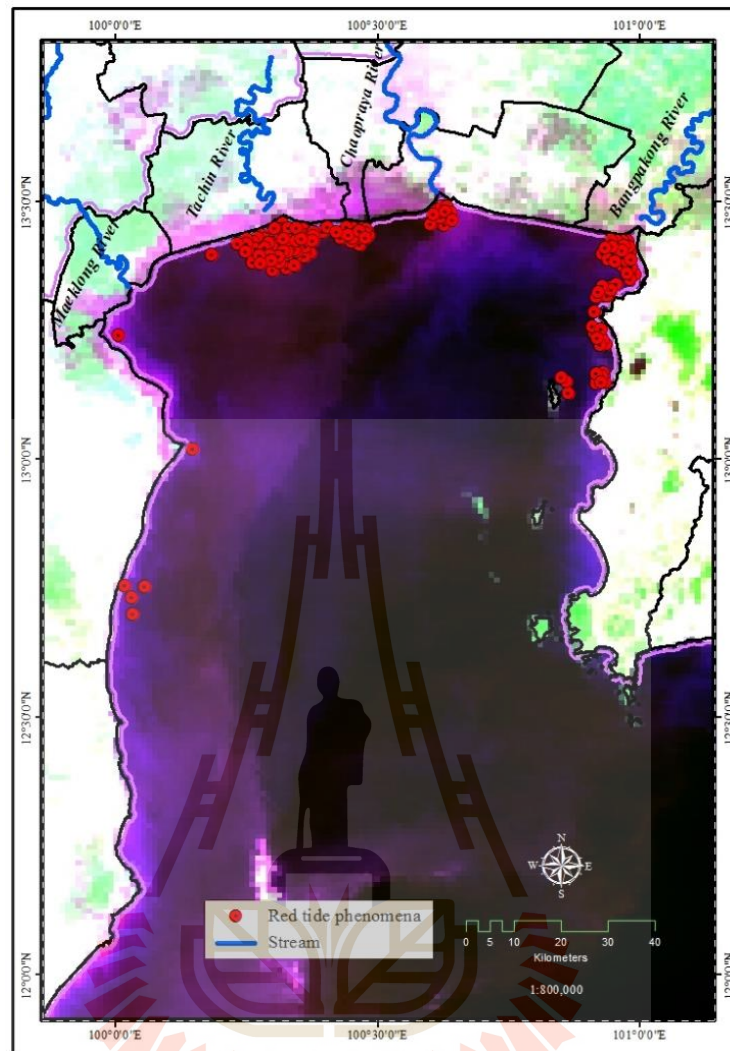


Figure 3.6 Examples of some past of red tide occurrence locations in the UGoT area.

3.3.2 Evaluation for optimal retrieval models

In this part, optimal retrieval models for each constituent concentration (Chl-a, TSS, CDOM) over UGoT area are evaluated based on comparative application of the proposed methods which are supported to the first objective. Details of work procedure are as follows.

(1) Five cruises surveyed from years 2003 to 2004 were investigated of three water constituents and PRR reflectance data. These were collected from seventeen station which accumulated as 84 records (one record was not available) (Matsumura et al., 2006). In situ measurements and collection of water samples for subsequent laboratory analyses are currently used to evaluate those constituent concentration.

(2) Dividing each set of constituent concentration data into two groups at random; one for the use in applied models (70%) and the other for the assessment of their prediction efficiency (30%).

(3) Implementing all the applied retrieval models as listed in Table 3.4 (for Chl-a), Table 3.5 (for TSS) and Table 3.6 (for CDOM) in the estimation of those respective constituent data based on knowledge of in situ data of the PRR reflectance at the preferred bands along with corresponding constituent data (70%). Consequently, the best results are then expressed in terms highest of coefficient of determination (R^2).

(4) Assessing efficiency of the incorporated models from step (3) in the prediction of reference constituent concentration data (30%). The yielded results are then expressed in terms of root mean square error (RMSE) and mean absolute of percent error (MAPE) from which an optimal method shall be identified for each considered marine constituent. Initially, first priority of the selection is given to level of the average efficiency seen from both factors (R^2 , RMSE and MAPE, respectively) and the second one is given on the complicated in structure or input data of the methods.

(5) Replacing the PRR reflectance data needed by the optimal methods gained in step (3) by suitable MODIS reflectance data based on the extracted mutual relationship between these two data sources. Necessary MODIS data could be acquired from the ocean color website.

(6) Building the ANN model to predict amount of each concerned constituent (Figure 3.1b). This shall start with input the spatial maps of Chl-a, TSS and CDOM which are dependent variables and then be modeled with the six bands of PRR reflectance.

(7) The gained of ANN process are determine which are systematically processed to find the best architecture that can simulate needed output data map. Consequently, The training variables of three constituents (based on PRR) are input to the next stage which based on MODIS analyze (independent variables) while the results are investigate of Chl-a, TSS and CDOM.

(8) Results from both of empirical and ANN models are compare and discuss with the principal statistical of R^2 and RMSE.

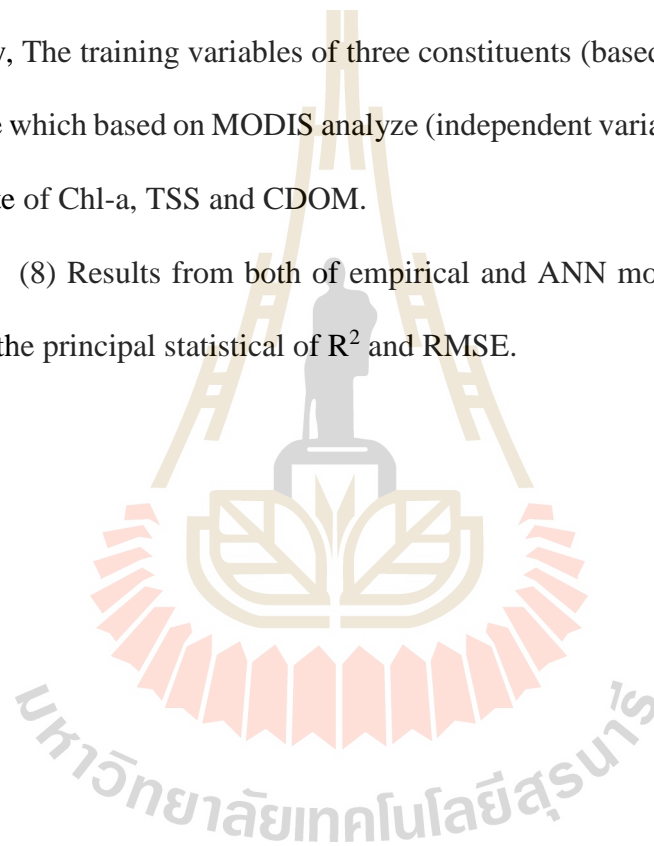


Table 3.4 The empirical models applied for the retrieval of Chl-a data in this research.

Models	Equation
1 OC3M	$C_{chla} = 10^{(a_0+a_1R+a_2R^2+a_3R^3+a_4R^4)}; R = \log_{10} \left[\max \left(\frac{R_{rs}(443)}{R_{rs}(550)}, \frac{R_{rs}(490)}{R_{rs}(550)} \right) \right]$
Reference: O'Reilly et al. (2000).	
2 DAAC-V4 Chlor_MODIS	$C_{chla} = 10^{0.07} \left[\frac{L_{wn}(443)}{L_{wn}(550)} \right]^{-1.40}$
Reference: Clark (1997) and Pinkerton et al. (2005) quoted in Jensen (2007).	
3 Aiken-1995	$\log[Chla] = c_0 + c_1 \log(r_{35}) + c_2 [\log(r_{35})]^2 + c_3 [\log(r_{35})]^3$ $r_{35} = \frac{R_{rs}(488)}{R_{rs}(551)}$
Reference: Aiken et al. (1995).	
4 Red-to-Green band ratio	$\ln(Chla) = 1.91 \ln(x) + 3.40$ $x = [R_{rs}(667) + R_{rs}(678)] / [R_{rs}(531) + R_{rs}(547)]$
Reference: Le et al. (2012).	
5 rGBr	$C_{chla} = C_1 \frac{R_{rs}(551)}{R_{rs}(443)} + C_2$
Reference: Ha, Koike, and Nhuan (2014).	
6 Applied SeaWiFs to MODIS	$C_{chla} = [R_{rs}(443)/R_{rs}(555)][R_{rs}(412)/R_{rs}(490)]^{-0.5}$
Reference: Tassan (1994).	
7 Chula model	$C_{chla} (\mu\text{g/l}) = 181.4 \exp(-4.74R); R = R_{rs}(520)/R_{rs}(565)$
Reference: Matsumura et al. (2006).	

Table 3.5 The empirical models applied for the retrieval of TSS data in this research.

Models	Equation
1 Apply SeaWiFs to MODIS	$SS = [Rrs(555) + Rrs(670)][Rrs(490)/Rrs(555)]^{-1.2}$
	Reference: Tassan (1994).
2 Global-Tassan's	$Log_{10}S = 1.83 + 1.26Log_{10}X_s$ $X_s = \{[Rrs(555) + Rrs(620)] \times [Rrs(555)/Rrs(490)]^{-1.2}\}$
	Reference: Tassan (1994).
3 Son-Wang-2012	$TSS = a + b (Kd_{490}), Kd_{490} = 0.2411(Rrs_{490}/Rrs_{565})^{-1.2753}$
	Reference: Son and Wang (2012).
4 GOCI standard-TSS	$TSS = 945.07 \times (Rrs(555))^{1.137}$
	Reference: Ruddick et al. (2012).
5 TSS _{s2011}	$log_{10}(TSS_{s2011}) = 0.738 + 22.79 * (Rrs_{555} + Rrs_{670}) - 0.574 * \frac{Rrs_{490}}{Rrs_{555}}$
	Reference: Siswanto et al. (2011).
6 SSCs	$SSCs = \{[Rrs(555) + Rrs(620)] + [Rrs(620)/Rrs(490)]^2\}$
	Reference: Sravanthi et al. (2013).
7 TSM	$TSM \left(\frac{mg}{l}\right) = 3.8813(nL_w(645))^3 - 13.822(nL_w(645))^2 + 19.61(nL_w(645))$
	Reference: Ondrusek et al. (2012).
8 Chula model	$\text{Total SS (mg/l)} = 1.16 \text{Ln}(Rrs(670,0-)) + 10.23$
	Reference: Matsumura et al. (2006).

Table 3.6 The empirical models applied for the retrieval of CDOM data in this research.

Models	Equation
1 Apply SeaWiFs to MODIS	$Y = [Rrs(412)/Rrs(490)][Rrs(443)]^{0.25}$
	Reference: Tassan (1994).
2 CDOM Band-ratio: I	$\log y = 1.1744 \ln(x) - 1.9558, \quad X = Rrs(510)/Rrs(555)$
	Reference: Reyes-Pesaresi (2010).
3 CDOM Band-ratio:II	$\log y = -3.3209 \ln(x) - 2.4245, \quad X = Rrs(443)/Rrs(510)$
	Reference: Reyes-Pesaresi (2010).
4 CDOM-440 Polynomial	$a_{g440} = 10^{(C_1 + C_2 \text{Log}_{10}(R) + C_3 \text{Log}_{10}^2(R))},$ $R = \left(\frac{Rrs_{490}}{Rrs_{555}} \right) (Rrs_{443})$
	Reference: Tang et al. (1994) quoted in Siswanto et al. (2011).
5 CDOM-400 Polynomial	$a_{g400} = 1.5 \times 10^{(C_0 + C_1 R_{15} + C_2 R_{15}^2 + C_3 R_{25} + C_4 R_{25}^2)},$ $R_{15} = \text{Log}_{10} \left(\frac{Rrs_{412}}{Rrs_{555}} \right) \text{ and } R_{25} = \text{Log}_{10} \left(\frac{Rrs_{443}}{Rrs_{555}} \right)$
	Reference: Carder et al. (2003).
6 Chula model	$\text{CDOM } k(412) = -0.1981 \text{Ln}(R) + 0.067,$ $R = Rrs(412,0-) / Rrs(565, 0-)$
	Reference: Matsumura et al. (2006).

3.4 Applications of the optimal method

After the suitable methods for each considered marine constituent were found, their applications to the observation and assessment of marine environmental situation and variation within the UGoT area from years 2010 to 2012 are carried out in this part. Details of work procedure are as follows:

(1) Producing concentration maps based on MODIS L2 satellite data to investigate the Chl-a, TSS, and CDOM from daily to weekly and monthly basis using optimal methods found in the previous part.

(2) Evaluating notable changes in values of the data maps obtained in the first step for all studied constituents in both spatial and temporal aspects.

(3) Applying information gained in step (2) to explore some listed issues, e.g.:

3.1 Effects of the mega flooding event in 2011 on amount of the Chl-a, TSS, and CDOM in the UGoT area. Initial processes are as follows:

3.1.1 Identify flooding period from the unusual increase in amount of the river discharge in 2011 compared to the data in normal years (2010 and 2012).

3.1.2 Prepare temporal maps of three concerned constituents during flooding period identified in the previous step then compare them with similar maps made for the normal years for each constituent (2010 and 2012).

3.1.3 Analyze the differences among the associated maps stated in the previous task for each constituent (i.e. maps for each year) and identify prominent changes between the mega-flood year (2011) and the two normal years that should be influenced by the huge amount for water discharge into the UGoT in that year.

3.2 Seasonal variation of the Chl-a, TSS, and CDOM in the UGoT area in both spatial and temporal aspects. Initial processes are as follows:

3.2.1 Prepare temporal maps of three listed constituents during normal period from years 2010 to 2012 (on monthly basis) from MODIS data using the optimal method identified in the 1st objective.

3.2.2 Analyze variation pattern of each constituent listed above on both spatial and temporal aspects, e.g. discharge volume, distance from river mouths.

3.3 UGoT trophic state and red tide analysis.

3.3.1 Build classified map of the obtained Chl-a concentration map gained in step 3.2.1 in terms of the trophic states based on the modification of criteria OECD (Table 3.6). This study used the annual mean of Chl-a for classification.

Table 3.7 Modified of OECD Fixed Boundary System (from Table 2.8) for UGoT performance.

Trophic state	Annual mean Chlorophyll-a ($\mu\text{g/l}$)
Ultra-oligotrophic	≤ 1.0
Oligotrophic	≤ 2.5
Mesotrophic	2.5 – 8.0
Eutrophic	8.0 – 25.0
Hyper-eutrophic	≥ 25.0

Source: OECD, 1982.

3.3.2 Identify red tide incidences from knowledge of trophic state illustrated in Table 3.7 from areas with eutrophic and hyper-eutrophic states (which are assign and represent to the red tide phenomenon) and make a record of the satellite-based red tide database.

3.5 Formulation of the red tide susceptibility maps

In this part, tendency of each specific location to have red tide incidence is evaluated from red tide susceptibility maps building by the two different approaches: the simple additive weighting (SAW) method and frequency ratio (FR) method, with five influencing factors are considered. These are TSS and CDOM concentration, water depth, distance from the river mouth, and current velocity, where 7 referred case studies (or scenarios) are examined. More details of work in this part are given in Chapter 6.

(1) Deriving the red tide susceptibility map by the SAW method (used multiple decision maker judgment) for each proposed scenarios. In this part, initial factor/class weights were derived from responses of nineteen interviewed experts on this field through prepared questionnaire (as detailed in Appendix F). Factor weighs were initially set to have score of 1 (least important) to 5 (most important) while their associated attribute weights (for each used factor) were given scores of 2, 4, 6, 8, and 10 (from low to high priority), respectively.

After that, appropriate factor weights were evaluated through multiple comparison method (Malczewski, 1999). In process, pairwise of preliminary weight are computed. Entire counting of criterion match paired which one more importance than other one and then be similar done for each pair of factors. Thus be summarize value as all factors in each column and divide by total of summarize (as all criteria). From the total preference score for each examined factor is evaluated and then used as a basis for the calculation of its proper normalized weight afterwards (from 0 to 1). Set of derived weights (for each factor) were then applied to calculate susceptibility score for each unit area (a pixel size of 1 km²) through linear combination of product between respective factor and their associated class weights of each identified unit area

(Adriyendi, 2015). The obtained scores are then classified into 5 categories (based on equal interval classification) of susceptibility level from very low (VL) to very high (VH) from which the classified map (for each scenario) can be formulated.

(2) Deriving the red tide susceptibility map using the FR method. In this case, specific weight (or FR value) for each attribute (of each associated factor) shall be evaluated based on general concept for FR index determination (as seen in Eq. 2.12 for landslide case). Then, the total weight, or susceptibility score, for each defined unit area can be established from the combination of associated FR values (from all factors under considerations) for each unit area (as detailed in Eq. 2.13). These scores are then classified (based on equal interval classification) and the susceptibility map output (for each scenario) can be formulated.

(3) Comparing/validating credibility of the produced susceptibility maps from both methods using the area under curve (AUC) accuracy assessment method.

Selection of the appropriate influencing parameters (as listed in Table 3.8) was carried out based on the literature review of red tide occurrence in Thailand and abroad. Low/high states mean low/high probability (or tendency) to have red tide incidence. However, actual mechanisms responsible for red tide formation are still inconclusive. In general, the bloom usually occurs during periods of freshwater discharge to the coast, which brings large amount of nutrients into the ocean (PCD and ARRI, 2003).

First criterion is total suspended solids (TSS) which are commonly associated with both the organic (living and non-living) and inorganic matters which make it become a main indicator of water quality assessment at present. In ocean, TSS material is regarded as a main source of nutrient load (that supports phytoplankton bloom) and is also a distinguish inhibitor of light penetration into deep water (from the arisen

turbidity). As phytoplankton growth, and subsequent colony expansion, is highly sensitive to environmental perturbations (e.g. nutrient inputs, light, and sea turbulence), amount of TSS materials mixed in coastal water shall become an important ingredient in the formation of red tide phenomenon (which is conceptually a harmful type of plankton bloom incidence). Next relevant factor is color dissolved organic matter (CDOM). More CDOM content means more dissolved organic nutrients in water body which might be sufficient to initiate appearance of phytoplankton bloom over the area (due to the substantial increase of plankton cells and rapid expansion of their colonies). As a result, CDOM has been regarded as key indicator for predicting occurrence of red tide events and was chosen to be used in this study.

Third criterion is sea water depth. Usually, deep water regions away from shore tend to have fewer dissolved nutrients and stronger movement of surface current which make red tide incidence less viable than those of shallow water near shore. Therefore, tendency of having red tide should be decreasing with depth (or in deeper water). The fourth parameter is distance from river mouth. An excessive amount of nutrients along with the usually low ocean current strength near shore make areas located near the river mouths more vulnerable to phytoplankton bloom incidence (and subsequent red-tide occurrence). Last factor, surface current is an important factor that fuels widespread distribution of nutrients (or sediment) from their original discharging sources situated near shore (especially main river mouths) into the deeper water zone away from shore. Typically, speed and moving direction of the surface ocean current shall determine how far in distance and in what direction that the embedded nutrients shall be carried away and accumulated. Low surface current indicates less distribution of concerned nutrients over the area which supports more likelihood of the red tide occurrence afterwards.

Table 3.8 Influencing parameters for red tide phenomena evaluation in UGoT.

Indicators	Units	Class of red tide occurrence					Reference
		Very Low	Low	Moderate	High	Very High	
1) Total suspended solids	mg/l	> 40	20-40	10-20	5-10	< 5	From Objective 2
2) CDOM	m ⁻¹	< 0.5	0.5-1.0	1.0-1.5	1.5-2.0	> 2.0	From Objective 2
3) Sea water depth	meter	> 20	15-20	10- 15	5-10	< 5	From Data-based
4) Distance from river mouths	km	> 30	20-30	10-20	5-10	< 5	From Data-based
5) Current (velocity)	m/sec	> 0.1	0.05-0.1	0.02-0.05	0.01-0.02	< 0.01	From Data-based

CHAPTER IV

MODIS-BASED EMPIRICAL MODEL DEVELOPMENT FOR MARINE CONSTITUENT CONCENTRATION ASSESSMENT OVER UGoT

This chapter reports conclusive results and related discussion of accomplished works to fulfill the first objective of the thesis stated in Chapter I. It was conducted to identify proper models for the determination of spatial concentration of three interested marine water constituents: chlorophyll-a (Chl-a), total suspended solid (TSS), color dissolved organic matter (CDOM), from the satellite-based MODIS reflectance data.

4.1 In situ data collection and preparation

This work was conducted to find the optimal models for the three main ocean color components (Chl-a, TSS, CDOM). Key optical data of these constituents in UGoT area were taken from Matsumara et al. (2006) based on field and lab data gained from five consecutive cruise surveys conducted over the area in 2003-2004 (Table 4.1) with seventeen measuring stations available (Figure 3.4).

Essential factor for describing the marine environment in UGoT is circulation (in Figure 4.1). Typical current pattern in each monsoon period including the northeast monsoon (NE) (from November to January), the transition period from the

northeast to the southwest monsoon (SW) (from February to April), the southwest monsoon (from May to August) and the transition period from SW to NE monsoon (from September to October). In NE monsoon, the circulation flows counter-clockwise while in NE-to-SW transition period, the circulation is rather weak but more complex. For SW monsoon, the circulation directs clockwise and SW-to-NE monsoon, it is similar to the previous transition period (Buranapratheprat et al., 2002).

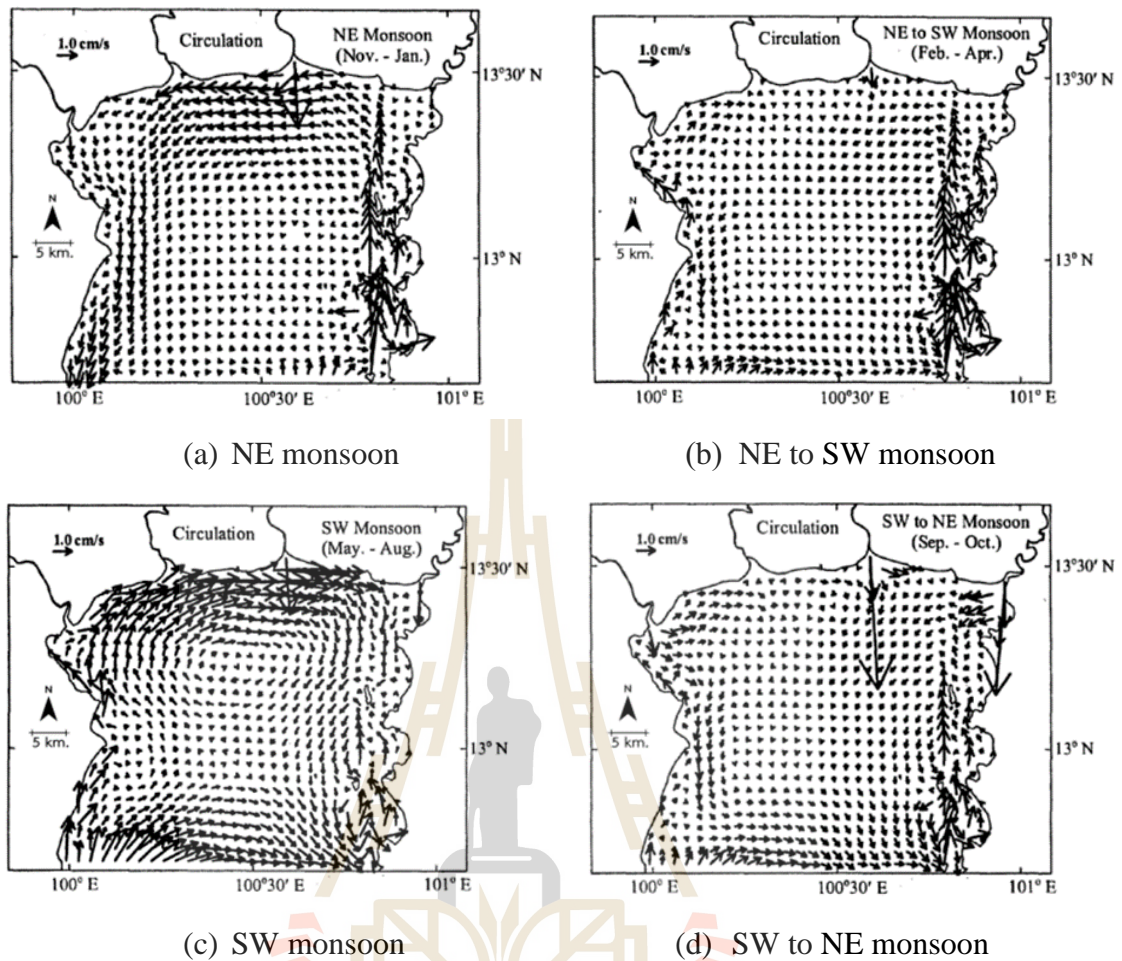
Table 4.1 Five cruises surveys in UGoT.

Cruise No.	Survey Periods	Monsoon	Seasonal
1	09-11 October 2003	Late southwest	Wet
2	04-06 December 2003	Early northeast	Dry
3	13-15 January 2004	Late northeast	Dry
4	12-15 May 2004	Early Southwest	Dry
5	07-10 October 2004	Late southwest	Wet

Source: Matsumara et al., 2006.

4.1.1 Data from field observation over UGoT area

Several water qualities and oceanographic parameters were measured or collected to accommodate this study such as secchi disc depth, nutrient concentrations, wind speed and water current characteristics. Values of three listed water constituents needed for model creation are shown in Appendix A while the ancillary data collected from oceanic water using conductivity-temperature-depth sensor (CTD) and acoustic equipment are summarized in Appendix B. In appendix C, data of nutrients and other oceanographic parameters, volume of the four main river discharges, PRR reflectance values and the MODIS satellite database (level-2) are presented.



Source: Buranapratheprat et al., 2002.

Figure 4.1 Seasonal circulation in the Upper Gulf of Thailand.

Field data of each examined constituent were extracted independently for each referred sampling station (Figure 3.4). The attained dataset from each cruise trip were then interpolated to produce corresponding maps of its spatial distribution using kriging method with cell size of 1 km² (Figures 4.2 to 4.4).

(1) Chlorophyll-a characteristic

In the first and second cruises, Chl-a was found prevalent at the NW portion of UGoT, typically at Mae Klong and Thachin River mouths (Figures 4.2a and 4.2b). These cruises were carried out during the transition period from SW to

NE monsoon when the surface water movement was typically in clockwise direction taking nutrients from land base in the north through the western part of the UGoT. As stated earlier, high nutrient accumulation can enhance phytoplankton growth resulting in high level of the Chl-a concentration. Cruise 3 was operated during 13-15 January 2004 (late NE monsoon with dry weather), Chl-a concentration in this cruise was moderate which highest values at the western side of UGoT close to Petchaburi Province (Figure 4.2c). During this time, anticlockwise surface current can introduce nutrient dispersion in large area with low river discharge which led to less phytoplankton bloom and consequently low of Chl-a. Cruise 4 was operated between 12-15 May 2004 (early SW monsoon season) from which Chl-a concentration data were found to be noticeably high at several locations such as near Pethaburi Province's coast, the Chao Phraya River mouth and the coastal zone of Chonburi Province (Figure 4.2d). These appearances were initiated by SW monsoon when clockwise surface current made Chl-a disperse and accumulate on the eastern side of UGoT. The last trip was done during 7-10 October 2004 (late SW monsoon or wet season) and found the highest Chl-a density at Thachin River mouth. However their concentration was rather low compared to the other cruises (Figure 4.2d).

(2) Total suspended solid Characteristic

In the first cruise, high TSS concentration was normally found at the Mae Klong and the Tha Chin River mouths as shown in Figure 4.3a while in the second cruise, TSS was found to be dispersed over large area close to Chao Phraya River mouth and the coast of Petchaburi Province (Figure 4.3b). TSS in cruise 3 accumulated at the Tha Chin and Chao Phraya River mouths and decreased continuously from the northern to the southern part of UGoT (Figure 4.3c). In cruise

4, notably high concentration was evidenced at the Bang Pakong River mouth. Since, the SW monsoon introduces clockwise movement of the surface current in the UGoT, TSS accumulated along west-to-east direction at the Bang Pakong River mouth as seen in Figure 4.3d. In Cruise 5, in the late SW monsoon season, TSS was found extended in large area of UGoT, especially along the western and the eastern coasts and also in the north of the gulf. Spatial distributions indicate more fluctuation along shore of the northern and western of UGoT.

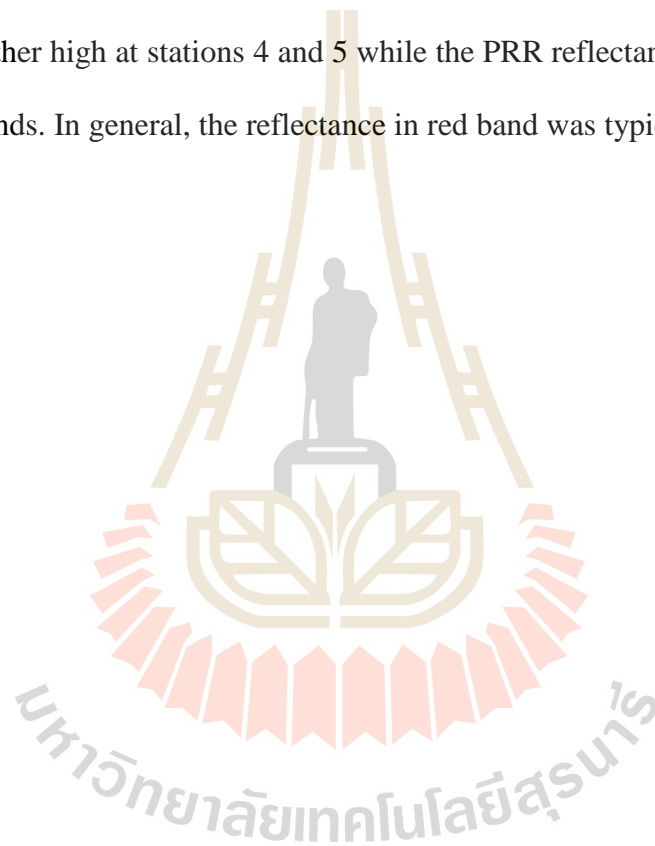
(3) Color dissolved organic matter characteristic

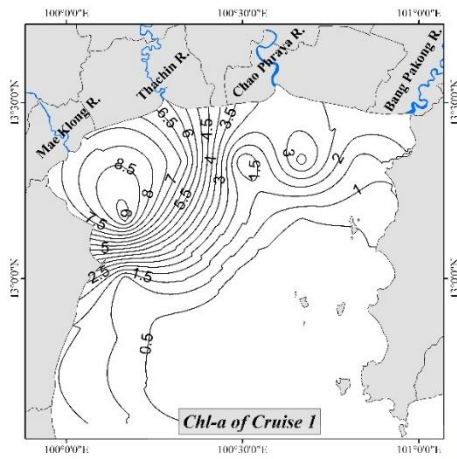
CDOM variation patterns in Cruise 1 and Cruise 2 were similar to those of observed Chl-a with high concentrations in the north-west coast of UGoT. High distributions located from the Mae Klong River mouth towards the coast of Petchaburi Province. Lowest concentrations were seen along the eastern coast as shown in Figures 4.4a/b. In Cruise 3, CDOM was not significantly high in general with no obvious pattern for spatial distribution appeared. In Cruise 4, CDOM was found in high abundant at the Chao Phraya River mouth and minimal at the south-east portion of UGoT (Figure 4.4d). In the last cruise, high CDOM was observed from the northwest to the west coast with highest one at the Thachin River mouth (Figures 4.4e).

4.1.2 Profiling reflectance radiometer (PRR) measurement

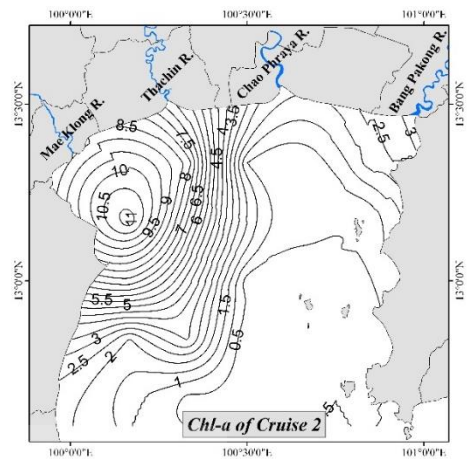
In situ spectral observations were performed using the PRR for 84 data records from all cruises (one record was not available). Optical spectrum based on PRR reflectance in Cruise 1 exhibited highest reflectance at 565 nm in the west coast (at station 5). Highest reflectance of blue bands (490 nm) occurred at the south-east of the offshore areas. Lowest reflectance was experienced in red band (670 nm) except at

stations 4 and 5 (Figure 4.5). Data from stations 1 to 7, or in the west and the north coast of UGoT, indicated high spectral variation. This might be due to high TSS concentration and variations in Chl-a and CDOM. For spatial variation of PRR in Cruise 2 (Figure 4.6), the reflectance data were grouped into 3 clusters as blue, green, and red distribution by station. Green bands were peaked from stations 1 to 6 (north to north-west) while blue band (490 nm) mostly peaked from stations 9 to 17 (SE coast). Chl-a was rather high at stations 4 and 5 while the PRR reflectance was lowest in blue and green bands. In general, the reflectance in red band was typically lowest.

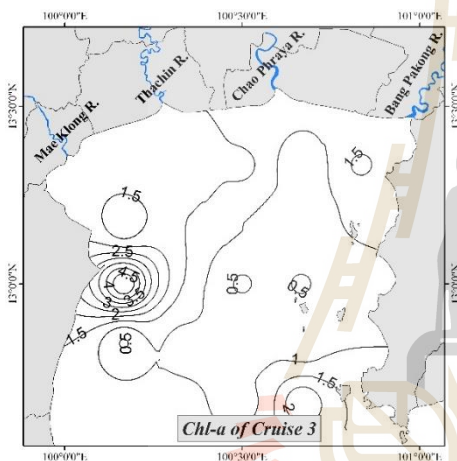




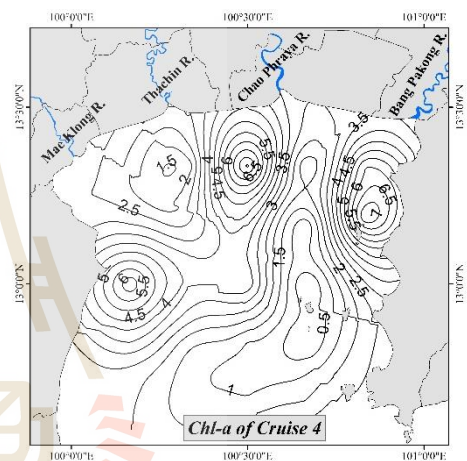
(a) Chl-a concentration of cruise 1.



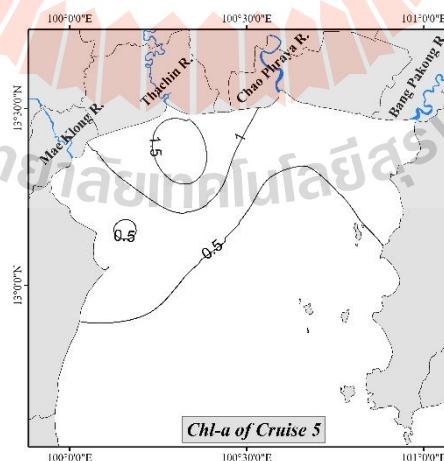
(b) Chl-a concentration of cruise 2.



(c) Chl-a concentration of cruise 3.

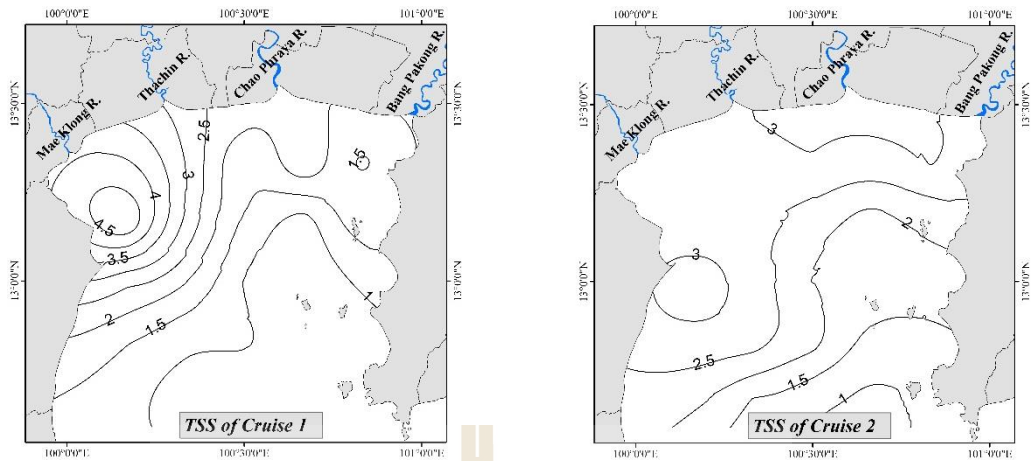


(d) Chl-a concentration of cruise 4.



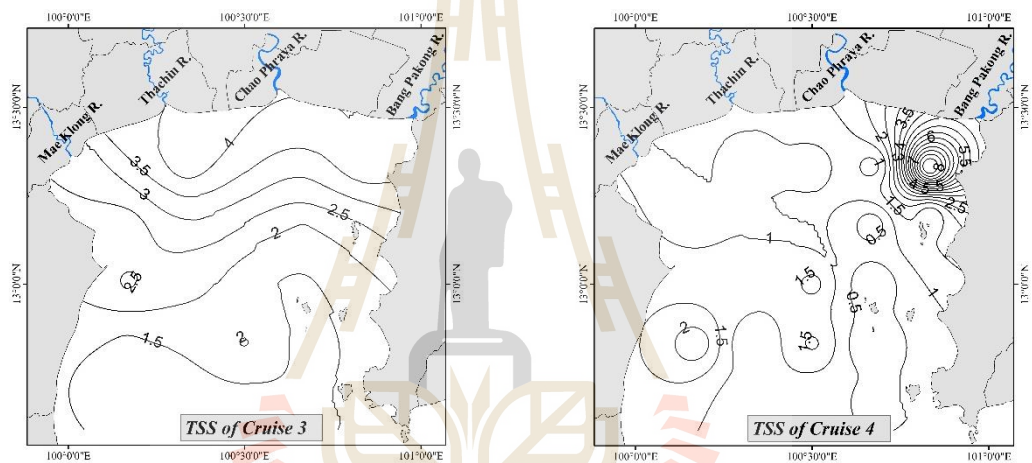
(e) Chl-a concentration of cruise 5.

Figure 4.2 Chlorophyll-a distribution maps from in situ data collected in UGoT from October 2003 to October 2004 (Cruise 1-5).



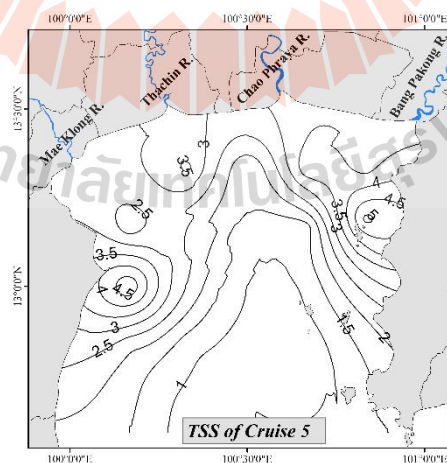
(a) TSS concentration of cruise 1.

(b) TSS concentration of cruise 2.



(c) TSS concentration of cruise 3.

(d) TSS concentration of cruise 4.



(e) TSS concentration of cruise 5.

Figure 4.3 Total suspended solid (TSS) distribution maps from in situ data collected in UGoT from October 2003 to October 2004 (Cruise 1-5).

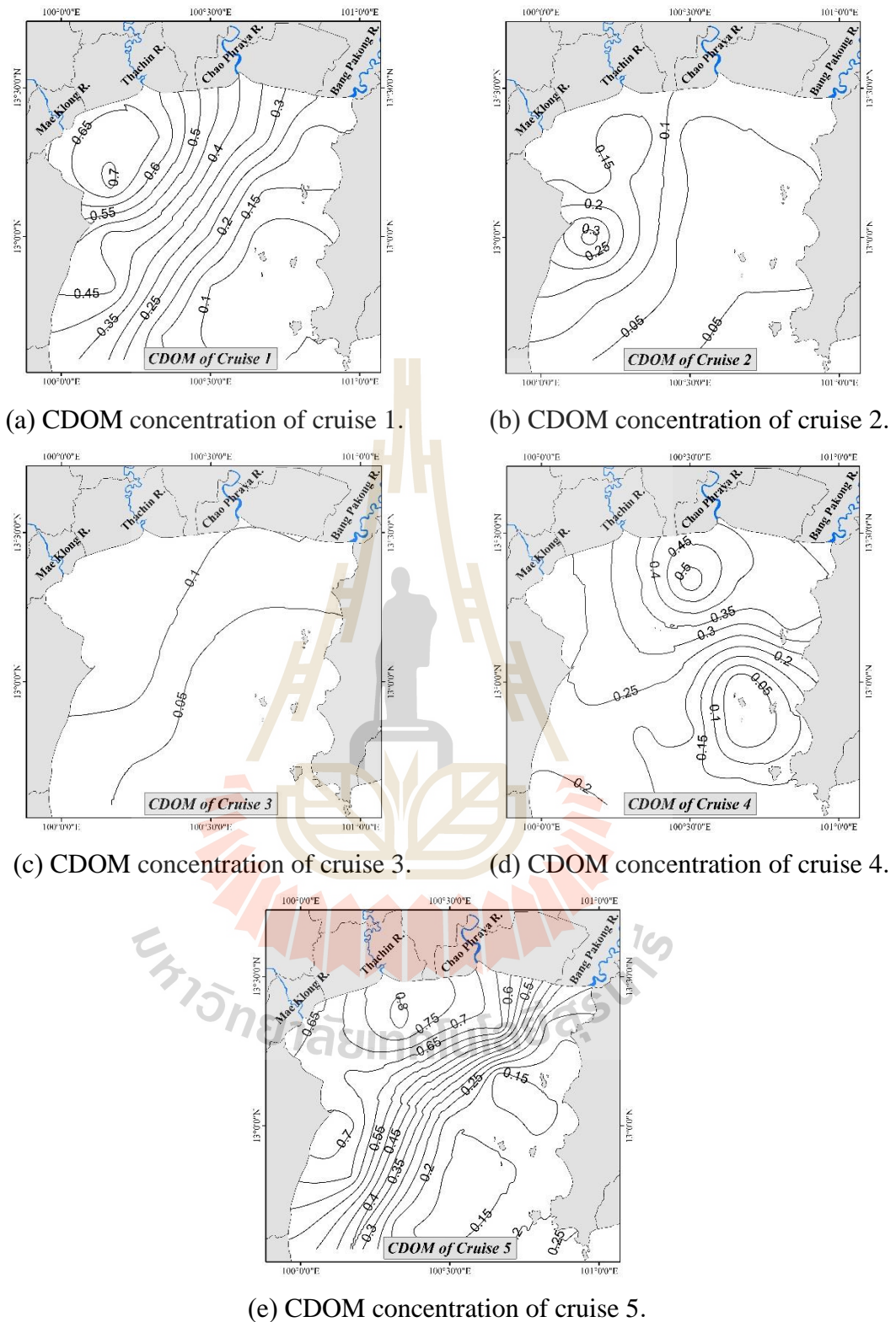


Figure 4.4 Color dissolved organic matter (CDOM) distribution maps from in situ data collected in UGoT from October 2003 to October 2004 (Cruise 1-5).

Figure 4.7 shows reflectance data of cruise 3 which illustrate spatial variation of PRR. Patterns of spectral signature were almost the same as those in previous cruises with high reflectances of green, blue and red bands from stations 1 to 6. PRR-based spectral signatures varied in each station in dry season during Cruise 4 (Figure 4.8). Reflectance data of green and blue bands were rather similar but concentrations of water constituents were different among locations. The reflectance at green bands were higher than those at the station from 1 to 7. Reflectance at red band was still lowest in the same way as those in previous cruises. In Cruise 5, high reflectance values of green bands were found in the north (stations from 1 to 7) while those of the blue bands dominated along the west coast (stations from 8 to 17). References at four main river mouths were always high in the green band. While those of the blue bands were high in the middle part of UGoT.

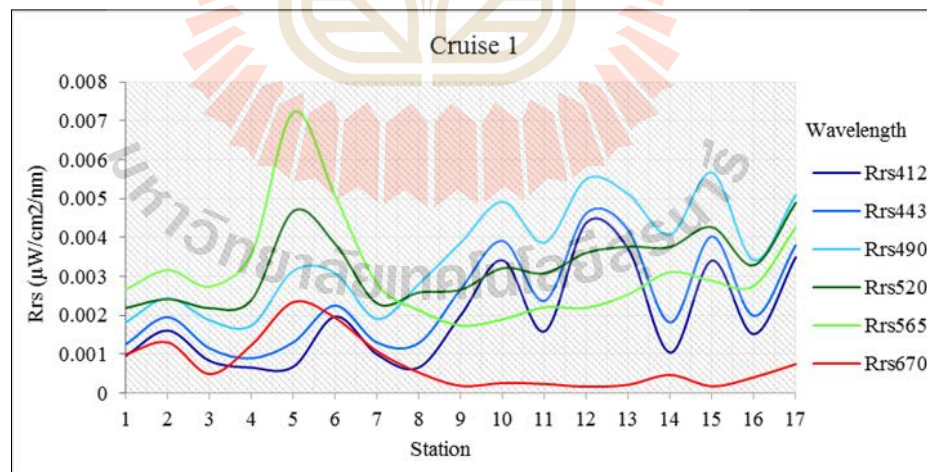


Figure 4.5 Spectral variations based on PRR measurement from cruise 1.

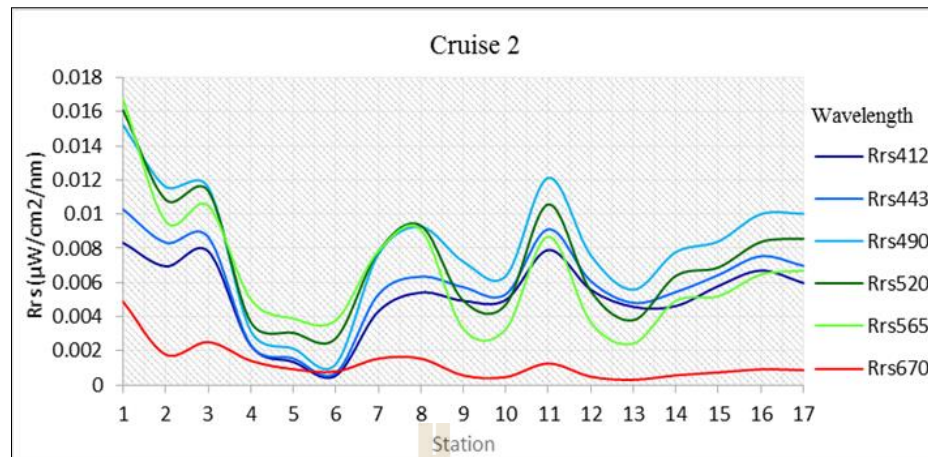


Figure 4.6 Spectral variations based on PRR measurement from cruise 2

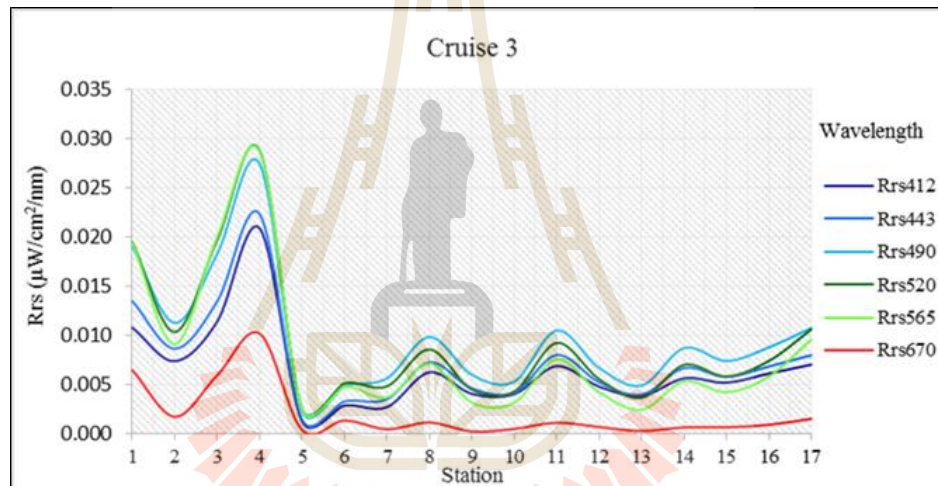


Figure 4.7 Spectral variations based on PRR measurement from cruise 3.

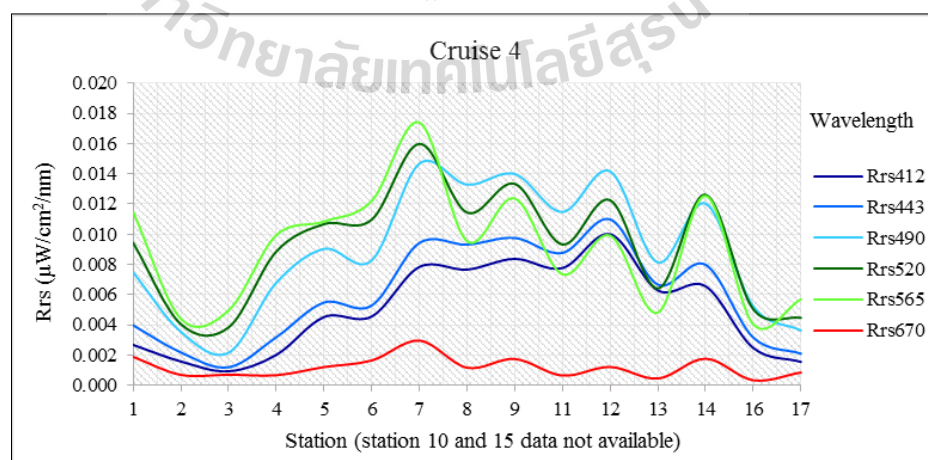


Figure 4.8 Spectral variations based on PRR measurement from cruise 4.

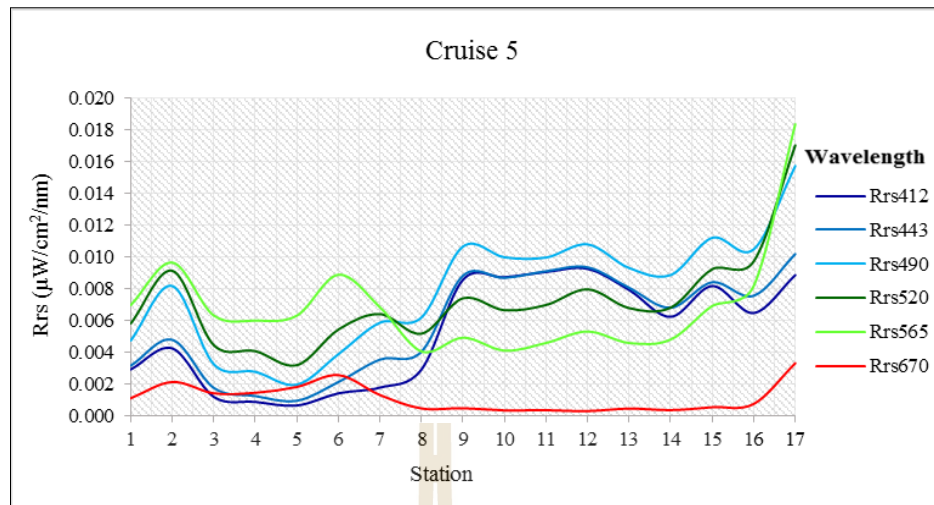


Figure 4.9 Spectral variations based on PRR measurement from cruise 5.

4.2 MODIS satellite dataset

This stage was carried out to extract spectral values from the acquired MODIS Level 2 dataset at the same sampling sites/collecting times of the aforementioned field observations. MODIS reflectance data of cruise 1 showed similar fluctuation patterns of the blue and green bands for all stations and almost similar to those of PRR (Figure 4.10). Highest reflectance in green bands occurred at stations from 1 to 7, 16, and 17 while those in the blue bands were found at stations from 8 to 15. High reflectance in the green bands always occurred at stations near four main river mouths where the influence of river discharge is high. In Cruise 2, the reflectances of all bands were highest at station 3 while those of the green bands were dominant at stations from 1 to 7 and those of the blue bands were high in other stations. The reflectance in the red bands were lowest at all stations except at stations from 3 to 6 where the values were high. All spectral variation curves were changed similarly as in the last cruise.

In Cruise 3, high reflectance data occurred at station 5 and the reflectance of red band was often lower than other wavelengths. High reflectance at station 5 might be due to the high Chl-a and CDOM concentration data. Noted that at stations 3, 4 and 6, reflectance data of the red bands were found higher than those of some blue bands. Data from cruise 4 showed high reflectance at station 6 (Figure 4.13) with reflectance data of the green bands dominated at the stations from 1 to 7 and blue bands dominated at station from 8 to 15. Reflectance of all the red bands was typically lowest at every stations. Highest reflectance at 531 nm was evidenced at all stations with highest peaks of all spectrums occurred at station 6. Noted that, reflectance data in this cruise are relatively lower than those in the other cruises. Also at stations from 4 to 7, the peak reflectance values were moved from the red bands (in the other cruises) to blue bands in this cruise. For cruise 5, reflectance patterns of blue and green bands were similar to those of cruise 1, but peak value was shifted for red bands (Figure 4.14). At stations from 8 to 16, reflectance spectral patterns were dominated primarily by blue and green bands. Reflectance data of blue bands at stations from 4 to 6 were found considerably lower than those of the other bands and spectral pattern of red bands appeared similarly to the previous cruises.

4.3 Modeling assessment

Empirical models based on the relationship between remotely sensed data and in situ data were developed to determine the water constituent concentration including Chl-a, TSS and CDOM over the UGoT from which the optimum model for each listed constituent was then identified. The yielded models were then applied to MODIS data to examine spatial/temporal variation of these studied constituents in the UGoT area.

Both linear relationship and non-linear relationships (such as polynomial, logarithm, power, exponential or linear models) were considered to achieve this purpose.

Relationships between PRR and MODIS level 2 reflectance dataset were made using five pairs of PRR/MODIS bands from the same cruise surveys with high level of correlation found (see Table 4.2). These results indicate rather strong relationship that supports the intended replacement of the PRR reflectance data by the associated MODIS data in the models to extract data of the three water constituents in UGoT.

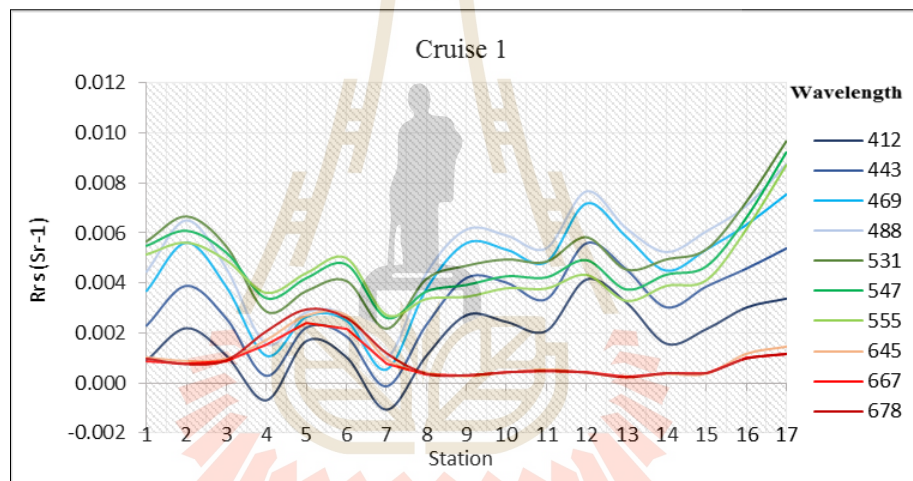


Figure 4.10 Spectral variations based on MODIS L2 reflectance in cruise 1.

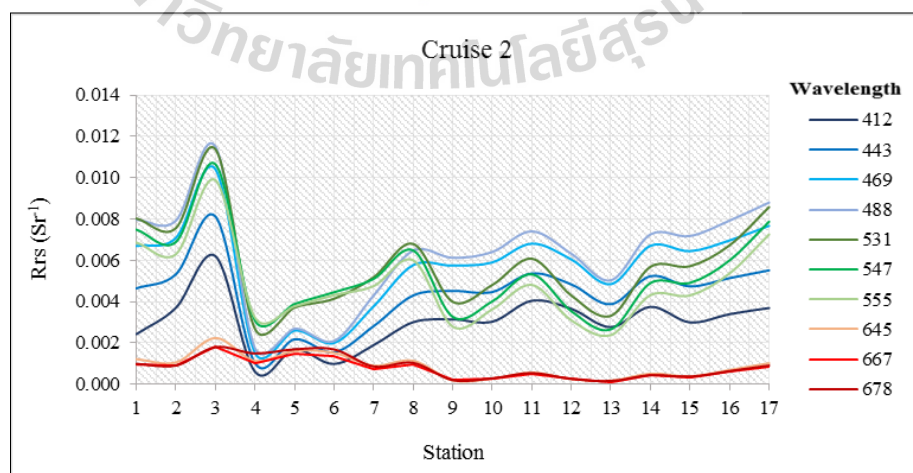


Figure 4.11 Spectral variations based on MODIS L2 reflectance in cruise 2.

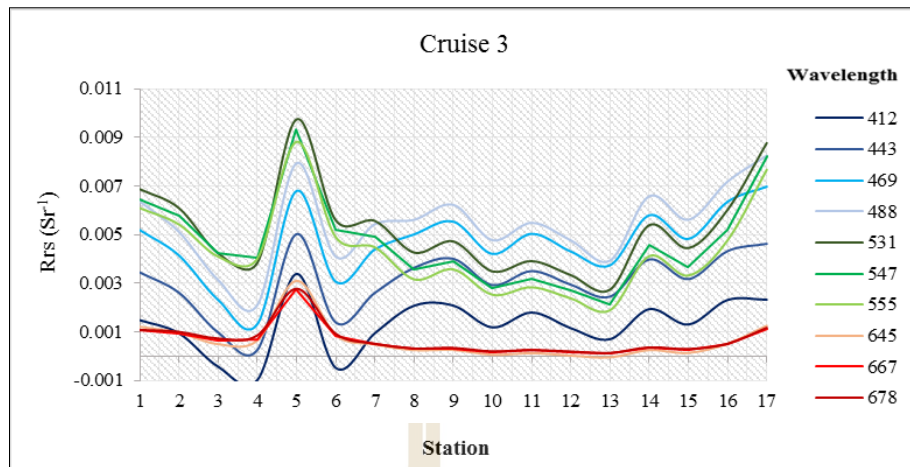


Figure 4.12 Spectral variations based on MODIS L2 reflectance in cruise 3.

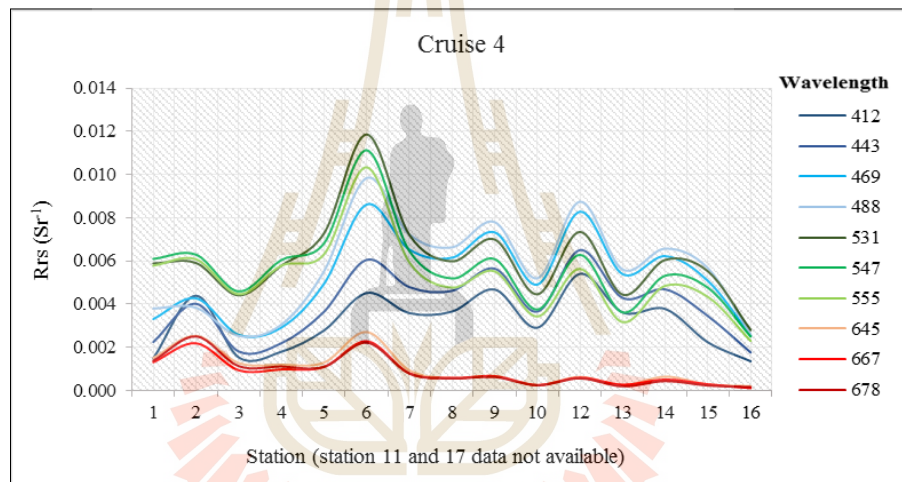


Figure 4.13 Spectral variations based on MODIS L2 reflectance in cruise 4.

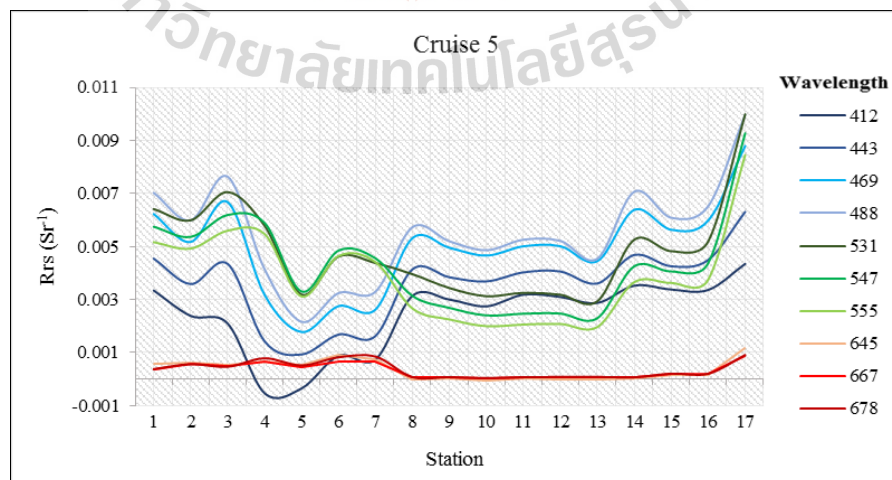


Figure 4.14 Spectral variations based on MODIS L2 reflectance in cruise 5.

The optimal models were identified based on the compared results of obtained statistical errors in three forms: coefficient of determination (R^2), root mean square error (RMSE) and mean absolute percentage error (MAPE).

4.3.1 Chl-a model modification

The first step was to transfer wavelengths from the original models to those of the PRR ones. An example process of the original OC3M model was established using three main wavelengths at 443, 490 and 550 nm. Due to discrepancy between the original model and PRR, the wavelength at 550 nm was replaced by that at 565 nm (the closest one) and then the coefficients of modified models were computed as shown in Table 4.3. Final results of model analysis for Chl-a using PRR data are shown in Table 4.4 in which the highest correlation with R^2 of 0.60 was seen for OC3M with RMSE and MAPE of 3.23 and 68.23, respectively. The new empirical models being used to estimate Chl-a concentration based on MODIS Level 2 data are summarized in Table 4.5 and Figure 4.15 with appropriate replacement of waveband data, e.g. 490 by 488 and 565 by 531 nm. The obtained Chl-a maps (on 4th December 2003) from MODIS data and the modified OC3M model are shown in Figure 4.16 with maximum value of 37.693 mg/m³ and minimum one of 0.037 mg/m³. High Chl-a density was frequently seen close to the Mae Klong and Tha Chin River mouths and Petchaburi's shore while low Chl-a water was dispersed on the eastern part of UGoT.

In this study shall be modified some wavebands to the new models which the blue/green ratio are more accurate than other visible bands (Lapucci et al., 2012). For observation, the lowest outcome are showed by red to green band ratio and rGBr, respectively. This is because, these models are comprise of the red bands which come to compute the Chl-a concentration. One reason which be support for local

OC3M become to the best result because the wavebands and model structure are similarly with the global OC3M.

Table 4.2 Coefficient of determination (R^2) of PRR reflectance and MODIS Level 2.

PRR Wavelengths	MODIS Level 2 Wavelengths (nm)									
	412	443	469	488	531	547	555	645	667	678
412	0.67	0.69	0.71	0.71	-	-	-	-	-	-
443	0.64	0.67	0.69	0.69	-	-	-	-	-	-
490	0.62	0.66	0.67	0.67	-	-	-	-	-	-
520	-	-	-	-	0.55	0.49	0.46	-	-	-
565	-	-	-	-	0.53	0.50	0.49	-	-	-
670	-	-	-	-	-	-	-	0.28	0.28	0.28

The empirical OC3M algorithm is extended from the OC4 and OC2 models developed for the SeaWiFS sensor and adopted to spectral bands of MODIS (Chen and Quan, 2013). An investigated of the relative between SeaWiFS and MODIS becomes to conformation. Calibration and processing methodologies can be produced the ocean color time-series from two very different spaceborne sensors. Thus, data used to model implementation to marine constituents was performed. According to, Franz et al. (2005) were reported the relative wavebands of SeaWiFS and MODIS (based on R^2) was over 0.86 of wavebands 490 nm and 488 nm, R^2 is 0.70 of wavebands 551 and 555 nm, and worst relative of 667 and 670 nm ($R^2 = 0.14$), respectively. From this result was indicated similarly work in this study of PRR reflectance and MODIS Level 2 (Table 4.2), which emphasize on band to band replacement based on local models were accepted and reliable. Consequently, similiary process are applied to TSS and CDOM models and so on.

4.3.2 TSS model modification

Model modification was performed to identify new coefficient for TSS analysis as that of the Chl-a (Table 4.6) and the gained results based on original PRR data were summarized in Table 4.7. There were four candidate models for TSS study including TSM, Chula, Applied SeaWiFs to MODIS and SSCs models which gave coefficients determination (R^2) between the predicted and in situ data of 0.72, 0.66, 0.66, and 0.64, respectively. Based on R^2 , the performance of all four models were rather acceptable but all of R^2 , RMSE and MAPE of the TSM was superior than the other models, therefore, it was selected for implementation due to its best statistical performances.

Considering two of the four best models are TSM and Chula, which are observed by those models was use only one of red band reflectance for predictions (667 nm). Conventional model structure of multi-regression was investigated. Which seems to be related to Ruddick et al. (2008) were reported as the linear regression performance of single-band model is usually best for low to moderate reflectance. In research of Hu et al. (2004) revealed best of regression between TSS and MODIS reflectance ($R^2 = 0.90$) which applied the difference band of 645 and 859 nm. While, an existing blue/green band-ratio model may not work in the complex like Case-II estuary waters.

The modified TSM model is illustrated in Table 4.8 and Figure 4.17. Yielded TSS map (on 4th December 2003) based on the implementation of TSM on MODIS data is shown in Figure 4.18 in which highest and lowest values of 11.213 and 0.001 g/m³, were found respectively. Spatial distribution of high values was located around all of four main river mouths and along the western coastline.

4.3.3 CDOM model modification

In this case, all applied models were modified with new coefficients (in the same way as those of the Chl-a and TSS) as summarized in Table 4.9 with gained results reported in Table 4.10. Among these, Chula model gained highest value of R^2 (0.78) followed by CDOM-400 polynomial (0.77) and Apply SeaWiFs to MODIS models (0.75), indicating that these models are credible for MODIS implementation. Eventually, Chula model was considered the best one for further application due to its high accuracy regarding RMSE (0.11) and MAPE (56.80) in CDOM estimation along with its simple/straightforward structure. Modified Chula model is illustrated in Table 4.11 and Figure 4.19 with spectral band ratio changed from 412/565 to 412/555.

This results, on the top of three CDOM models, two of the three best models are used the blue/green band. Knowledge of CDOM have been sensitive as shortwave of blue bands (440 nm) thus be usually useful to the model because it corresponds to the maximal absorption by algal pigments (Keith, Yoder, and Freeman, 2002). Furthermore, CDOM has been always linked to chlorophyll or other biomass amount (Corbett, 2007), consequently this model perform shall be not accurately with only blue or green bands to the model like the Apply to SeaWiFs (used only blue-band) or CDOM Band-ratio: I (used only green-band) models in this studied for UGoT.

Figure 4.20 shows CDOM concentration map (on 4th December 2003) generated by the MODIS-based modified Chula model where the highest and lowest values of 3.529 m^{-1} and 0.001 m^{-1} , were found respectively. Here, high CDOM values were mainly found at UGoT near shore (typically at the Bang Pakong River mouth).

Table 4.3 Modified empirical models for Chl-a estimation based on in situ and PRR dataset.

No.	Models name	Models structure	PRR modified structure	Validation			Remark
				RMSE	MAPE	n	
1	OC3M	$C_{\text{chla}} = 10^{(a_0+a_1R+a_2R^2+a_3R^3+a_4R^4)},$ $R = \log_{10} \left[\max \left(\frac{R_{rs}(443)}{R_{rs}(550)}, \frac{R_{rs}(490)}{R_{rs}(550)} \right) \right]$	$C_{\text{chla}} = 10^{(0.0513-1.5884R-5.5887R^2-5.4592R^3+16.977R^4)}$ $R = \log_{10} \left[\max \left(\frac{R_{rs}(443)}{R_{rs}(565)}, \frac{R_{rs}(490)}{R_{rs}(565)} \right) \right]$ $R^2 = 0.60, n = 57$	3.25	68.23	25	Replaced Rrs 550 by 565
2	DAAC-V4 Chlor_MODIS	$C_{\text{chla}} = 10^a \left[\frac{L_{wn}(443)}{L_{wn}(550)} \right]^{-b}$	$C_{\text{chla}} = 10^{0.5} \left[\frac{L_{wn}(443)}{L_{wn}(565)} \right]^{-0.8082}$ $R^2 = 0.44, n = 59$	3.03	817.39	25	Replaced Rrs 550 by 565
3	Aiken-1995	$\log[\text{Chla}] = c_0 + c_1 \log(r_{35})$ $+ c_2 [\log(r_{35})]^2$ $+ c_3 [\log(r_{35})]^3$ $r_{35} = \frac{R_{rs}(488)}{R_{rs}(550)}$	$\log[\text{Chla}] = -0.1308 + 1.2767 \log(r_{35})$ $- 1.3613 [\log(r_{35})]^2$ $+ 0.2678 [\log(r_{35})]^3$ $r_{35} = \frac{R_{rs}(490)}{R_{rs}(565)}$ $R^2 = 0.51, n = 59$	3.35	67.78	25	Replaced Rrs 488 by 490 and 550 by 565
4	Red to Green band ratio	$\ln(\text{Chla}) = a \ln(x) + b$ $x = [R_{rs}(678)]/[R_{rs}(531) + R_{rs}(547)]$	$\ln(\text{Chla}) = 1.2475 \ln(x) + 2.7387$ $x = [R_{rs}(670)]/[R_{rs}(520) + R_{rs}(565)]$ $R^2 = 0.27, n = 59$	3.54	78.43	25	Excluded Rrs 667, replaced 678 by 670, 531 by 520 and 547 by 565

Table 4.3 Modified empirical models for Chl-a estimation based on in situ and PRR dataset (Continued).

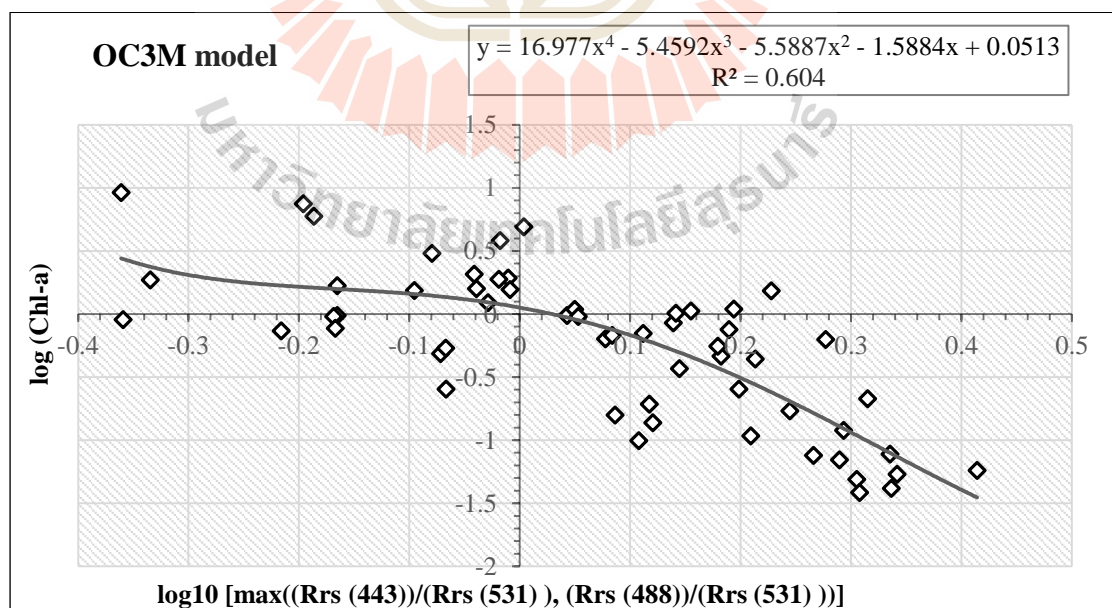
No.	Models name	Models structure	PRR modified structure	Validation			Remark
				RMSE	MAPE	n	
5	rGBr	$C_{\text{chla}} = C_1 \frac{R_{\text{rs}}(551)}{R_{\text{rs}}(443)} + C_2$	$C_{\text{chla}} = 0.6828 \left(\frac{R_{\text{rs}}(565)}{R_{\text{rs}}(443)} \right) + 0.1842$ $R^2 = 0.22, n = 59$	3.00	212.95	25	Rrs 551 replaced by 565
6	Applied SeaWiFs to MODIS	$C_{\text{chla}} = [R_{\text{rs}}(443) / R_{\text{rs}}(555)] [R_{\text{rs}}(412) / R_{\text{rs}}(490)]^{-0.5}$	$C_{\text{chla}} = 5.1419e^{-1.87x}$ $R^2 = 0.50, n = 59$ $X = [R_{\text{rs}}(443) / R_{\text{rs}}(565)] [R_{\text{rs}}(412) / R_{\text{rs}}(490)]^{-0.5}$	3.067	67.90	25	Replaced Rrs 555 by 565
7	Chula	$C_{\text{chla}} = 181.4 \exp(-4.74R);$ $R = R_{\text{rs}}(520) / R_{\text{rs}}(565)$	$C_{\text{chla}} = 30.511 \exp(-3.647R)$ $R = R_{\text{rs}}(520) / R_{\text{rs}}(565)$ $R^2 = 0.55, n = 51$	3.21	68.64	25	

Table 4.4 The performance of Chl-a models based on PRR data for Chl-a prediction.

Order	Models name	R ²	RMSE	MAPE
1	OC3M	0.60	3.23	68.23
2	Chula	0.55	3.21	68.64
3	Aiken-1995	0.51	3.35	67.78
4	Applied SeaWiFs to MODIS	0.50	3.07	67.90
5	DAAC-V4 Chlor_MODIS	0.44	3.03	817.39
6	Red to Green band ratio	0.27	3.35	78.43
7	rGBr	0.22	3.00	212.95

Table 4.5 The optimal model for Chl-a extraction from MODIS data (OC3M).

Model	PRR modified structure	MODIS implement	Remark
OC3M	$C_{chl-a} = 10^{\left(\frac{0.0513 - 1.5884R - 5.5887R^2 - 5.4592R^3}{+16.977R^4} \right)}$ $R = \log_{10} \left[\max \left(\frac{R_{rs}(443)}{R_{rs}(565)}, \frac{R_{rs}(490)}{R_{rs}(565)} \right) \right]$	$C_{chl-a} = 10^{\left(\frac{0.0513 - 1.5884R - 5.5887R^2 - 5.4592R^3}{+16.977R^4} \right)}$ $R = \log_{10} \left[\max \left(\frac{R_{rs}(443)}{R_{rs}(531)}, \frac{R_{rs}(488)}{R_{rs}(531)} \right) \right]$	Replaced Rrs 490 by 488 and 565 by 531

**Figure 4.15** MODIS-based OC3M model performance for Chl-a prediction/mapping.

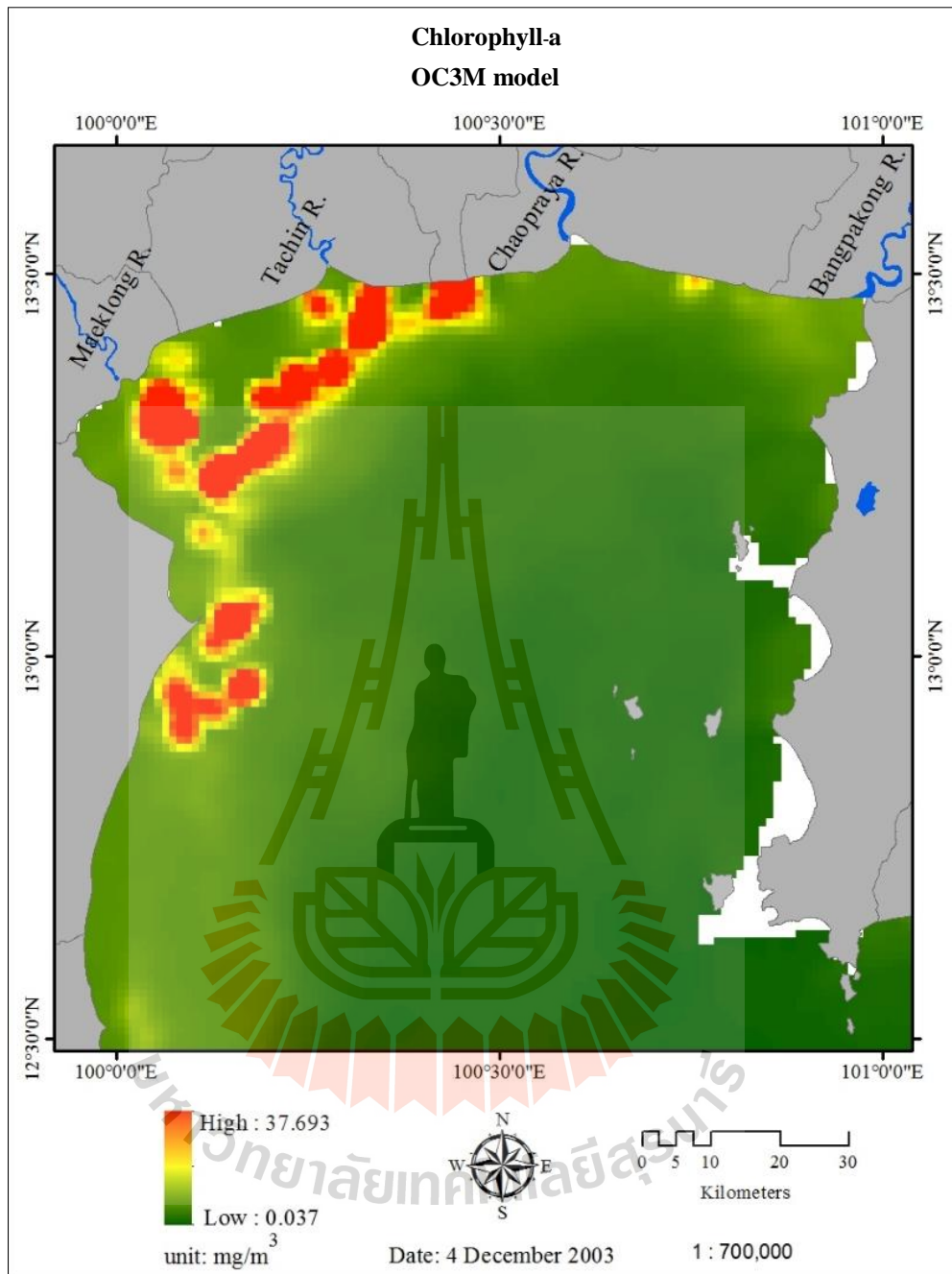


Figure 4.16 MODIS-based Chl-a concentration map derived by the OC3M model.

Table 4.6 Modified empirical models for TSS predictions based on in situ and PRR dataset.

No.	Models name	Models structure	PRR modified structure	Validation			Remark
				RMSE	MAPE	n	
1	Apply SeaWiFs to MODIS	$SS = [R_{rs}(555) + R_{rs}(670)][R_{rs}(490)/R_{rs}(555)]^{-1.2}$	$SS = 425.79x^2 + 112.14x + 0.8618$ $X = [R_{rs}(565) + R_{rs}(670)][R_{rs}(490)/R_{rs}(565)]^{-1.2}$ $R^2 = 0.66, n = 57$	1.16	41.23	25	Replaced Rrs 555 by 565
2	Global- Tassan's	$\text{Log}_{10}S = 1.83 + 1.26\text{Log}_{10}X_s$ $X_s = \{[R_{rs}(555) + R_{rs}(620)] \times [R_{rs}(555)/R_{rs}(490)]^{-1.2}\}$	$\text{Log}_{10}S = 0.639 + 0.2237\text{Log}_{10}X_s$ $X_s = \left\{ \begin{array}{l} [R_{rs}(565) + R_{rs}(670)] \\ \times [R_{rs}(565)/R_{rs}(490)]^{-1.2} \end{array} \right\}$ $R^2 = 0.14, n = 59$	0.27	119.89	25	Replaced Rrs 555 by 565 and Rrs 620 by 670
3	Son-Wang- 2012	$TSS = a + b (Kd490),$ $Kd490 = 0.2411(R_{rs}490/R_{rs}565)^{-1.2753}$	$TSS = 1.0651 + 4.0594 (Kd490),$ $Kd490 = 0.2411(R_{rs}490/R_{rs}565)^{-1.2753}$ $R^2 = 0.1975, n = 59$	1.04	72.13	25	
4	GOCI	$TSS = 945.07 \times R_{rs}(555)^{1.137}$	$TSS = 43.437 \times R_{rs}(565)^{0.6503}$ $R^2 = 0.2826, n = 59$	0.98	46.29	25	Replaced Rrs 555 by 565

Table 4.6 Modified empirical models for TSS predictions based on in situ and PRR dataset (Continued).

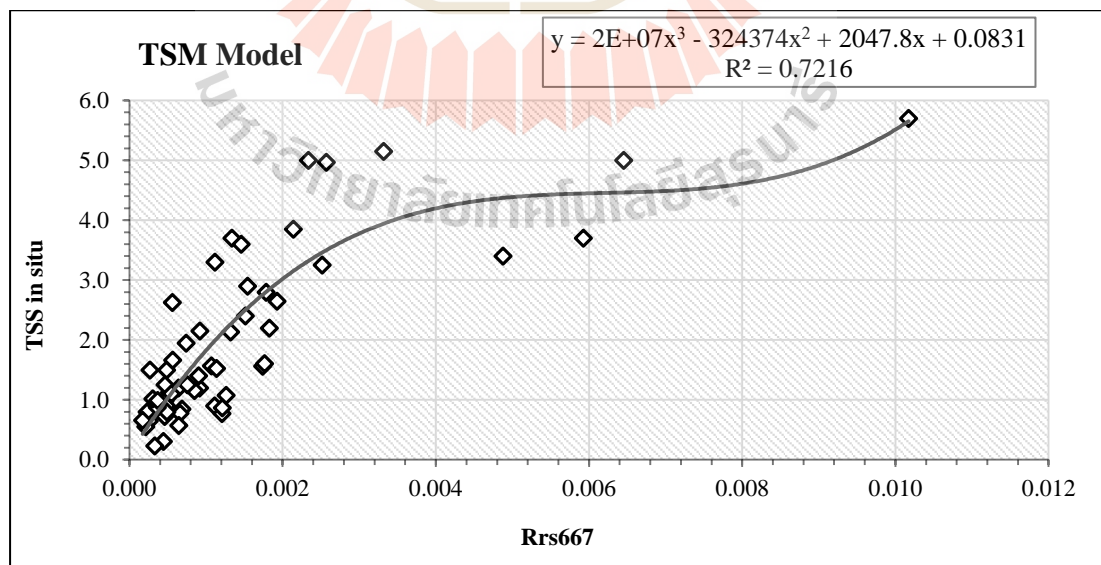
No.	Models name	Models structure	PRR modified structure	Validation			Remark
				RMSE	MAPE	n	
5	TSSs2011	$\log_{10}(\text{TSS}_{\text{S2011}}) = 0.738 + 22.79$ $\times (\text{Rrs555} + \text{Rrs670}) - 0.574$ $\times \frac{\text{Rrs490}}{\text{Rrs555}}$	$\log_{10}(\text{TSS}_{\text{S2011}}) = 0.3014 + 20.322$ $\times (\text{Rrs565} + \text{Rrs670}) - 0.223 \times \frac{\text{Rrs490}}{\text{Rrs565}}$ $R^2 = 0.432, n = 59$	0.19	98.18	25	Replaced Rrs 555 by 565
6	SSCs	$\text{SSCs} = \{[\text{R}_{\text{rs}}(555) + \text{R}_{\text{rs}}(620)] + [\text{R}_{\text{rs}}(620)/\text{R}_{\text{rs}}(490)]^2\}$	$\text{SSCs} = -321.99x^4 + 529x^3 - 276.08x^2 + 53.53x$ $+ 0.4858$ $X = \left\{ \begin{array}{l} [\text{R}_{\text{rs}}(565) + \text{R}_{\text{rs}}(670)]^2 \\ + [\text{R}_{\text{rs}}(670)/\text{R}_{\text{rs}}(490)] \end{array} \right\}$ $R^2 = 0.64, n = 58$	1.10	56.65	25	Replaced Rrs 555 by 565 and Rrs 620 by 670
7	TSM	$\text{TSM} = 3.8813(\text{nL}_w(645))^3 - 13.822(\text{nL}_w(645))^2 +$ $19.61(\text{nL}_w(645))$	$\text{TSM} = 2E + 07(\text{nL}_w(670))^3 - 324374$ $(\text{nL}_w(670))^2 + 2047.8(\text{nL}_w(670)) +$ 0.0831 $R^2 = 0.72, n = 57$	0.77	38.98	25	Replaced Rrs 645 by 670
8	Chula	$\text{Total SS (mg/l)} = 1.16 \text{Ln}(\text{Rrs}(670)) + 10.23$	$\text{Total SS (mg/l)} = 1.2727\text{Ln}(\text{Rrs}(670)) +$ 10.822 $R^2 = 0.66, n = 57$	0.78	46.78	25	

Table 4.7 The performance of TSS models based on PRR data for TSS prediction.

Order	Models name	R ²	RMSE	MAPE
1	TSM	0.72	0.77	38.97
2	Chula	0.66	0.78	46.78
3	Apply SeaWiFs to MODIS	0.66	1.16	41.23
4	SSCs	0.64	1.10	56.65
5	TSSs2011	0.43	0.19	98.18
6	GOCI	0.28	0.98	46.29
7	Son-Wang-2012	0.20	1.04	72.13
8	Global-Tassan's	0.14	0.27	119.89

Table 4.8 The optimal model for TSS extraction from MODIS data (TSM).

Model	PRR modified structure	MODIS implementation	Remark
TSM	$\text{TSM} = 2\text{E} + 07(\text{nL}_w(670))^3 - 324374(\text{nL}_w(670))^2 + 2047.8(\text{nL}_w(670)) + 0.0831$	$\text{TSM} = 2\text{E} + 07(\text{nL}_w(667))^3 - 324374(\text{nL}_w(667))^2 + 2047.8(\text{nL}_w(667)) + 0.0831$	Replaced Rrs 670 by 667

**Figure 4.17** MODIS-based TSM model performance for TSS prediction/mapping.

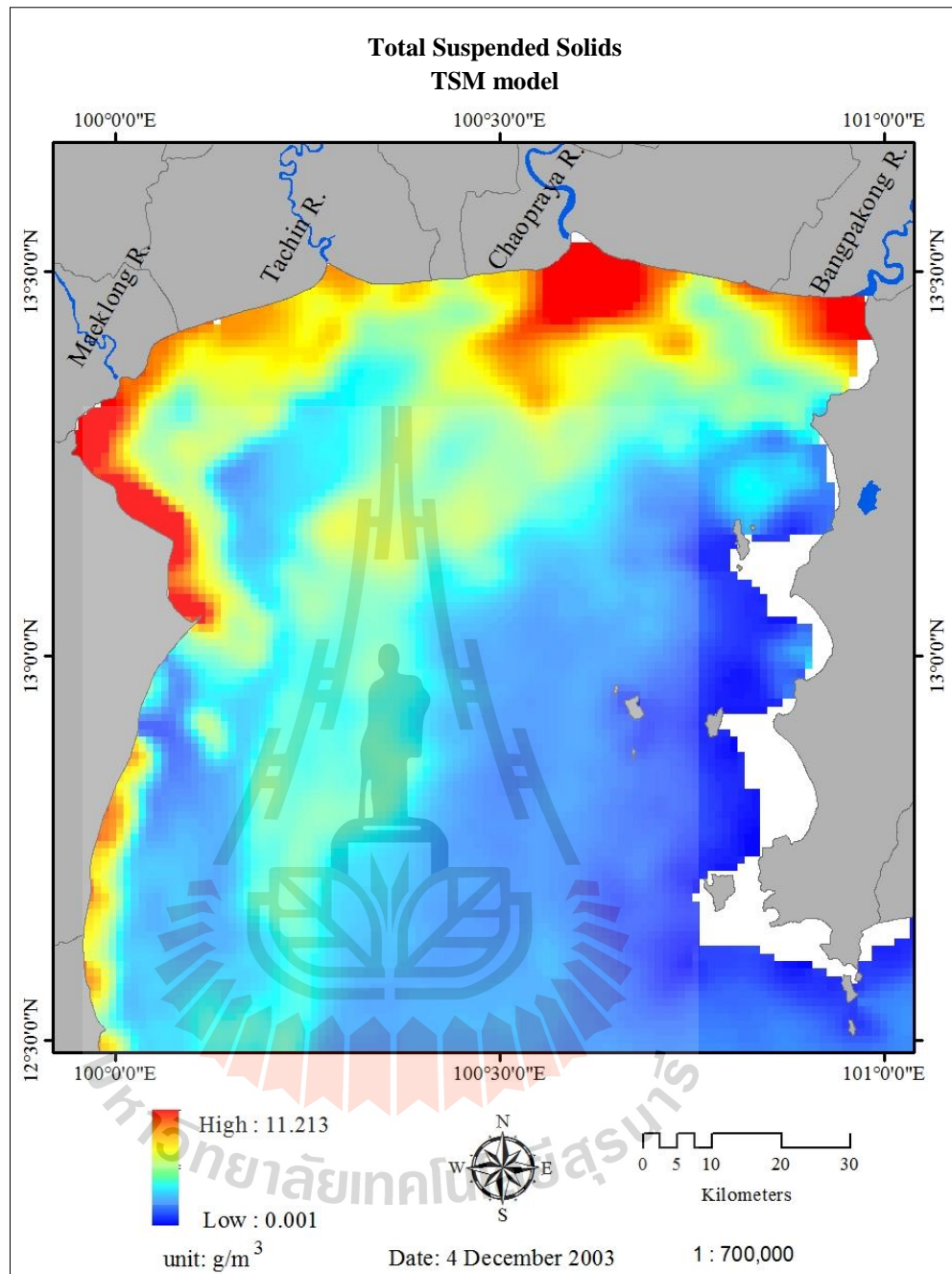


Figure 4.18 MODIS-based TSS concentration map derived by the TSM model.

Table 4.9 Modified empirical models for CDOM predictions based on in situ and PRR dataset.

No.	Models name	Models structure	PRR modified structure	Validation			Remark
				RMSE	MAPE	n	
1	Apply SeaWiFs to MODIS	$Y = [\text{Rrs}(412)/\text{Rrs}(490)][\text{Rrs}(443)]^{0.25}$	$y = -3411.7x^4 + 2445x^3 - 596.91x^2 + 55.244x - 1.1992$ $R^2 = 0.75, n = 53$ $X = \left[\frac{\text{Rrs}(412)}{\text{Rrs}(490)} \right] [\text{Rrs}(443)]^{0.25}$	0.13	62.17	21	
2	CDOM Band-ratio:I	$\log y = 1.1744 \ln(x) - 1.9558,$ $X = \text{Rrs}(510)/\text{Rrs}(555)$	$\log y = -1.1643 \ln(x) - 0.7647,$ $X = \text{Rrs}(520)/\text{Rrs}(565)$ $R^2 = 0.42, n = 58$	0.36	40.68	24	Replaced Rrs 510 by 520 and 555 by 565
3	CDOM Band-ratio:II	$\log y = -3.3209 \ln(x) - 2.4245,$ $X = \text{Rrs}(443)/\text{Rrs}(510)$	$\log \text{CDOM} = -0.868 \ln(x) - 1.177$ $R^2 = 0.49, n = 58$ $X = \text{Rrs}(443)/\text{Rrs}(520)$	0.38	44.45	24	Replaced Rrs 510 by 520
4	CDOM-440 Polynomial	$ag_{440} = 10^{(C_1 + C_2 \log_{10}(R) + C_3 \log_{10}(R)^2)},$ $R = \left(\frac{\text{Rrs}_{490}}{\text{Rrs}_{555}} \right) (\text{Rrs}_{443})$	$ag_{440} = 10^{(-1.6527 - 0.0308 \log_{10}(R) + 0.1328 \log_{10}(R)^2)}$ $R^2 = 0.47, n = 58$ $R = \left(\frac{\text{Rrs}_{490}}{\text{Rrs}_{565}} \right) (\text{Rrs}_{443})$	0.40	46.22	24	Replaced Rrs 555 by 565

Table 4.9 Modified empirical models for CDOM predictions based on in situ and PRR dataset (Continued).

No.	Models	Models structure	PRR modified structure	Validation			Remark
				RMSE	MAPE	n	
5	CDOM-400 Polynomial	$ag_{400} = 1.5 \times 10^{(C_0 + C_1 R_{15} + C_2 R_{15}^2 + C_3 R_{25} + C_4 R_{25}^2)}$, $R_{15} = \text{Log}_{10} \left(\frac{Rrs_{412}}{Rrs_{555}} \right)$ and $R_{25} = \text{Log}_{10} \left(\frac{Rrs_{443}}{Rrs_{555}} \right)$	$ag_{400} = 1.5 \times 10^{(0 + 15.326 R_{15} + 15.1693 R_{15}^2 - 16.0815 R_{25} - 20.4818 R_{25}^2)}$	0.20	91.14	21	Replaced Rrs 555 by 565
			$R^2 = 0.77, n = 58$ $R_{15} = \text{Log}_{10} \left(\frac{Rrs_{412}}{Rrs_{565}} \right)$ $R_{25} = \text{Log}_{10} \left(\frac{Rrs_{443}}{Rrs_{565}} \right)$				
6	Chula model	$\text{CDOM } k(412) = -0.1981 \text{Ln}(R) + 0.067,$ $R = Rrs(412, 0-) / Rrs(565, 0-)$	$\text{CDOM } k(412) = 0.0768R^2 - 0.1274R + 0.0876$ $R^2 = 0.78, n = 56$ $R = Rrs(412) / Rrs(565)$	0.11	56.80	21	

Table 4.10 The performance of CDOM models based on PRR data for CDOM prediction.

Order	Models	R ²	RMSE	MAPE
1	Chula model	0.78	0.11	56.80
2	CDOM-400 Polynomial	0.77	0.20	91.14
3	Apply to SeaWiFs	0.75	0.13	62.17
4	CDOM Band-ratio:II	0.49	0.36	44.45
5	CDOM-440 Polynomial	0.47	0.40	46.22
6	CDOM Band-ratio:I	0.42	0.36	40.68

Table 4.11 The optimal model for CDOM extraction from MODIS data (Chula model).

Model	PRR modified structure	MODIS implementation	Remark
Chula model	$\text{CDOM } k(412) = 0.0768R^2 - 0.1274R + 0.0876$ $R = \text{Rrs}(412,0-) / \text{Rrs}(565, 0-)$	$\text{CDOM } k(412) = 0.0768R^2 - 0.1274R + 0.0876$ $R = \text{Rrs}(412) / \text{Rrs}(531)$	Replaced Rrs 565 by 531

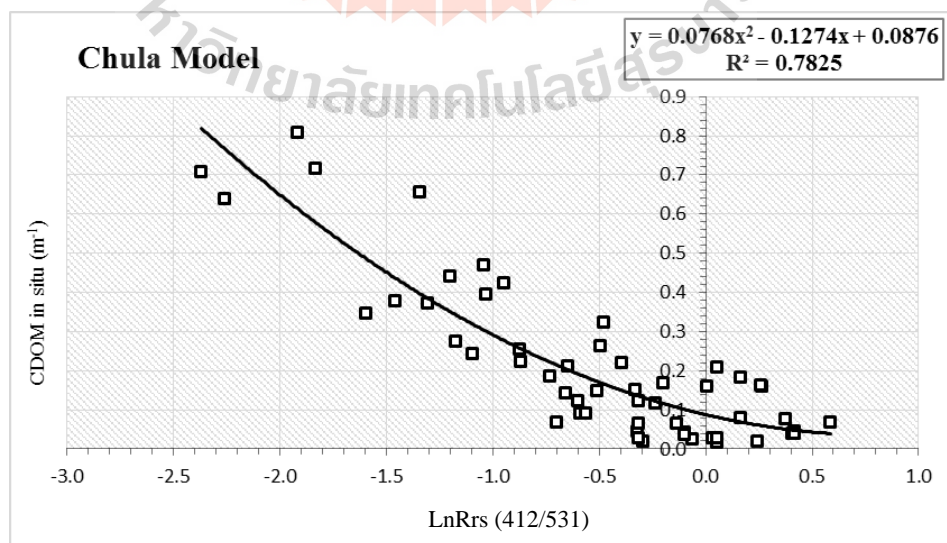


Figure 4.19 MODIS-based Chula model performance for CDOM prediction/mapping.

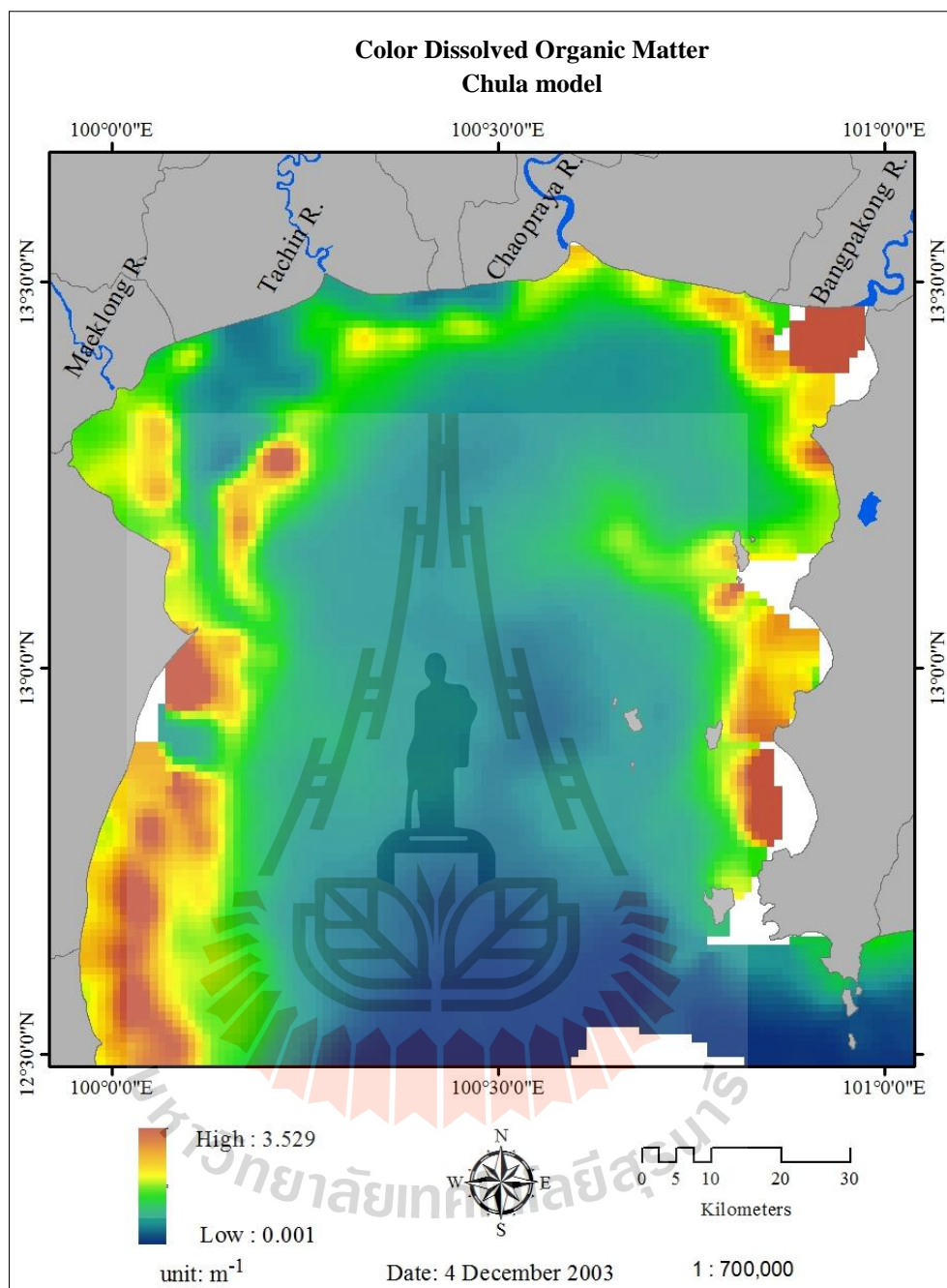


Figure 4.20 MODIS-based CDOM concentration map derived by the Chula model.

4.4 Artificial neural network (ANN) model

This section describes potential application of the preferred ANN model in the estimation of three main water component in UGoT (Chl-a, TSS and CDOM) wherein the multi-layer perceptron neural network (MLP-NN) model with back propagation (BP) algorithm was applied (Recknagel, 2006). Here, the model's training session was done based on known information of spectral waveband reflection of MODIS imagery in relation to the concurrent constituent data of interest.

Relevant parameters were investigated by five cruises as previously mentioned and fifteen MODIS images recorded the same time of field data collection were used. In the study, the reflectance data of MODIS L2 (10 bands) were used as independent variable with the associated in-situ data of Chl-a, TSS and CDOM concentration were considered as dependent variable. Both groups of variable data were fed as prior input data for the aforementioned MLP neural network to fulfil initial need of automatically producing thematic maps of studied water constituents from MODIS reflectance data. To help the model work more efficiently (faster converge), all applied input data were normalized accordingly to downscale units of each used factor to be in the same range of 0 to 255 (unsigned 8-bit float data) (Kiener and Yan, 1998).

The applied ANN structure included four main processing layers: input layer including ten spectral wavebands of MODIS, two hidden layers and one output layer, as seen in Figure 4.21. First hidden layer was consisting of 30 nodes while the second one had 10 nodes (these numbers were concluded from the trial and error experiment). Though, the overall model's structure became 10:30:10:1 where the input data files are as shown in Table 4.12. The ANN analysis was done on regression algorithm with the final learning rate of 0.01, momentum factor setting at around 0.5, Sigmoid

constant of 1, acceptable RMS not more than 0.01 and the iteration of 10000 rounds (Table 4.13). Eventually, the accomplished results of the training RMS, testing RMS and R^2 had become 0.0831, 0.0974 and 0.7854, respectively. This achievement indicates high efficiency of the ANN structure in use.

ANN outputs were determined by various statistics regarding prior knowledge gained from the learning process which includes weight information of neurons across layers. For examples, Table 4.14 reports weight data between input layer neurons and hidden layer 1 neuron while Table 4.15 presents those of hidden layers 1 and 2, and Table 4.16 for those of hidden layer 2 and the output layer. In addition, to examine influence of each input parameter (MODIS L2 reflectance), sensitivity analysis was performed on each listed independent variable. This task included three scenarios as described in Tables 4.17 to 4.19. The first one forced a single independent variable to be constant at a time and considered a noticeable change in working efficiency of the adjusted ANN model (in term of R^2). As seen in Table 4.17, the most important variable in this case was reflectance data at 443 nm waveband and the least crucial one was 488 nm band. In the second scenario, things were operated other way round by forcing all independent variables to be fixed except the single one of preference, and in the third scenario, number of input variables being forced to be fixed increased in a stepwise pattern, one after one. In both cases, influence of each listed variable on ANN efficiency was also determined by the observed change of R^2 compared to the optimal one as shown in Tables 4.18 and 4.19, respectively. Typically, removing low significance variables might benefit in reducing the likelihood of overfitting and slightly increase efficiency of the used model (Eastman, 2016).

Prediction of Chl-a concentration from 15 MODIS datasets by the ANN model process gained rather high correlation coefficient ($R^2 = 0.67$) in which the most influential and least influential ones were blue-band data (Table 4.20). For the TSS prediction, good correlation coefficient was also achieved ($R^2 = 0.77$) and the most crucial input factors were also the blue-band data (Table 4.21). These findings were also evidenced for the CDOM with R^2 of 0.78 (Table 4.22). These obtained results indicate that reflectance data of MODIS blue bands are very essential for efficient work of the applied ANN model in the UGoT area. Finally, examples of the derived concentration map for each listed constituent (Chl-a, TSS and CDOM) over UGoT area derived from yielded output of the applied ANN model are presented in Figures 4.22 to 4.24, respectively.

Three water constituents were the most successfully estimated parameters by the ANN model. Rather high of coefficient by the process was investigated in the complex of coastal areas like UGoT which outperform by linear function method (Table 4.23). In this process, there is no theoretical background about how many hidden layers and node to be appropriate, thus must be determine the proper network structure which supported by trial and error. Most importance point to be certain of the ANN approach do better than conventional empirical models which can be deal with the difficulty and complexity as well, and more adaptable with the influences factors that control the sources of primary productivity in the coastal zone (Scardi and Harding, 1999). ANN model indicated the sufficient tools for estimating the contribution of specific constituents, such as chl-a, TSS and CDOM (Canziani, Ferrati, Marinelli, and Dukatz, 2008).

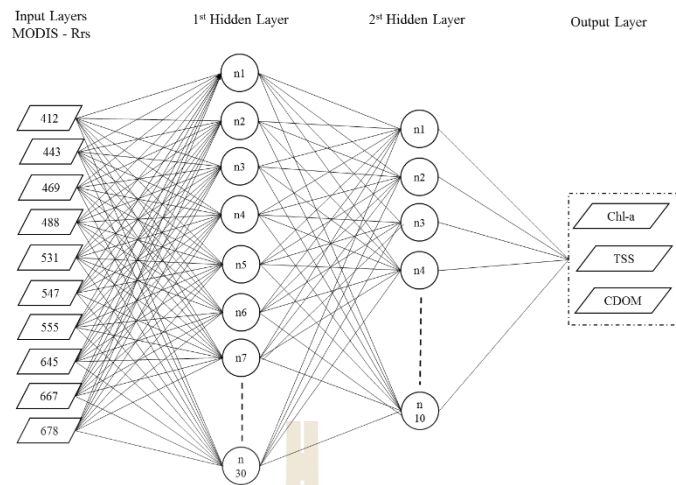


Figure 4.21 ANN structure for the Chl-a/TSS/CDOM prediction from MODIS data.

Table 4.12 Detail of input parameters for the applied ANN model.

Variables	Name of input files
Dependent variable	Chl-a of Cruise 4
Independent variable 1	a27042004_band_412
Independent variable 2	a27042004_band_443
Independent variable 3	a27042004_band_469
Independent variable 4	a27042004_band_488
Independent variable 5	a27042004_band_531
Independent variable 6	a27042004_band_547
Independent variable 7	a27042004_band_555
Independent variable 8	a27042004_band_645
Independent variable 9	a27042004_band_667
Independent variable 10	a27042004_band_678
Training mask file	NONE
Study area mask file	NONE

Table 4.13 Details of the parameter and performance data of the applied ANN model.

Parameters	Performance
Application type	Regression
Input layer neurons	10
Hidden layers	2
Hidden layer 1 neurons	30
Hidden layer 2 neurons	10
Output layer neurons	1
Maximum requested samples	1000
Final learning rate	0.01
Momentum factor	0.5
Sigmoid constant	1
Acceptable RMS	0.01
Iterations	10000
Training RMS	0.0831
Testing RMS	0.0974
R square	0.7854

Table 4.14 Weights information of neurons across layers;

(1) Weights between input layer neurons and hidden layer 1 neurons.

i-Neuron	h1-Neuron														
	1	2	3	4	5	6	7	8	9	10	11	12	13	14	15
1	-0.1213	-0.4924	-0.7567	0.1433	0.0723	-0.5259	0.2662	-0.0312	0.0819	0.0076	0.3448	1.0952	0.2949	-0.1171	-0.3207
2	-0.2649	-0.4631	-0.0735	-0.0642	0.1296	-0.4452	0.8174	0.0564	-0.2923	0.4352	0.2013	0.4472	-0.0030	-0.5540	-0.1784
3	-0.4081	0.0415	-0.3307	-0.1475	0.0626	-0.1353	0.4620	0.1644	0.0026	-0.1226	-0.0782	0.2601	0.0751	-0.0714	-0.1092
4	-0.1588	-0.1015	-0.3940	0.0519	0.1167	-0.0346	0.2301	0.1004	0.0065	-0.1746	0.1308	0.5642	-0.1268	-0.2802	-0.2514
5	0.0114	0.1551	-0.7549	0.1754	0.1984	0.3175	-0.4551	0.1025	0.3617	-0.2142	0.1075	0.7076	-0.4058	0.2923	0.1799
6	0.3794	0.2969	-0.5521	0.0030	-0.0561	0.5059	-0.2013	-0.1121	0.1416	-0.1699	0.0870	0.7027	-0.1220	0.4002	0.3336
7	0.4681	-0.0642	-0.4540	-0.1719	0.0735	0.3391	-0.4002	-0.1276	0.4099	-0.1361	0.0768	0.8243	-0.1813	0.2884	0.3731
8	0.6872	0.8399	-0.7536	-0.1308	-0.1904	0.7859	-1.0855	-0.2175	0.6090	-0.6202	0.2623	1.1259	-0.4197	0.7995	0.1159
9	0.6721	0.8097	-0.7866	-0.1514	-0.1341	0.7755	-0.8983	-0.0575	0.1769	-0.5276	0.2684	1.0803	-0.3748	0.6028	0.4504
10	0.3931	0.7859	-0.8147	0.2402	0.0403	0.8512	-1.2202	0.0574	0.2818	-0.5374	0.0721	1.0435	-0.2364	0.5984	0.3894

(Continued)

i-Neuron	h1-Neuron														
	16	17	18	19	20	21	22	23	24	25	26	27	28	29	30
1	-0.4350	1.6785	-0.0053	-0.1237	0.4445	0.4129	0.3325	-0.1988	0.2784	-0.3311	0.6245	-0.2876	-0.3599	0.4369	0.3090
2	-0.6483	0.8832	0.3528	-0.8311	0.7620	0.2547	0.6839	0.2496	0.4332	0.0802	0.2438	0.2398	-0.6124	0.3645	0.4969
3	-0.0604	0.4334	0.1168	-0.3653	0.2546	0.2510	-0.0402	-0.1083	0.2871	0.0390	0.1968	-0.0611	-0.3644	0.2880	0.1153
4	-0.0803	0.9853	0.0862	0.1555	-0.1623	0.0213	-0.0379	-0.2460	-0.0130	-0.2407	0.3105	-0.1681	-0.0714	0.2236	-0.1420
5	0.3147	1.3640	-0.4820	0.5032	-0.4691	-0.3226	-0.4050	-0.0181	-0.3202	0.1194	0.5615	-0.5219	0.4295	-0.2260	-0.1275
6	0.3512	1.1055	-0.4247	0.2917	-0.2112	-0.0518	-0.2407	-0.5148	-0.1611	-0.2896	0.5724	-0.4737	0.5095	-0.3491	-0.2553
7	0.3755	1.0204	0.0159	0.2764	-0.0640	-0.1830	-0.0878	-0.1171	-0.4309	-0.2924	0.2704	-0.4843	0.4552	-0.2205	-0.0922
8	0.9786	1.2019	-0.7623	0.9697	-0.9290	-0.3951	-0.5733	-0.1740	-0.4374	0.2041	0.9013	-0.9397	1.1173	-0.8907	-0.7638
9	0.8989	1.3121	-0.5033	0.9901	-0.5667	-0.8017	-0.5439	-0.0780	-0.7870	0.1257	0.8853	-0.5942	0.6552	-0.7537	-0.7728
10	0.8583	1.4050	-0.6348	0.8880	-1.0507	-0.8016	-0.7442	-0.2081	-0.4794	0.1058	0.7074	-0.6640	0.7829	-0.8996	-0.4431

Table 4.15 Weights information of neurons across layers;

(2) Weights between hidden layer 1 neurons and hidden layer 2 neurons.

Neuron	h2-Neuron									
	1	2	3	4	5	6	7	8	9	10
h1-Neuron 1	-0.2850	0.2184	-0.1550	0.1637	-0.1680	-0.4864	-0.8950	-0.4804	-0.1619	-0.2674
h1-Neuron 2	-0.4127	0.0884	0.0189	0.3145	0.0298	-0.0458	-1.1430	-0.6213	-0.5647	-0.2989
h1-Neuron 3	0.4417	0.1685	0.2484	-0.1006	0.0271	0.1643	0.9908	0.7791	0.2977	0.9283
h1-Neuron 4	-0.2286	-0.1883	-0.0197	0.0234	-0.0056	0.2361	0.1913	-0.0742	-0.2095	-0.1708
h1-Neuron 5	0.0702	-0.1417	-0.1414	-0.0402	0.0814	0.0128	0.2599	-0.0941	-0.1604	0.1621
h1-Neuron 6	-0.6206	0.0939	-0.4030	0.2641	-0.0024	-0.3408	-1.1635	-0.4107	-0.6711	-0.7057
h1-Neuron 7	0.3252	-0.1618	-0.0679	-0.2482	0.0659	0.6910	1.8110	0.7014	0.6579	1.0456
h1-Neuron 8	-0.1857	0.1745	-0.1635	0.1945	0.0667	0.3270	0.2639	-0.0889	-0.0273	0.0598
h1-Neuron 9	-0.0435	0.2345	-0.2201	-0.0555	0.0826	-0.3655	-0.4600	-0.1392	-0.3225	-0.5021
h1-Neuron 10	0.4657	-0.3209	0.1517	0.3128	0.1167	0.7583	0.7293	0.6307	0.2551	0.7488
h1-Neuron 11	-0.2635	0.1805	-0.1468	-0.2415	0.1077	-0.4205	-0.1524	-0.0813	-0.1030	0.1537
h1-Neuron 12	-0.7179	-0.2777	-0.2001	0.3565	-0.1569	0.2446	-1.2520	-0.8409	-0.3986	-1.0913
h1-Neuron 13	0.2676	-0.3329	0.0195	-0.0173	-0.0304	0.7190	0.4365	0.4387	0.0638	0.3341
h1-Neuron 14	-0.3242	0.2085	-0.0360	0.3159	-0.2831	-0.1349	-0.9421	-0.6062	-0.2090	-0.4858
h1-Neuron 15	-0.0377	0.0633	-0.2033	0.0858	-0.3058	-0.3569	-0.6400	0.0313	-0.1156	-0.0959
h1-Neuron 16	-0.2991	-0.0040	-0.3152	0.1690	0.0025	-0.2793	-1.0971	-0.7819	-0.6038	-0.9893
h1-Neuron 17	-0.8177	-0.0603	-0.1204	0.3160	-0.1762	0.1141	-1.8837	-1.1666	-0.7243	-1.5472
h1-Neuron 18	0.4796	0.0004	-0.0146	0.1578	-0.2152	0.7637	0.9822	0.5857	0.5969	0.5241
h1-Neuron 19	-0.4888	-0.0015	-0.0305	0.3023	-0.2122	-0.0463	-1.3923	-0.6897	-0.6225	-0.7044
h1-Neuron 20	0.4662	-0.0862	-0.0942	-0.0051	0.1076	0.4566	1.4911	0.5333	0.3243	0.7569
h1-Neuron 21	0.3341	0.0631	0.2321	0.0775	-0.0770	0.4553	1.0519	0.3026	0.2633	0.6493
h1-Neuron 22	0.2369	0.1102	-0.1240	-0.1505	0.1606	0.4111	1.0643	0.6143	0.5401	0.3714
h1-Neuron 23	0.0309	-0.3044	0.2028	0.1347	0.0357	0.6663	0.4094	0.1701	0.1127	0.0217
h1-Neuron 24	0.1735	-0.4130	-0.1974	0.1230	-0.1609	0.8287	0.9978	0.5566	0.3895	0.4242
h1-Neuron 25	0.1719	-0.1703	-0.0397	0.0424	-0.0491	0.3187	-0.3137	0.1278	0.0825	-0.0956
h1-Neuron 26	-0.5190	0.0561	0.0227	0.0802	0.0311	0.1835	-0.6541	-0.8132	-0.5313	-0.9249
h1-Neuron 27	0.3135	0.1243	0.1360	-0.0826	-0.1000	0.5033	1.0058	0.5739	0.6131	0.9895
h1-Neuron 28	-0.5973	0.1985	-0.3072	0.2270	-0.3523	-0.1123	-1.2512	-0.3604	-0.5004	-0.8921
h1-Neuron 29	0.3662	0.0824	0.0429	-0.1294	-0.0461	0.6949	1.3555	0.6801	0.2420	0.6191
h1-Neuron 30	0.4403	-0.2395	0.2204	-0.1484	0.0247	0.4798	0.9535	0.4773	0.4975	0.4733

Table 4.16 Weights information of neurons across layers;

(3) Weights between hidden layer 2 neurons and output layer neurons network.

Neuron	Weights
H2-Neuron 1	-1.2480
H2-Neuron 2	-0.8286
H2-Neuron 3	0.2440
H2-Neuron 4	-0.7605
H2-Neuron 5	0.0055
H2-Neuron 6	1.8679
H2-Neuron 7	-4.5841
H2-Neuron 8	-2.1169
H2-Neuron 9	-1.3838
H2-Neuron 10	-2.6794

Table 4.17 Sensitivity of model to forcing independent variables to be constant;

(1) Forcing a single independent variable to be constant.

Model	R-square	Influence order
With all variables	0.7854	N/A
Var. 1 constant	0.7724	6
Var. 2 constant	0.7004	1 (most influential)
Var. 3 constant	0.7788	8
Var. 4 constant	0.7857	10 (least influential)
Var. 5 constant	0.7666	5
Var. 6 constant	0.7750	7
Var. 7 constant	0.7789	9
Var. 8 constant	0.7542	2
Var. 9 constant	0.7567	3
Var. 10 constant	0.7573	4

Table 4.18 Sensitivity of Model to forcing independent variables to be constant;

(2) Forcing all independent variables except one to be constant.

Model	R-square
With all variables	0.7854
All constant but var. 1	0.0000
All constant but var. 2	0.0000
All constant but var. 3	0.0000
All constant but var. 4	0.0000
All constant but var. 5	0.0880
All constant but var. 6	0.0133
All constant but var. 7	0.0000
All constant but var. 8	0.1406
All constant but var. 9	0.0938
All constant but var. 10	0.1292

Table 4.19 Sensitivity of model to forcing independent variables to be constant;

(3) Backwards stepwise constant forcing.

Model	Variables included	R-square
With all variables	All variables	0.7854
Step 1: var.[4] constant	[1,2,3,5,6,7,8,9,10]	0.7857
Step 2: var.[4,3] constant	[1,2,5,6,7,8,9,10]	0.7806
Step 3: var.[4,3,7] constant	[1,2,5,6,8,9,10]	0.7826
Step 4: var.[4,3,7,1] constant	[2,5,6,8,9,10]	0.7654
Step 5: var.[4,3,7,1,6] constant	[2,5,8,9,10]	0.7467
Step 6: var.[4,3,7,1,6,2] constant	[5,8,9,10]	0.6576
Step 7: var.[4,3,7,1,6,2,5] constant	[8,9,10]	0.6762
Step 8: var.[4,3,7,1,6,2,5,9] constant	[8,10]	0.5324
Step 9: var.[4,3,7,1,6,2,5,9,10] constant	[8]	0.1406

Table 4.20 Summary of coefficient and wavebands influence results of ANN model based on Chl-a assessment.

Cruise no.	Satellite Date	MODIS R ²	wavelengths Influence Order of MODIS	
			Most influential (nm)	Least influential (nm)
1	A1010-2003	0.29	488-B	412-B
1	A2810-2003	0.69	469-B	531-G
1	T2810-2003	0.75	469-B	645-R
2	A0412-2003	0.71	488-B	443-B
2	A0612-2003	0.68	488-B	443-B
2	T0412-2003	0.80	488-B	443-B
2	T0612-2003	0.72	412-B	443-B
3	A1601-2004	0.62	469-B	443-B
3	T1601-2004	0.55	412-B	645-R
3	T0701-2004	0.46	469-B	645-R
4	A2704-2004	0.79	443-B	488-B
4	A3105-2004	0.80	443-B	678-R
5	T1510-2004	0.83	412-B	469-B
5	A3110-2004	0.67	555-B	645-R
5	T3110-2004	0.62	412-B	469-B

Table 4.21 Summary of coefficient and wavebands influence results of ANN model based on TSS assessment.

Cruise no.	Satellite Date	MODIS R ²	wavelengths Influence Order of MODIS	
			Most influential (nm)	Least influential (nm)
1	A1010-2003	0.60	488-B	678-R
1	A2810-2003	0.80	469-B	443-R
1	T2810-2003	0.72	469-B	645-R
2	A0412-2003	0.80	488-B	443-B
2	A0612-2003	0.87	443-B	547-G
2	T0412-2003	0.90	547-G	488-B
2	T0612-2003	0.88	412-B	488-B
3	A1601-2004	0.77	488-B	443-B
3	T1601-2004	0.74	531-G	469-B
3	T0701-2004	0.70	412-B	678-R
4	A2704-2004	0.69	443-B	469-B
4	A3105-2004	0.85	412-B	645-R
5	T1510-2004	0.76	412-B	469-B
5	A3110-2004	0.79	555-G	667-G
5	T3110-2004	0.68	443-B	488-B

Table 4.22 Summary of coefficient and wavebands influence results of ANN model based on CDOM assessment.

Cruise no.	Satellite Date	MODIS R ²	wavelengths Influence Order of MODIS	
			Most influential (nm)	Least influential (nm)
1	A1010-2003	0.80	488-B	443-B
1	A2810-2003	0.82	469-B	488-B
1	T2810-2003	0.77	469-B	678-R
2	A0412-2003	0.64	412-B	678-R
2	A0612-2003	0.69	488-B	667-R
2	T0412-2003	0.70	412-B	443-B
2	T0612-2003	0.68	412-B	678-R
3	A1601-2004	0.88	678-R	469-B
3	T1601-2004	0.89	412-B	469-B
3	T0701-2004	0.85	531-G	645-R
4	A2704-2004	0.85	412-B	531-B
4	A3105-2004	0.94	469-B	531-B
5	T1510-2004	0.79	443-B	645-R
5	A3110-2004	0.88	412-B	488-B
5	T3110-2004	0.53	443-B	645-R

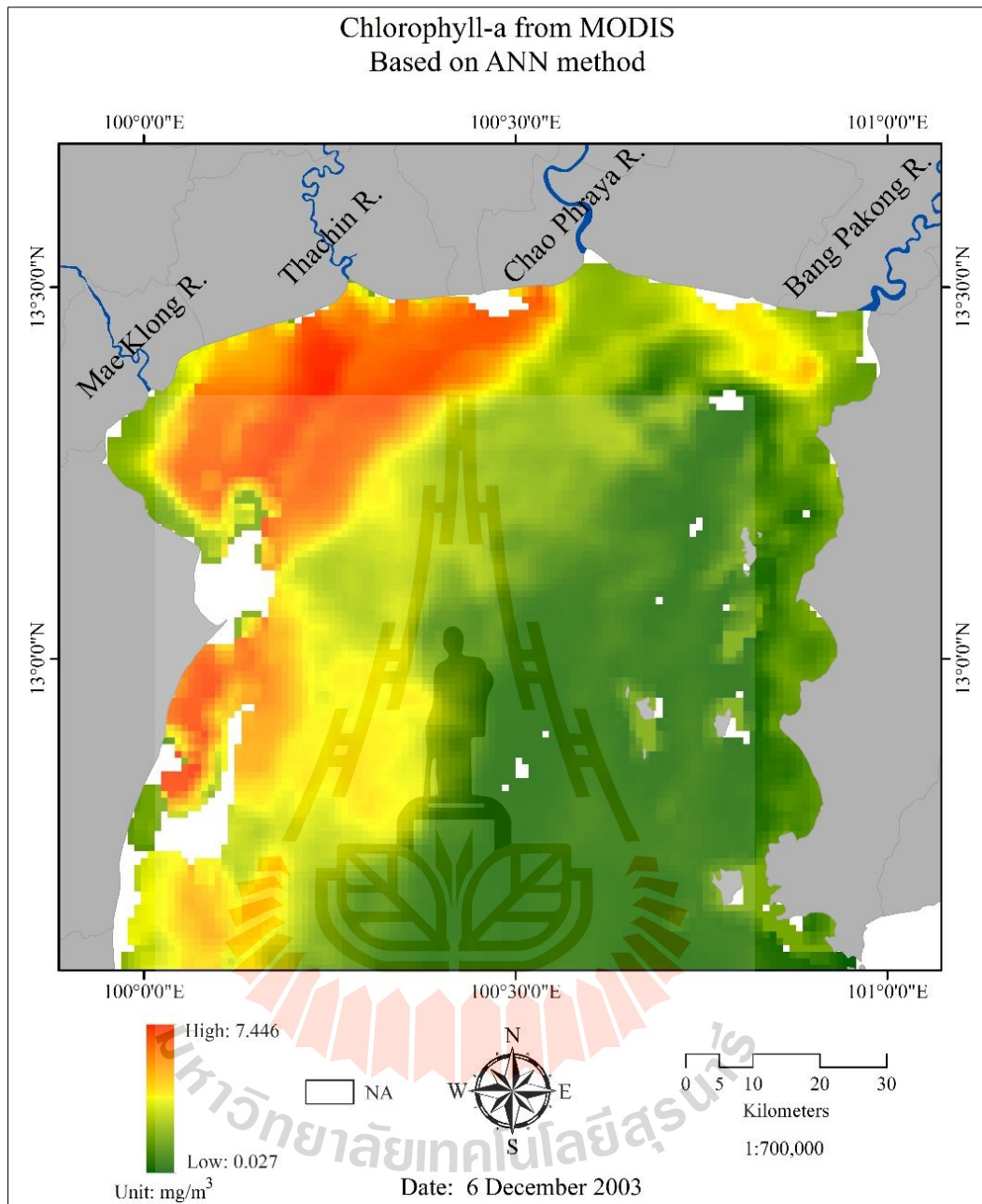


Figure 4.22 Example of Chl-a concentration map derived by the applied ANN model.

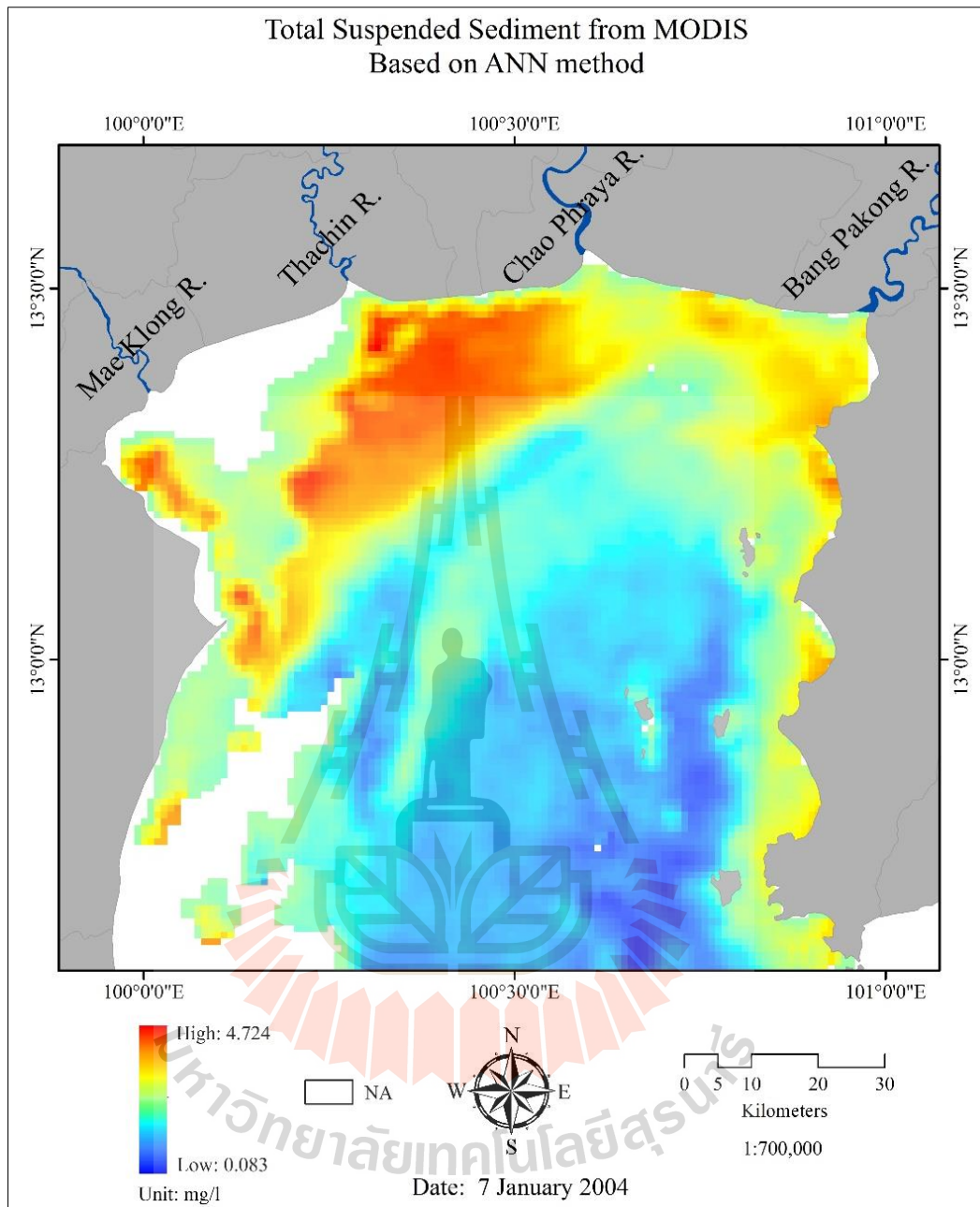


Figure 4.23 Example of TSS concentration map derived by the applied ANN model.

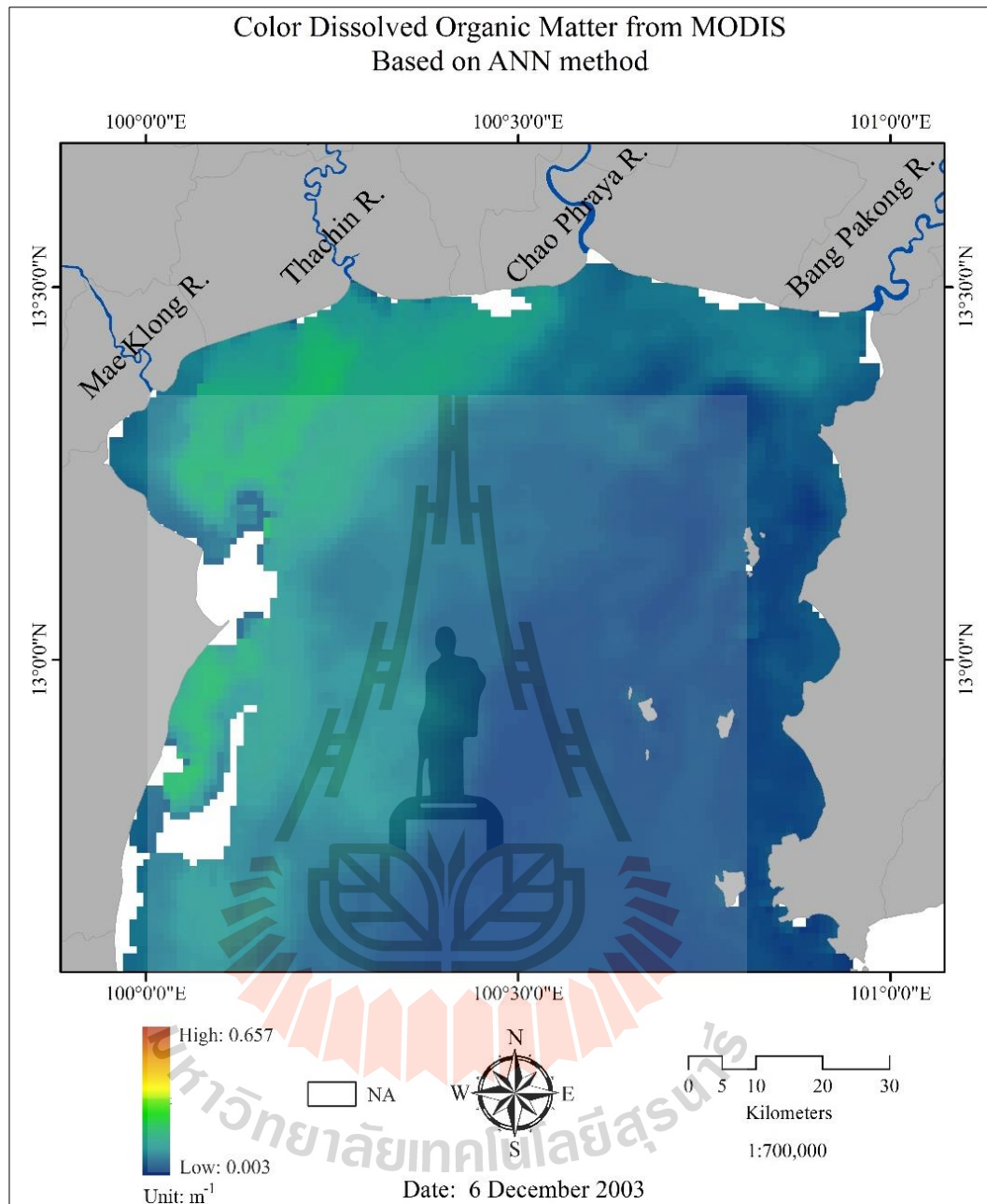


Figure 4.24 Example of CDOM concentration map built by the applied ANN model.

Statistical of three water constituents based on ANN models are computed and then be compared with the results from empirical model, thus both of ANN and empirical maps are validated by four imageries which coincide from in situ data. Here, the empirical maps of all components are used the preference models as aforementioned. Table 4.23 summarizes observed efficiency in concentration determination for each studied constituent by the used ANN model and the preferred empirical models (in terms of R^2 and RMSE) reported earlier. In general, the gained ANN results seem to remarkably outperform those of the empirical one in all cases of listed constituents. However, due to its rather complicated structure and somewhat lengthy (and not well comprehensible) computing process, the true merit of its routine application compared to the preferred empirical one (with simple/straightforward working structure) should be a subject of further intensive investigation.

Table 4.23 Comparison of ANN and empirical models performance.

Type of Models	Statistical	Chl-a	TSS	CDOM
ANN	R-square	0.87	0.92	0.94
	RMSE	1.59	0.85	0.21
Empirical	R-square	0.76	0.84	0.85
	RMSE	3.57	1.39	0.20

4.5 Conclusion

The research in this part was conducted to identify the appropriate models for estimating selected key water constituents in UGoT area. In-situ data collected from five past field surveys were used for model development and verification at first then suitable MODIS L2 reflectance data were applied as a replacement for the respective original reflectance data gained from the in-situ measurements. Yielded results of this study indicate that Chl-a concentration was normally high near the main river mouths and relatively low further away into the central region. Spatial variations of TSS and CDOM concentration were similar to that of the Chl-a but their temporal variations were different. High CDOM was always bound to river mouths with specific locations changed with time. PRR characteristics displayed similar trends in all field-survey cruises. Reflectance at green bands were found dominant at stations 1 to 7 (near river mouths) and red bands regularly had lowest reflectance rate in all considered cruises. Finally, three respective empirical models (for the determination of Chl-a, TSS and CDOM concentration over UGoT area) were established based on the best outcome of statistical analysis in terms of R^2 , RMSE and MAPE. These were OC3M (for Chl-a), TSM (for TSS) and Chula models (for CDOM), respectively.

Results from this work emphasize the importance of the blue/green band ratio application in all selected empirical models mentioned earlier which was also reported in other works (satellite-based analysis). For examples, Islam and Tat (2001) reported that the optimal model for Chl-a determination was OC2-v4 (based on SeaWiFs data), also Marghany and Hashim (2010) identified the best blue/green band ratio for their work using Aiken model (MODIS-based). Furthermore, O'Reilly et al. (2000), found that the blue/green band ratio was the best overall single band ratio index seen in their

work. However, the red/green band ratio was also applied in some cases, e.g. Le et al. (2012) used it to develop local non-linear regression model for the estimation of Chl-a concentration from MODIS data.

In addition, the artificial neural network (ANN) was proved to be a promising tool for mapping key constituent concentration over UGoT from associated MODIS reflectance data. As seen here, the multi-layer perceptron neural network (MLP-NN) model with back propagation (BP) algorithm (and the structure model of 10:30:10:1) was able to provide high accuracy in the determination of all considered constituents with R^2 of 0.87 for Chl-a, 0.92 for TSS, and 0.94 for CDOM. These accuracy results were showed better than the empirical model by 0.76 for Chl-a, 0.84 for TSS and 0.85 for CDOM. This finding is similar to that of Kishino, Tanaka and Ishizaka, (2005) which revealed reasonably accurate output of TSS and Chl-a while CDOM was not reliable. In addition, Palani, Liong and Tkalich, (2008) suggested that ANN had great potential to water quality prediction to increase efficiency in generating needed unavailable data for the water quality model.

CHAPTER V

MODIS-BASED MONITORING OF COASTAL ENVIRONMENT IN THE UPPER GULF OF THAILAND

This chapter describes the application of MODIS data for monitoring concentrations (spatial and temporal variations) of the three target constituents: Chl-a, TSS and CDOM during years from 2010 to 2012 over UGoT area. In addition, the trophic states of UGoT during this time were also assessed based on knowledge of Chl-a data. MODIS/Aqua-Terra level 2 dataset were applied to fulfill the primary need of work in this part which is to evaluate the impact of mega-flooding event over central Thailand in late 2011 on the subsequent coastal environment situation of the UGoT.

5.1 Main river discharges into the UGoT

Basically, the amount of rainfall and subsequent surface water in Thailand is under strong influence of the occupying monsoonal systems over the area. These comprise of the SW monsoon, which brings rain to most part of Thailand during wet season, and the NE monsoon, which brings cold air and dryness to Thailand during country's winter period and takes moisture over the Thai Gulf to become rain along the eastern part of the south during that time as (Table 5.1). The seasonal fluctuation of rainwater as such has led to similar change in water discharges of the main rivers across

the country as shown in Figure 5.1. There are four main rivers in central Thailand: Mae Klong, Thachin, Chao Phraya and Bang Pakong, which are the main contributors of nutrient and freshwater for UGoT, especially the Chao Phraya River (Figure 5.1 and Table 5.2).

River discharge data in Tables 5.4 and Figure 5.1 displayed distinctively high volume for the Chao Phraya River in the year 2011 compared to that of the year 2010 and 2012 due primarily to mega flooding occurrence over central Thailand in that year (August-December). Table 5.3 shows the annual rainfall of four main river basin from the past years from 1985 to 2014.

Table 5.1 Monsoonal seasons in Thailand.

Periods	Monsoon	Seasonal
November-January	North-East	Dry
February-April	North-East to South-West	Dry
May-August	South-west	Wet
September-October	South-west to North-East	Wet

Source: Buranapratheprat et al., 2002.

Table 5.2 Main river discharges into UGoT in year 1997.

	River name			
	Mae Klong	Thachin	Chao Phraya	Bang Pakong
Drainage area (km ²)	30,837	14,199	160,000	8,706
Length (km)	520	325	1,352	434
Annually runoff (m ³ /s)	273	3.7	117	9.02
Annual rainfall (mm)	1,146.5	1,390.6	1,487.3	1,895
Land use type Forest	73.35%	7.5%	2.1%	10.6%
Bush	3.65%	-	-	-
Agriculture & city	19.85%	90.8%	92.7%	89.2%
Water resources	3.15%	1.7%	5.2%	0.2%

Source: Shi et al., 2015.

Table 5.3 Annual rainfall of four river basin from years from 1985 to 2014.

River name	mm/year
Mae Klong	1,392.00
Thachin	988.40
Chao Phraya	1,020.60
Bang Pakong	1,305.50

Source: Royal irrigation department, 2015.

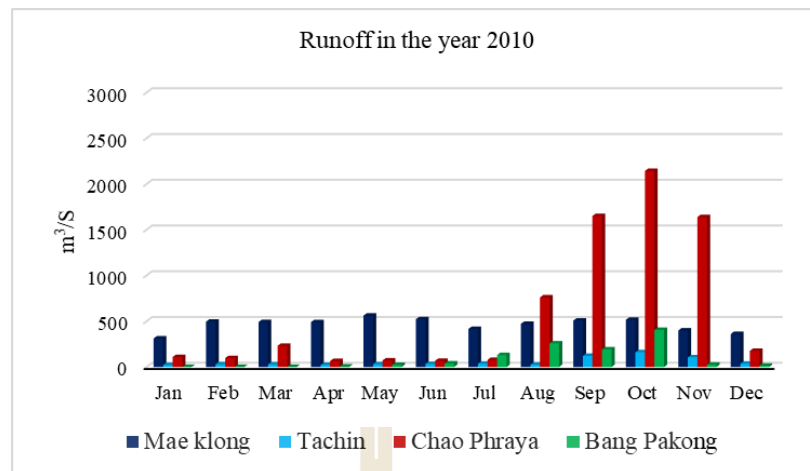
Table 5.4 Annual river discharges into UGoT from years 2010 to 2012.

Unit: m³/s.

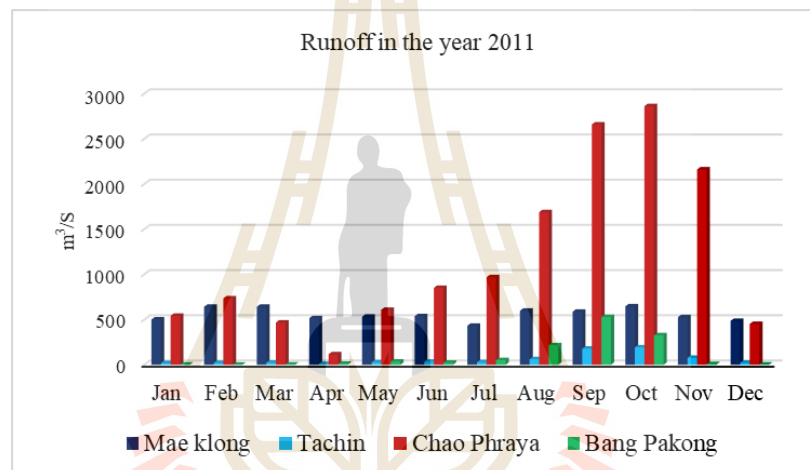
Month	Year 2010				Year 2011				Year 2012			
	MK	TC	CH	BK	MK	TC	CH	BK	MK	TC	CH	BK
January	312.10	22.05	109.57	0.52	501.31	19.59	541.67	2.64	406.81	25.38	46.30	18.77
February	495.64	30.04	96.84	0.52	641.50	20.44	734.57	0.52	448.76	22.95	46.30	17.11
March	490.87	29.14	231.87	1.09	641.66	23.72	467.21	3.16	562.20	23.05	38.19	4.35
April	490.71	23.15	65.59	5.34	515.76	8.99	115.74	10.80	685.55	25.35	116.51	5.88
May	561.71	31.15	71.76	23.50	532.31	27.92	608.02	35.20	569.28	39.70	195.22	5.60
June	523.05	33.92	67.52	39.31	537.15	33.98	850.31	22.63	467.74	35.48	399.31	21.46
July	416.78	36.88	77.93	130.50	431.64	29.10	968.75	51.78	472.63	42.64	202.93	51.05
August	472.30	26.43	761.19	258.69	598.17	61.97	1687.89	216.74	737.14	38.90	257.72	84.76
September	508.25	121.99	1,650.85	193.80	587.33	178.40	2658.56	528.12	788.18	160.82	1519.68	570.24
October	516.00	161.95	2,143.90	406.00	646.53	192.92	2861.11	326.00	702.17	145.02	1066.36	187.21
November	400.38	106.73	1,638.89	26.39	526.33	77.48	2161.27	7.05	552.20	54.18	150.46	31.26
December	361.44	36.60	176.70	14.62	485.04	22.57	451.77	2.95	492.48	24.52	76.39	22.19

MK: Mae Klong River, TC: Thachin River, CH: Chao Phraya River, BK: Bang Pakong River

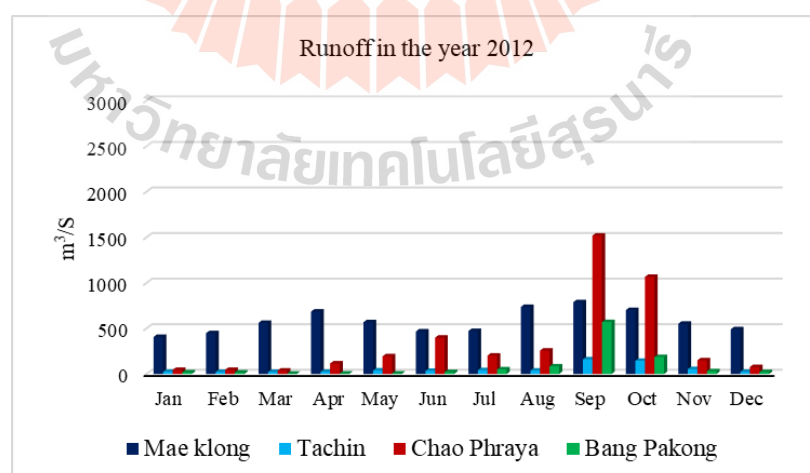
Source: Royal irrigation department, 2015.



a) Four main river discharges in year 2010.



b) Four main river discharges in year 2011.



c) Four main river discharges in year 2012.

Source: Royal irrigation department, 2015.

Figure 5.1 Four main river discharges from years 2010 to 2012.

The disastrous flood is believed to be the impacts of strong La Niña originated in the Pacific Ocean during years from 2010 to 2012. Considerably high rainfall and several strong tropical storms including Haima (June), Nok-Ten (July) and Nesat, Haitang and Nalgae (September and October) occurred in Thailand during those years.

5.2 MODIS-based observations of target constituents in 2010-2012

To evaluate spatial/temporal distributing patterns of the three proposed targets (Chl-a, TSS, CDOM) during the chosen time period (2010 to 2012) over UGoT, monthly concentration maps for each referred constituent were derived through the use of respective optimal retrieval models identified in Chapter IV. These are the OC3M model for Chl-a mapping, the TSM model for TSS mapping and the Chula model for CDOM mapping as detailed in Chapter IV. Here, each monthly map was prepared by the integration of the available daily maps for each studied constituent (using optimal model and daily Aqua/Terra MODIS data). In addition, the local maximum fitting algorithm (LMF) was applied to reduce irregular fluctuation of the originally gained MODIS dataset which make the subsequent analysis more effective. The multiple daily dataset were then proceeded to weekly level in which maximum pixel values were combined to establish the monthly dataset and maps.

5.2.1 Spatial/temporal variations of Chl-a concentration

Figures 5.2-5.4 present yielded monthly Chl-a maps over UGoT area for years 2010 (Figure 5.2), 2011 (Figure 5.3), 2012 (Figure 5.4), respectively. For 2010, high average Chl-a was evidenced in rainy season from June to September, with maximum value of about 91.28 mg/m^3 in September while the lowest concentration

appeared in March (4.68 mg/m^3) (Table 5.5 and Figure 5.5a). High values were often noticed close to shore and the main river mouths, especially those of the Mae Klong and the Thachin Rivers (Figure 5.2). In addition, monthly variation patterns of the maximum and average values of observed Chl-a concentration in year 2010 were similar with peak values for both cases observed in rainy season, especially in July and September (Figure 5.5b). Relatively low values were dominant in dry season.

In 2011, unlike 2010, top values of the derived concentration happened from dry season to early wet season (March to July) as detailed in Table 5.6. The highest value of 104.08 mg/m^3 was observed in June. After that, Chl-a concentration started to decline sharply toward the end of year. The lowest values was witnessed in December (20.608 mg/m^3). The prominent drop in Chl-a from August to December was coincided with large influx of freshwater into UGoT as a result of the 2011 mega flooding over central Thailand (Figure 5.1b). This could dramatically increase the amount of nutrient over the area.

In 2012, more fluctuation was observed for high Chl-a with peak values in April (44.431 mg/m^3), June (46.134 mg/m^3) and October (49.723 mg/m^3) (Figure 5.5 and Table 5.7). Prominent Chl-a was often evidenced close to shore and around the river mouths. However, the highest of the derived Chl-a density was not as high as those in 2011 and 2010. In general, variation patterns of maximum and mean values of Chl-a density in 2012 and 2011 (Figure 5.5) were somewhat resemble with difference to those of the 2010.

Regarded as a normal year, mean/maximum Chl-a concentrations over the area were lowest during dry season (January-April). The data then rose steadily during wet season (May to September) with notable drop in August. This rising trend ended around

September and started to gradually fall from that point onwards throughout winter. This finding was supported by relevant work of Boonkwan (2013) which found the highest diversity index in August and the lowest in March. Thaipichitburapa (2013) also reported higher Chl-a concentration in wet season than in dry season at the Thachin River mouth and nutrients in water were high in almost entire year. Years 2011 and 2012 were regarded as flood-affected years, therefore variation trends of Chl-a over the area (maximum/mean) were expected to have different characteristics compared to those of 2010 (considered a normal year) as described earlier. These differences were evidenced quite clearly during the time of mega-flood appearance (August-December, 2011), when Chl-a density (maximum and mean) dropped significantly compared to those in 2010. However difference was shown when flood's effect gradually declined in 2012 (Figure 5.5).

Like in 2010, maximum Chl-a in 2012 had the peak value in dry season but in different month (December for 2010 and April for 2012). During these three years, the months with most excessive Chl-a distribution in the UGoT seemed to be July and September 2010 and also peak in May and June for 2011 (before storms was attacked). In addition, the missing data in September 2011 might make the thorough analysis, described earlier, uncertain.

Recently, high Chl-a concentration at the Thachin River mouth during years 2010 to 2012 was reported by Chuennyom, Meksumpun, and Meksumpun (2012). Main source of phytoplankton bloom was believed to be some specific land-based activities along the river's floodplain. In addition, Wattayakorn and Jaiboon (2014) found that photosynthesis was larger than decomposition plus bottom release in wet

season while those similar in dry season. Which indicated Chl-a in wet season higher than dry season over the UGoT area.



Figure 5.2 Spatial distribution of monthly Chl-a in year 2010.

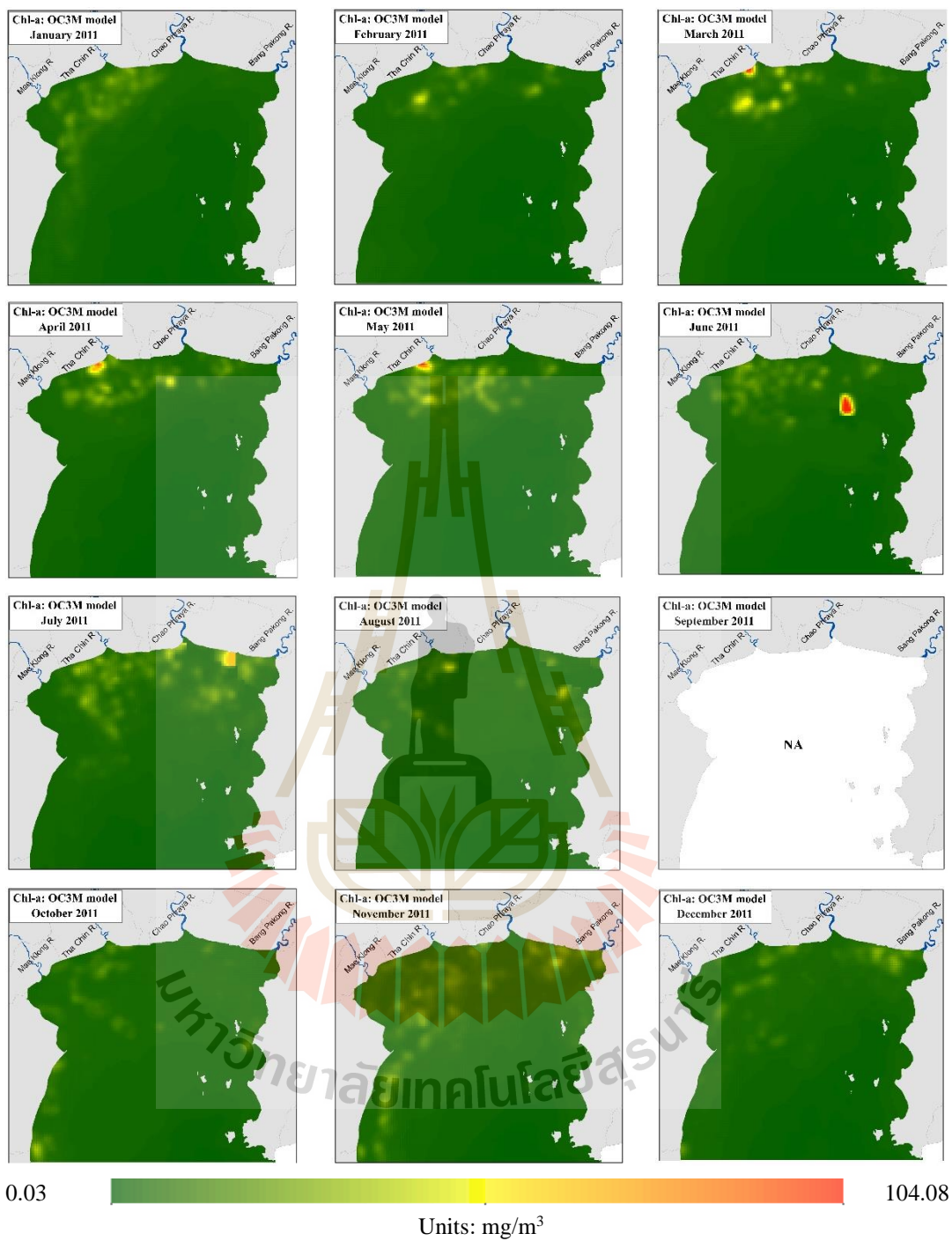


Figure 5.3 Spatial distribution of monthly Chl-a in year 2011.



Figure 5.4 Spatial distribution of monthly Chl-a in year 2012.

Table 5.5 Standard statistics of Chl-a concentration in year 2010.Unit: mg/m³

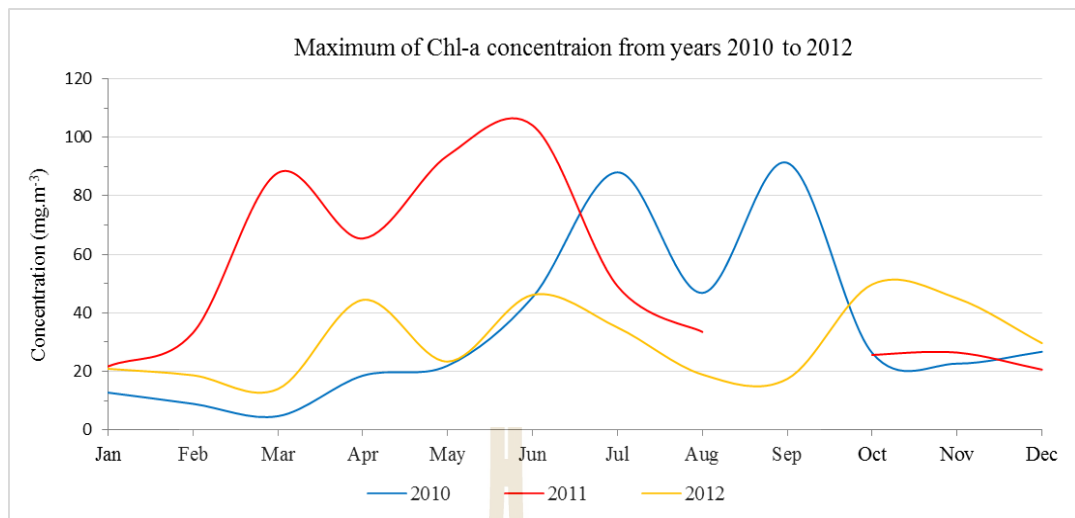
Year 2010	Maximum	Minimum	Mean	Std Dev.
January	12.721	0.218	1.565	1.352
February	8.912	0.243	1.238	0.777
March	4.678	0.299	1.218	0.495
April	18.534	0.249	1.996	2.067
May	21.960	0.273	2.525	2.967
June	45.337	0.449	4.222	5.264
July	88.031	0.318	5.139	7.683
August	46.820	0.377	3.338	4.392
September	91.279	0.318	5.030	8.596
October	26.316	0.420	2.880	2.652
November	22.625	0.409	2.439	2.874
December	26.704	0.359	2.239	2.815

Table 5.6 Standard statistics of Chl-a concentration in year 2011.Unit: mg/m³

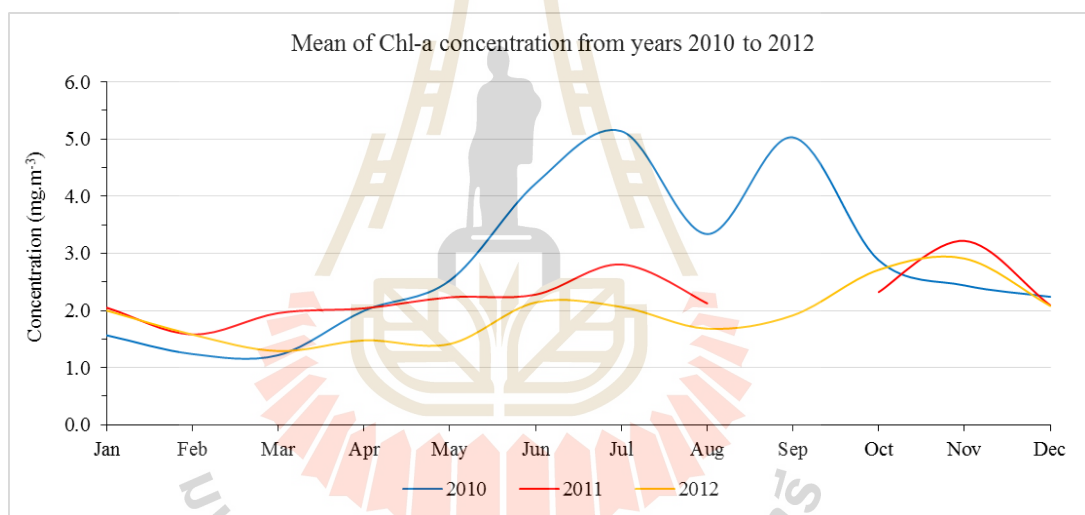
Year 2011	Maximum	Minimum	Mean	Std Dev.
January	21.721	0.311	2.049	2.479
February	33.211	0.177	1.581	2.111
March	87.866	0.130	1.955	4.054
April	65.411	0.109	2.038	3.767
May	93.772	0.097	2.231	4.360
June	104.079	0.096	2.278	5.027
July	49.133	0.100	2.807	4.144
August	33.484	0.428	2.125	2.105
September	NA	NA	NA	NA
October	25.619	0.120	2.323	1.923
November	26.427	0.179	3.219	3.042
December	20.608	0.316	2.091	2.164

Table 5.7 Standard statistics of Chl-a concentration in year 2012.Unit: mg/m³

Year 2012	Maximum	Minimum	Mean	Std Dev.
January	20.880	0.120	1.998	2.479
February	18.665	0.107	1.578	1.777
March	13.971	0.139	1.290	1.000
April	44.431	0.091	1.477	3.059
May	23.345	0.237	1.414	1.294
June	46.134	0.272	2.141	4.057
July	34.986	0.287	2.062	3.081
August	18.915	0.229	1.682	1.678
September	17.427	0.229	1.915	1.977
October	49.723	0.128	2.712	2.792
November	44.967	0.031	2.909	3.993
December	29.640	0.043	2.081	2.522



(a) Maximum concentration of Chl-a.



(b) Mean concentration of Chl-a.

Figure 5.5 Maximum/mean Chl-a concentration from years 2010 to 2012

(OC3M model).

5.2.2 Spatial/temporal variation of TSS concentration

The TSM model was applied on MODIS reflectance data to estimate TSS distribution over UGoT area, and the results are reported as monthly TSS maps during 2010 to 2012 (Figures 5.6-5.8). In general, top values of TSS concentration were commonly located close to shore and the main river mouths like those of Chl-a, especially near the Chao Phraya River (most frequent and dominant), and the Bang Pakong and Mae Klong River (less frequent/outstanding). However, peak values of the maximum or mean for each year might appeared at different months. In 2010, the maximum data tended to gradually increase from dry season to wet season and beyond with two highest peaks in September (61.551 g/m^3) and November (73.004 g/m^3). However, the mean values in 2010 exhibited low fluctuation all year round (with mean value around 3 g/m^3) except some noticeable surge found in September (Table 5.8).

In 2011, peak locations of maximum data occurred in May (38.582 g/m^3) and October (31.420 g/m^3) while mean values decreased from dry season to wet season (Table 5.9). If focus only during wet season (not include September), the concentrations of TSS over UGoT in 2011 (maximum/mean) tended to drop significantly from that of 2010 (the assumed normal year). This finding might be explained by the same reason used for the Chl-a case stated earlier (i.e., from direct influence of exceptionally large amount of freshwater discharge to UGoT in late 2011 contributed from the mega flooding event over central Thailand in that year). In 2011, the TSS pollution was apparently severe in the areas close to the Chao Phraya and Bang Pakong River mouths in May.

However, in 2012 (after the mega-flooding year), TSS density seemed to follow the same normal trend as in 2010 with gradual rise in values from dry season

with a prominent top value in August (58.940 g/m³). The data trend changed in winter with dramatic drop of monthly maximum values toward new year (Table 5.10). For the mean data, a single peak was evidenced in March (4.821 g/m³) and steadily decline throughout the rest of the year (Figure 5.9). Apparently, from May to September, severe TSS pollution was shown at most river mouths, except at the Thachin. The most serious one was at the Chao Phraya River (Figure 5.8), while in winter the situation was normal.

In conclusion, the levels of TSS over the entire UGoT area vary significantly with place and time. This information can be extracted quite well by the available MODIS daily data. In normal year, maximum TSS concentrations tend to be low in dry season and gradually increase toward wet season with peak values during that time. Also, the hotspots for TSS pollution incidences normally occur at the main river mouths, with critical zones often attached to the Chao Phraya River mouth. On the contrary, critical zones of Chl-a were usually found further away from the river mounts. Also Chumnantana (2006) found that the highest TSS concentration was often appeared in August and the lowest in December. Both situations were found located near the Bang Pakong River mouth, similar to this study. However, the occurrence of unexpected influencing factors, like the 2011 mega-flood, might make the thoughtful analysis on this issue (TSS distributing pattern regarding to place/time) much more difficult. According to, Bidorn, Chanyotha, Kish, Donoghue, Bidorn, and Mama (2015), TSS transported from the Chao Phraya River basin into UGOT in mega flooding year was more than twice of the 60 years average. However, as found in this study, impact of this sharp increase of nutrient loading into the area (through the Chao Phraya River).

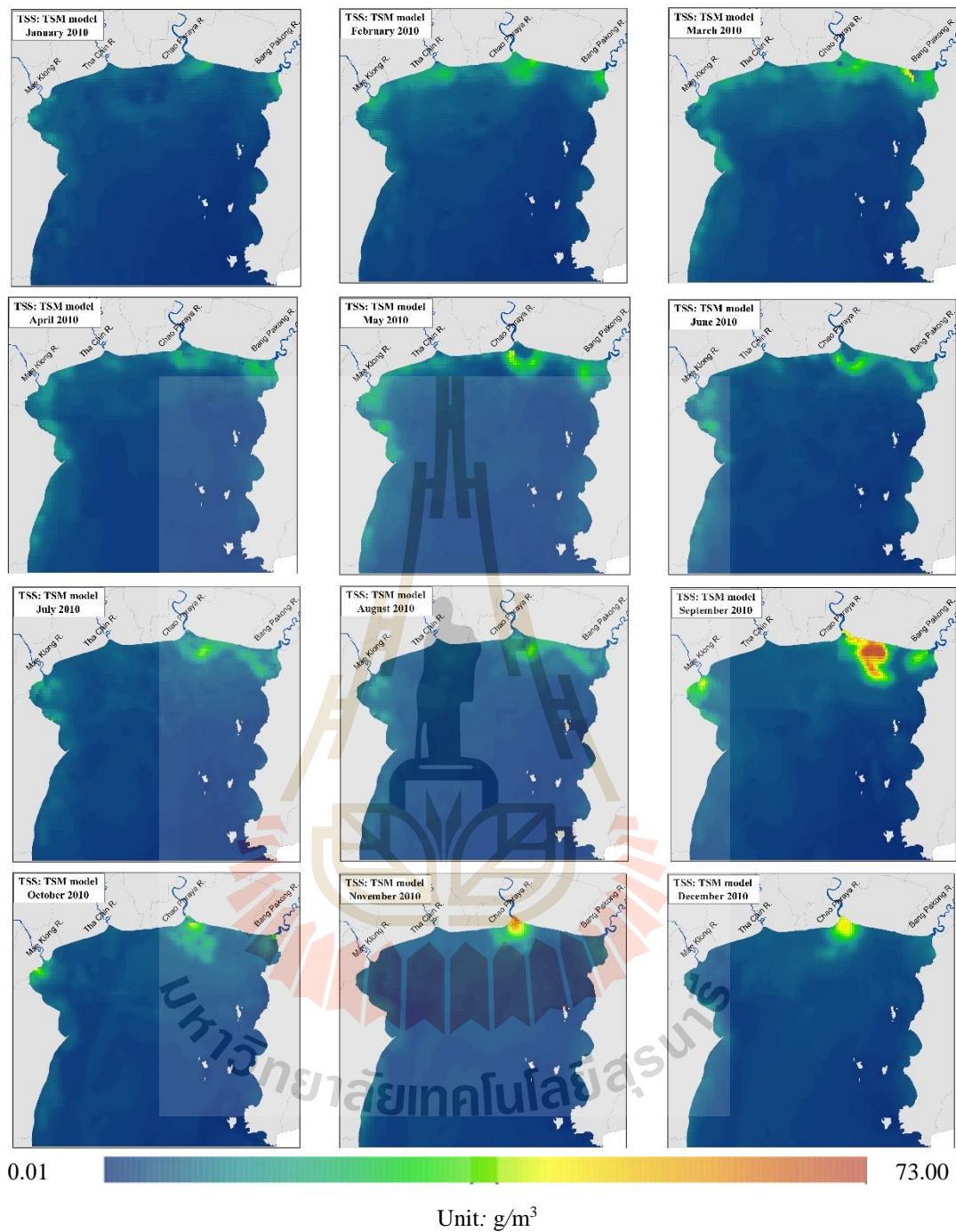


Figure 5.6 Spatial distribution of monthly TSS in year 2010.

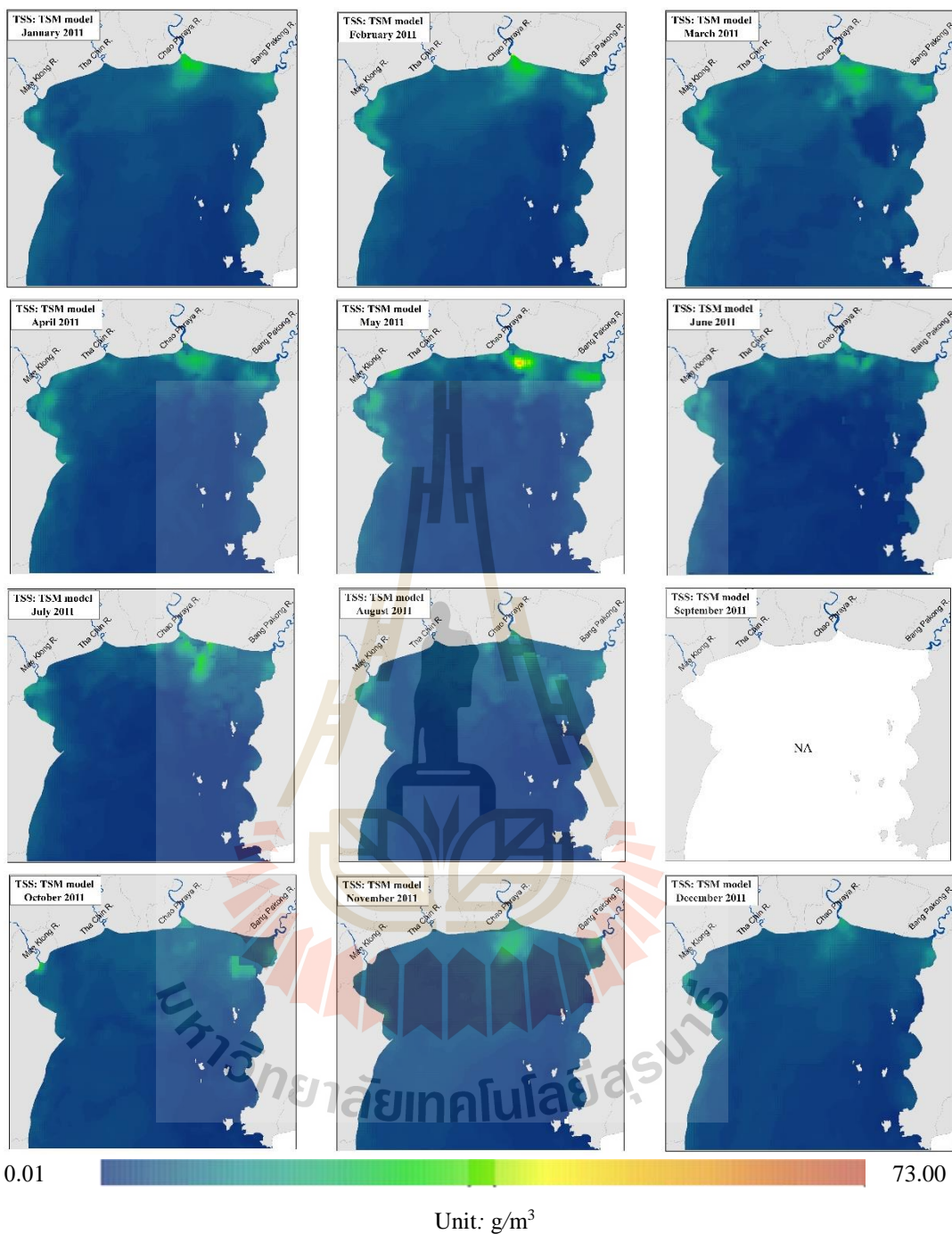


Figure 5.7 Spatial distribution of monthly TSS in year 2011.

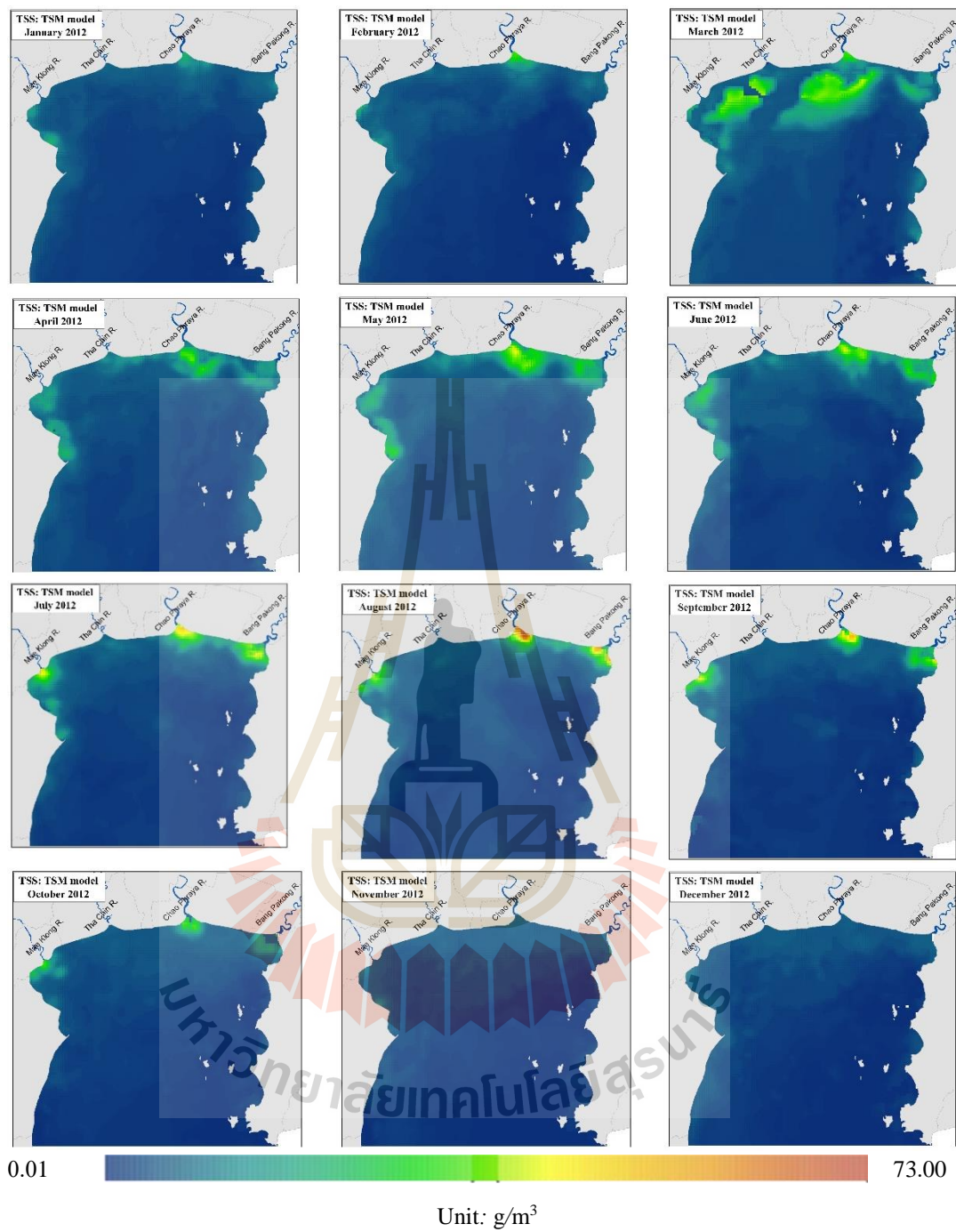


Figure 5.8 Spatial distribution of monthly TSS in year 2012.

Table 5.8 Standard statistics of TSS concentrations in year 2010.Unit: g/m³

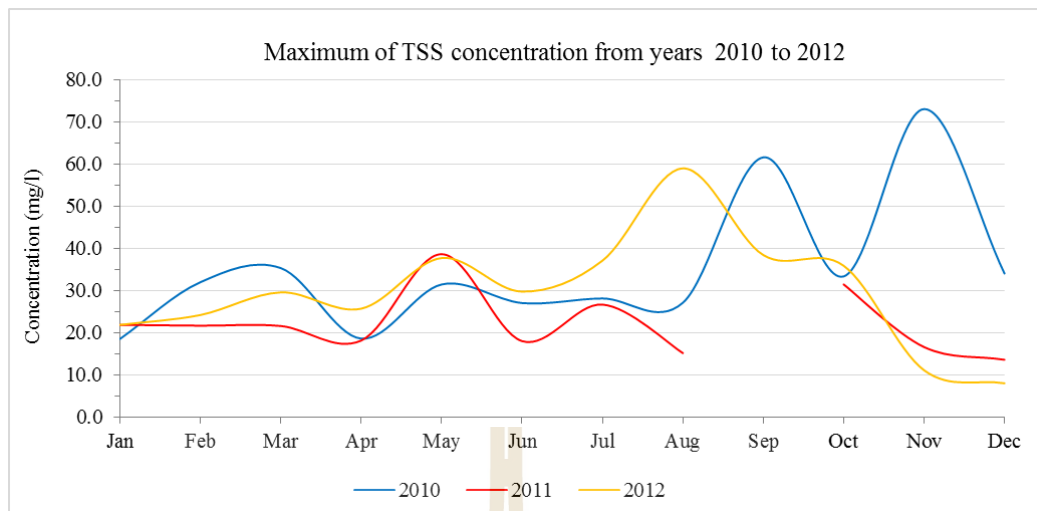
Year 2010	Maximum	Minimum	Mean	Std Dev.
January	18.459	0.049	2.648	1.776
February	31.940	0.113	3.381	3.088
March	35.281	0.278	3.598	3.093
April	18.551	0.462	3.154	2.320
May	31.397	0.525	3.547	3.252
June	26.997	0.358	3.164	2.548
July	28.076	0.011	2.942	2.432
August	27.063	0.064	2.901	2.360
September	61.551	0.011	4.227	6.481
October	33.307	0.055	2.977	2.424
November	73.004	0.222	2.989	3.405
December	33.996	0.244	3.090	2.825

Table 5.9 Standard statistics of TSS concentrations in year 2011.Unit: g/m³

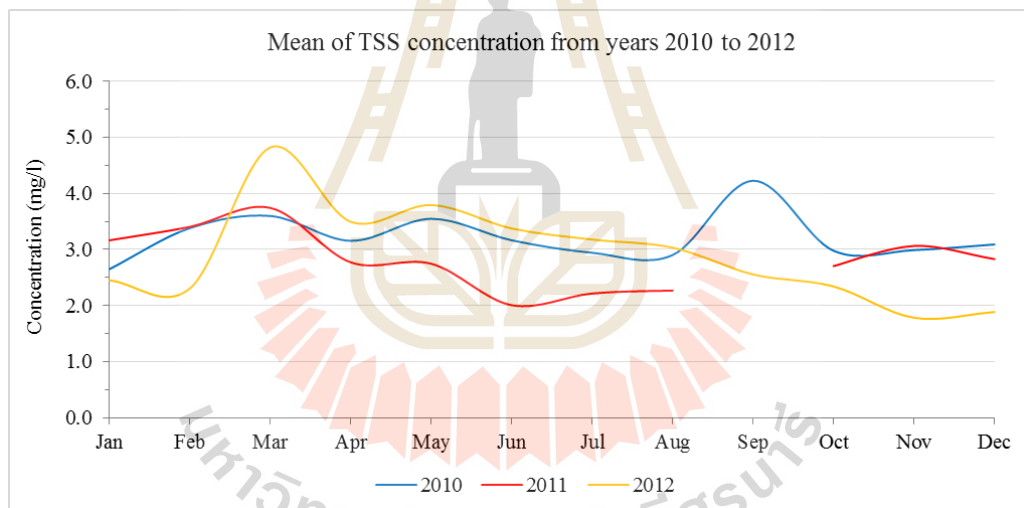
Year 2011	Maximum	Minimum	Mean	Std Dev.
January	21.809	0.290	3.164	2.131
February	21.618	0.079	3.403	2.526
March	21.543	0.058	3.742	2.319
April	18.092	0.061	2.770	2.427
May	38.582	0.061	2.745	3.231
June	17.955	0.011	2.006	1.950
July	26.636	0.016	2.215	2.424
August	15.119	0.028	2.267	1.800
September	NA	NA	NA	NA
October	31.420	0.210	2.703	1.650
November	16.538	0.050	3.062	1.913
December	13.533	0.115	2.827	1.513

Table 5.10 Standard statistics of TSS concentrations in year 2012.Unit: g/m³

Year 2012	Maximum	Minimum	Mean	Std Dev.
January	18.613	0.329	2.449	1.675
February	24.153	0.056	2.305	2.122
March	29.520	0.014	4.821	5.206
April	25.655	0.272	3.493	2.943
May	32.455	0.567	3.793	3.944
June	29.694	0.016	3.374	3.647
July	37.044	0.016	3.177	4.241
August	58.940	0.016	3.032	4.475
September	38.380	0.026	2.554	3.550
October	26.107	0.041	2.340	2.385
November	11.026	0.013	1.781	1.304
December	7.955	0.012	1.884	1.335



(a) Maximum concentration of TSS.



(b) Mean concentration of TSS.

Figure 5.9 Maximum/mean TSS concentration from years 2010 to 2012 (TSM model).

5.2.3 Spatial/temporal variations of CDOM concentration

In the case of the CDOM, Chula model was used for CDOM mapping from years 2010 to 2012 presented in Figures 5.10-5.13 and Tables 5.11-5.13, respectively. In general, places with relatively high amount of CDOM concentration were found more widespread into the deep water zone away from the main river mouths than those of Chl-a or TSS reported earlier. Naturally, biogeochemical processes are proportionally related to the volume of CDOM which are originated from terrestrial environment and transported to coastal zone. As seen in Figure 5.13, for the maximum data of CDOM concentration, similar gradual increasing trends from late dry season towards the end of wet season were observed in years 2010 and 2012 with peak values of both years arose in September (at around 2.0 m^{-1}) while base data in dry season were rather constant at around 1.0 m^{-1} for all months. This means, most serious situations of CDOM pollution were tended to appear in wet season, especially, on final months of the season. However, in 2011, the apparent peak location for the CDOM maximum data was shifted to be in June (at 1.980 m^{-1}) instead and they seem to maintain a downward moving trend thereafter (contrary to what found in 2010 and 2012).

In terms of mean concentration data, their variation patterns look closely resemble each other in those three years with high-value during winter and dry months and the low-value in wet season. This information indicates that moderate/high levels of CDOM incidence should be found more widespread during dry/winter months from 2010 to 2012 than those in wet season of those years (as illustrated in Figures 5.10 to 5.12).

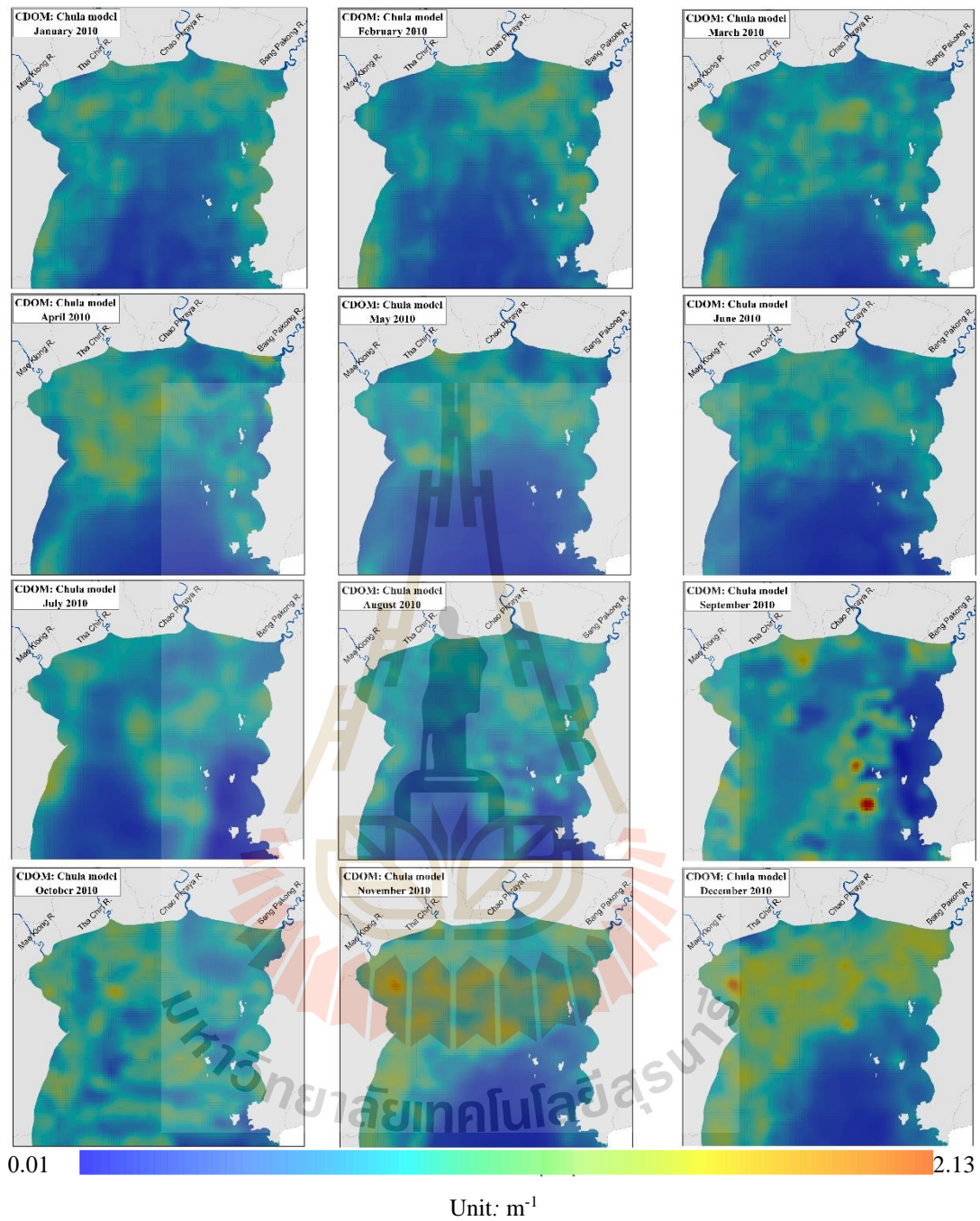


Figure 5.10 Spatial distributions of monthly CDOM in year 2010.

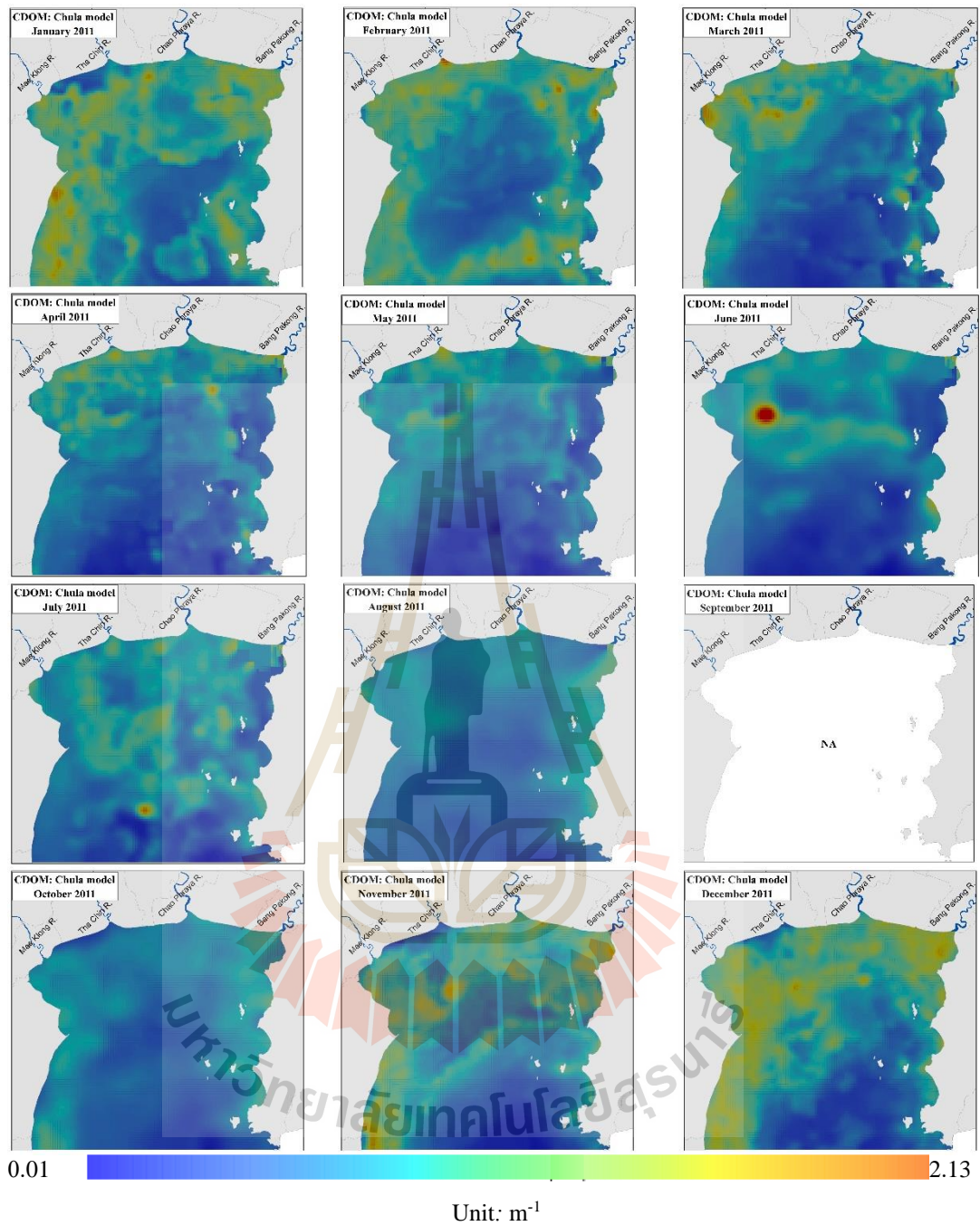


Figure 5.11 Spatial distributions of monthly CDOM in year 2011.

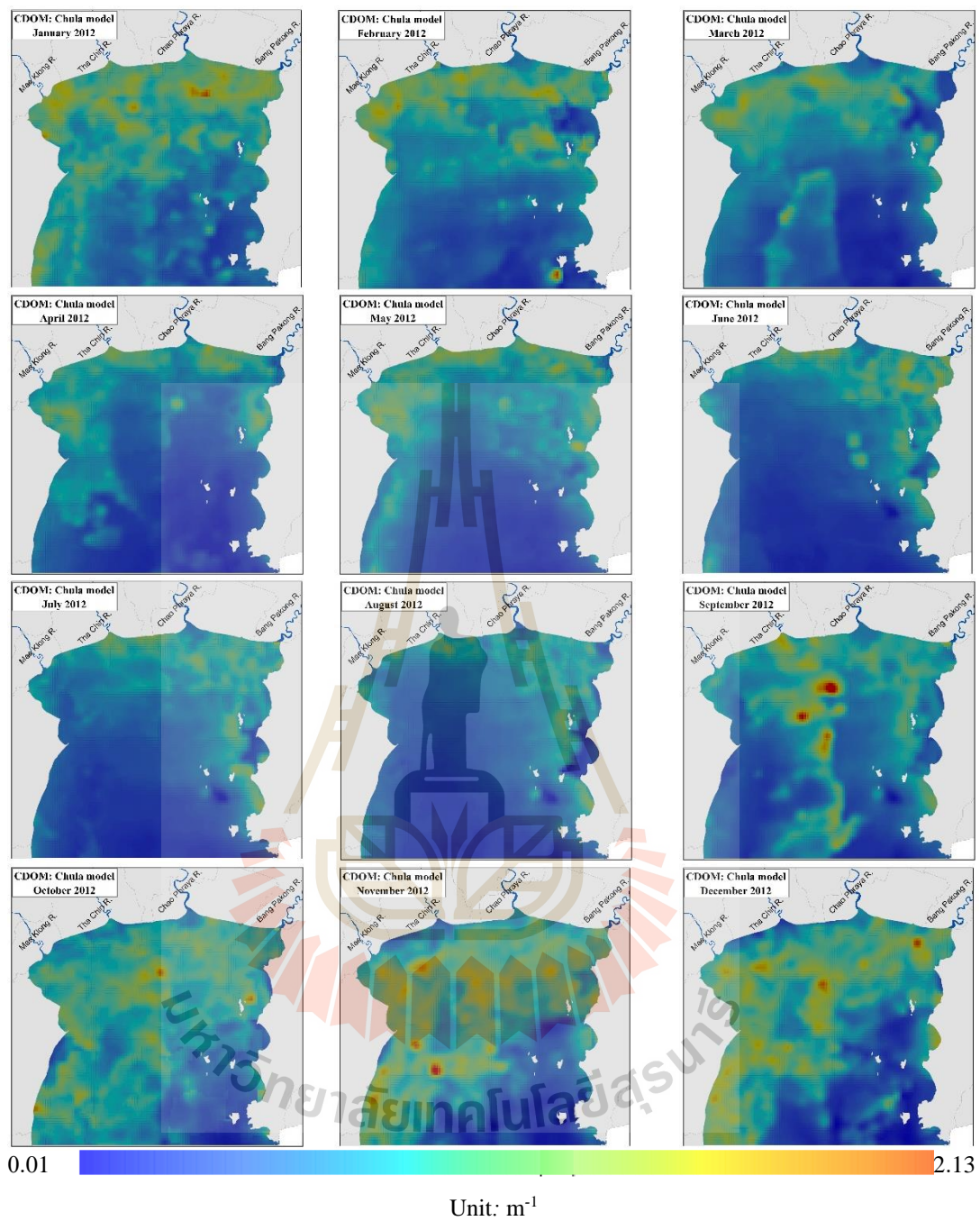


Figure 5.12 Spatial distributions of monthly CDOM in year 2012.

Table 5.11 Standard statistics of CDOM concentraions in year 2010.Unit: m⁻¹

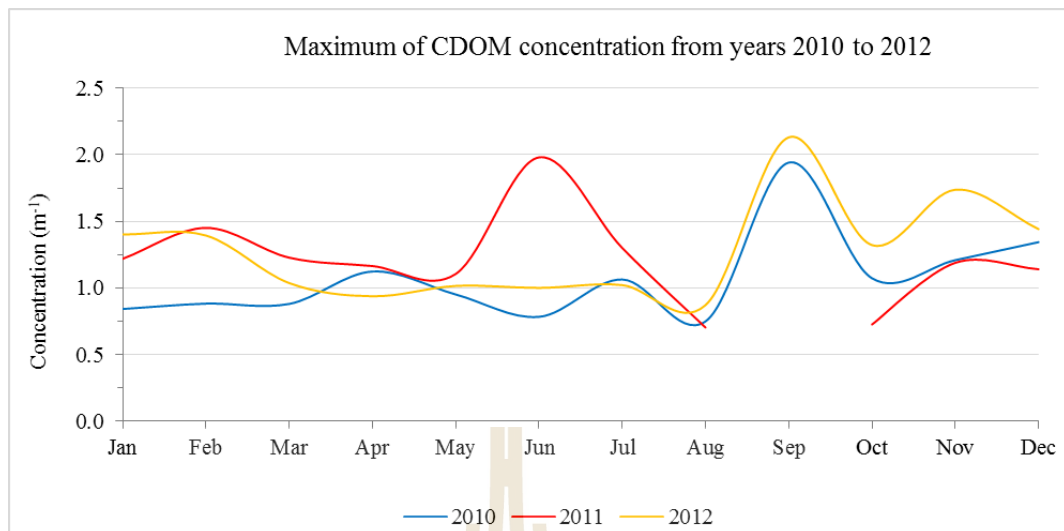
Year 2010	Maximum	Minimum	Mean	Std Dev.
January	0.843	0.143	0.448	0.145
February	0.883	0.163	0.428	0.145
March	0.881	0.148	0.447	0.131
April	1.124	0.113	0.465	0.171
May	0.952	0.098	0.385	0.166
June	0.784	0.111	0.397	0.154
July	1.064	0.040	0.411	0.170
August	0.750	0.091	0.425	0.129
September	1.941	0.060	0.482	0.192
October	1.073	0.209	0.543	0.121
November	1.209	0.118	0.526	0.219
December	1.344	0.131	0.577	0.244

Table 5.12 Standard statistics of CDOM concentraions in year 2011.Unit: m⁻¹

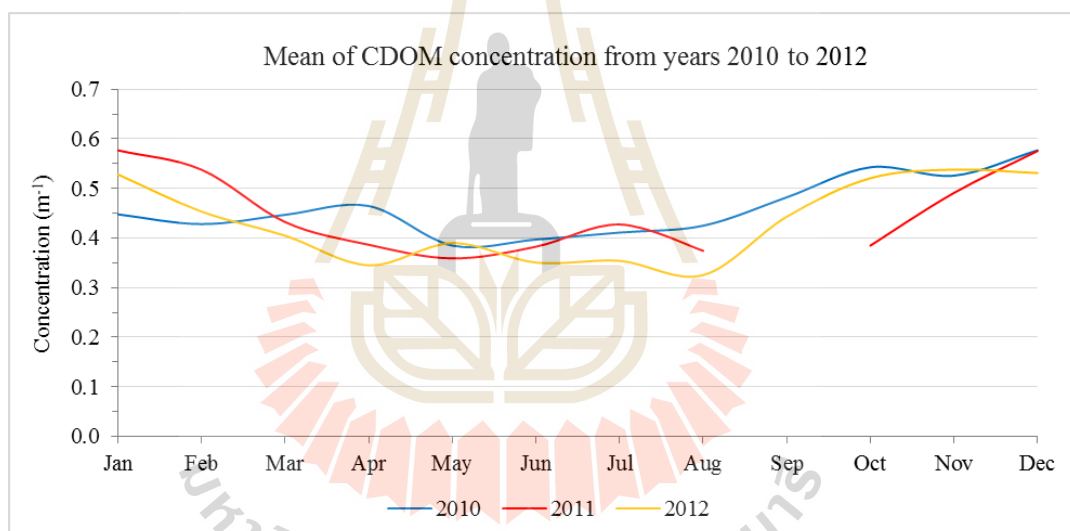
Year 2011	Maximum	Minimum	Mean	Std Dev.
January	1.220	0.211	0.575	0.185
February	1.451	0.047	0.538	0.171
March	1.228	0.110	0.432	0.188
April	1.165	0.033	0.387	0.153
May	1.106	0.020	0.359	0.148
June	1.980	0.031	0.383	0.177
July	1.300	0.022	0.427	0.144
August	0.704	0.146	0.374	0.092
September	NA	NA	NA	NA
October	0.727	0.073	0.385	0.102
November	1.189	0.051	0.491	0.198
December	1.141	0.121	0.576	0.243

Table 5.13 Standard statistics of CDOM concentraions in year 2012.Unit: m⁻¹

Year 2012	Maximum	Minimum	Mean	Std Dev.
January	1.402	0.159	0.528	0.191
February	1.394	0.079	0.453	0.192
March	1.037	0.047	0.405	0.180
April	0.938	0.037	0.345	0.178
May	1.016	0.070	0.390	0.187
June	1.001	0.045	0.351	0.175
July	1.022	0.038	0.354	0.159
August	0.872	0.033	0.325	0.144
September	2.130	0.042	0.443	0.199
October	1.322	0.055	0.521	0.167
November	1.737	0.029	0.538	0.232
December	1.442	0.011	0.539	0.248



(a) Maximum concentration of CDOM.



(b) Mean concentration of CDOM.

Figure 5.13 Maximum/mean CDOM concentration from years 2010 to 2012

(Chula model).

5.3 Relationships of Chl-a, TSS and CDOM

The compositions and optical properties of coastal water play an important role for the water quality assessment. The relationships among Chl-a, TSS and CDOM for UGoT area from years 2010 to 2012 were investigated here. Conclusive results of this work are presented in Figure 5.14 and Tables 5.14 and 5.15, respectively, wherein correlation coefficient (R) is used to identify the degree of mutual correlation between a pair of targets from 0 (none) to 1 (perfect).

For Chl-a and TSS in year 2010, moderate correlation was found in dry season from January to March (with R around 0.4-0.5), however the correlation level dropped continuously throughout the year with lowest R values ranges around 0.1-0.2. In 2011, the correlation level in general appeared to be relatively low with R data fluctuated mostly between 0.1-0.3, except in the wet season (July/August). R values started to move up substantially to be around 0.35 before moving down again later to be at 0.17 in October and then rising again to be around 0.40 in December. In 2012, moderate correlation level (R values around 0.4-0.5) was evidenced in several months during dry season (January-May/November-December) while lowest levels were found in wet season (July-August) with R around 0.2. In conclusion, moderately-strong correlation between Chl-a and TSS often observed in dry season ($R \approx 0.4-0.5$) and weak correlation often evidenced in wet season ($R \approx 0.1-0.2$), except in 2011.

For Chl-a and CDOM in 2010, relatively strong correlation was shown in several months during dry season (January-June, except April) with $R \approx 0.5-0.7$ and the downward trend was seen during the wet season (from June to October) with poor results in September and October ($R = 0.28$ and 0.20 , respectively). In 2011, relatively low correlation level was seen all year round ($R \approx 0.3-0.4$), except in November and

December that showed sign of improvement with $R \approx 0.5$ (0.50 and 0.53). And in 2012, moderate correlation level was dominant from dry season to middle wet season from January to August ($R \approx 0.4-0.6$) with peak values appeared in May ($R = 0.58$) and August ($R = 0.55$). Then, the downward trend finally took place for the rest of the year (from August to December) with values of R dropped from 0.55 (in August) to 0.24 (in December). Therefore, in conclusion, moderately-strong correlation between Chl-a and CDOM often prevailed in dry season till early wet season (from January to June) with R ranging around 0.4-0.6 and weak correlation often evidenced in late wet season around September/October with R ranging around 0.2-0.4. However, in 2011, relatively weak correlation was evidenced nearly all year round with R around 0.3-0.4 except in November and December that stronger correlation with R around 0.5 was found.

For TSS and CDOM, their correlation level in 2010 was seen rather low all year round with R less than 0.2 except in January and during May-August that R values ranges around 0.2-0.4. However in 2011, correlation level moved up significantly with R values at around 0.3-0.5 in most months with peak values mainly evidenced in dry season (March-April/November-December). For 2012, moderately-strong correlation dominated during dry season towards early wet season (January-July) with R values around 0.4-0.6. After that, the downward trend was taken place from June to October with R value dropped from 0.43 in June to 0.17 in October followed by sharp increase in R value in November and December.

In conclusion, correlation levels of three considered water constituents over the UGoT area during 2010 to 2012 were investigated. Correlation of Chl-a and TSS was found moderate in dry season (from January to May and November to December) with $R \approx 0.4-0.6$. While relative low was indicated in wet season, especially in September

and October. Reason for this finding might originate from the fact that both necessary nutrient loads (for Chl-a production by phytoplankton) and main TSS materials are normally carried along into the UGOT by main attached from rivers (Chuenniyom et al., 2012, Wattayakorn and Jaiboon, 2014). Therefore, those correlation was expected moderate to strong which depend on seasonal, the highest value was normally found in dry months.

Among these, correlation level of Chl-a and CDOM was found more stable throughout the year than other pair of constituents under consideration (as shown in Figure 5.14). However, in work of Das et al. (2016), CDOM was not found to exhibit any statistically significant correlation to Chl-a unlike what was in this found study. Typically, main sources of the TSS and CDOM materials are ongoing discharge from main rivers into UGoT from which CDOM was risen as product of soluble organic nutrients. Similarly, Das et al. (2016) reported the positive relationship of TSM and CDOM and suggested that the relationship may be not as good at lower concentration of the TSM. In addition, Reyes-Pesaresi (2010) found that the resuspension process of the bottom sediments can support CDOM variation in water bank during dry season. And TSS materials (sediments loading) are mostly carried to the sea by river discharges. Therefore, they tend to rapidly subside and settle to the sea floor close to the river mouth location, especially if the sea current speed over the area is low (Coble, Hu, Gould, Chang, and Wood, 2004).

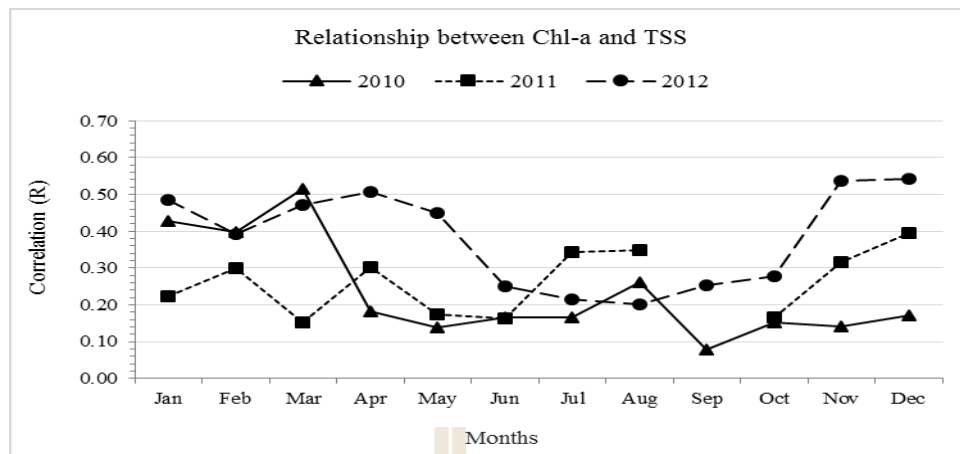
Table 5.14 Previous researches concerned the relationship of Chl-a, TSS and CDOM.

No.	Topic	Relative status			Author	Remark
		Chl-a	TSS	CDOM		
1	Colored dissolved organic matter in the coastal ocean: An optical tool for coastal zone environmental assessment and management.	X		X	Coble et al. (2004)	CDOM related with salinity, the higher-salinity, lower-CDOM in offshore waters. CDOM associated with high turbidity. Most CDOM comes from rivers containing organic materials leached from soils.
2	Dynamics of chromophoric dissolved organic matter, CDOM, in coastal tropical waters	X		X	Reyes-Pesaresi, (2010).	Correlation analysis between Chl-a, vs. CDOM suggests that phytoplankton is not a dominant source of CDOM in Mayagüez Bay waters. TSS at inshore was related to CDOM.
3	Spatial and Temporal Distribution of Colored Dissolved Organic Matter (CDOM) in Narragansett Bay, Rhode Island: Implications for Phytoplankton in Coastal Waters	Y		Y	Keith, Yoder, and Freeman, (2002)	CDOM can be affects to the light absorption in coastal water. Results suggested CDOM is related to the salinity and variation is related to seasonal change of freshwater input from watershed. Phytoplankton blooms will affect to properties of CDOM concentrations.

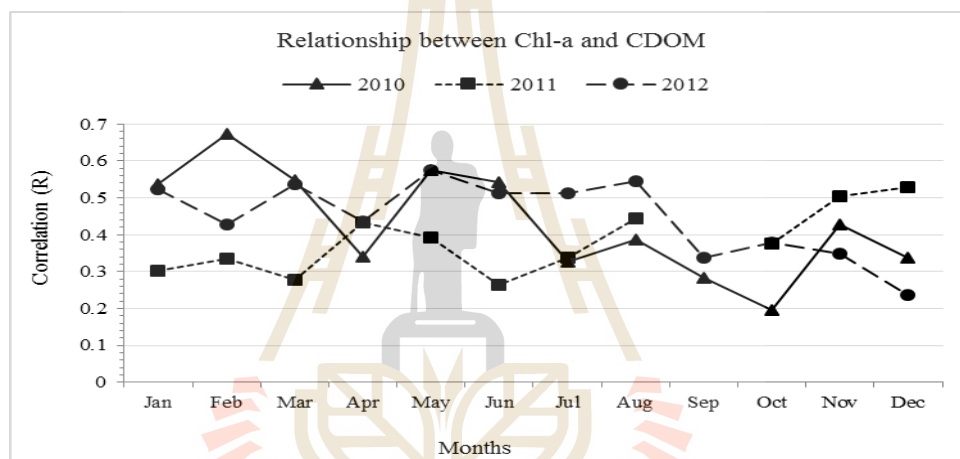
Note: X = not relative, Y = Relative, NA = Not appear

Table 5.15 Correlation (R) matrix of Chl-a, TSS and CDOM from 2010 to 2012.

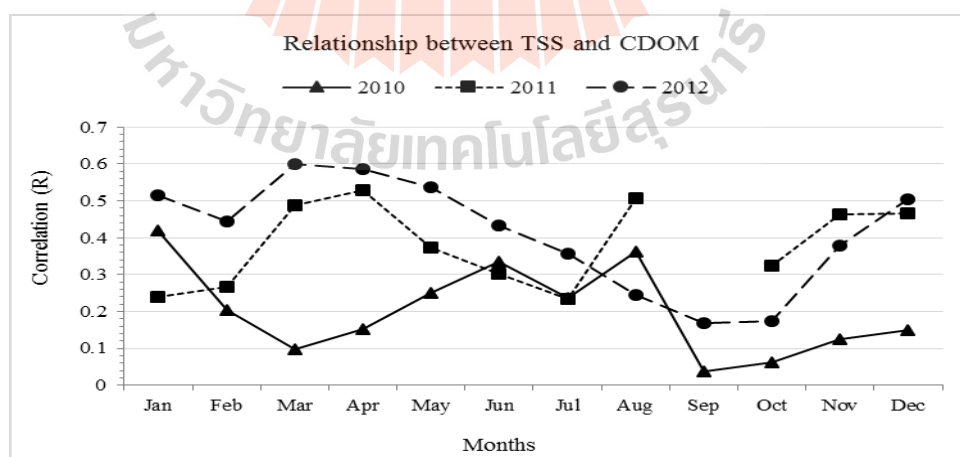
Months	Years	2010			2011			2012		
	Factors	Chl-a	TSS	CDOM	Chl-a	TSS	CDOM	Chl-a	TSS	CDOM
January	Chl-a	1			1			1		
	TSS	0.43	1		0.22	1		0.48	1	
	CDOM	0.54	0.42	1	0.30	0.24	1	0.52	0.52	1
February	Chl-a	1			1			1		
	TSS	0.40	1		0.30	1		0.39	1	
	CDOM	0.67	0.21	1	0.34	0.27	1	0.43	0.44	1
March	Chl-a	1			1			1		
	TSS	0.51	1		0.15	1		0.47	1	
	CDOM	0.55	0.10	1	0.28	0.49	1	0.54	0.60	1
April	Chl-a	1			1			1		
	TSS	0.18	1		0.30	1		0.51	1	
	CDOM	0.34	0.15	1	0.43	0.53	1	0.44	0.59	1
May	Chl-a	1			1			1		
	TSS	0.14	1		0.17	1		0.45	1	
	CDOM	0.58	0.25	1	0.39	0.37	1	0.58	0.54	1
June	Chl-a	1			1			1		
	TSS	0.17	1		0.16	1		0.25	1	
	CDOM	0.54	0.33	1	0.26	0.30	1	0.51	0.43	1
July	Chl-a	1			1			1		
	TSS	0.17	1		0.34	1		0.22	1	
	CDOM	0.33	0.24	1	0.34	0.24	1	0.51	0.36	1
August	Chl-a	1			1			1		
	TSS	0.26	1		0.35	1		0.20	1	
	CDOM	0.39	0.36	1	0.45	0.51	1	0.55	0.25	1
September	Chl-a	1			na			1		
	TSS	0.08	1		na	na		0.25	1	
	CDOM	0.28	0.04	1	na	na	na	0.34	0.17	1
October	Chl-a	1			1			1		
	TSS	0.15	1		0.17	1		0.28	1	
	CDOM	0.20	0.06	1	0.38	0.32	1	0.38	0.17	1
November	Chl-a	1			1			1		
	TSS	0.14	1		0.32	1		0.54	1	
	CDOM	0.43	0.13	1	0.50	0.46	1	0.35	0.38	1
December	Chl-a	1			1			1		
	TSS	0.17	1		0.40	1		0.54	1	
	CDOM	0.33	0.15	1	0.53	0.47	1	0.24	0.51	1



(a) Chlorophyll-a and total suspended solid



(b) Chlorophyll-a and color dissolved organic matter



(c) Total suspended solid and color dissolved organic matter

Figure 5.14 Correlation data (R) of three water constituents from years 2010 to 2012.

5.4 Trophic states over the UGoT area from years 2010 to 2012

Knowledge of Chl-a concentration over UGoT area from 2010 to 2012 is useful for the assessment of trophic states over the area based on the classification criteria proposed by the OECD (1982) (as described in Table 3.6). Five trophic classes were identified, i.e., (1) ultra-oligotrophic (UT), (2) oligotrophic (OT), (3) mesotrophic (MT), (4) eutrophic (ET) and (5) hyper-eutrophic (HT). Results of the study are reported in Figures 5.15-5.21 and Tables 5.16-5.18, respectively.

In 2010, oligotrophic state was found prevalent all year round with covering proportion of around 40-60% with lowest value of about 30% in June, followed by the ultra-oligotrophic class. Here the classified ultra-oligotrophic state (with lowest Chl-a density) was mostly in the deep-water zone and far away from dry land. Most severe cases of eutrophic and hyper-eutrophic states were found close to shore and known locations at the main river mouths. Thachin and Chao Phraya River mouths, during wet season from June to September was large amount of freshwater which released into the UGoT (Figure 5.15).

In 2011, the ultra-oligotrophic and oligotrophic classes still occupied most areas all year round (except in winter months that ultra-oligotrophic area dropped dramatically) with more than 90% in total area from February to May. And the eutrophic and hyper-eutrophic zones covered few percentages of the area throughout the year similar to that of 2010. However, it was obvious that the occurrences of the concerned eutrophic and hyper-eutrophic incidences were remarkably dropped in 2011, especially during the wet season (Figure 5.17) due primarily to the impact of the mega-flooding event over central Thailand. In addition, critical areas this year often attached to the Thachin River mouth, especially during dry season, from January to May.

In 2012, amount of areas occupied by ultra-oligotrophic and oligotrophic classes were still dominant in most months (except October for ultra-oligotrophic) with the eutrophic and hyper-eutrophic shared of the total area normally less than 5% as usual. From Figure 5.19 and Table 5.18, two critical months primarily seen this year were in June and November due mainly to the greatest expansion of the hyper-eutrophic zone (in June) and eutrophic zone (in November). In June, critical areas were found located mostly close to the Bang Pakong River mouth along the NE coast, however in November, those areas were more widespread covering many parts of the coastal zone, especially along the NW coast close to Mae Klong River mouth.

The classified eutrophic and hyper-eutrophic zones reported here will be used as a representative of the red tide occurrence in UGoT. Therefore, regarding to this assumption, the occurrences of red tide events should be low during dry season (January-April/October-December) and their locations should be close to some specific river mouths only. However, the occurrences of the red tide event should be seen more often during wet season (June to September) covering much more widespread area than that of the studied dry season. Massive discharge in 2011 was not influence to seasonal trophic state formation but it was impact on the variation of the trophic class area such as hyper-eutrophic zone which was rather high in wet season and low in dry season.

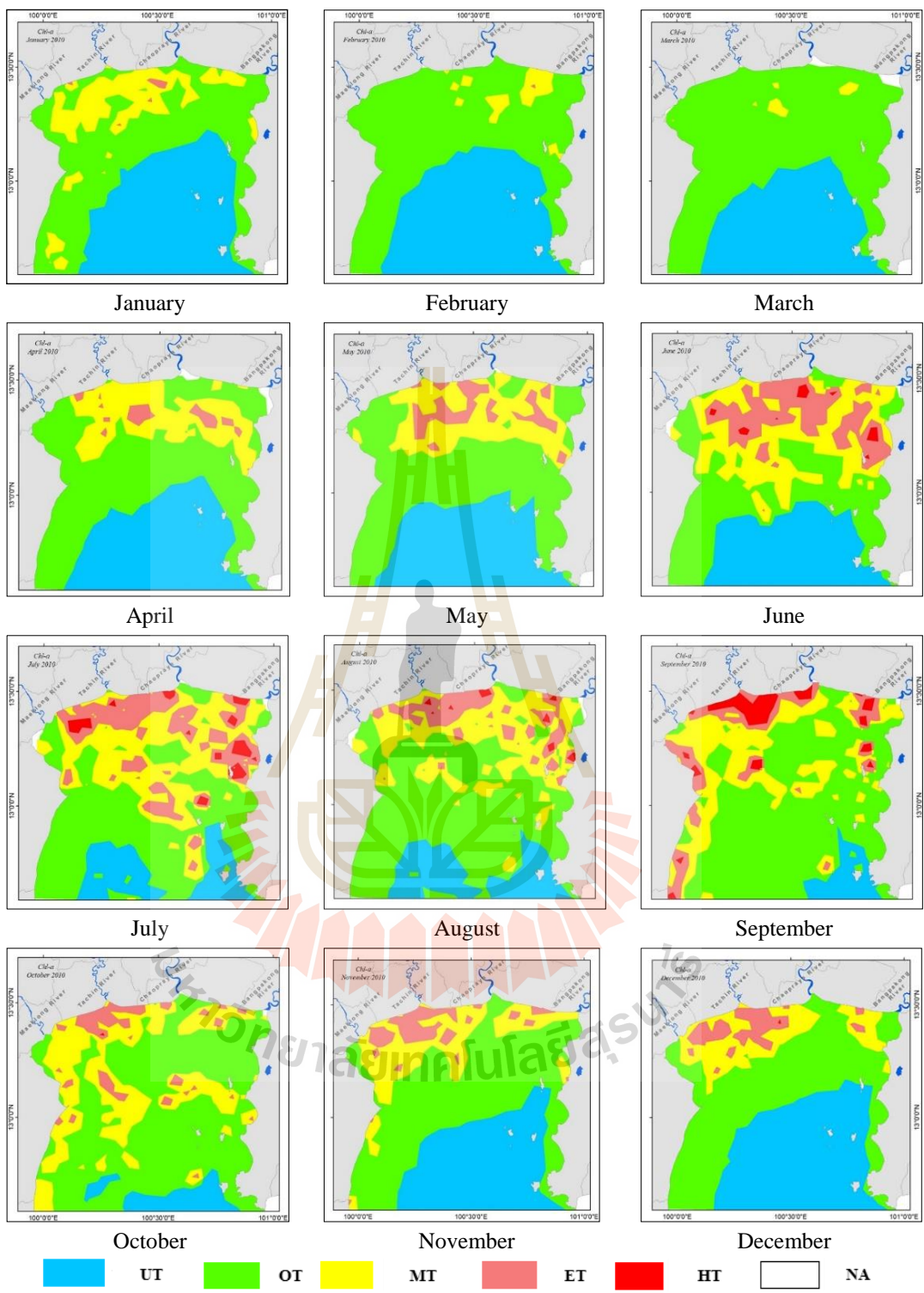
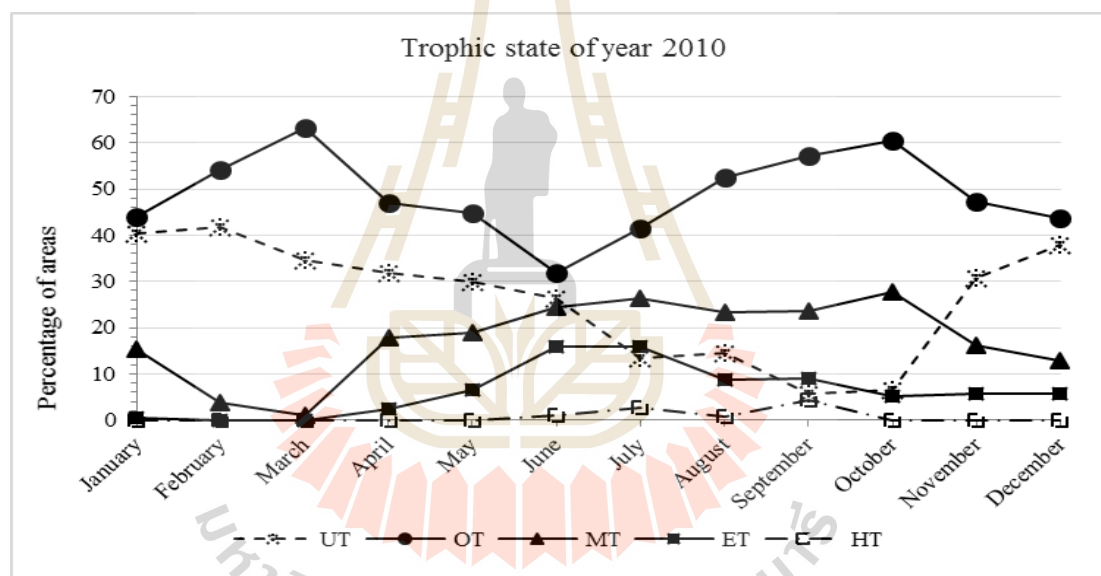


Figure 5.15 Trophic state maps of Chl-a based on OC3M model in year 2010.

Table 5.16 The results of trophic state classification in year 2010.

Unit: km²

Months	Classes										Remark	
	UT	%	OT	%	MT	%	ET	%	HT	%	NA	%
January	3,520.97	40.34	3,825.10	43.83	1,346.86	15.43	30.40	0.35	0	0	3.97	0.05
February	3,645.70	41.77	4,736.74	54.27	335.91	3.85	2.32	0.03	0	0	6.64	0.08
March	3,030.33	34.72	5,517.38	63.22	97.34	1.12	0	0	0	0	82.2	0.94
April	2,774.53	31.79	4,112.25	47.12	1,564.84	17.93	209.35	2.40	0	0	66.3	0.76
May	2,605.12	29.85	3,910.97	44.81	1,643.39	18.83	561.52	6.43	0	0	6.30	0.07
June	2,297.98	26.33	2,787.28	31.94	2,135.49	24.47	1,392.4	15.96	79.55	0.91	34.5	0.40
July	1,163.24	13.33	3,631.54	41.61	2,291.93	26.26	1,378.1	15.79	221.0	2.53	41.4	0.47
August	1,262.97	14.47	4,577.42	52.45	2,024.18	23.19	757.76	8.68	55.95	0.64	49.0	0.56
September	502.68	5.76	4,989.23	57.17	2,068.12	23.70	779.47	8.93	377.1	4.32	10.6	0.12
October	575.13	6.59	5,272.83	60.42	2,408.22	27.59	459.22	5.26	1.35	0.02	10.5	0.12
November	2,690.21	30.83	4,114.01	47.14	1,415.52	16.22	507.56	5.82	0	0	0	0
December	3,300.32	37.82	3,804.41	43.59	1,114.97	12.78	502.70	5.76	1.37	0.02	3.54	0.04

**Figure 5.16** Area percentage of classified trophic state in year 2010.

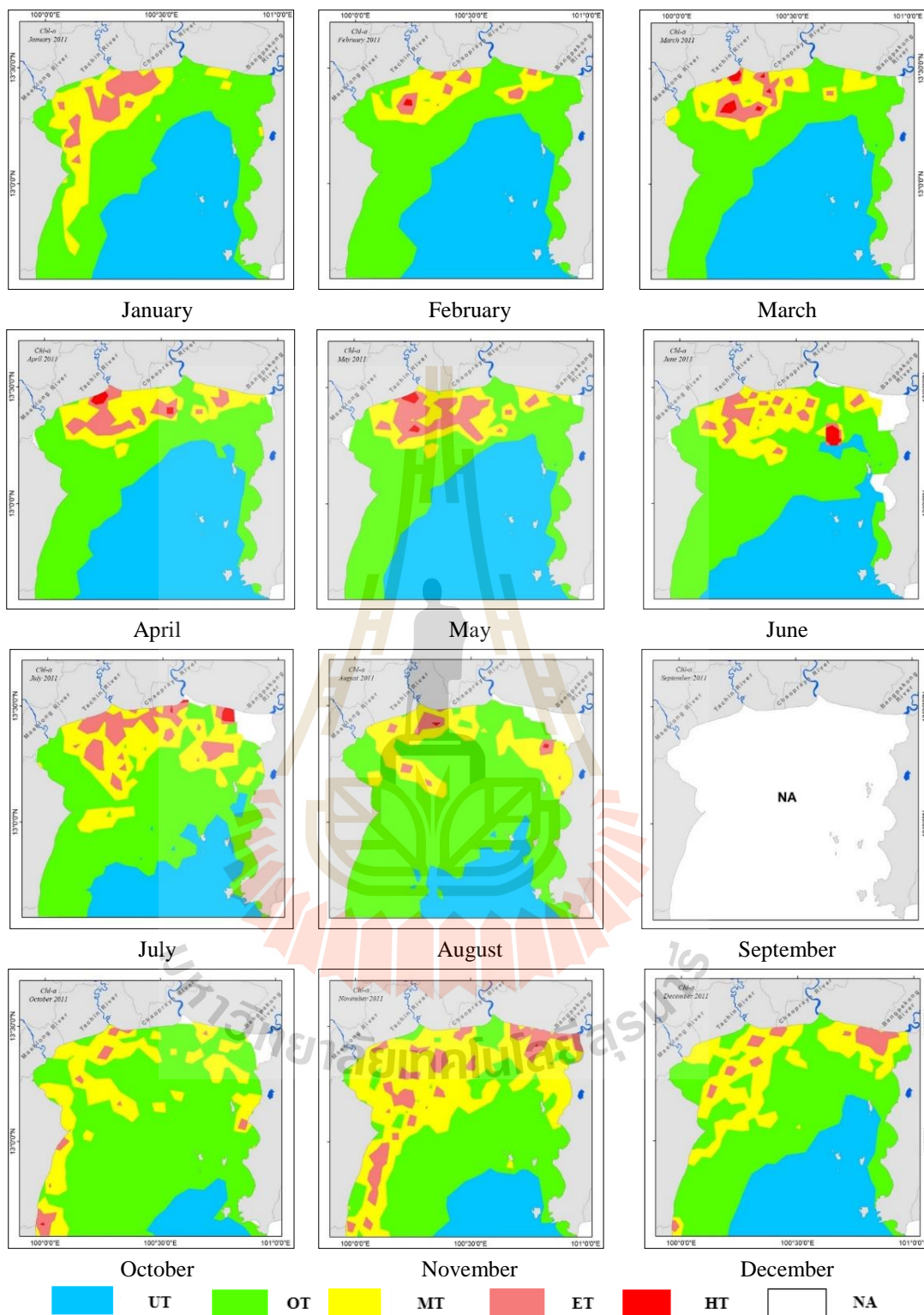
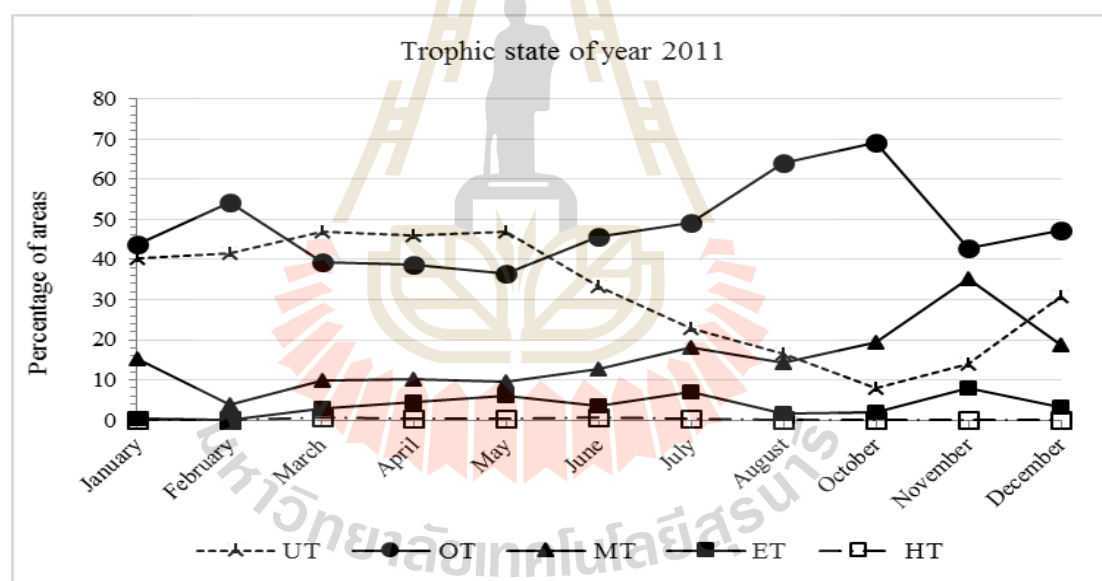


Figure 5.17 Trophic states maps of Chl-a based on OC3M model in year 2011.

Table 5.17 The results of trophic state classification in year 2011.

Unit: km²

Months	Classes										Remark	
	UT	%	OT	%	MT	%	ET	%	HT	%	NA	%
January	3,520.97	40.26	3,825.10	43.74	1,346.86	15.40	30.40	0.35	0	0	22.25	0.25
February	3,645.70	41.69	4,736.74	54.16	335.91	3.84	2.32	0.03	0	0	24.92	0.28
March	4,110.47	47.00	3,439.45	39.33	862.99	9.87	261.77	2.99	53.21	0.61	17.69	0.20
April	4,029.18	46.07	3,375.11	38.59	895.03	10.23	380.19	4.35	36.89	0.42	29.19	0.33
May	4,104.38	46.93	3,182.48	36.39	827.04	9.46	543.17	6.21	32.05	0.37	56.46	0.65
June	2,913.20	33.31	4,006.61	45.81	1,118.84	12.79	323.34	3.70	47.52	0.54	336.07	3.84
July	1,995.21	22.81	4,288.87	49.04	1,574.98	18.01	603.75	6.90	37.90	0.43	244.87	2.80
August	1,440.52	16.47	5,601.73	64.05	1,247.62	14.27	148.87	1.70	7.64	0.09	299.21	3.42
September	NA	NA	NA	NA	NA	NA	NA	NA	NA	NA	NA	NA
October	690.10	7.89	6,047.02	69.14	1,699.89	19.44	164.98	1.89	1.35	0.02	142.24	1.63
November	1,231.58	14.08	3,734.09	42.70	3,081.87	35.24	697.36	7.97	0.68	0.01	0	0
December	2,685.16	30.70	4,140.00	47.34	1,649.81	18.86	269.79	3.08	0	0	0.82	0.01

**Figure 5.18** Area percentage of classified trophic state in year 2011.

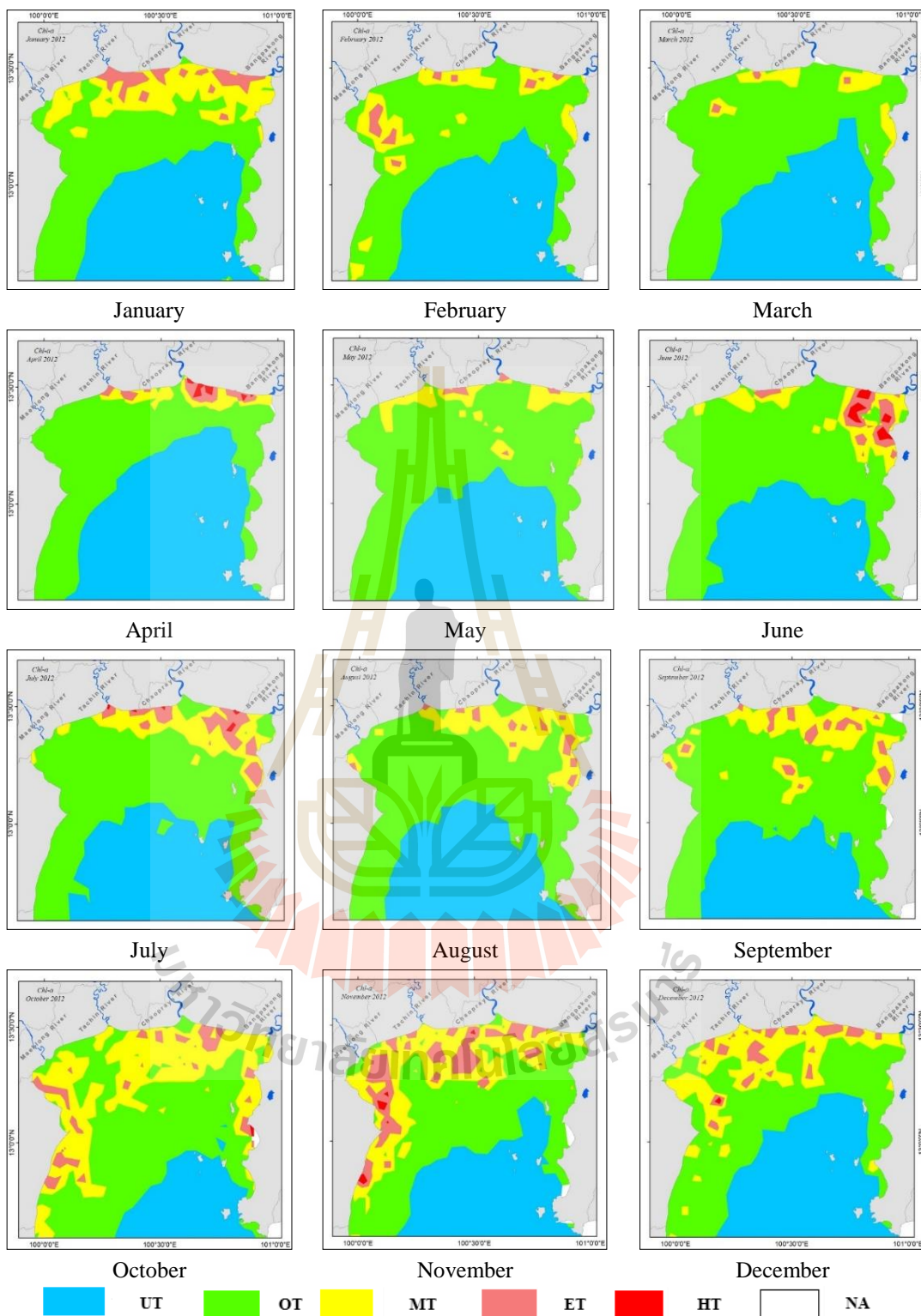
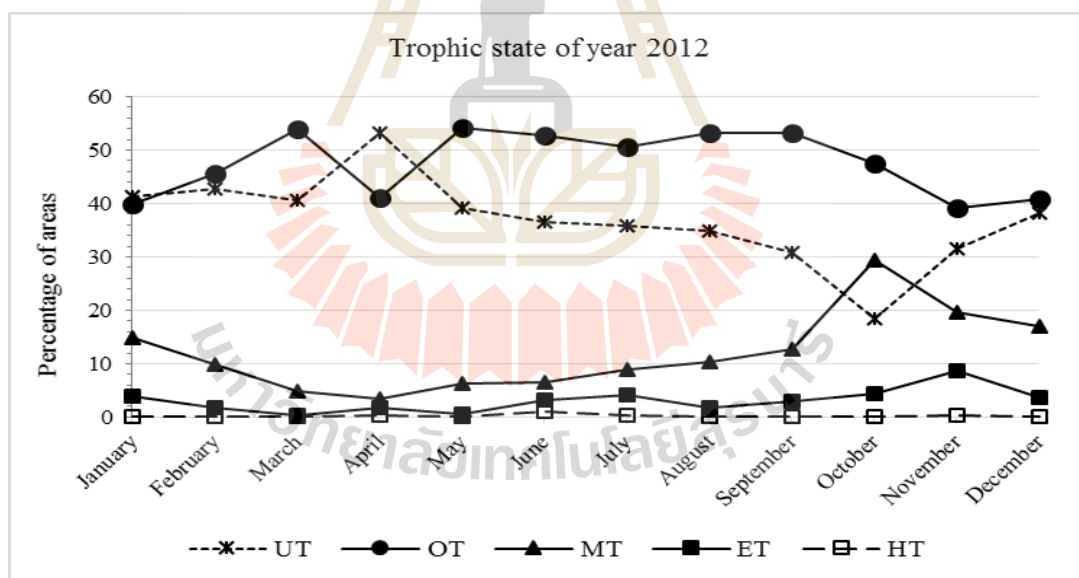


Figure 5.19 Trophic state maps of Chl-a based on OC3M model in year 2012.

Table 5.18 The results of trophic state classification in year 2012.

Unit: km²

Months	Classes										Remark	
	UT	%	OT	%	MT	%	ET	%	HT	%	NA	%
January	3,603.31	41.18	3,494.66	39.94	1,309.84	14.97	341.77	3.91	0	0	0	0
February	3,738.57	42.73	3,981.40	45.50	867.07	9.91	157.15	1.80	0	0	5.39	0.06
March	3,547.27	40.54	4,712.24	53.86	424.64	4.85	31.34	0.36	0	0	34.11	0.39
April	4,654.82	53.20	3,600.11	41.15	294.05	3.36	152.40	1.74	37.56	0.43	10.66	0.12
May	3,417.32	39.06	4,740.12	54.18	539.63	6.17	52.48	0.60	0	0.00	0.04	0.00
June	3,196.71	36.54	4,610.96	52.70	576.88	6.59	274.44	3.14	90.57	1.04	0.04	0
July	3,138.41	35.87	4,433.49	50.67	786.77	8.99	370.47	4.23	18.65	0.21	1.79	0.02
August	3,040.25	34.75	4,653.70	53.19	906.96	10.37	145.44	1.66	0	0	3.24	0.04
September	2,702.31	30.89	4,647.26	53.11	1,111.22	12.70	248.42	2.84	0	0	40.38	0.46
October	1,606.55	18.36	4,155.25	47.49	2,571.14	29.39	390.93	4.47	5.86	0.07	19.84	0.23
November	2,766.46	31.62	3,428.45	39.18	1,710.77	19.55	766.46	8.76	29.26	0.33	48.19	0.55
December	3,349.30	38.28	3,568.01	40.78	1,497.62	17.12	329.74	3.77	4.92	0.06	0	0

**Figure 5.20** Area percentage of classified trophic state in year 2012.

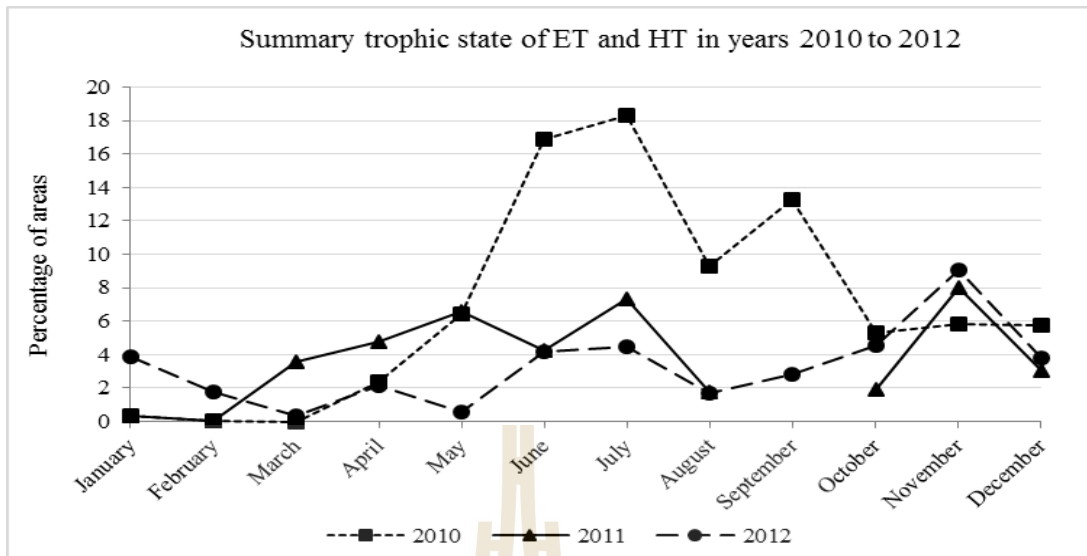


Figure 5.21 Summary trophic state of ET and HT from years 2010 to 2012.

5.5 Conclusions

This chapter describes the application of temporal MODIS data for monitoring concentrations (spatial and temporal variations) of the three target constituents: Chl-a, TSS and CDOM during years from 2010 to 2012 over UGoT area along with the trophic states of UGoT during this time. The extraction and mapping of concentration data for each stated constituent were achieved through the use of respective optimal algorithms as explained in Chapter IV.

In general, Chl-a concentration data in normal year (2010) were relatively low in dry season (January-April) and gradually rose afterwards with peak values achieved in wet season (July/September). This rising trend ended in October and data started to gradually fall from that point onwards throughout winter. High data values were often noticed close to shore and the main river mouths, especially those of the Thachin and the Chao Phraya Rivers. However, the effects of 2011 mega flood over central Thailand

had led to different characteristics of the data variation where the most notable one was great drop in Chl-a density (maximum/mean) during wet season of 2011.

For TSS case, maximum concentration tended to be low in dry season and then gradually increase towards wet season with peak values achieved during that time (like Chl-a). Also, hotspots for TSS pollution were often seen at the main river mouths, mostly at the Chao Phraya River. Unlike Chl-a case in which critical zones were usually found at far away from river mounts. For the CDOM concentration, low values were seen dominant in dry season and peak values were seen in wet season like others. However, critical zones of CDOM pollution were found more widespread into the deep-water zone than those of the Chl-a or TSS.

Correlation among the studied constituents were also assessed and it was found that correlation levels of these constituents were normally found to be moderately strong during dry season (from January to June) with $R \approx 0.4-0.6$ while the relatively low correlation level was often seen in wet season, especially September and October. Among these, correlation of Chl-a and CDOM was found to be more stable throughout the year than other pair of constituents.

In conclusion, moderately-strong correlation between Chl-a and TSS often observed in dry season and weak correlation appeared in wet season, except in 2011. Moderately-strong correlation between Chl-a and CDOM was often shown in dry season till early wet season and weak correlation often showed in late wet season. Correlation of TSM and CDOM mostly peaked in dry season (except in 2010) while it was relatively low in wet period. This finding was supported by work of Das et al. (2016) which found positive relationship of TSM and CDOM and suggested that the relationship might be weakened at the lower concentration of TSM.

One of the main difficult extracted Chl-a concentration from the satellite-based (like MODIS) is strong sunlight absorption of CDOM material in sea water over wavelengths similar to Chl-a. This makes the final estimation of the Chl-a by typical ocean color algorithms less robust (Keith et al., 2002). In general, CDOM absorption can reduce light energy by 20-40% during plankton bloom incidence.

Finally, the trophic state maps of UGoT were generated from gained maps of Chl-a concentration over the area in 2010-2012 from which the classified eutrophic and hyper-eutrophic zones were used as a representative of red tide occurrence in UGoT area as they indicate much higher amount than usual of Chl-a density over a specific location. This led to the prior conclusion that occurrences of red tide events should be rather low in dry season (January-April/October-December) and their locations should be restricted to sea areas close to some specific river mouths only. However, the occurrences of red tide event should be found more often during wet season (June to September) covering much more widespread area than that of the dry season. For Thachin estuary, nutrients condition was found as hypertrophic state condition while the red tide phenomena was often occurred during November to December. High nutrient condition could fuel fast development of the red tide phenomenon with the cycle rate of appearing might be less than one week (Chuennyom, Meksumpun, and Meksumpun, 2012).

CHAPTER VI

RED TIDE SUSCEPTIBILITY ANALYSIS

Red tide phenomenon was evidenced more prevalently over the UGoT zone in recent years and has become a critical threat to natural marine ecosystem of the area at present. Therefore, to determine influence of key environmental factors associated to red tide occurrence over the area in the past which can help identify places with high chances of having the incidences in the future, the associated susceptibility maps for explaining likelihood of red tide occurrence in the UGoT region were formulated using two popular methods: the Frequency ratio (FR) and Simple additive weighting (SAW). To achieve this stated objective, five factors believed to be crucial for red tide formation were taken into consideration, which are, TSS and CDOM concentrations, water depth, distance from the river mouth, and current velocity.

Here, the TSS and CDOM concentration maps were derived from the relevant MODIS dataset through their respective optimal models and the mapping process detailed earlier in Chapters IV and V, while water depth and distance from key river mouths are static data accumulated from responsible government's agencies, and water speed data were acquired from associated expert in this field. In addition, fifteen daily maps of the identified red tide occurrence over UGoT (i.e., ones with eutrophic/ hyper-eutrophic trophic states) between 2006 and 2015 were also

synthesized for further implementation in model's assessment process (12 maps) and map's validation process (3 maps).

6.1 Preparation of necessary factors for model's analysis

6.1.1 Reference red tide occurrence maps

For the preparation of red tide susceptibility maps from the two chosen methods [i.e., the simple additive weighting (SAW) and the frequency ratio (FR)], reference data of past red tide occurrences over the area were crucially required for the model's operating process (the FR method) and the validation process of yielded susceptibility maps from both methods. In this regard, fifteen daily maps of identified red tide events occurred over UGoT from 2005 to 2015 (i.e., areas classified with eutrophic and hyper-eutrophic trophic states described in Table 3.6) were built to fulfil the aforementioned tasks. These reference data comprise of 12 red-tide maps for model's analysis process (Figure 6.1) and 3 maps for the result's validation process (Figure 6.2).

The derivation of red tide reference maps started with the development of daily Chl-a concentration maps over the UGoT area from the associated MODIS data during 2005 to 2015 by the optimal model found for Chl-a (the OC3M model). The original Chl-a concentration maps of the preferred dates (with predominant red tide appearance) were then finally classified to represent five classes of trophic states based on the applied OECD system (Table 3.6). After that, the red-tide occupied areas (i.e., those classified with eutrophic and hyper-eutrophic trophic states) were then identified and mapped as shown in Figures 6.1 and 6.2, respectively. Note that, three

red-tide reference maps in Figure 6.2(a) were merged to make a single map shown in Figure 6.2(b) . Typically, red-tide cases were often evidenced near shore within vicinity of the four river mouths (i.e., Mae Klong, Thachin, Chao Phraya and Bang Pakong).

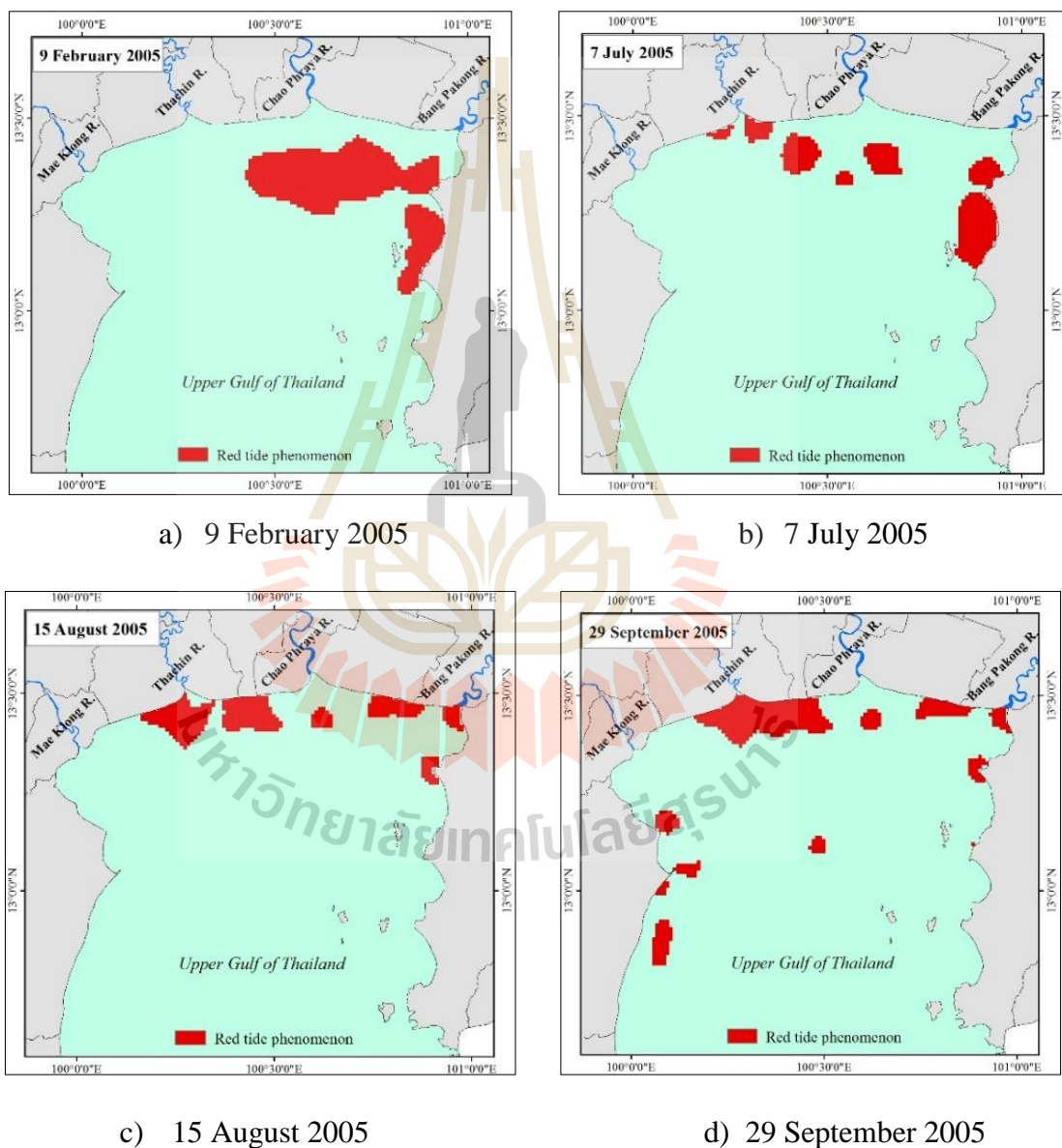


Figure 6.1(a) Reference red-tide maps for model's application process.

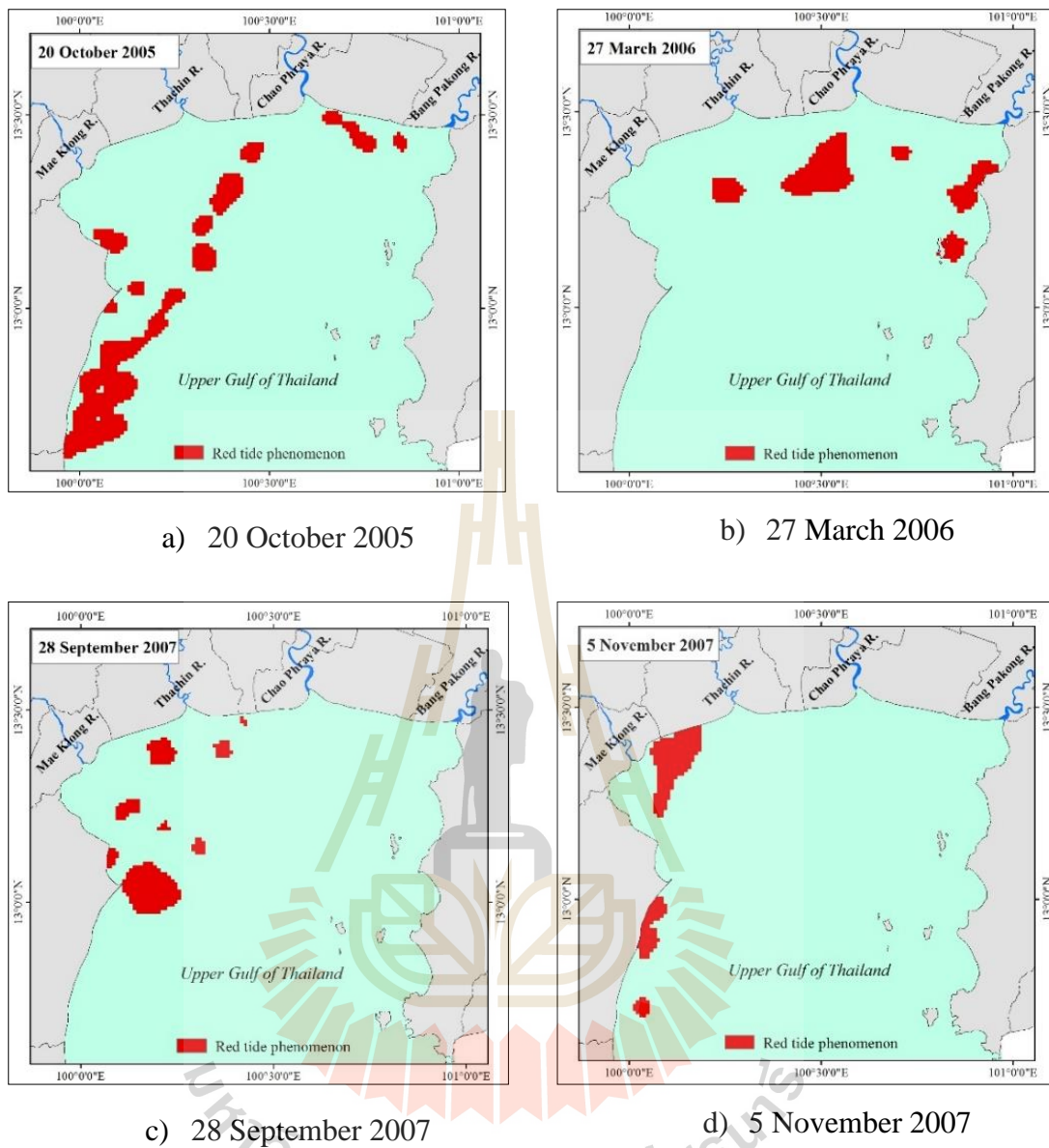


Figure 6.1(b) Reference red-tide maps for model's application process.

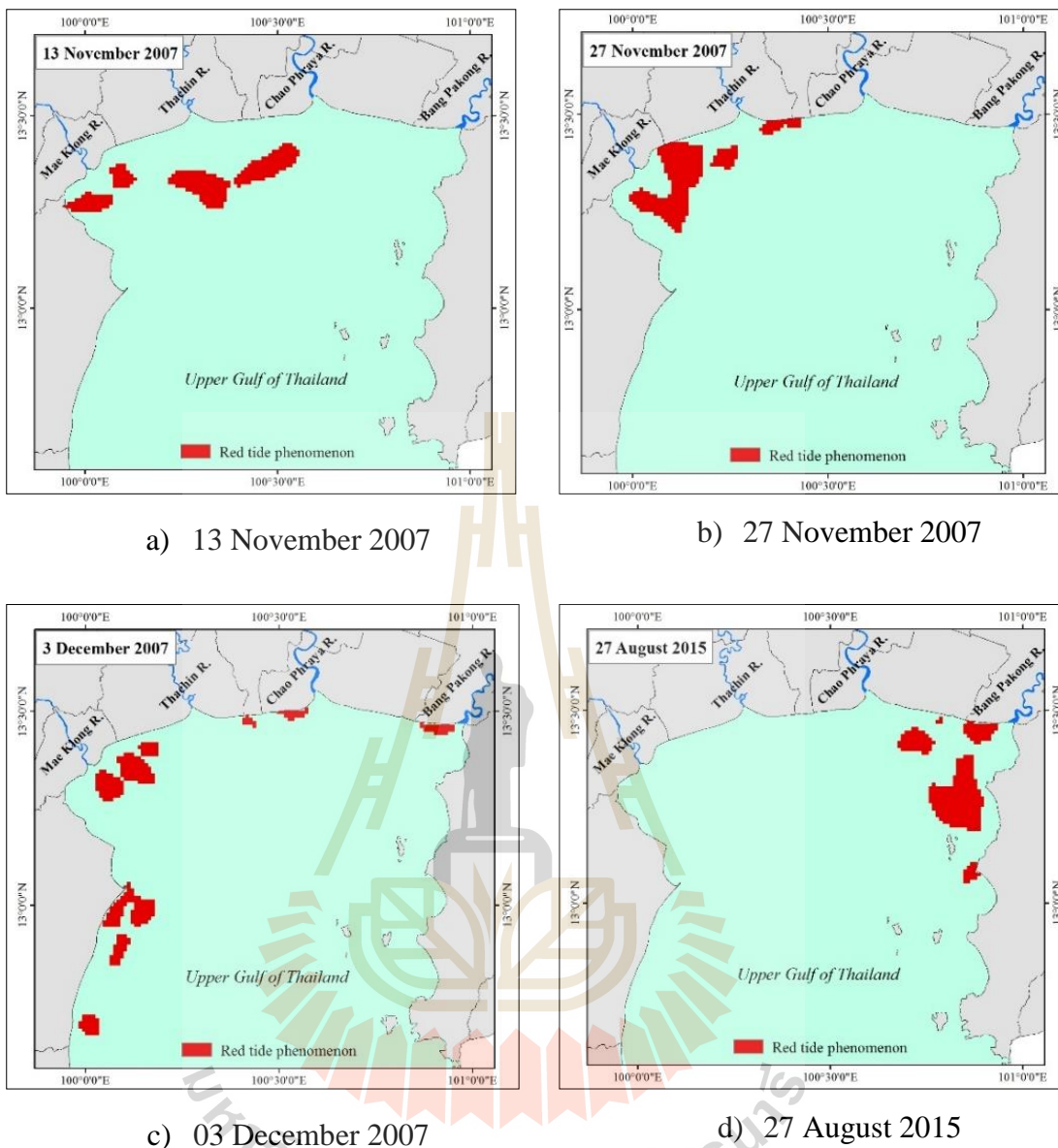
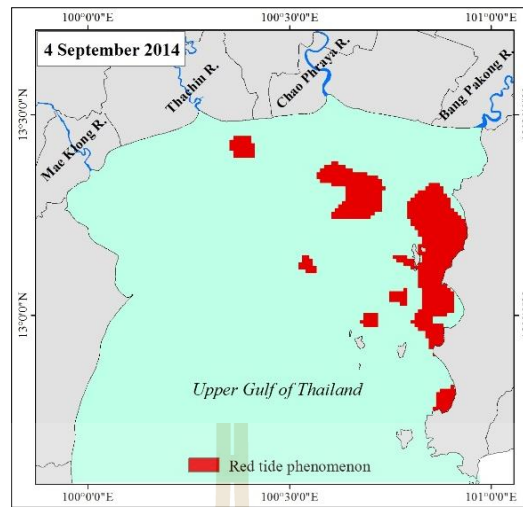
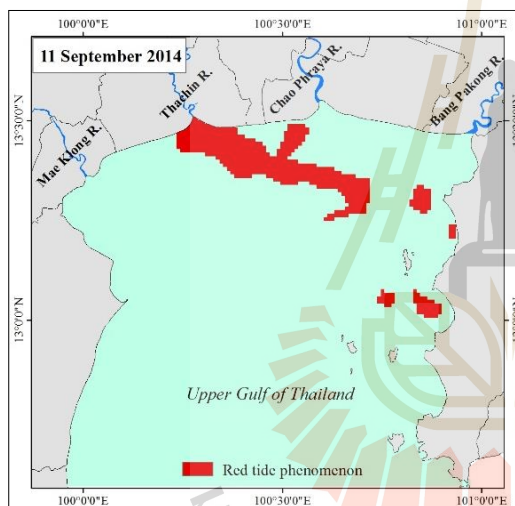


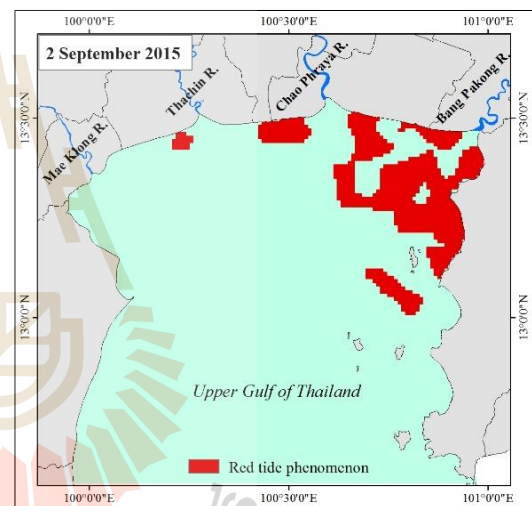
Figure 6.1(c) Reference red-tide maps for model's application process.



a) 4 September 2014



b) 11 September 2014



c) 2 September 2014

Figure 6.2(a) Reference red-tide maps for susceptibility map's validation process.

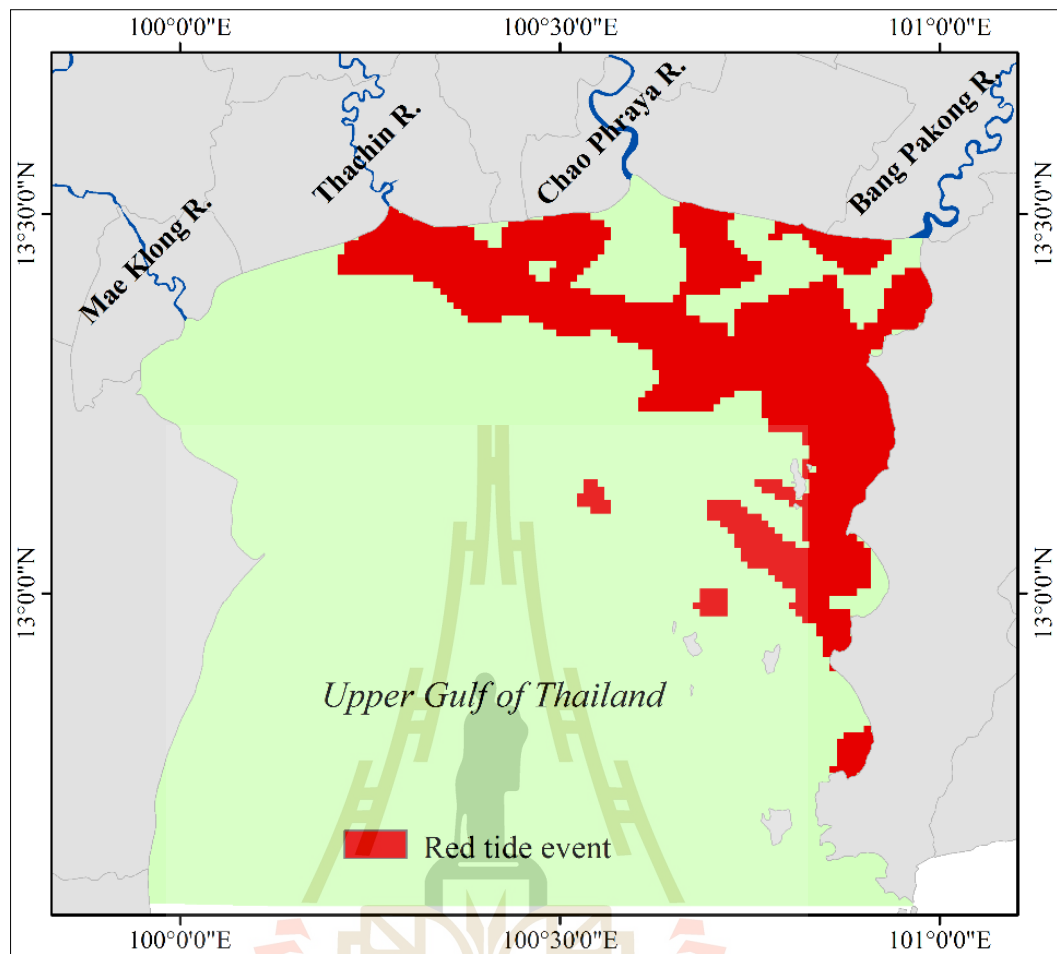


Figure 6.2(b) Conclusive red-tide map for susceptibility map's validation process.

6.1.2 Total suspended solids

Total suspended solids (TSS) was one of the total five key factors to be integrated in the red tide susceptibility analysis and mapping for the UGoT area in this work. In general, TSS-led nutrients can support occurrence of the plankton bloom over a specific area, however, prominent lack of sunlight from rising turbidity in surface water layer shall eventually result in gradual decline in number of the living phytoplankton cells (due to lack of efficient photosynthesis activity). This knowledge indicates inevitably complicated relationship manner between the observed TSS and Chl-a concentration data in coastal water as seen in Table 5.15 and Figure 5.14(a) for examples, in which moderate-to-low correlation levels were evidenced. According to the present OECD criteria for trophic state classification for water quality assessment described in Tables 2.7/2.8, turbidity level of water (expressed in terms of secchi disk depth) can be related straightforwardly to the level of its trophic states in which more turbidity (with lower secchi depth) indicates worse trophic state of the water under consideration. Here, original TSS concentration maps on the same dates of red tide maps shown in Figures 6.1/6.2 were prepared by the chosen model (TSM) and then classified into five levels as detailed in Table 3.8.

Figures 6.3(a) and (b) present classified TSS concentration maps for twelve specific dates (those of the red tide mapping reported in Figure 6.1) in which five classes of red-tide occurrence tendency based on the extracted TSS density were identified (from very-low to very-high level as said in Table 3.8). Results showed that most areas were belonged to the very high tendency (of red-tide occurrence) class (mainly over deep water region away from shore) and tendency levels shall decrease

continuously (from class four to class one) for areas with shallow water located closer to shore and to the main river mouths. The extracted TSS concentration range seen in this work was appeared to be ranging from 0.109 to 66.425 mg/l (both were found on 27 September 2007) as detailed in Table 6.2. This finding is partly in accordance with TSS values reported by Chumnantana (2006) which found (by in situ measurements) that the TSS concentration data in the UGoT area were varying from 33.60 to 127.64 mg/l with predominant portion appeared close to the Bang Pakong River mouth.



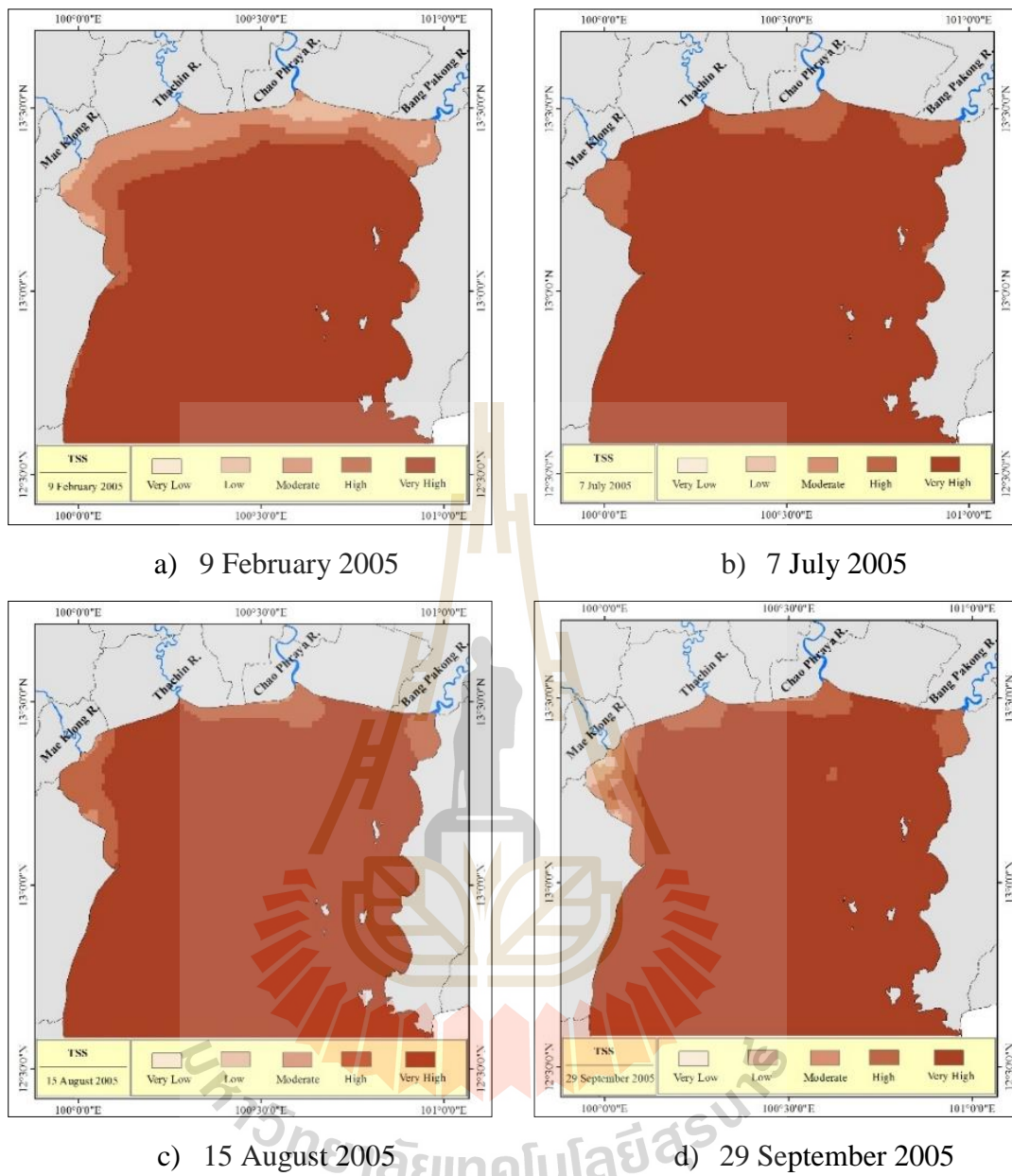


Figure 6.3(a) Classified TSS-based red-tide tendency of occurrence maps.

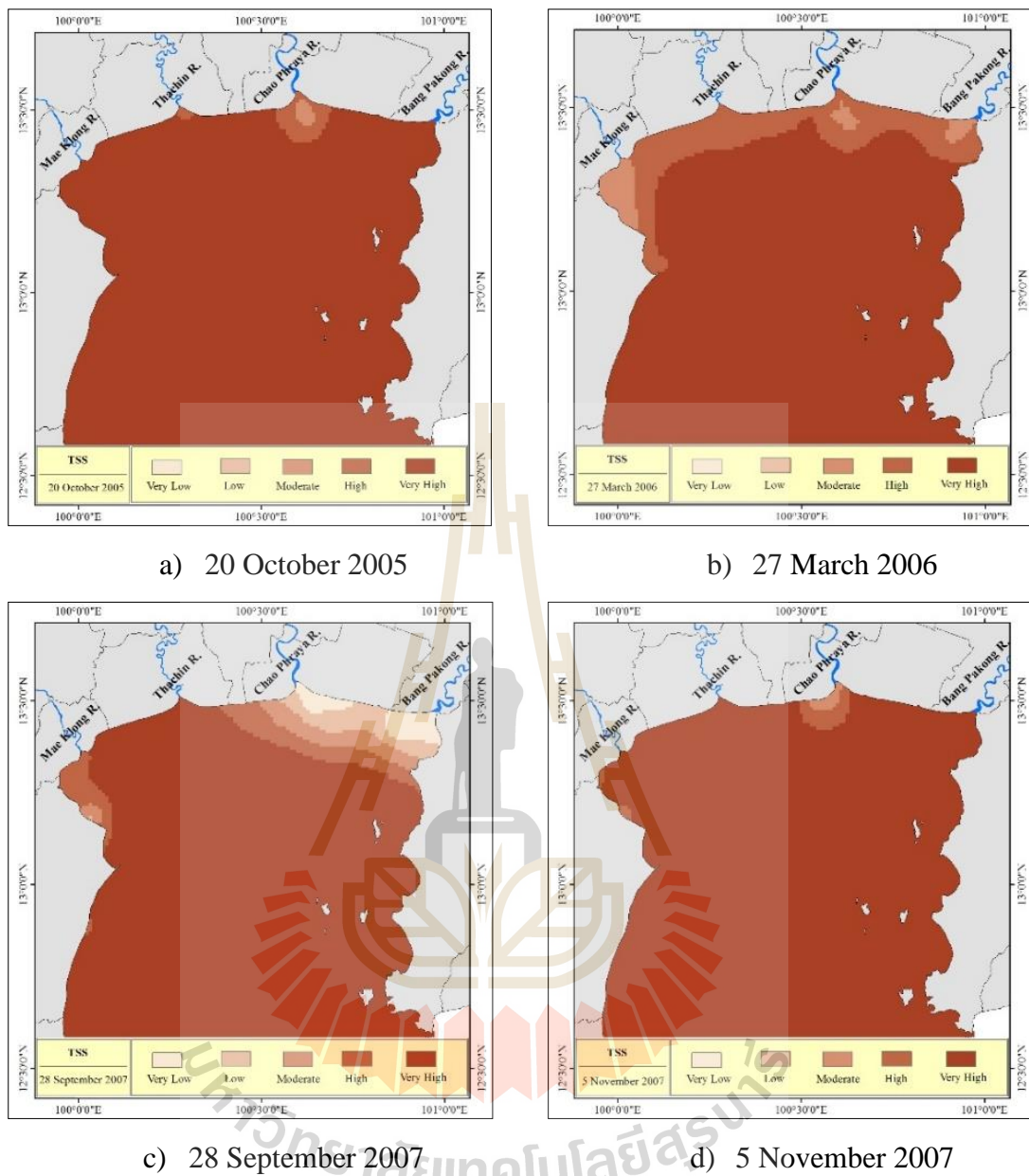


Figure 6.3(b) Classified TSS-based red-tide tendency of occurrence maps.

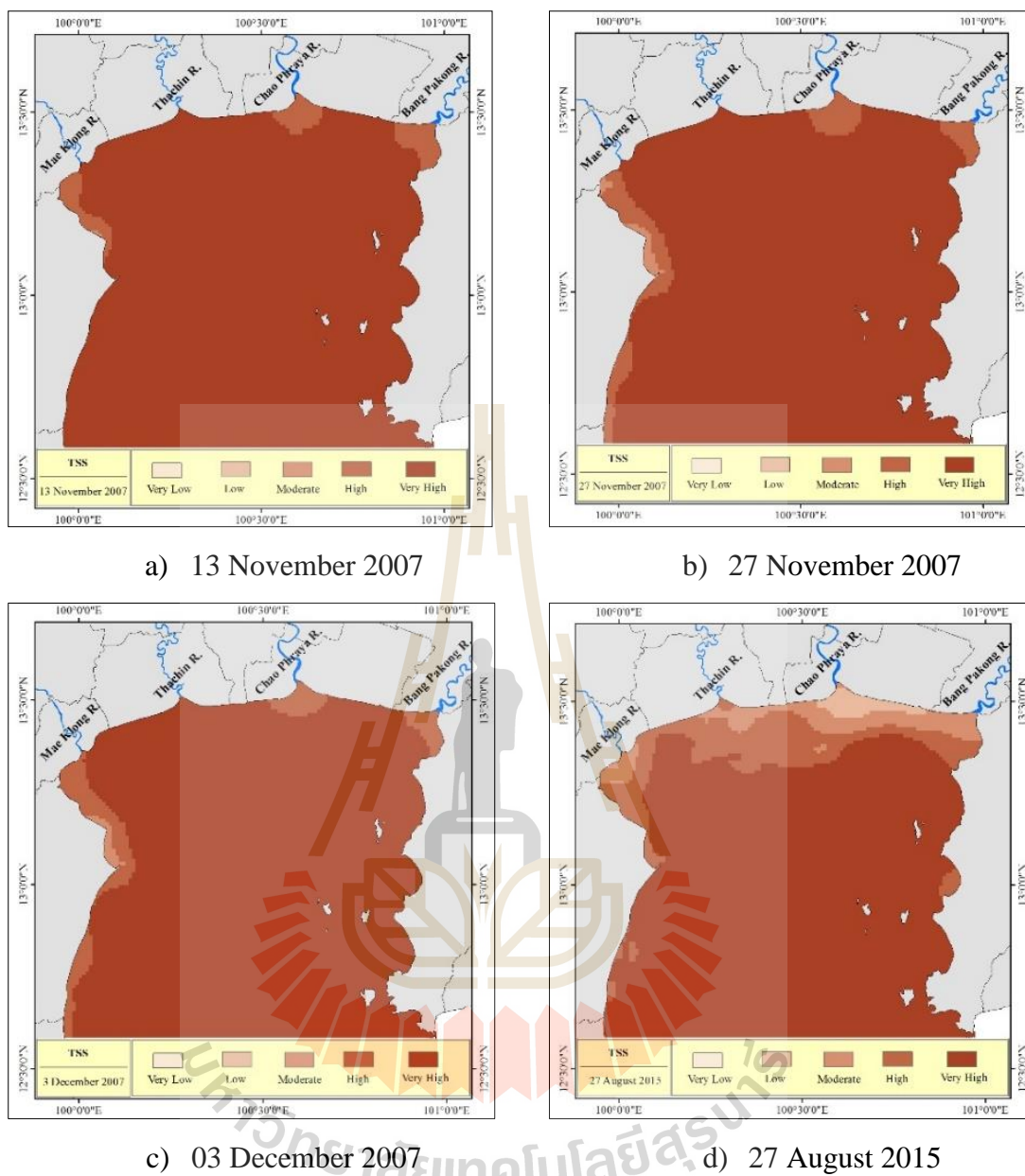


Figure 6.3(c) Classified TSS-based red-tide tendency of occurrence maps.

Table 6.1 Classified area for the TSS-based tendency maps in Figure 6.3.

Unit: sq.km

Classes	09 Feb 05	07 Jul 05	15 Aug 05	29 Sep 05	20 Oct 05	27 Mar 06	28 Sep 07	05 Nov 07	13 Nov 07	27 Nov 07	03 Dec 07	27 Aug 15
1	0	0	0	8	0	0	245	0	0	0	0	0
2	232	0	0	68	0	0	288	0	0	0	0	164
3	998	0	62	146	36	273	286	48	7	85	65	566
4	750	737	727	668	163	1,257	541	134	411	651	641	1,204
5	8,265	9,508	9,456	9,355	10,046	8,715	8,885	10,063	9,827	9,509	9,539	8,311

1 = Very Low, 2 = Low, 3 = Moderate, 4 = High, 5 = Very High.

Table 6.2 Standard statistics of original TSS data of the classified maps in Figure 6.3.

Unit: mg/l

No	Date	Minimum	Maximum	Mean	Std.Dev.
1	9 February 2005	0.158	32.479	4.097	4.932
2	7 July 2005	0.127	9.796	1.675	1.648
3	15 August 2005	0.168	17.625	2.092	1.891
4	29 September 2005	0.389	44.987	3.013	3.091
5	20 October 2005	0.234	15.462	2.438	1.501
6	27 March 2006	0.203	15.415	2.854	2.483
7	28 September 2007	0.109	66.425	4.649	9.216
8	5 November 2007	0.299	15.780	1.878	1.235
9	13 November 2007	0.283	10.419	2.261	1.341
10	27 November 2007	0.199	16.391	2.600	1.749
11	03 December 2007	0.375	15.364	2.559	1.650
12	27 August 2015	0.879	32.534	3.975	4.061

6.1.3 Color dissolved organic matter

Typically, CDOM is the large reserve of organic material in the aquatic environment that indicates nutrients abundance and, thereby, indirectly associates to eutrophication state. Like the TSS case reported earlier, CDOM concentration data for the preferred dates (like those of the TSS) were extracted from the corresponding MODIS imagery dataset through application of the identified optimal model (Chula model). These obtained CDOM dataset were then classified and mapped into five main categories representing five degrees of red tide occurrence tendency regarding to CDOM density seen in the area. The classification criteria for this purpose are as detailed in Table 3.8 from very low ($< 0.5 \text{ m}^{-1}$) to very high ($> 2.0 \text{ m}^{-1}$) and results are shown in Figure 6.4 in which concentration data ranging from 0.003 to 2.699 m^{-1} were found (Table 6.4). As seen in Table 6.3, regarding CDOM-based tendency maps displayed in Figure 6.4, areas with high to very high tendency were very low (for all dates) while most areas were found having very low to low tendency in this regard, especially those located further away from shore. Also, areas with moderate to very-high occurrence tendency were distributed sporadically close to shore on both sides of the gulf with no obvious regular pattern. Influence of river mouths on these CDOM-based tendency maps was not clearly evidenced (compared to the TSS case) for most dates under consideration.

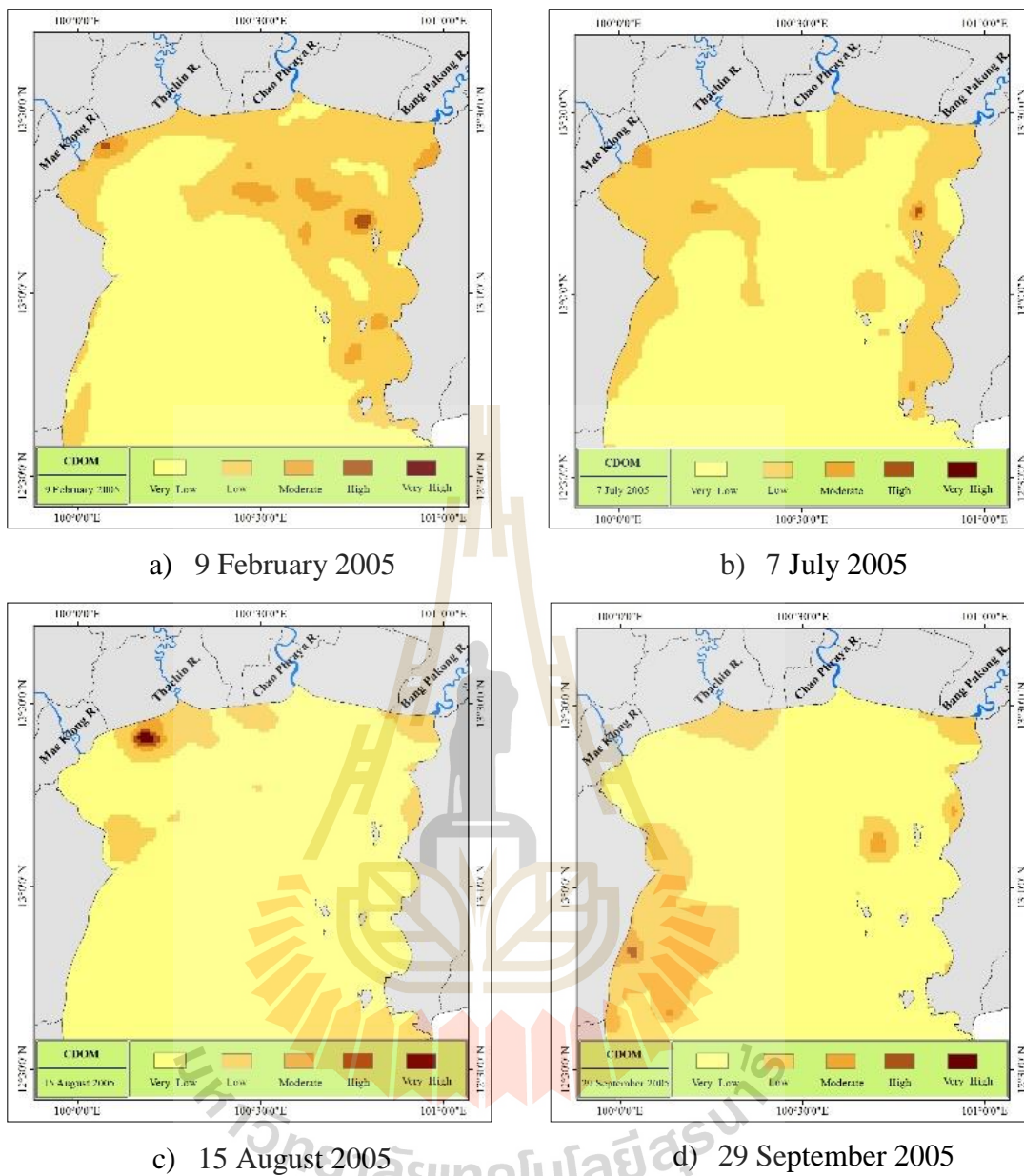


Figure 6.4(a) Classified CDOM-based red-tide tendency of occurrence maps.

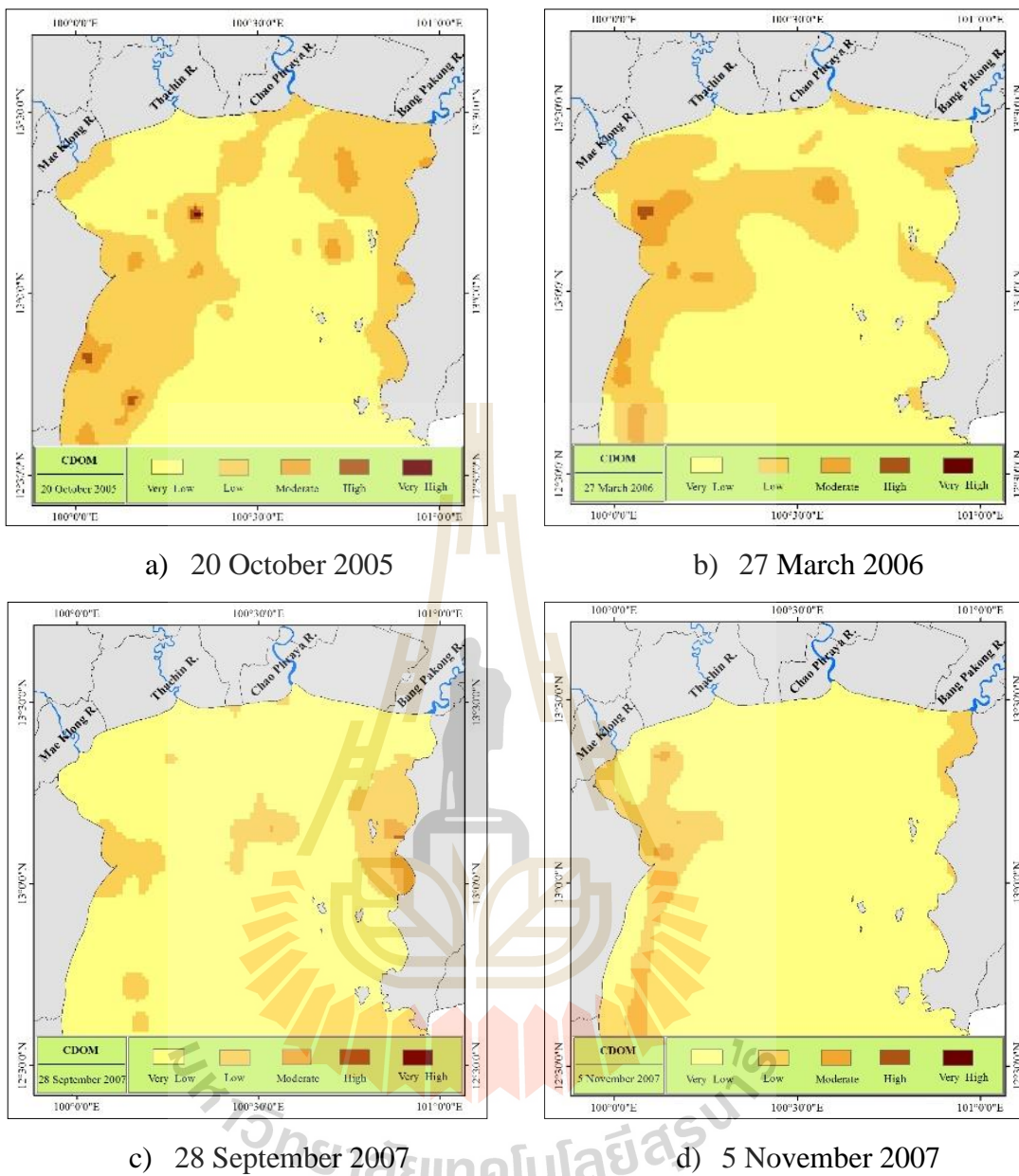


Figure 6.4(b) Classified CDOM-based red-tide tendency of occurrence maps.

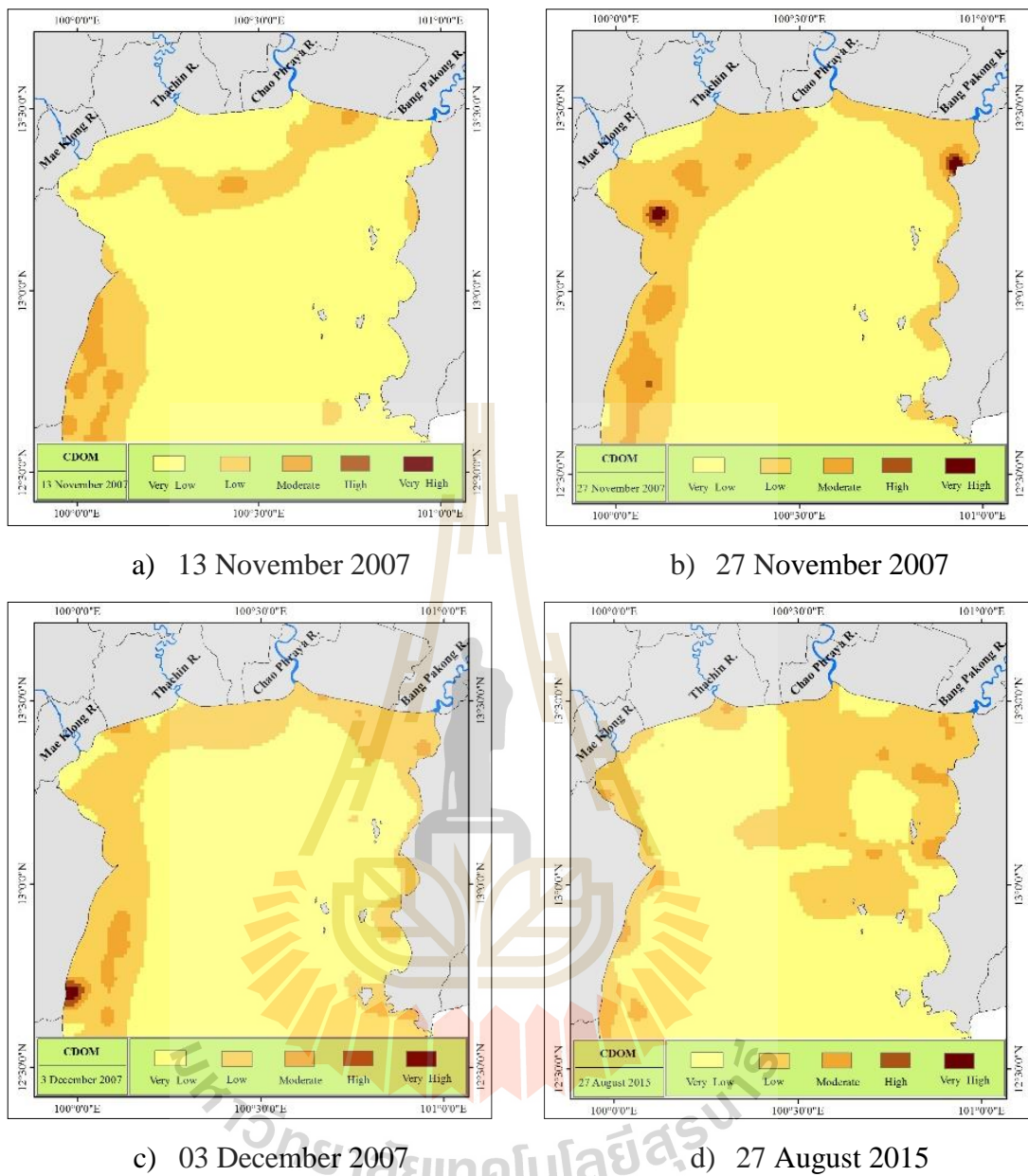


Figure 6.4(c) Classified CDOM-based red-tide tendency of occurrence maps.

Table 6.3 Classified area for the CDOM-based tendency maps in Figure 6.4.

Unit: sq.km

Classes	09 Feb 05	07 Jul 05	15 Aug 05	29 Sep 05	20 Oct 05	27 Mar 06	28 Sep 07	05 Nov 07	13 Nov 07	27 Nov 07	03 Dec 07	27 Aug 15
1	5,946	6,472	9,394	8,266	5,643	6,694	8,925	9,051	8,109	6,883	7,034	6,745
2	3,899	3,675	763	1,867	4,230	3,136	1,201	1,157	1,786	2,767	2,953	3,317
3	377	93	57	104	346	398	115	37	347	534	219	183
4	23	5	19	8	24	17	4	0	3	34	23	0
5	0	0	12	0	2	0	0	0	0	27	16	0

1 = Very Low, 2 = Low, 3 = Moderate, 4 = High, 5 = Very High,

Table 6.4 Standard statistics of original CDOM data of classified maps in Figure 6.4.Unit: m⁻¹

No	Date	Minimum	Maximum	Mean	Std.Dev
1	09 February 2005	0.091	1.832	0.475	0.254
2	07 July 2005	0.055	1.640	0.418	0.228
3	15 August 2005	0.004	2.500	0.240	0.208
4	29 September 2005	0.037	1.608	0.385	0.193
5	20 October 2005	0.043	2.093	0.503	0.258
6	27 March 2006	0.131	1.580	0.481	0.247
7	28 September 2007	0.019	1.689	0.367	0.181
8	05 November 2007	0.003	1.212	0.252	0.199
9	13 November 2007	0.037	1.786	0.332	0.264
10	27 November 2007	0.122	2.699	0.454	0.299
11	03 December 2007	0.117	2.167	0.414	0.252
12	27 August 2015	0.146	1.427	0.448	0.210

6.1.4 Sea water depth and distance from river mouth

Phytoplankton bloom is under influence of many ecological conditions such as water depth, sunlight, temperature, salinity, nutrient amount, ocean current (velocity/direction). In this work, water depth data of the UGoT were separated into five groups based on criteria given in Table 3.8 ranging from the very low tendency level (depth > 20 m) to the very high level (depth < 5 m) and the associated map was produced as illustrated in Figure 6.5.

In case of the distance from river mouth, this factor is very crucial for the analysis of red tide occurrence potential as most key nutrients were carried along (from upstream land) to the gulf's coastal zone by large amount of the water discharge released at four examined river mouths (that of the Chao Phraya River in particular). Figure 6.6 shows map of the red-tide occurrence tendency regarding the distance-from-river-mouth criteria stated in Table 3.8, from the very low (> 30 km) to the very high tendency level (< 5 km). Both factors stated here gave highest priority of red tide occurrence to areas situated close to shore due to higher amount of needed nutrients and rather calm ocean current over there. Chances of having red tide seem to drop rapidly with the distance away from shore and from the river mouths as evidenced in Figure 6.6 and Table 6.5.

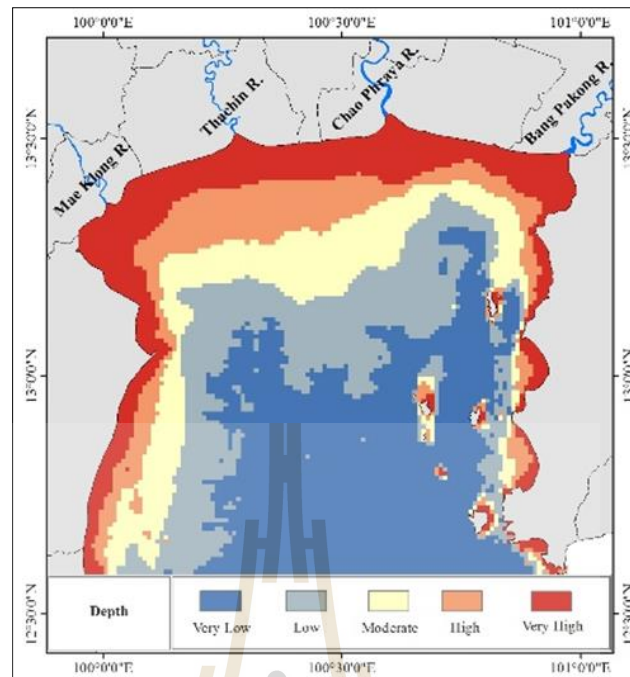


Figure 6.5 Classified red-tide tendency of occurrence map based on water depth.

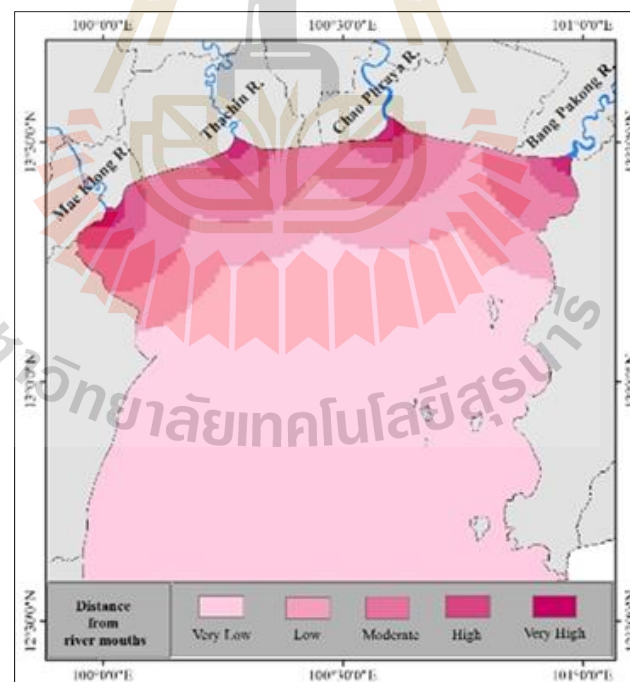


Figure 6.6 Classified red-tide tendency of occurrence map based on distance away from four main river mouths.

Table 6.5 Classified area for the tendency maps in Figures 6.5 (based on water-depth) and 6.6 (based on distance-from-river-mouth).

Unit: sq.km

Classes	Sea Water Depth		Distance from River mouths	
	Area	%	Area	%
1) Very low	3,393	33.12	7,240	70.67
2) Low	2,141	20.90	1,232	12.03
3) Moderate	1,509	14.73	1,304	12.73
4) High	1,246	12.16	361	3.52
5) Very high	1,956	19.09	108	1.05

6.1.5 Velocity of surface current

Primarily, movement characteristics of sea currents over the UGoT is under dominant control of the prevailing monsoon systems over the area which are the NE monsoon during winter to early dry season and SW monsoon during the local wet (or monsoon) season (Buranapratheprat, 2000). However, as movements of the surface sea current are usually quite dynamics all year round, therefore, current's velocity/direction maps (derived from proper ocean current simulation model for the UGoT) must reflect these characteristics as well like in Figures 6.7(a)-(c). In general, current velocity in UGoT was often found not higher than 0.15 m/sec except during wet season.

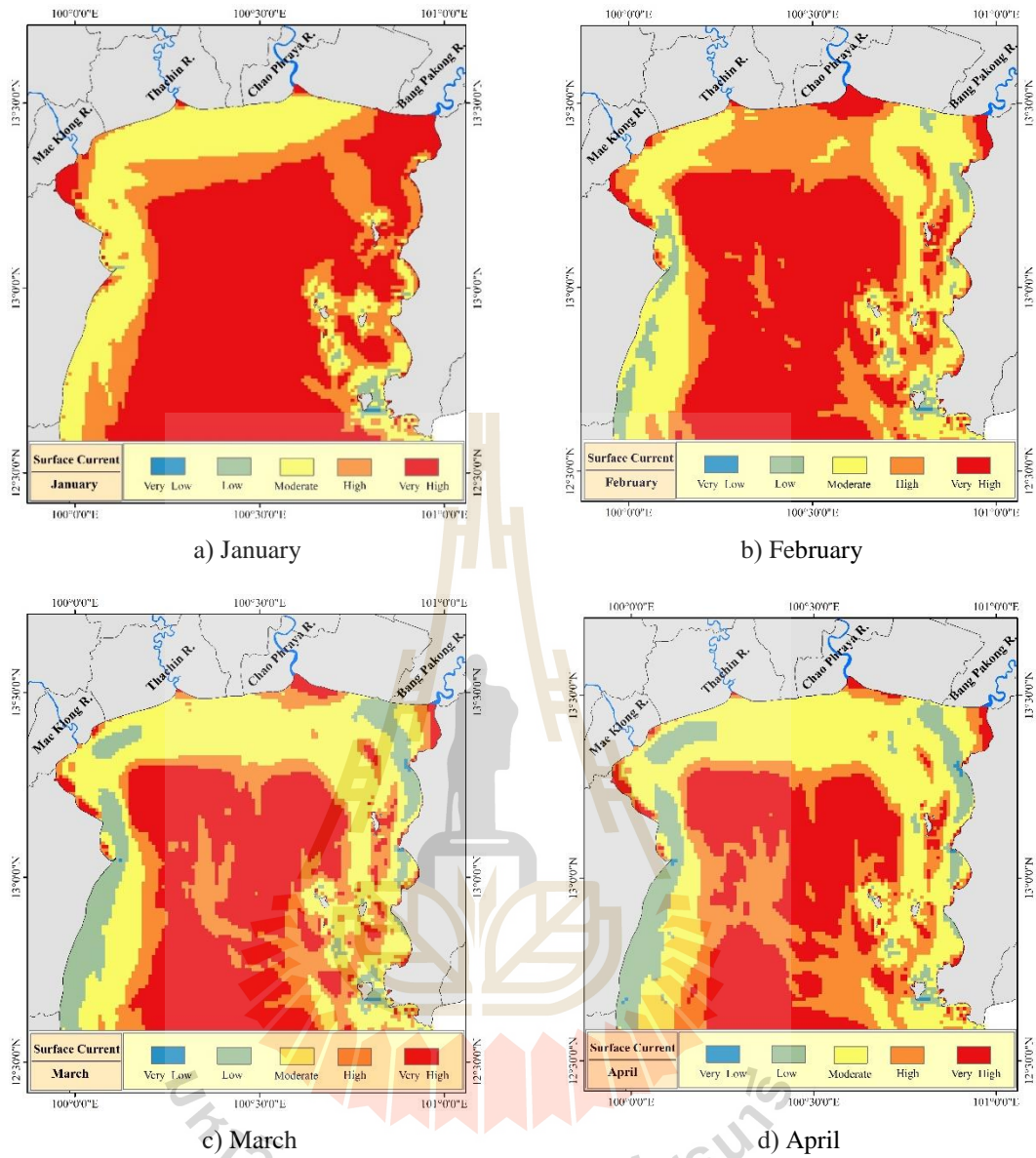


Figure 6.7(a) Surface current maps of the UGoT from January to April.

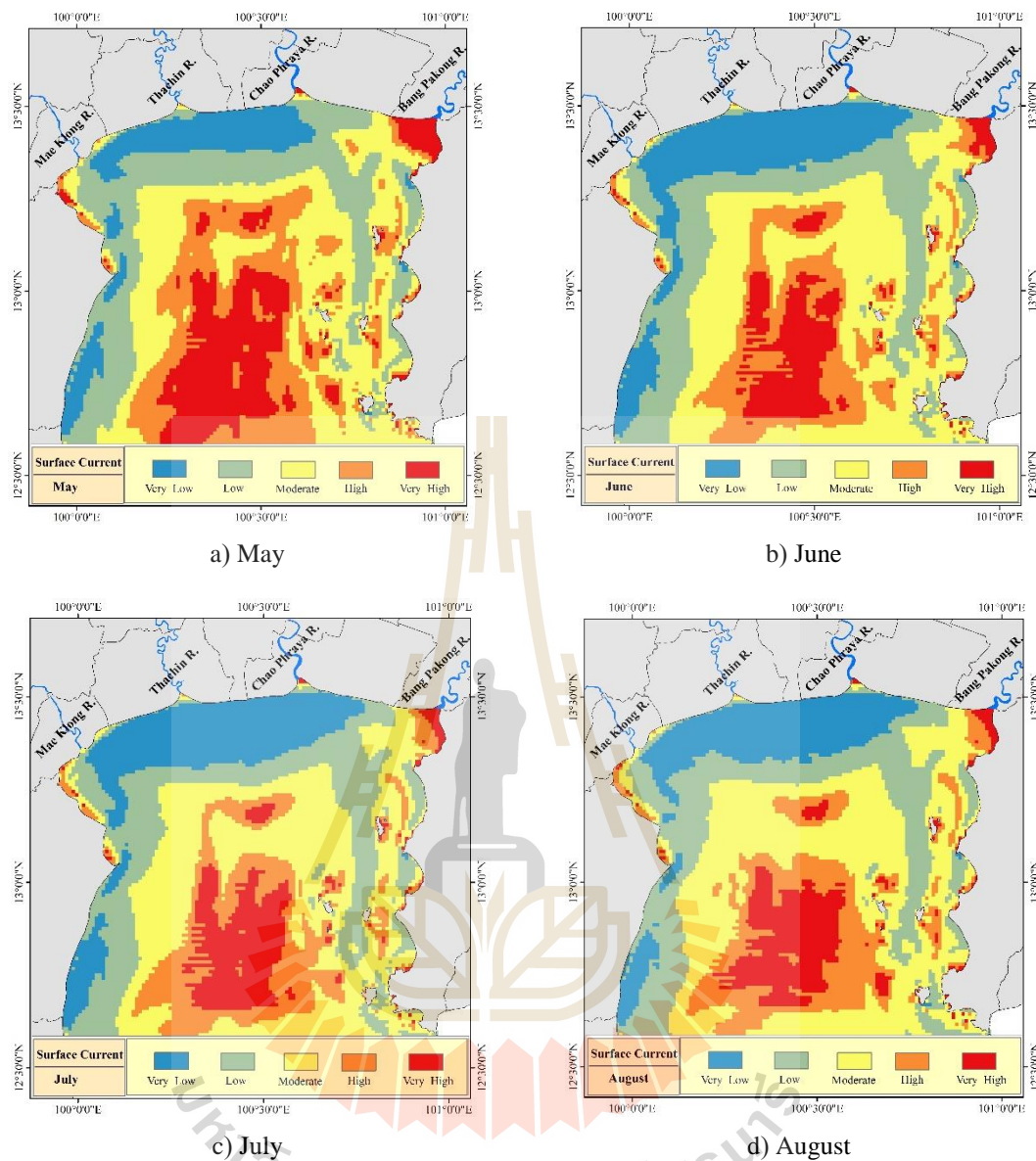


Figure 6.7(b) Surface current maps of the UGoT from May to August.

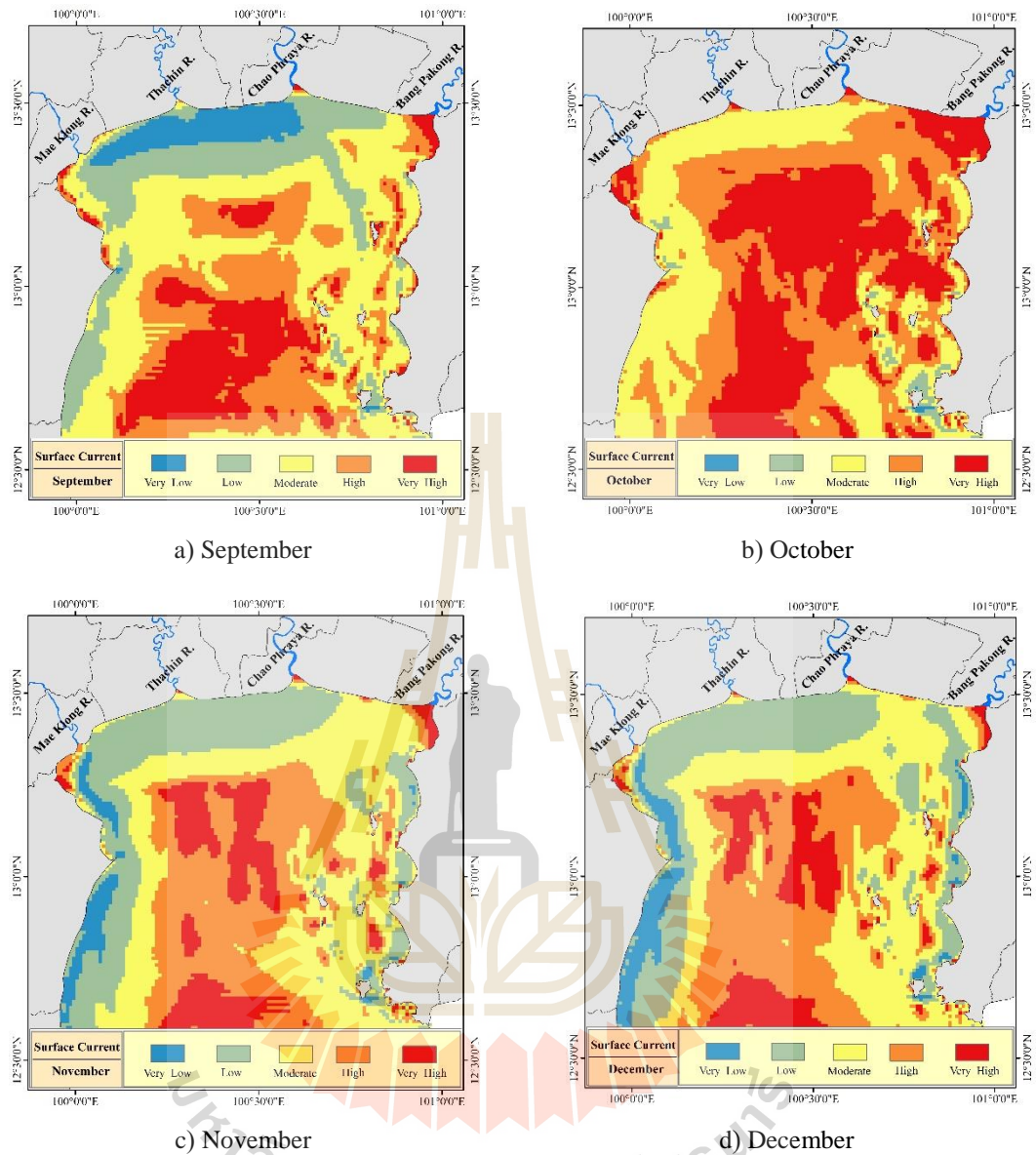


Figure 6.7(c) Surface current maps of the UGoT from September to December.

Table 6.6 Classified area for the tendency maps seen in Figure 6.7.

Unit: sq.km

Classes	Jan	Feb	Mar	Apr	May	Jun	Jul	Aug	Sept	Oct	Nov	Dec
1) Very low	0	0	2	0	0	151	315	253	0	0	2	5
2) Low	16	14	101	166	1,775	2,074	2,006	2,005	969	44	945	837
3) Moderate	69	378	818	843	1,630	1,684	1,688	1,603	1,370	152	1,725	1,945
4) High	2,425	2,565	3,309	3,479	3,037	3,535	3,462	3,611	3,620	2,567	3,482	3,463
5) Very high	7,735	7,288	6,015	5,757	3,803	2,801	2,774	2,773	4,286	7,482	4,091	3,995

Table 6.7 Standard statistics of the derived monthly surface current velocity data.

Unit: m/sec

Month	Minimum	Maximum	Mean	Std.Dev
January	0.00011	0.14196	0.01288	0.01184
February	0.00017	0.14687	0.01657	0.01446
March	0.00017	0.15503	0.02161	0.01880
April	0.00016	0.14281	0.02349	0.01976
May	0.00018	0.16165	0.04222	0.03509
June	0.00021	0.17325	0.05022	0.04056
July	0.00022	0.17759	0.05167	0.04223
August	0.00023	0.17732	0.04951	0.04075
September	0.00018	0.15002	0.03457	0.02944
October	0.00014	0.16840	0.01668	0.01198
November	0.00015	0.16522	0.03660	0.02837
December	0.00018	0.17325	0.03741	0.02927

6.2 Red tide susceptibility mapping by SAW method

In this part, the preferred simple additive weighting (SAW) decision method was applied to identify susceptibility level of the red tide occurrence over the UGoT area based on the assigned factor and class (or attribute) weights for each influencing factor in use yielded from the expert judgments. These weights reflect priority of each attribute to the development of red tide over the area. Advantages of this method are its simple structure and straightforward concept to derive susceptibility map.

In the analysis process, initial factor/class weights were drawn from responses of nineteen interviewed experts on this field (the corresponding marine specialists) through the prepared questionnaire (as detailed in Appendix F). Factor weights were initially proposed to have score of 1 (least important) to 5 (most important) while their associated attribute weights (for each used factor) were given scores of 2, 4, 6, 8, and 10 (from low to high priority), respectively. After that, the appropriate factor weights were determined through multiple comparison method (Malczewski, 1999). This set of derived weights were then applied to calculate susceptibility score for each defined unit area (a pixel size of 1 km²) through the linear combination of product between respective factor and class weights for each identified unit area (Adriyendi, 2015). In the preparation of preferred susceptibility maps, seven different scenarios were considered based on different combinations of input factors in the susceptibility analysis as explained in Table 6.8, starting from case 1 (or scenario Type 1) where all five factors were used to case 7 where only CDOM/current velocity were included. The multiple comparison analysis weight were computed which counted of criterion match paired, which one more importance than other one and then be similar done for each pair of factors. Summarize value as all factors in each column and divide by total of summarize (as all criteria). Relevant factor weights for each case are given in Table 6.9 factor.

Table 6.8 Seven examined scenarios for red-tide susceptibly mapping (Type 1-7).

Factors	Scenario type						
	Type 1	Type 2	Type 3	Type 4	Type 5	Type 6	Type 7
1) Total suspended solids	√	√	√	√	√	√	-
2) Color dissolved organic matter	√	√	√	√	√	√	√
3) Water depth	√	√	√	-	-	-	-
4) Distance from river mouth	√	√	-	√	-	-	-
5) Current velocity	√	-	√	√	√	-	√

Table 6.9 Evaluation of preference score (PS) by the multiple comparison analysis.

Factors	Total suspended solids	Color dissolved organic matter	Water depth	Distance from river mouth	Current velocity
1) Total suspended solids	-	7	8	9	6
2) Color dissolved organic matter	5	-	5	7	4
3) Water depth	5	9	-	9	5
4) Distance from river mouth	1	3	2	-	1
5) Current velocity	7	10	8	13	-
Total preference score (Type-1)	18	29	23	38	16

Table 6.10 Total preference score (from Table 6.9) and final normalized weight for individual factor included in each listed scenario (Type 1-7) presented in Table 6.8.

Total PS /Normalized weight	Total suspended solids	Color dissolved organic matter	Water depth	Distance from river mouth	Current velocity
Type 1: Total PS	18	29	23	38	16
Type 1: Normalized weight	0.145	0.234	0.185	0.306	0.129
Type 2: Total PS	11	19	15	25	-
Type 2: Normalized weight	0.157	0.271	0.214	0.357	-
Type 3: Total PS	17	26	21	-	15
Type 3: Normalized weight	0.215	0.329	0.266	-	0.190
Type 4: Total PS	13	20	-	29	11
Type 4: Normalized weight	0.178	0.274	-	0.397	0.151
Type 5: Total PS	12	17	-	-	10
Type 5: Normalized weight	0.308	0.436	-	-	0.256
Type 6: Total PS	5	7	-	-	-
Type 6: Normalized weight	0.417	0.583	-	-	-
Type 7: Total PS	-	10	-	-	4
Type 7: Normalized weight	-	0.714	-	-	0.211

Note: Normalized weight = Total PS/∑ Total PS

Table 6.11 Associated class (or attribute) weights for input factors in SAW model.

Factors	Class weights				
	Class 1	Class 2	Class 3	Class 4	Class 5
1) Total suspended solids	2.22	4.88	5.53	7.71	8.50
2) Color dissolved organic matter	2.42	4.00	6.00	7.31	9.07
3) Water depth	2.47	3.67	6.22	8.11	10.00
4) Distance from river mouth	2.59	4.47	6.11	8.00	9.75
5) Current velocity	2.78	5.05	6.21	7.33	7.41

Based on gained preference scores for each pair of examined factors displayed in Table 6.9 (e.g. 7 for CDOM over TSS or 5 for TSS over CDOM), the normalized weight for each factors in each proposed scenarios (Type 1-7) were then established from the known total preference score for each factor (of each scenario) as detailed in Table 6.10. For example, in Type 1 case where all five initial factors were examined, the obtained total score for TSS, CDOM, water depth, distance from the river mouth and current velocity were 18, 29, 23, 38, and 16, respectively (with total sum of 124). As a result, their associated normalized weights became 0.145, 0.234, 0.185, 0.306, and 0.129, accordingly. Result in this case means the corresponding experts gave top priority to distance from river mouth in average (for red-tide susceptibility mapping) if compared to other considered factors (followed by CDOM) while the least favorite ones here were current velocity and TSS. Similar outcomes were evidenced in Type 2 and 4 scenarios where top preference list was distance from the river mouth in both cases while the lowest ranks were TSS (in Type 2) and current velocity (in Type 4). For other cases where distance from river mouth was excluded (i.e., Type 3 and 5-7), foremost priority belonged to CDOM (the second-most favorite one in Type 1 case).

The yielded normalized factor weights seen in Table 6.9 were then integrated with the associated class (or attribute) weights for each listed factor in each scenario derived from collective expert's opinions given through the distributed questionnaires. The original proposed class weights were 2, 4, 6, 8, and 10 (from low to high priority) and average values (from 19 responses available) were used as ultimate class weight for each factor of interest as described in Table 6.11. The red-tide susceptibility maps for proposed scenarios were then constructed by SAW technique detailed in Chapter

III from which the pixel-based total red-tide susceptibility score were classified into five categories: very low (VL), low (L), moderate (M), high (H), and very high (VH). Five value classes were defined by equal interval method of classification. This is because the yield maps were derived become to be draw a comparison between several scenarios in the end.

Figures 6.8(a)-(b) display classified red-tide susceptibility maps formulated through the SAW method for the UGoT area for each relevant scenarios (Type 1 to 7). In general, output susceptibility maps of Type 1-4 scenarios display expected pattern of red-tide tendency map with top probability (e.g. the H/VH classes) appeared over shallow water zone near shore and close to the main river mouths, especially those of the Thachin and Bang Pakong Rivers, while low occurrence tendency zone was mainly evidenced further away from shore and main river mouths into the deep water zone (e.g. VL/L classes). Note that, influence of huge annual the Chao Phraya River's discharge on red tide occurrence tendency over UGoT area was rather weak/moderate in Type 1-4 analysis. In addition, data of classified area for the mapped trophic states for Type 3 case (without distance-to-river-mount factor) seems rather different from that of other cases as the "low" class was predominant in deep water zone instead of the "very low" tendency class as usual (36.7% for L and 2.3% for VL) (as detailed in Table 6.12). This result indicates high influence of the distance-to-river-mount factor (that was abandoned in this case) in the creation of susceptibility map in this analysis if compared to the output map of Type 1 case (with all factors applied), Type 2 case (without current-velocity factor) and Type 4 case (without water-depth factor). This work also highlights low influence of current-velocity and water-depth exclusion on

red-tide susceptibility mapping for the UGoT area done at this stage (as evidenced in the expert-based preference weights reported in Table 6.10).

For susceptibility analysis and mapping in the Type 5-7 cases (where distance-to-river-mount and water-depth were excluded), outlook of the obtained maps appears distinctively different from the output map of the Type 1 scenario (the reference case). For examples, now the “moderate” and “high” susceptibility portions were apparently prevalent over the area while the classified “very low” and “low” susceptibility zones appear to be much inferior. For examples, in Type 5 (TSS+CDOM+current velocity) and 6 (TSS+CDOM) scenarios, about 94% of the total area was belonged to the “M” and “H” classes while just only around 2% was occupied by the “VL” and “L” states. However, for Type 7 case (CDOM+current velocity), the established map looks more realistic as the “VL” and “L” states now covered about 39% of total area while that of the “H” and “VH” stayed about 60 %. Also, highly prone areas (“H” and “VH” levels) were found spreading sporadically over UGoT region and not bound to shallow water zone near shore/close to main river mounts as observed in Type 1-4 cases.

To evaluate general ability of the established susceptibility maps on explaining the presumed occurrences of red tide incidences [Figure 6.2(b)], the area under curve (AUC) method for map accuracy assessment was done for all examined cases (Type 1-7 scenarios) and final results are reported in Table 6.13 and Figure 6.9, respectively. Among these cases, best AUC results were found belonged to Type 6 (TSS+CDOM) with the AUC of 0.94 and Type 5 (TSS+CDOM+current velocity) with AUC of 0.89. Performances of Type 1-4 cases were rather similar with moderate AUC data of 0.54 (Type 2) to 0.66 (Type 3) were discovered. The worst result gained in this evaluation

was for Type 7 case where AUC of 0.28 was found indicating low predictability of its map for past happening of reference red tide incidences.

Note that, all three highest AUC outcomes (Types 6/7/3) were yielded from cases with no distance-to-river-mount factor incorporated. This fact made the output susceptibility maps be more in favor of the moderate (M) to high (H) tendency level of red tide occurrence, even in the remote deep water zone far away from shore. Also, the hotspots for red tide occurrence likelihood (H/VH zones) were then not bound to the near shore/close to main river mouths as usual due to the ignorance of distance to river mount and water depth in map preparation process. In principle, this kind of map (M/H favourite) tends to offer notable “true-positive” prediction accuracy as well as excessive “false-positive/false-alarm” prediction also. Therefore, the interpretation of AUC results gained in this situation should be cautiously carried out as the associated susceptibility maps (with high AUC outcome) might not validly represent the realistic nature of the red tide occurrence tendency regarding conventional believe or prevailed theory, as key parameters, i.e. distance to main river mount and water depth factors, were discarded in the analysis. To achieve more comprehensive accuracy assessment of the established susceptibility map in each case, some other accuracy assessment methods (apart from AUC) might be required to ensure of its effectiveness as needed.

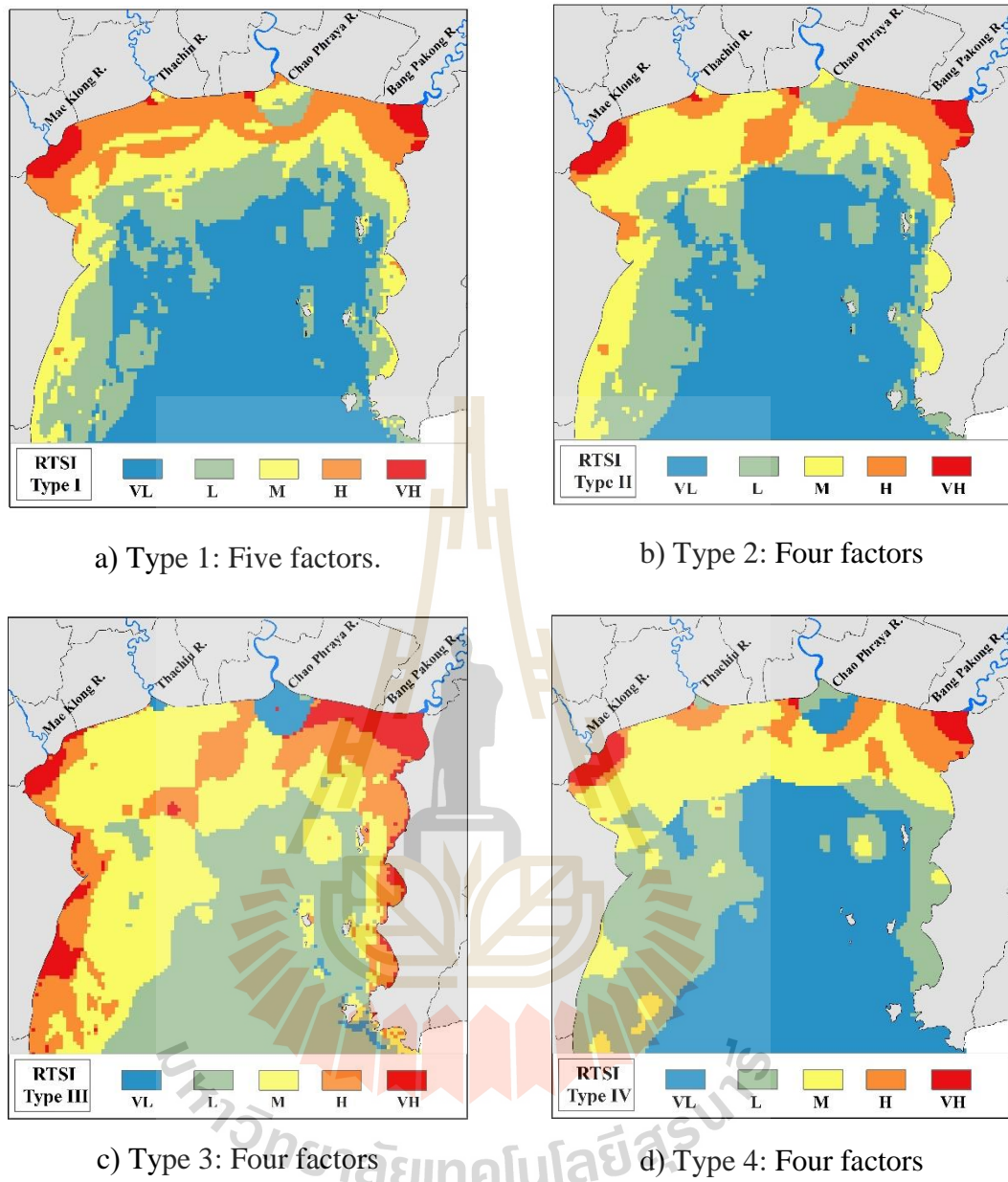
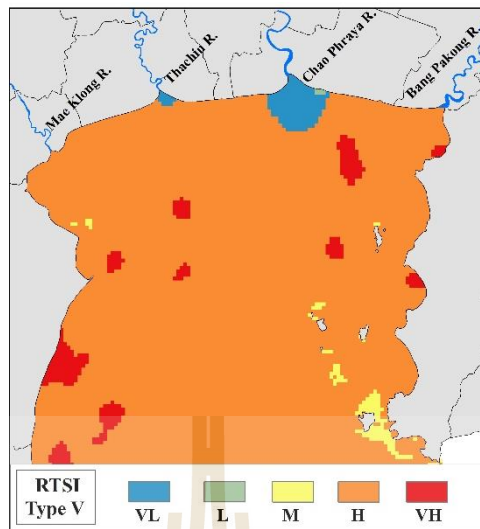
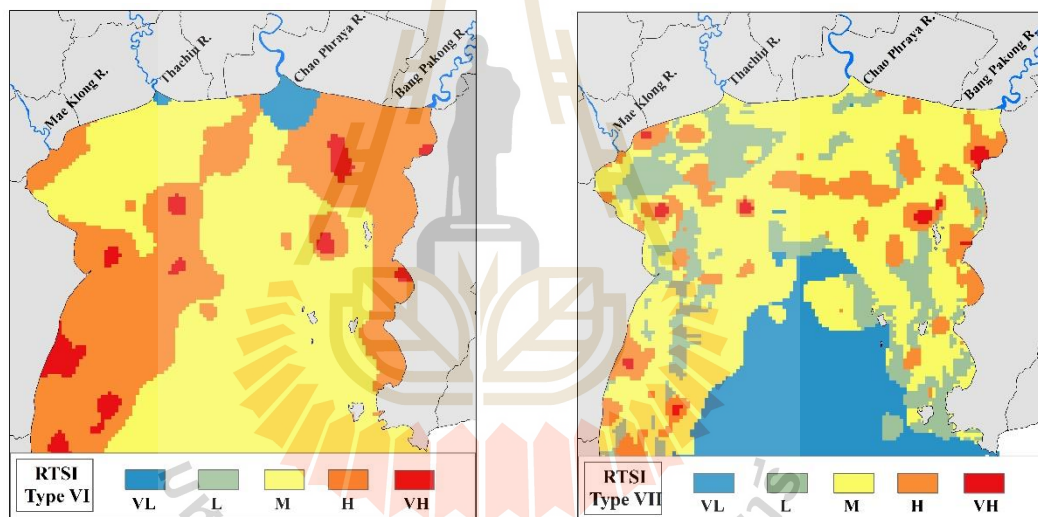


Figure 6.8(a) Red-tide susceptibility maps by SAW method (Type 1-4 cases).



a) Type 5: Three factors.



b) Type 6: Two factors

c) Type 7: Two factors

Figure 6.8(b) Red-tide susceptibility maps by SAW method (Type 5-7 cases).

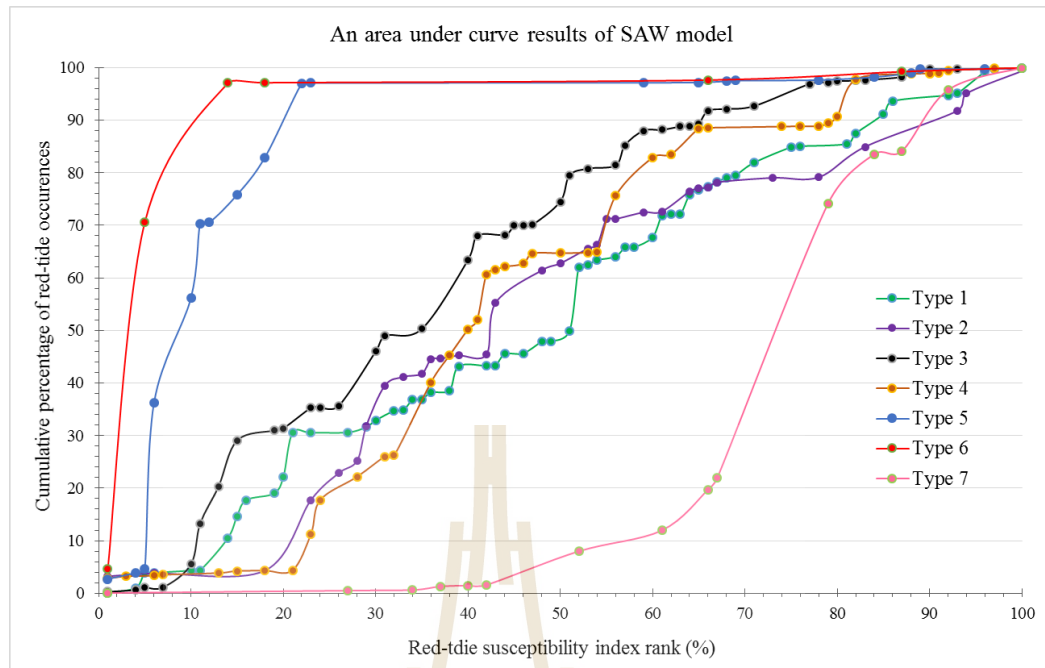


Figure 6.9 An accuracy assessment result based on AUC method of SAW model.

Table 6.12 Classified area for red-tide susceptibility category based on SAW model.

Unit: sq.km

Types	RTSI Condition	VL	%	L	%	M	%	H	%	VH	%
1	Five Factors	4,533	44.2	2,495	24.4	1,745	17.0	1,248	12.2	224	2.2
2	Four Factors	4,572	44.6	2,338	22.8	2,214	21.6	866	8.5	255	2.5
3	Four Factors	240	2.3	3,759	36.7	3,738	36.5	1,775	17.3	733	7.2
4	Four Factors	4,318	42.1	2,884	28.2	2,182	21.3	623	6.1	238	2.3
5	Three Factors	193	1.9	6	0.1	128	1.2	9,546	93.2	372	3.6
6	Two Factors	199	1.9	0	0	5,557	54.3	4,117	40.2	372	3.6
7	Two Factors	2,245	21.9	1,709	16.7	4,914	48.0	1,282	12.5	95	0.9

Total of areas: 10,245.

Table 6.13 The results of accuracy assessment based on SAW model.

Type of validation	Scenario type						
	Type 1	Type 2	Type 3	Type 4	Type 5	Type 6	Type 7
SAW-AUC	0.55	0.54	0.66	0.56	0.89	0.94	0.28

Type 1 : Five factors. TSS, CDOM, Depth, Distance from the river mouth and Speed of surface current

Type 2 : Four factors; TSS, CDOM, Depth and Distance from the river mouth

Type 3 : Four factors. TSS, CDOM, Depth and Speed of surface current

Type 4 : Four factors. TSS, CDOM, Distance from the river mouth and Speed of surface current

Type 5 : Three factors. TSS, CDOM and Speed of surface current

Type 6 : Two factors. TSS and CDOM

Type 7 : Two factors. CDOM and Speed of surface current

6.3 Red tide susceptibility mapping by FR method

In this part, the red-tide susceptibility maps (for each specified scenarios stated in Table 6.8) were established by the popular frequency ratio (FR) method described in Chapters II and III. In essence, FR is a quantitative susceptibility analysis/mapping frequently used for the formulation of landslide susceptibility maps around the world but its application in red-tide susceptibility analysis/mapping has not been seen so far. Here, the FR method was introduced to generate scenario-based red-tide susceptibility maps for the UGoT based on the assessed quantitative relationships between red-tide occurrence locations and the associated attributes of each considered factors (for each proposed scenarios). These relationships were expressed in form of class (or attribute) weight ranging from 0 (no relation) onwards to 1 (average correlation) and to greater values (> 1) (higher correlation). Total sum of all corresponding class weights (from each associated factor) for a specific unit area (1 km^2), or a pixel, shall become its red-tide susceptibility index (RTSI) for that pixel which indicates likelihood of having

red tide incidence over that area. Note that, in the FR case, the specific factor weight was not required in the susceptibility assessment process like that in the SAW case.

Tables 6.14(a)-(c) demonstrate examples of the yielded FR attribute weight for the three reference red-tide dominant dates, i.e., 07 July 2005, 27 March 2006 and 03 December 2007. Each specific FR class weight was determined from computed ratio of the red-tide area percentage (for that attribute) over class-occupied area percentage where higher FR value means higher correlation to red tide occurrence frequency seen in that attribute state (or class). For examples, on 07 July 2005, the most influential attributes related to the observed red tide incidences on that date (based on FR values) were distance from river mouth of 5-30 km (FR=2.54-2.97), water depth of 5-10 meter (FR=2.76) and relatively strong current speed of > 0.1 m/s (FR=2.48). Similar trends were found on the other dates under consideration.

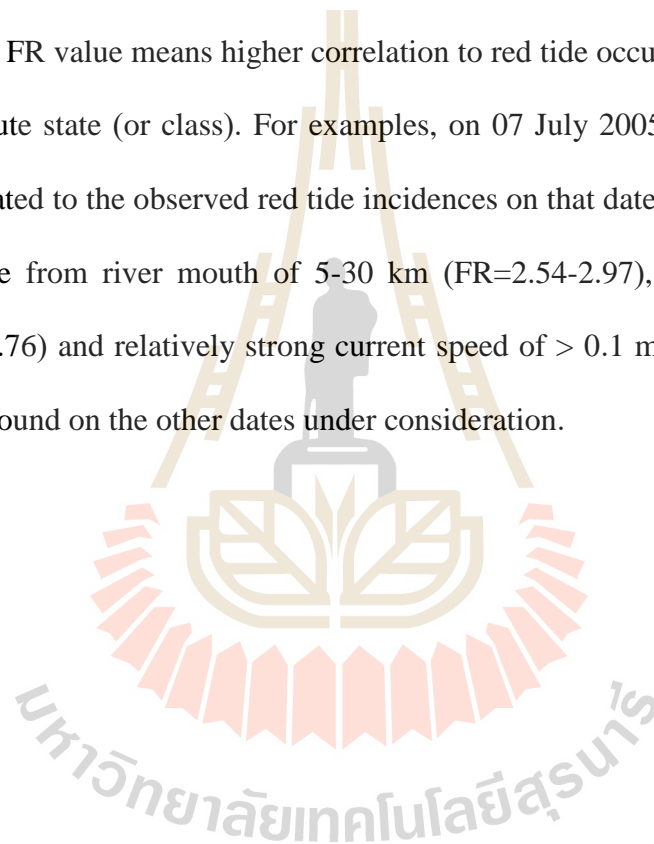


Table 6.14(a) Derivation of the associated FR attribute weights on 07 July 2005.

Factors	Class	Total number of pixels		Red tide event sites pixels		Frequency
		Area (sq.km)	%	Area (sq.km)	%	Ratio
TSS (mg/l)						
1	> 40	0	0	0	0	0
2	20 - 40	0	0	0	0	0
3	10 - 20	0	0	0	0	0
4	5 - 10	737	7.19	60	11.70	1.63
5	< 5	9,508	92.81	453	88.30	0.95
CDOM (m⁻¹)						
1	< 0.5	6,472	63.17	114	22.22	0.35
2	0.5 - 1.0	3,675	35.87	399	77.78	2.17
3	1.0 - 1.5	93	0.91	0	0	0
4	1.5 - 2.0	5	0.05	0	0	0
5	> 2.0	0	0	0	0	0
Depth (m)						
1	> 20	2,791	27.24	14	2.73	0.10
2	15 - 20	2,634	25.71	21	4.09	0.16
3	10 - 15	1,576	15.38	111	21.64	1.41
4	5 - 10	1,325	12.93	183	35.67	2.76
5	< 5	1,919	18.73	184	35.87	1.91
Distance from river mouth (km)						
1	>30	7,240	70.67	112	21.83	0.31
2	20-30	1,232	12.03	183	35.67	2.97
3	10-20	1,304	12.73	166	32.36	2.54
4	5 - 10	361	3.52	48	9.36	2.66
5	< 5	108	1.05	4	0.78	0.74
Current – velocity (m/sec)						
1	> 0.1	1,672	16.32	208	40.55	2.48
2	0.05 - 0.1	2,386	23.29	104	20.27	0.87
3	0.02 - 0.05	3,452	33.69	140	27.29	0.81
4	0.01 - 0.02	1,664	16.24	51	9.94	0.61
5	< 0.01	1,071	10.45	10	1.95	0.19

Total cell of event = 513

Total cell of all areas = 10,245

Table 6.14(b) Derivation of the associated FR class weights on 27 March 2006.

Factors	Class	Total pixels		Red tide event pixels		Frequency
		Area (sq.km)	%	Area (sq.km)	%	Ratio
TSS (mg/l)						
1	> 40	0	0	0	0	0
2	20 - 40	0	0	0	0	0
3	10 - 20	273	2.66	0	0	0
4	5 - 10	1,257	12.27	29	6.70	0.55
5	< 5	8,715	85.07	404	93.30	1.10
CDOM (m⁻¹)						
1	< 0.5	6,694	65.34	212	48.96	0.75
2	0.5 - 1.0	3,136	30.61	214	49.42	1.61
3	1.0 - 1.5	398	3.88	7	1.62	0.42
4	1.5 - 2.0	17	0.17	0	0	0
5	> 2.0	0	0	0	0	0
Depth (m)						
1	> 20	2,791	27.24	20	4.62	0.17
2	15 - 20	2,634	25.71	13	3.00	0.12
3	10 - 15	1,576	15.38	135	31.18	2.03
4	5 - 10	1,325	12.93	213	49.19	3.80
5	< 5	1,919	18.73	52	12.01	0.64
Distance from River Mouth (km)						
1	>30	7,240	70.67	55	12.70	0.18
2	20-30	1,232	12.03	278	64.20	5.34
3	10-20	1,304	12.73	100	23.09	1.81
4	5 - 10	361	3.52	0	0	0
5	< 5	108	1.05	0	0	0
Current – velocity (m/sec)						
1	> 0.1	13	0.13	4	0.92	7.28
2	0.05 - 0.1	966	9.43	30	6.93	0.73
3	0.02 - 0.05	3,341	32.61	246	56.81	1.74
4	0.01 - 0.02	2,161	21.09	101	23.33	1.11
5	< 0.01	3,764	36.74	52	12.01	0.33

Total cell of event = 433

Total cell of all areas = 10,245

Table 6.14(c) Derivation of the associated FR class weights on 03 December 2007.

Factors	Class	Total number of pixels		Red tide event sites pixels		Frequency
		Area (sq.km)	%	Area (sq.km)	%	Ratio
TSS (mg/l)						
1	> 40	0	0	0	0	0
2	20 - 40	0	0	0	0	0
3	10 - 20	65	0.63	2	0.57	0.91
4	5 - 10	641	6.26	64	18.23	2.91
5	< 5	9,539	93.11	285	81.20	0.87
CDOM (m ⁻¹)						
1	< 0.5	7,034	68.66	12	3.42	0.05
2	0.5 - 1.0	2,953	28.82	302	86.04	2.99
3	1.0 - 1.5	219	2.14	24	6.84	3.20
4	1.5 - 2.0	23	0.22	8	2.28	10.15
5	> 2.0	16	0.16	5	1.42	9.12
Depth (m)						
1	> 20	2,791	27.24	0	0	0
2	15 - 20	2,634	25.71	12	3.42	0.13
3	10 - 15	1,576	15.38	67	19.09	1.24
4	5 - 10	1,325	12.93	99	28.21	2.18
5	< 5	1,919	18.73	173	49.29	2.63
Distance from River Mouth (km)						
1	>30	7,240	70.67	157	44.73	0.63
2	20 - 30	1,232	12.03	0	0	0
3	10 - 20	1,304	12.73	126	35.90	2.82
4	5 - 10	361	3.52	61	17.38	4.93
5	< 5	108	1.05	7	1.99	1.89
Current – velocity (m/sec)						
1	> 0.1	508	4.96	71	20.23	4.08
2	0.05 - 0.1	2,387	23.30	246	70.09	3.01
3	0.02 - 0.05	3,321	32.42	26	7.41	0.23
4	0.01 - 0.02	2,861	27.93	5	1.42	0.05
5	< 0.01	1,168	11.40	3	0.85	0.07

Total cell of event = 351

Total cell of all areas = 10,245

Table 6.15. Summary of FR class weights for all reference red tide maps and the average FR for each specific attribute.

Factors	Class	Frequency Ratio of Red Tide Occurrences												FR
		7-Jan-05	9-Feb-05	29-Sep-05	20-Oct-05	15-Aug-05	27-Mar-06	27-Nov-07	28-Sep-07	3-Dec-07	5-Nov-07	13-Nov-07	27-Aug-15	average
TSS-C1	> 40	0	0	0	0	0	0	0	0	0	0	0	0	0
TSS-C2	20 - 40	0	0	0	0	0	0	0	0	0	0	0	0.46	0.04
TSS-C3	10 - 20	0	0	0	0	0	0	0	0	0.91	0	0	3.89	0.40
TSS-C4	5 - 10	1.63	1.64	4.97	1.35	3.46	0.55	0.70	0.86	2.91	0	1.68	0.90	1.72
TSS-C5	< 5	0.95	1.05	0.73	1.00	0.82	1.10	1.03	1.10	0.87	1.02	0.98	0.89	0.96
CDOM 1	< 0.5	0.35	0.13	0.46	0.14	0.47	0.75	0.37	0.64	0.05	0.90	0.74	0.04	0.43
CDOM -2	0.5 - 1.0	2.17	2.28	3.39	1.99	6.66	1.61	2.43	3.80	2.99	1.51	2.36	0.23	2.78
CDOM -3	1.0 - 1.5	0	1.59	0.75	2.36	12.29	0.42	1.03	0	3.20	8.60	0	0.38	3.41
CDOM -4	1.5 - 2.0	0	0	0	8.64	3.46	0	3.60	0	10.15	0	0	0.54	2.15
CDOM -5	> 2.0	0	0	0	0	0	0	0	0	9.12	0	0	0	0
Depth -1	> 20	0.10	0.14	0	0.07	0	0.17	0	0.04	0	0	0	0.01	0.06
Depth -2	15 - 20	0.16	0.71	0.18	0.59	0	0.12	0	1.71	0.13	0	0	0.04	0.35
Depth -3	10 - 15	1.41	2.49	0.35	2.25	0	2.03	0.35	1.22	1.24	0.32	0.40	0.11	1.22
Depth -4	5 - 10	2.76	2.36	1.58	2.47	1.47	3.80	3.07	1.48	2.18	2.31	5.41	0.21	2.55
Depth -5	< 5	1.91	0.49	3.72	0.88	4.32	0.64	2.93	0.91	2.63	3.48	1.28	0.17	2.01
Total cell of events		513	955	657	840	468	433	335	330	351	322	326	342	
Total cell of all areas		10,245	10,245	10,245	10,245	10,245	10,245	10,245	10,245	10,245	10,245	10,245	10,245	10,245

Units: TSS: mg/l, CDOM: m⁻¹ and Depth: meter

Table 6.15 Summary of FR class weights for all reference red tide maps and the average FR for each specific attribute (Continued).

Factors	Class	Frequency Ratio of Red Tide Occurrences												FR average
		7-Jan-05	9-Feb-05	29-Sep-05	20-Oct-05	15-Aug-05	27-Mar-06	27-Nov-07	28-Sep-07	3-Dec-07	5-Nov-07	13-Nov-07	27-Aug-15	
Dist-1	>30	0.31	0.29	0.25	1.02	0	0.18	0	0.87	0.63	0.49	0	0.04	0.37
Dist-2	20 - 30	2.97	4.91	1.05	1.59	0.96	5.34	0.20	0.58	0	0	4.31	0.21	2.13
Dist-3	10 - 20	2.54	1.58	3.93	0.64	5.09	1.81	6.75	2.45	2.82	4.42	3.04	0.25	3.06
Dist-4	5 - 10	2.66	0	4.10	0.24	5.15	0	3.30	0	4.93	2.56	2.70	0.25	2.27
Dist-5	< 5	0.74	0	4.91	0	5.27	0	0	0	1.89	0	0	0.27	1.07
Current-1	> 0.1	2.48	0.00	7.90	0.00	4.98	7.28	1.41	3.12	4.08	6.55	1.29	0.29	3.28
Current-2	0.05 - 0.1	0.87	0.79	1.86	1.45	0.71	0.73	3.73	1.38	3.01	3.27	2.37	1.30	1.79
Current-3	0.02 - 0.05	0.81	1.69	0.46	1.94	0.14	1.74	0.26	0.99	0.23	0.11	1.06	1.46	0.91
Current-4	0.01 - 0.02	0.61	1.72	0.05	0.77	0.09	1.11	0.00	0.74	0.05	0.00	0.17	0.78	0.51
Current-5	< 0.01	0.19	0.25	0.31	0.43	0.60	0.33	0.00	0.28	0.07	0.00	0.15	0.11	0.23
Total cell of events		513	955	657	840	468	433	335	330	351	322	326	342	
Total cell of all areas		10,245	10,245	10,245	10,245	10,245	10,245	10,245	10,245	10,245	10,245	10,245	10,245	10,245

Units: Distance from river mouth: kilometer and Current-velocity: m/s

Table 6.15 reports data of the average FR class weights for all applied factors (based primary on relevant data accumulated from 12 reference dates) for further use in susceptibility score analysis and mapping. Regarding the FR values, top preference attributes for red tide occurrence over UGoT were CDOM of 1.0-1.5 m^{-1} (FR = 3.41), current velocity of > 0.1 m/s (FR = 3.28) and distance from river mouth of 10-20 km (FR = 3.06), while lowest preference ones were TSS (FR = 0.04) which concentration of 20-40 mg/l and water depth levels > 20 m (FR = 0.06) and 15-20 km (FR = 0.35), current velocity of < 0.01 m/s (FR = 0.23), and distance from river mouth of > 30 km (FR = 0.37). In conclusion, preference conditions for the occurrence of red tide events in the UGoT from FR analysis (e.g. ones with $\text{FR} \geq 2$ in Table 6.15) are relatively low density of TSS (5-10 mg/l), moderate/high concentration of CDOM (0.5-2.0 m^{-1}), relatively shallow water near shore (at depth of ≤ 10 m), and moderate distance from the main river mouths (5-30 km) and relatively strong current velocity (> 0.1 m/s).

If consider factor by factor, the preference order of classified attributes found in the FR analysis for each applied factor (Table 6.15) might look somewhat different from that seen in the SAW analysis (Table 6.11). For TSS, the orders of preference in both methods share similar pattern form low to high scores in average for high to low concentration scale (Class 1 to 5). For CDOM, peak weighting scores were evidenced at Class 4-5 (high concentration level) for the SAW case while those of the FR case were observed at Class 2-3 (moderate level) instead. For water depth, similar trends were seen where weighting scores tend to decline with increasing depth. For distance from river mouth, closest distance (< 5 km) was most favorite (Class 5) in SAW case, but further away distance level (10-20 km) was found most favorable in the FR case. For current velocity, these two methods yielded rather opposite outcome as most

preferable condition in SAW method was the gentle current velocity (Class 5) but that of the FR case was the strong current velocity one (Class 1). These stated differences are results from the different concepts of weighting determination for map preparation process in both methods. This is because the SAW method judges specific weight for each classified attribute based principally on cumulative expert opinions, which tend to follow conventional believes (qualitative approach), while FR method relies mainly on available evidences of the considered event (not on opinion/personal believes) to judge appropriate conclusion on attribute weights (quantitative approach). Therefore, map products gained from these two methods shall directly reflect weight information gained from their associated sources which makes validity assessment (of these maps) become a crucial task to identify superior method on this map preparation matter.

Figures 6.10(a)-(b) illustrate red-tide susceptibility maps for the UGoT for all seven scenarios under consideration (Type 1-7 cases) based on the direct combination of the derived susceptibility maps for each stated case from all twelve reference dates. The pixel-based total red-tide susceptibility score were classified into five categories: very low (VL), low (L), moderate (M), high (H), and very high (VH) which used the equal interval method for classification same as SAW method. In general, susceptibility maps in all cases display similar pattern of red-tide tendency in which top probability (e.g. the H/VH classes) appeared in shallow water zone near shore and close to main river mouths, especially that of the Thachin and Bang Pakong Rivers, while low occurrence tendency zones were often evidenced further away from shore/main river mouths into deeper water zone (e.g. the VL/L classes). This outcome indicates less effect of the distance-to-river-mouth and water-depth exclusion (in Type 5-7 cases) on the preparation of final susceptibility map for the area if compared to

that of the reference case (Type 1). The map validation process also provided rather good AUC outcome for all examined cases, from 0.51 in Type 2 case to 0.75 in Type 6 case (CDOM+TSS) as described in Table 6.17.

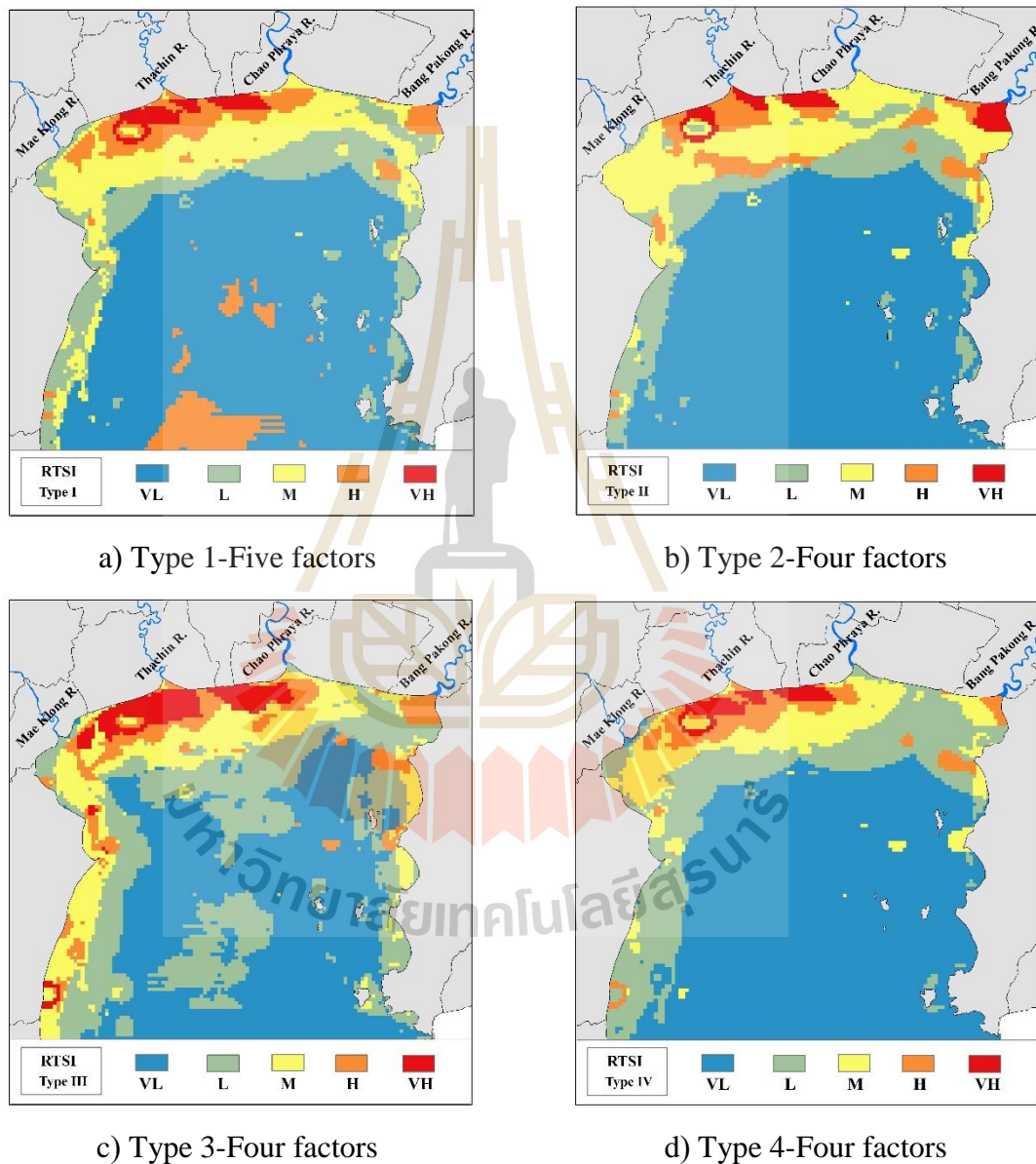
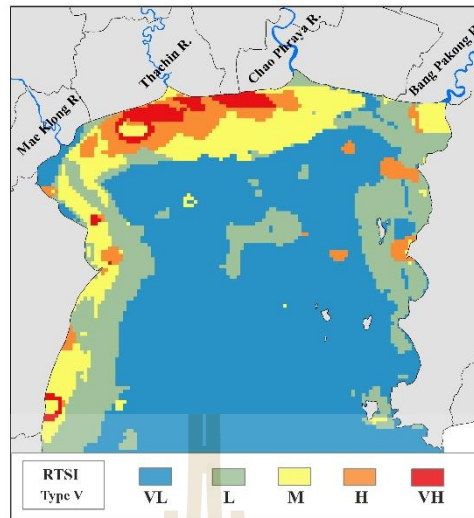
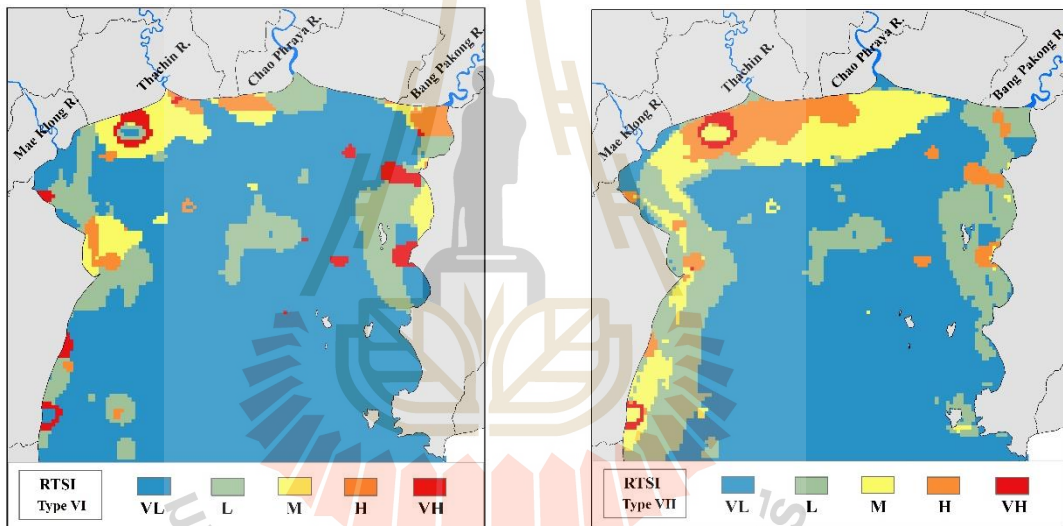


Figure 6.10(a) Red-tide susceptibility maps by FR method (Type 1- 4 scenarios).



a) Type 5-Three factors



b) Type 6-Two factors

c) Type 7-Two factors

Figure 6.10(b) Red-tide susceptibility maps by FR method (Type 5 - 7 scenarios).

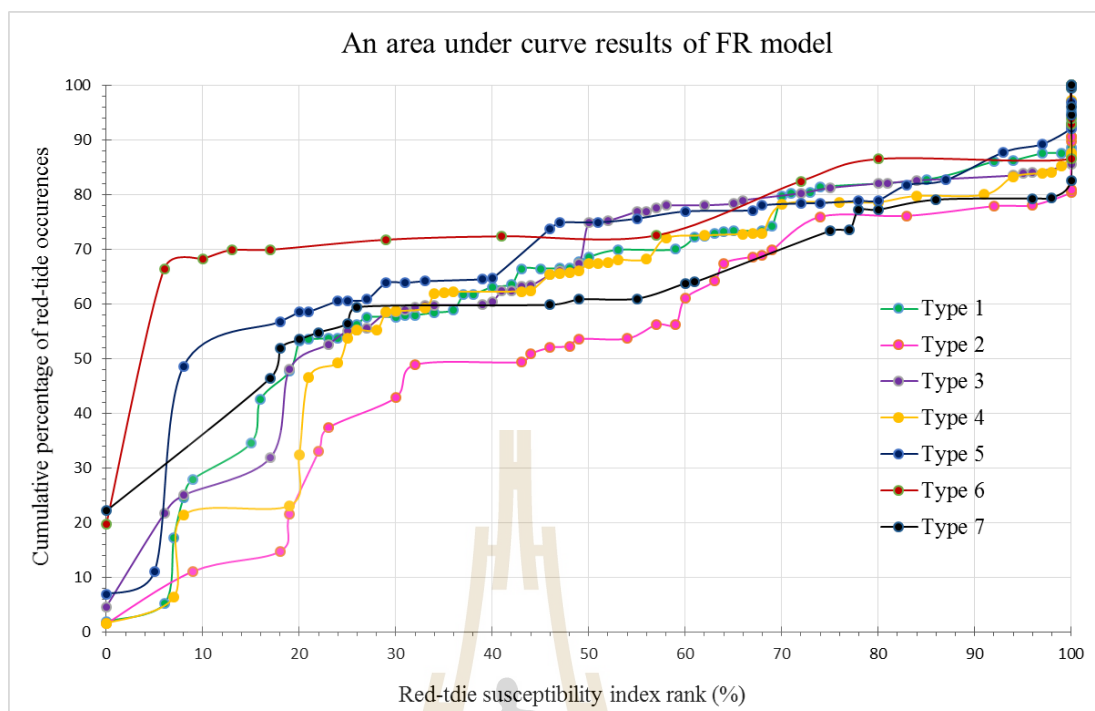


Figure 6.11 An accuracy assessment result based on AUC method of FR model.

Table 6.16 Classified area for red-tide susceptibility category based on FR method.

Unit: sq.km

Types	RTSI Condition	VL	%	L	%	M	%	H	%	VH	%
1	Five Factors	5,931	57.9	1,549	15.1	1,503	14.7	1,069	10.4	193	1.9
2	Four Factors	6,506	63.5	1,381	13.5	1,576	15.4	541	5.3	241	2.4
3	Four Factors	4,487	43.8	3,127	30.5	1,520	14.8	679	6.6	432	4.2
4	Four Factors	6,324	61.7	2,115	20.6	1,122	11.0	494	4.8	190	1.9
5	Three Factors	6,245	61.0	2,034	19.9	1,210	11.8	537	5.2	219	2.1
6	Two Factors	7,788	76.0	1,386	13.5	546	5.3	286	2.8	239	2.3
7	Two Factors	6,435	62.8	2,075	20.3	1,035	10.1	625	6.1	75	0.7

Total of areas: 10,245.

Table 6.17 The results of accuracy assessment base on FR model.

Type of validation	Type of Performance						
	Type 1	Type 2	Type 3	Type 4	Type 5	Type 6	Type 7
FR - AUC	0.62	0.51	0.63	0.59	0.67	0.75	0.61

Type 1: Five factors. TSS, CDOM, Depth, Distance from the river mouth and Speed of surface current

Type 2: Four factors; TSS, CDOM, Depth and Distance from the river mouth

Type 3: Four factors. TSS, CDOM, Depth and Speed of surface current

Type 4: Four factors. TSS, CDOM, Distance from the river mouth and Speed of surface current

Type 5: Three factors. TSS, CDOM and Speed of surface current

Type 6: Two factors. TSS and CDOM,

Type 7: Two factors. CDOM and Speed of surface current

6.4 Conclusion

In this part, the red-tide occurrence tendency over UGoT region was evaluated and mapped through two popular susceptibility analysis methods: the simple additive weighting (SAW) and the frequency ratio (FR) methods, with five crucial influencing parameters of red tide formation were used, i. e., TSS and CDOM concentrations, water depth, distance from the river mouth, and current velocity. Fifteen daily maps of the identified red tide occurrence over UGoT (i. e., ones having eutrophic/ hyper-eutrophic states) between 2006 to 2015 were also synthesized to fulfill needs in model's assessment process (12 maps) and map's validation process (3 maps). In map preparation process, seven different scenarios were considered based on different combinations of factors included in the susceptibility analysis as explained in Table 6.8, starting from case 1 (or Scenario type 1) where all five initial factors were incorporated to case 7 analysis where only CDOM and current velocity were considered.

In SAW-based susceptibility analysis, the corresponding experts (19 in total) experts mainly gave top priority to distance from river mouth (for red-tide formation

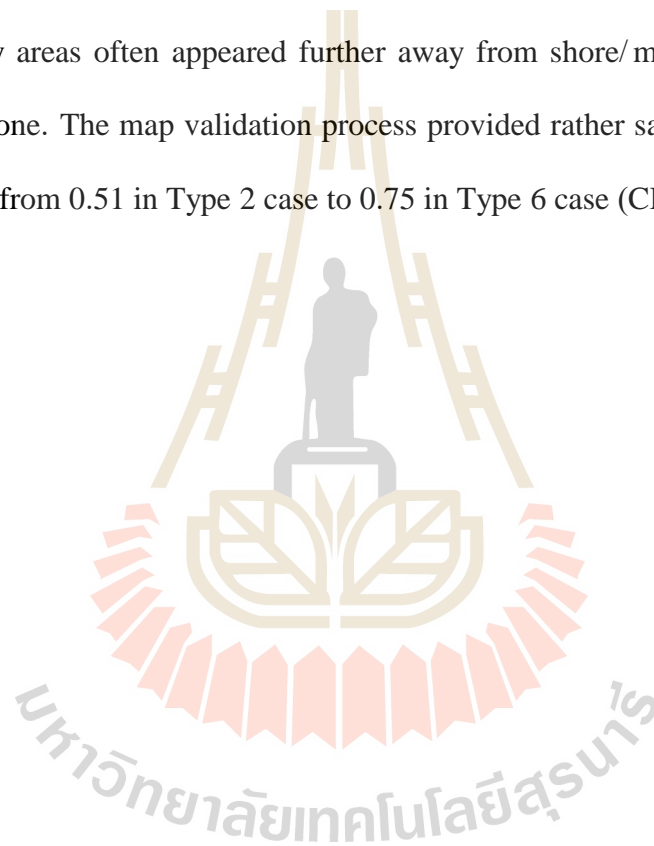
in UGoT) followed by CDOM while the least favorite ones here were current velocity and TSS, in general. The output susceptibility maps of Type 1 to 4 scenarios in SAW case displayed expected pattern of red-tide tendency map with top potential appeared in shallow water zone near shore/close to main river mouths, especially the Thachin and the Bang Pakong Rivers, while low tendency areas were normally evidenced far away from shore and main river mouths into the deep water zone. This conclusion was supported by several previous works, e.g. Chumnantana (2006), Buranapratheprat et al. (2008), Buranapratheprat et al. (2009), and Vasinamakin et al. (2008).

However, in cases 5-7, where distance-to-river-mouth and water-depth were excluded, outlook of the gained maps seems somewhat unrealistic as moderate to high tendency of red tide occurrence was prevalent over most area even in clear deep water zone far away from shore. In principle, this kind of map (M/H favourite) tends to have high accuracy outcome (by the AUC method), e.g. 0.89 for Type 5 or 0.94 for Type 6 but it shall conceptually contain high rate of false prediction (or false alarm) also. Therefore, its prediction ability should be assessed with great caution.

In FR-based susceptibility analysis (an evidence-based approach), it was found that, regarding the obtained FR value, preference conditions for occurrence of red tide events in the UGoT area are relatively low density of TSS (5-10 mg/l), moderate/high concentration of CDOM ($0.5-2.0 \text{ m}^{-1}$), relatively shallow water near shore (at depth of $\leq 10 \text{ m}$), and moderate distance from the main river mouths (5-30 km) and relatively strong current velocity ($> 0.1 \text{ m/s}$). If consider factor by factor, the preference order of classified attributes found in the FR analysis look partially different from that seen in the SAW analysis especially for the CDOM and current velocity. These differences

were principally resulted from the different concepts of weighting determination used in SAW method (based on gained expert opinions on red-tide preference conditions) and FR method (based on data of past red-tide evidences).

In general, susceptibility maps in all FR-based cases display similar pattern of red-tide tendency with top probability appeared in shallow water zone near shore and close to main river mouths, especially the Thachin and the Bang Pakong Rivers, while low tendency areas often appeared further away from shore/main river mouths into deep water zone. The map validation process provided rather satisfied AUC outcome for all cases, from 0.51 in Type 2 case to 0.75 in Type 6 case (CDOM+TSS).



CHAPTER VII

CONCLUSIONS AND RECOMMENDATIONS

This chapter summarizes main findings in this thesis work regarding three given objectives described in Chapter I. Conclusions shall be presented for the results gained from works in each objective in respective order, while some recommendations for the further works on these topics are addressed in the final part of this chapter.

7.1 Model development for marine constituent determination

This part aims to identify appropriate models for estimating selected key marine water constituents (Chl-a, TSS, CDOM) over UGoT area. In-situ data collected from five field surveys were used for model development and verification at first then suitable MODIS L2 reflectance data were applied as a replacement for the respective original reflectance data gained from the in-situ records. Results of the study indicates that the level of Chl-a concentration was typically high near river mouths and relatively low in central UGoT. Spatial variations of the TSS and CDOM concentration were found similar to that of the Chl-a but their temporal variations were different. High CDOM was always seen at the river mouths with specific locations changed with time. PRR characteristics displayed similar trends in all field-survey cruises. Finally, three optimal models (for the Chl-a, TSS and CDOM observation) were identified based on the statistical outcome in terms of R^2 , RMSE and MAPE. These are OC3M (for Chl-a), TSM (for TSS) and Chula models (for CDOM), respectively (as detailed in Table 7.1).

Table 7.1(a) The optimal model for Chl-a extraction from MODIS data (OC3M).

Model	PRR modified structure	MODIS implement	Remark
OC3M	$C_{\text{chla}} = 10^{\left(\frac{0.0513 - 1.5884R - 5.5887R^2 - 5.4592R^3}{+16.977R^4}\right)}$ $R = \log_{10} \left[\max \left(\frac{R_{rs}(443)}{R_{rs}(565)}, \frac{R_{rs}(490)}{R_{rs}(565)} \right) \right]$	$C_{\text{chla}} = 10^{\left(\frac{0.0513 - 1.5884R - 5.5887R^2 - 5.4592R^3}{+16.977R^4}\right)}$ $R = \log_{10} \left[\max \left(\frac{R_{rs}(443)}{R_{rs}(555)}, \frac{R_{rs}(488)}{R_{rs}(531)} \right) \right]$	Replaced Rrs 490 by 488 and 565 by 531

Table 7.1(b) The optimal model for TSS extraction from MODIS data (TSM).

Model	PRR modified structure	MODIS implementation	Remark
TSM	$\text{TSM} = 2E + 07(nL_w(670))^3 -$ $324374(nL_w(670))^2 +$ $2047.8(nL_w(670)) + 0.0831$	$\text{TSM} = 2E +$ $07(nL_w(667))^3 -$ $324374(nL_w(667))^2 +$ $2047.8(nL_w(667)) +$ 0.0831	Replaced Rrs 670 by 667

Table 7.1(c) The optimal model for CDOM extraction from MODIS data (Chula model).

Model	PRR modified structure	MODIS implementation	Remark
Chula model	$\text{CDOM } k(412) = 0.0768R^2 - 0.1274R$ $+ 0.0876$ $R = R_{rs}(412, 0-) / R_{rs}(565, 0-)$	$\text{CDOM } k(412) = 0.0768R^2 - 0.1274R$ $+ 0.0876$ $R = R_{rs}(412) / R_{rs}(531)$	Replaced Rrs 565 by 531

Results from this work emphasize the importance of the blue/green band ratio application in all selected empirical models mentioned earlier which was also reported in other works (satellite-based analysis).

In addition, developed artificial neural network (ANN) system was also proved to be a promising tool for the extraction of listed constituents from MODIS reflectance data. In this work, multi-layer perceptron neural network (MLP-NN) model with back

propagation (BP) algorithm was employed using structure model (for each processing layer) of 10:30:10:1. This was able to provide high accuracy in the determination of all considered constituents with R^2 of 0.87 (for Chl-a), 0.92 (for TSS), and 0.94 (for CDOM), respectively. In general, these ANN outcomes seem to remarkably outperform those of the chosen empirical ones for all listed constituents, which are, R^2 of 0.76 (for Chl-a), 0.84 (for TSS), and 0.85 (for CDOM), respectively. However, due to its rather complicated structure and somewhat lengthy (and not well comprehensible) computing process, true merit of the ANN system for routine application compared to the preferred empirical one (with rather simple and straightforward structure) should be a subject of further intensive investigation.

7.2 MODIS-based monitoring of coastal environment in UGoT

This part focuses on mapping extracted concentration data of Chl-a, TSS and CDOM from associated MODIS reflectance data by the respective optimal algorithm for these constituents identified earlier during years 2010 to 2012. The initial purposes of this work were to investigate effect of the mega flooding event over central Thailand in 2011 on UGoT water quality variation as well as to evaluate the associated trophic states of UGoT area from the daily MODIS data for effective water quality (and red tide incidence) assessment and management purpose, from which the classified eutrophic/hyper-eutrophic trophic states were used as a representative of red tide incidences over the area.

In general, Chl-a concentration in normal year (2010) was relatively low in dry season (January-April) and gradually rising towards its peak value in wet season (July-September) before the declining trend took place from October onwards throughout the

winter season. High concentration data were often evidenced over shallow water, close to shore and the main river mouths, especially those of the Thachin and the Chao Phraya Rivers. The effects of the 2011 mega flood had led to apparent different characteristics of the data variation where the most notable one was great drop in Chl-a density data (maximum/mean) during wet season of 2011.

For TSS case, maximum concentration data tended to be low in dry season and then gradually increase towards wet season with peak values achieved during that time (like Chl-a). Also, hotspots for TSS pollution were often seen at locations of main river mouths, mostly at that of the Chao Phraya River, unlike Chl-a case in which critical zones were usually found somewhere further away from river mounts. For the CDOM concentration, low values were seen dominant in dry season and peak values were seen in wet season like others. However, critical zones of CDOM pollution were found more widespread into the deep-water zone than those of the Chl-a or TSS.

Mutual correlation among the studied constituent were found moderately strong during dry season (from January to June) with $R \approx 0.4-0.6$ while the relatively low correlation was often seen in wet season, especially September and October. Among these, correlation of Chl-a and CDOM was found to be more stable throughout the year than other pair of constituents. Finally, the generated trophic state maps of UGoT area from the associated Chl-a concentration maps in 2010 to 2012 (from which the classified eutrophic/hyper-eutrophic states were used as a representative of red tide incidences over the area) indicate that occurrences of red tide events should be low in dry season (January-April/October-December) and their preferred locations should be restricted to sea areas located close to some specific river mouths only. However, the

occurrences of the red tide incidence should be seen more often during wet season (June to September) covering much more widespread area than that of the dry season.

In addition, the occurrence of red tide phenomena was always affected the fisheries economic and aquatic resources. Thus, this event was risen on large and long-lasting area, resulted in migratory of marine life and also make the benthic fauna will be died. Trophic state management in UGoT will be used for indicator of red tide phenomenon, which can be tracking and monitoring of the occurrence. Consequently, should be take avoiding of aquatic activities in that area and also to reduce the economic losses. Typically over the four main river mouths, such the Thachin River mouth.

7.3 Red tide susceptibility analysis and mapping

This part evaluates red-tide occurrence tendency over UGoT based on derived susceptibility maps by two popular methods: the simple additive weighting (SAW) where the weights were generated by multiple comparison method, and the frequency ratio (FR) methods in which five crucial influencing parameters of red tide formation were considered, i.e., TSS/CDOM concentrations, water depth, distance from the river mouth, and current velocity. In map preparation process, seven different scenarios were considered based on different combinations of factors included in the susceptibility analysis as detailed in Table 6.8, starting from case 1 (or Scenario type 1) where all five initial factors were incorporated to case 7 where only CDOM and current velocity were considered (as detailed in Table 7.2).

In SAW-based susceptibility analysis, the priority of each incorporated factor was assessed based on opinions of corresponding experts (19 in total) from which top

priority was normally given to distance from river mouth (for red-tide formation in UGoT) followed by CDOM while the least favorite ones here were current velocity and TSS. In general, the output susceptibility maps of Type 1 to 4 scenarios in SAW case

Table 7.2 Seven examined scenarios for red-tide susceptibility mapping (Type 1-7).

Factors	Scenario type						
	Type 1	Type 2	Type 3	Type 4	Type 5	Type 6	Type 7
1) Total suspended solids	√	√	√	√	√	√	-
2) Color dissolved organic matter	√	√	√	√	√	√	√
3) Water depth	√	√	√	-	-	-	-
4) Distance from river mouth	√	√	-	√	-	-	-
5) Current velocity	√	-	√	√	√	-	√

displayed expected pattern of the red-tide tendency map with top potential appeared in shallow water zone near shore and close to main river mouths, especially the Thachin and the Bang Pakong Rivers, while low tendency ones were usually evidenced far away from shore and main river mouths into deep water zone. This conclusion was supported by several previous works, e.g. Chumnantana (2006), Buranapratheprat et al. (2008), Buranapratheprat et al. (2009), and Vasinamakin et al. (2008).

However, in cases 5-7, where distance-to-river-mount and water-depth were excluded, outlook of the gained maps seems somewhat unrealistic as moderate to high tendency of red tide occurrence was prevalent over most area even in clear deep water zone far away from shore. In principle, this kind of map (M/H favorite) tends to have high accuracy outcome (by the AUC method), e.g. 0.89 for Type 5 or 0.94 for Type 6 but it shall conceptually have high potential of false prediction (or false alarm) also as the high tendency was so notably widespread (overestimation of the incidences). Therefore, its prediction ability should be assessed with thoughtful interpretation.

For the FR-based susceptibility analysis (an evidence-based approach), it was found that, regarding the obtained FR value, preference conditions for occurrence of red tide events in UGoT area are relatively low density of the TSS (5-10 mg/l), moderate/high concentration of CDOM (0.5-2.0 m^{-1}), relatively shallow water near shore (at depth of ≤ 10 m), and moderate distance from the main river mouths (5-30 km) and relatively strong current velocity (> 0.1 m/s). If consider factor by factor, the preference order of classified attributes found in the FR analysis look partially different from that evidenced in the SAW analysis especially for the CDOM and current velocity. These differences were principally resulted from the different concepts of weighting determination used in SAW method (based on accumulated expert opinions on red-tide preference conditions) and FR method (based on data of past red-tide evidences). These differences were led to contrast outlook of the derived susceptibility maps afterwards

In general, susceptibility maps in all FR-based cases display similar pattern of red-tide tendency with top probability appeared in shallow water zone near shore and close to main river mouths, especially the Thachin and the Bang Pakong Rivers, while low tendency areas often appeared further away from shore/main river mouths into deeper water zone. The map validation process provided rather satisfied AUC outcome for all examined cases, from 0.51 in Type 2 case to 0.75 in Type 6 case.

7.4 Recommendations

The achievements of all proposed works done in this thesis demonstrate great merit of the MODIS-level 2 data for the effective mapping and monitoring of important marine constituents (Chl-a, TSS, CDOM) over UGoT region as well as the extensive

assessment of sea water quality condition regarding concentration of these constituents, especially that of Chl-a which becomes primary indicator for the occurrence of red tide incidence known so far. However, to make further works on this topic in Thailand more robust, some broad recommendations arisen from experience and eventual outcome of works reported in this thesis are addressed here as follows.

1) Empirical and ANN models can be generated directly by the data collection from field survey and satellite. The PRR reflectance from field survey can be ignored in such a case.

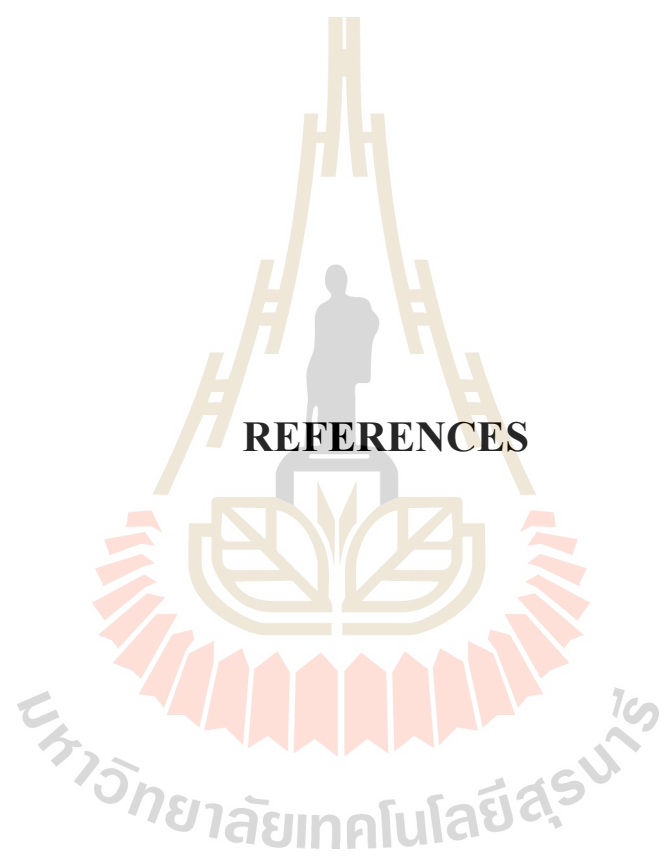
2) Long-term data (5-10 years) are required for model establishment to improve the accuracy and precision of predicting results.

3) This research used only MODIS satellite data. Data from other sensors such as the ocean-based satellite sensor of ISRO (OCM-2), NOAA (VIIRS), and ESA/EUMETSAT (OLCI) or the land-based satellite sensor of Landsat-8 or Hyper-spectral sensor should be examined for local model establishment.

4) For SAW/FR method, suitable factors and categorized classes are the most importance to model accuracy. Inappropriate class assignment may generate significant error in the results.

5) For input factor, the direction of surface current should be applied to the SAW/FR model because it is related to phytoplankton distribution.

6) Because of spatial and temporal variations in trophic states over UGoT, the future local model should take them into consideration for more accuracy in model prediction.



REFERENCES

REFERENCES

- พระราชบัญญัติกำหนดเขตจังหวัดในอำเภอไทยตอนใน (2502). เล่ม 76 ตอนที่ 92 ราชกิจจานุเบกษา
ลงวันที่ 29 กันยายน 2502.
- Abdullah, L., and Adawiyah, R. (2014). Simple additive weighting methods of multi-criteria decision making and applications: a decade review. **International Journal of Information Processing and Management (IJIPM)**. 5(1).
- Adriyendi. (2015). Multi attribute decision making using simple additive weighting and weighted product in food choice. **Information Engineering and Electronic Business**. (6): 8-14. doi:10.5815/ijieeb.2015.06.02.
- Aiken, J., Moore, G. F., Trees, C. C., Hooker, S. B., and Clark, D. K. (1995). **The SeaWiFS CZCS-type pigment algorithm, in SeaWiFS Technical Report Series**. vol. 29, edited by S.B. Hooker and E.R. Firestone, Goddard Space Flight Center, Greenbelt, MD.
- Alves, G., Flores-Montes, M., Gaspar, F., Gomes, J., and Feitosa, F. (2013). Eutrophication and water quality in a tropical Brazilian estuary. **Journal of Coastal Research**. Special Issue No. 65.
- Ambarwulan, W. (2010). **Remote sensing of tropical coastal water: study of the Berau estuary, east Kalimantan, Indonesia**. Ph.D. Dissertation, University of Twente, ITC, P.O. Box 6, 7500 AA Enschede, The Netherlands.

- Amin, A. R. M., and Abdullah, K. (2010). Sediment and shallow coastal water detection utilizing MODIS land channels over Gulf of Martaban. **Applied Physics Research**. 2: 2. doi:10.5539/apr.v2n2p61.
- Baruah, P. J. (2002). Application of remote sensing and smart algorithms for modelling of water quality in Lake Kasumigaura. **Doctoral dissertation in Engineering**. University of Tsukuba. Japan. 154 p.
- Behrenfeld, M. J., and Falkowski, P. G. (1997). A consumer's guide to phytoplankton primary productivity models. **Limnology and oceanography**. 42(7): 1479-1491.
- Bhatrasataponkul, T. (2004). Development of ocean colour algorithms for the upper gulf of Thailand. Master of Science Dissertation. Department of Marine Science. Faculty of Science, Chulalongkorn University, Thailand.
- Bidorn, B., Chanyotha, S., Kish, S. A., Donoghue, J. F., Bidorn, K., and Mama, R. (2015). The effects of Thailand's Great Flood of 2011 on river sediment discharge in the upper Chao Phraya River basin, Thailand. **International Journal of Sediment Research**. (30): 328-337. doi:10.1016/j.ijsrc.2015.10.001.
- Biospherical Instruments Inc. (2002). **User's manual profiling reflectance radiometer system (PRR-2600)**. 5340 Riley Street San Diego, CA 92110-2621. Version 004961UC.DOC.
- Boonkwan, S. (2013). **Seasonal variations of phytoplankton and primary production in the inner gulf of Thailand**. Master of Science Dissertation in Aquatic science. Burapha University. Thailand.

- Bruckner, M. (2013). **Red tide-Harmful algal blooms**. Microbial life education resources. Montana State University, USA. [On-line]. Available: <http://serc.carleton.edu/microbelife/topics/redtide/index.html>.
- Buranapratheprat, A. (2000). **Hydrodynamic model for investigation of circulation in the Bang Pakong estuary**. Department of Aquatic science, Faculty of science, Burapha University, Thailand.
- Buranapratheprat, A. (2007). **Surface chlorophyll distributions in the Upper Gulf of Thailand investigated using satellite imagery and ecosystem model**. Doctoral Dissertation in Geography. Department of Geography, University of Victoria, Canada.
- Buranapratheprat, A., Niemann, K. O., Matsumura, S., and Yanagi, T. (2009). MERIS imageries to investigate surface chlorophyll in the upper Gulf of Thailand. **Coastal Marine Science**. 33(1): 22-28.
- Buranapratheprat, A., Yanagi, T., and Matsumura, S. (2008). Seasonal variation in water column conditions in the upper Gulf of Thailand. **Continental Shelf Research**. 28: 2509-2522.
- Buranapratheprat, A., Yanagi, T., Niemann, K.O., Matsumura, S., and Sojisuporn, P. (2008). Surface chlorophyll-a dynamics in the Upper Gulf of Thailand Revealed by a coupled hydrodynamic-ecosystem model. **Journal of Oceanography**. (64): 639-656.
- Buranapratheprat, A., Yanagi, T., and Sawangwong, P. (2002). Seasonal variations in circulation and salinity distribution in the upper Gulf of Thailand: modeling approach. **La Mer**. (40): 147-155.

- Burger, J. B. (2006). A review of their use in the environmental literature 1970-2005. **Environmental Bioindicators**. 1(2): 136-44.
- Burzel, A., Dassanayake, D. R., and Oumeraci, H. (2012). **Spatial modelling of tangible losses in an integrated risk analysis**. Leichtweiß-Institute for Hydraulic Engineering and Water Resources, Technische Universität Braunschweig.
- Canziani, G., Ferrati, R., Marinelli, C., and Dukatz, F. (2008). Artificial neural networks and remote sensing in the analysis of the highly variable PAMPEAN shallow lakes. **Mathematical Biosciences and Engineering**. 5(4). doi:10.3934/mbe.2008.5.691.
- Carder, K. L., Chen, F. R., Lee, Z., Hawes, S. K., and Canizzaro, J. P. (2003). **MODIS ocean science team algorithm theoretical basis document, ATBD 19, Case 2 Chlorophyll-a**. College of marine science University of South Florida.
- Chang, N. B., Xuan, Z., and Yang, Y. J. (2013). Exploring spatiotemporal patterns of phosphorus concentrations in a coastal bay with MODIS images and machine learning models. **Remote Sensing of Environment**. 134: 100-110. doi: 10.1016/j.rse.2013.03.002.
- Chen, J., and Quan, W. (2013). An improved algorithm for retrieving chlorophyll-a from the Yellow River Estuary using MODIS imagery. **Environment Monitoring Assess.** 185: 2243-2255. doi:10.1007/s10661-012-2705-y.
- Chuennyom, W., Meksumpun, C., and Meksumpun, S. (2012). Impacts of nutrients and related environmental factors on distribution and size structure of Noctiluca scintillans populations of the Eutrophic Tha Chin Estuary, Thailand. **Water Science & Technology**. 65: 11. doi:10.2166/wst.2012.099.

- Chumnantana, R. (2006). **Causative phytoplankton of red tide phenomena in the Upper Gulf of Thailand**. Phuket Marine Biological Center. Department of Marine and Coastal Resources. Ministry of Natural Resources and environment. Technical Paper no. 1/2006.
- Cloern, J. E. (2001). Our evolving conceptual model of the coastal eutrophication problem. **Marine Ecology Progress Series**. 210: 223-253.
- Coble, P., Hu, C., Gould, R. W. Jr., Chang, G., and Wood. A. M. (2004). Colored dissolved organic matter in the coastal ocean: An optical tool for coastal zone environmental assessment and management. **Oceanography**. 17(2): 50-59. doi: 10.5670/oceanog.2004.47.
- Corbett, C. A. (2007). **Colored dissolved organic matter (CDOM) workshop summary**. Reports. Paper 2. Charlotte Harbor National Estuary Program. University of South Florida, USA.
- Das, S., Hazra, S., Lotlikar, A. A., Das, I., Giri, S., Chanda, A., Akhand, A., Maity, S., and Kumar, T. S. (2016). Delineating the relationship between chromophoric dissolved organic matter (CDOM) variability and biogeochemical parameters in a shallow continental shelf. **Egyptian Journal of Aquatic Research**. 42: 241-248. doi:10.1016/j.ejar.2016.08.001.
- Eastman, J. R. (2016). **TerrSet manual: Geospatial monitoring and modeling system manual**. Clark Labs. Clark University. 950 Main Street. Worcester, MA. 01610-1477. USA.
- EEA. (2001). **Eutrophication in Europe's coastal waters (Vol. 7)**. Copenhagen: European Environmental Agency.

- Falkowski, P. G., Behrenfeld, M. J., Esaias, W. E., Balch, W., Campbell, J. W., Iverson, R. L., Kiefer, D. A., Morel, A., and Yoder, J. A. (1998). **Satellite primary productivity data and algorithm development: a science plan for mission to planet earth.** In S. B. Hooker and E. R. Firestone (Eds.), SeaWiFs Technical Report Series (Vol. 42, pp. 36): NASA. doi:10.1016/j.jenvman.2012.08.019.
- Ferrari, G. M., Dowell, M. D., Grossi, S., and Targa, C. (1996). Relationship between the optical properties of chromophoric dissolved organic matter and total concentration of dissolved organic carbon in the southern Baltic Sea region. **Marine Chemistry.** 55: 299-316.
- Ferreira, J. G., Andersen, J. H., Borja, A., Bricker, S. B., Camp, J., Cardoso da Silva, M., Garcés, E., Heiskanen, A.-S., Humborg, C., Ignatiades, L., Lancelot, C., Menesguen, A., Tett, P., Hoepffner, N., and Claussen, U. (2011). Overview of eutrophication indicators to assess environmental status within the European Marine Strategy Framework Directive. **Estuarine, Coastal and Shelf Science.** 93(2): 117-131. doi:10.1016/j.ecss.2011.03.014.
- Franz, B. A., Werdell, P. J., Meister, G., Bailey, S. W., and Eplee, J. R. E. (2005). **The continuity of ocean color measurements from SeaWiFS to MODIS.** Proceeding of SPIE 5882, Earth Observing Systems X, 58820W (September 08, 2005). doi:10.1117/12.620069.
- Franz, B. A., Werdell, P. J., Meister, G., Kwiatkowska, E. J., Bailey, S.W., Ahmad, Z., and McClain, C. R. (2006). MODIS land bands for ocean remote sensing applications. **Proceeding Ocean Optics XVIII.** Montreal, Canada, 9-13 October 2006.

- Giardino, C., Bresciani, M., Pilkaityt, R., Bartoli, M., and Razinkovas, A. (2010). In situ measurements and satellite remote sensing of case 2 waters: first results from the Curonian Lagoon. **Oceanologia**. 52 (2): 197-210.
- Gitelson, A. A., Gurlin, D., Moses, W., and Barrow, T. (2009). A bio-optical algorithm for the remote estimation of the chlorophyll-*a* concentration in case 2 waters. **Environmental Research Letters**. 4: 045003. doi:10.1088/1748-9326/4/4/045003.
- Ha, N. T. T., Koike, K., and Nhuan, M. T. (2014). Improved accuracy of chlorophyll-*a* concentration estimates from MODIS imagery using a two-band ratio algorithm and geostatistics: As applied to the monitoring of eutrophication processes over Tien Yen Bay (Northern Vietnam). **Remote Sensing**. 6: 421-442. doi:10.3390/rs6010421.
- Harn, S. D. (1991). **Simple estimation for the movement of the red tides in small bay**. Recent approaches on red tides, Proceeding of "1990 Korean-French Seminar on red tides" held, November 9-10, 1990 at National fisheries research and development agency, Republic of Korea.
- Helsinki Commission, (2009). **Eutrophication in the Baltic Sea**. Helsinki Commission. [On-line]. Available: <http://www.helcom.fi/stc/files/Publications/Proceedings/bsep115A.pdf>.
- Horning, N., Robinson, J. A., Sterling, E. J., Turner, W., and Spector, S. (2010). **Remote sensing for ecology and conservation: a handbook of techniques**. United States: Oxford University Press Inc., New York.
- Hu, C., Chen, Z., Clayton, T. D., Swarzenski, P., Brock, J. C., and Muller-Karger, F. E. (2004). Assessment of estuarine water-quality indicators using MODIS

- medium-resolution bands: Initial results from Tampa Bay, FL. **Remote Sensing of Environment**. 93: 423-441. doi:10.1016/j.rse.2004.08.007.
- Huo, S., He, Z., Su, J., Xi, B., and Zhu, C. (2013). Using artificial neural network models for eutrophication prediction. **Procedia Environmental Sciences**. 18: 310-316. doi:10.1016/j.proenv.2013.04.040.
- Hutchinson, G. E. (1967). A treatise on limnology. Introduction to lake biology and the limnoplankton, Volume II. New York: John Wiley & Sons. Quoted in Kitsiou, D., and Karydis, M. (2011). Coastal marine eutrophication assessment: a review on data analysis. **Environment International**. 37(4): 778-801. doi:10.1016/j.envint.2011.02.004.
- Institute of Marine Science. (2006). **Marine environmental monitoring program and protection management of red tide in the coastal water of Chon Buri Province**. Burapha University, Thailand.
- Intarawichian, N., and Dasananda, S. (2010). Analytical hierarchy process for landslide susceptibility mapping in lower mae chaem watershed, northern Thailand. **Suranaree Journal of Science Technology**. 17(3): 277-292.
- Islam, Md. M., and Tat, C. W. (2001). **A comparison of empirical algorithms for chlorophyll concentration in Singapore regional waters**. The 22nd Asian conference on Remote Sensing, 5-9 November 2001, Singapore.
- IOCCG. (2000). **Remote sensing of ocean colour in coastal, and other optically-complex, waters**. In Stuart, V. (Ed.), Reports of the International Ocean-Colour Coordinating Group (Vol. 3, pp. 140). Dartmouth, Canada.
- Jang, K., and Yang, K. (2001). Improving principal component analysis (PCA) in automotive body assembly using artificial neural networks. **Journal of**

- Manufacturing Systems.** 20(3): 188-197. doi:10.1016/S0278-6125(01)80040-6.
- Jensen, J. R. (2007) **Remote sensing of environment: An earth resources perspective (second edition)**. Pearson education, Inc. pp. 442 (592 p).
- Keith, D. J., Yoder, J. A., and Freeman, S. A. (2002). Spatial and temporal distribution of coloured dissolved organic matter (CDOM) in Narragansett Bay, Rhode Island: implications for phytoplankton in coastal waters. **Estuarine, Coastal and Shelf Science.** 55(5): 705-717. doi:10.1006/ecss.2001.0922.
- Khan, F. A., and Aliansari, A. (2005). Eutrophication: an ecological vision. **The Botanical Review.** 71(4): 449-482.
- Kiener, L. E., and Yan, X. H. (1998). A neural network model for estimating sea surface chlorophyll and sediments from thematic mapper imagery. **Remote sensing environment.** 66: 153-165.
- Kishino, M., Tanaka, A., and Ishizaka, J. (2005). Retrieval of Chlorophyll-a, suspended solids, and colored dissolved organic matter in Tokyo Bay using ASTER data. **Remote Sensing of Environment.** 99: 66-74. doi:10.1016/j.rse.2005.05.016.
- Kitsiou, D., and Karydis, M. (1998). Development of categorical mapping for quantitative assessment of eutrophication. **Journal of Coastal Conservation.** 4: 35-42, Opulus Press Uppsala. Printed in Sweden.
- Kitsiou, D., and Karydis, M. (2011). Coastal marine eutrophication assessment: a review on data analysis. **Environmental International.** 37(4): 778-801. doi: 10.1016/j.envint.2011.02.004.
- Kobayashi, H., Toratani, M., Matsumura, S., Siripong, A., Lirdwitayaprasit, T., and Jintaseranee, P. (2010). Optical properties of inorganic suspended solids and

their influence on coastal ocean color remote sensing. *International Archives of the Photogrammetry. Remote Sensing and Spatial Information Science*, XXXVIII (Part 8).

Koponen, S., Pulliainen, J., Kallio, K., and Hallikainen, M. (2002). Lake water quality classification with airborne hyperspectral spectrometer and simulated MERIS data. *Remote Sensing of Environment*. 79: 51-59.

Kowalczyk, P., Stedmon, C. A. and Markager, S. (2006). Modeling absorption by CDOM in the Baltic Sea from season, salinity and chlorophyll. *Marine Chemistry*. 101: 1-11. doi:10.1016/j.marchem.2005.12.005.

Kungvalchokechai, S., and Sawada, H. (2013). The filtering of satellite imagery application using meteorological data aiming to the measuring, reporting and verification (MRV) for REDD. *Asian Journal of Geoinformatics*. 13(3).

Lapucci, C., Rella, M. A., Brandini, C., Ganzin, N., Gozzini, B., Maselli, F., Massi, L., Nuccio, C., Ortolani, A., and Trees, C. (2012). Evaluation of empirical and semi-analytical chlorophyll algorithms in the Ligurian and North Tyrrhenian Seas. *Journal of Applied Remote Sensing*. 6(1): 1931-3195. doi:10.1117/1.JRS.6.063565.

Le, C., Hu, C., English, D., Cannizzaro, J., Chen, Z., Feng, L., Boler, R., Kovach, C. (2012). Towards a long-term chlorophyll-a data record in a turbid estuary using MODIS observations. *Progress in Oceanography*. 109: 90-103. doi:10.1016/j.pocean.2012.10.002.

Lee, S., Park, I., Koo, B. J., Ryu, J., Choi, J., and Woo, H. J. (2013). Macrobenthos habitat potential mapping using GIS-based artificial neural network models. *Marine Pollution Bulletin*. 67: 177-186. doi:10.1016/j.marpobul.2012.10.023.

- Lirdwitayaprasit, T. (nd). **Red tide in the inner Gulf of Thailand**. Department of Marine Science, Chulalongkorn University, Thailand.
- Lundberg, C., Lonroth, M., Numers, M. V., and Bonsdorff, E. (2005). A multivariate assessment of coastal eutrophication. Examples from the Gulf of Finland, northern Baltic Sea. **Marine Pollution Bulletin**. 50:1185-1196. doi:10.1016/j.marpolbul.2005.04.029.
- Malczewski, J. (1999). **GIS and multicriteria decision analysis**. John Willey & Son, Inc. 392 p.
- Marghany, M., and Hashim, M. (2010). MODIS satellite data for modeling chlorophyll-a concentrations in Malaysian coastal waters. **International Journal of the Physical Sciences**. 5(10):7.
- Matsumura, S., Siripong, A., and Lirdwitayaprasit, T. (2006). Underwater optical environment in the Upper Gulf of Thailand. **Coastal Marine Science**. 30(1): 36-43.
- Mélin, F., and Hoepffner, N. (2011). **Monitoring phytoplankton productivity from satellite: an aid to marine resources management**. J. Morales, V. Stuart, T. Platt and S. Sathyendranath (Eds.), Handbook of Satellite Remote Sensing Image Interpretation: Applications for Marine Living Resources Conservation and Management (pp. 293).
- Menasveta, P. (n.d.). **Marine pollution problems in Thailand water**. Department of Marine Science Faculty of Science. Chulalongkorn University Bangkok Thailand.
- NASA-Ocean Color. (2012). **MODIS specification**. [On-line]. Available: <http://oceancolor.gsfc.nasa.gov/>.

- Nixon, S. W. (1995). Coastal marine eutrophication: a definition, social causes, and future concerns. **Ophelia**. 41:199-219.
- OECD. (1982). **Eutrophication of waters: monitoring, assessment and control**. Organization for economic and co-operative development, Paris, France. Quoted in Stednick, J. D., and Hall, E. B. (2003). Applicability of trophic status indicators to colorado plains reservoirs. **Completion Report No. 195**. Colorado Water Resources Research Institute. Colorado State University, USA.
- Ondrusek, M., Stengel, E., Kinkade, C., Vogel, R., Keegstra, P., Hunter, C., and Kim, C. (2012) The development of a new optical total suspended matter algorithm for the Chesapeake Bay. **Remote Sensing of Environment**. 119: 243-254. doi:10.1016/j.rse.2011.12.018.
- O'Reilly, J. E., Maritorena, S., Mitchell, B. G., Siegel, D. A., Carder, K. L., Garver, S. A., Kahru, M., and McClain, C. (1998). Ocean color chlorophyll algorithms for SEAWIFS. **Journal of geophysical research**. 103: 24937-24953.
- O'Reilly, J. E., Mitchell, B. G., Kahru, M., Chavez, F. P., Strutton, P., Cota, G. F., Hooker, S. B., McClain, C. R., Carder, K. L., Muller-Karger, F., Harding, L., Phinney, D., Moore, G. F., Aiken, J., Arrigo, K. R., Letelier, R., and Culver, M. (2000). **Ocean color chlorophyll-a algorithms for SeaWiFS, OC2 and OC4: version 4**. SeaWiFS Postlaunch Calibration and Validation Analyses, Part 3.
- Palani, S., Liong, S. Y., and Tkalich, P. (2008). An ANN application for water quality forecasting. **Marine Pollution Bulletin**. 56: 1586-1597.
- Pan, Y., Tang, D., and Weng, D. (2010). Evaluation of the SeaWiFs and MODIS Chlorophyll-a algorithms used for the Northern South China Sea during the

- summer season. **Terrestrial Atmospheric and Oceanic Sciences**. 21: 997-1005. doi:10.3319/TAO.2010.02.11.01(Oc).
- PCD and ARRI. (2003). **Red tide monitoring phenomena in Thailand**. Pollution control department and Chulalongkorn University. Thailand (in Thai).
- Phoomwongpitak, W. (2003). **Meteorological factors associated with chlorophyll-a concentration in the gulf of Thailand as studied by remote sensing technique**. Master thesis in environmental science. Chulalongkorn University, Thailand.
- Poudyal, C. P., Chang, C., Oh, H. J., and Lee, S. (2010). Landslide susceptibility maps comparing frequency ratio and artificial neural network: a case study from the Nepal Himalaya. **Environmental Earth Sciences**. 61: 1049-1064. doi: 10.1007/s12665-009-0426-5.
- Primpas, I., Tsirtsis, G., Karydis, M., and Kokkoris, G. D. (2010). Principal component analysis: development of a multivariate index for assessing eutrophication according to the European water framework directive. **Ecological Indicators**. 10: 178-83.
- Quetglas, A., Ordines, F., and Guijarro, B. (2011). **The use of artificial neural Networks (ANNs) in aquatic ecology, artificial neural networks application**. Chi Leung Patrick Hui (Ed.), ISBN: 978-953-307-188-6, InTech, [Online] Available: <http://www.intechopen.com/books/artificial-neural-networks-application/the-use-of-artificial-neural-networks-anns-in-aquatic-ecology>.
- Ramsey, E. W. (2005). **Remote sensing of coastal environments**. In M. L. Schwartz (Ed.), Encyclopedia of Earth Sciences Series:Encyclopedia of Coastal Science

- (pp. 797). Netherlands: Springer, PO Box 17, 3300 AA Dordrecht, The Netherlands.
- Recknagel, F. (2006). **Ecological informatics scope, techniques and applications (2nd edition)**. School of earth and environmental sciences.the University of Adelaide. Australia. Springer-Verlag Berlin Heidelberg. Printed in Germany.
- Reyes-Pesaresi, P. (2010). **Dynamics of chromophoric dissolved organic matter, CDOM, in coastal tropical waters**. Doctoral dissertation in marine science. University of Puerto Rico.
- Royal irrigation department. (2015). **Monthly volume of water-runoff. Office of water management and hydrology**. Ministry of Agriculture and Cooperatives. Thailand. [On-line]. Available: <http://water.rid.go.th/hyd/PORTAL/submenu/4-03.html>
- Ruddick, K., Nechad, B., Neukermans, G., Park, Y., Doxaran, D., Sirjacobs, D., and Beckers, J. M. (2008). **Remote sensing of suspended particulate matter in turbid waters: state of the art and future perspectives**. Published in the CDROM Proceedings of the Ocean Optics XIX conference held in Barga, 6-10 October, 2008.
- Scardi, M., and Harding, L. W. J. (1999). Developing an empirical model of phytoplankton primary production: a neural network case study. **Ecological Modelling**. 120: 213-223.
- Shen, L., Xu, H., and Guo, X. (2012). Satellite remote sensing of harmful algal blooms (HABs) and a potential synthesized framework. **Sensors**. 12: 7778-7803). doi: 10.3390/s120607778.

- Shi, X., Liu, S., Fang, X., Qiao, S., Khokiattiwong, S., and Kornkanitnan, N. (2015). Distribution of clay minerals in surface sediments of the western Gulf of Thailand: Sources and transport patterns. **Journal of Asian Earth Sciences**. 105: 390-398.
- Siswanto, E., Tang, J., Yamaguchi, H., Ahn, Y. H., Ishizaka, J., Yoo, S., Kim, S. W., Kiyomoto, Y., Yamada, K., Chiang, C., and Kawamura, H. (2011). Empirical ocean-color algorithms to retrieve chlorophyll-a, total suspended matter, and colored dissolved organic matter absorption coefficient in the Yellow and East China Seas. **Journal of Oceanography**. 67: 627. doi:10.1007/s10872-011-0062-z.
- Smith, M. J. D., Goodchild, M. F., and Longley, P. (2007). **Geospatial analysis: A comprehensive guide to principles, techniques and software tools (second edition)**. British Library Cataloguing in Publishing Data, UK. 491 p.
- Smith, V. H., and Schindler, D. W. (2009). Eutrophication science: where do we go from here. **Trend in Ecology and Evolution**. 24(4): 201-207.
- Smith, V. H., Tilman, G. D., and Nekola, J. C. (1999). Eutrophication: impacts of excess nutrient inputs on freshwater, marine, and terrestrial ecosystems. **Environmental Pollution**. 100: 179-196.
- Son, S. H., and Wang, M. (2012). Water properties in Chesapeake Bay from MODIS-Aqua measurements. **Remote Sensing of Environment**. 123: 163-174.
- Sravanthi, N., Ramana, I. V., Yunus Ali, P., Ashraf, M., Ali, M. M., and Narayana, A. C. (2013). An algorithm for estimating suspended sediment concentrations in the coastal waters of India using remotely sensed reflectance and its application

to coastal environments. **International Journal Environment Resources**. 7(4): 841-850. ISSN: 1735-6865.

Stednick, J. D., and Hall, E. B. (2003). **Applicability of trophic status indicators to colorado plains reservoirs**. Completion Report No. 195. Colorado Water Resources Research Institute. Colorado State University, USA.

Steele, J. H. (1974). **The structure of marine ecosystems**. Cambridge: Harvard Univ. Press. Quoted in Kitsiou, D., and Karydis, M. (2011). Coastal marine eutrophication assessment: a review on data analysis. **Environmental International**. 37(4): 778-801. doi:10.1016/j.envint.2011.02.004.

Subramanian, A. N. (n.d.). **Introduction: Marine Environment**. [On-line]. Available: <http://ocw.unu.edu/international-network-on-water-environment-nd-health/unu-inweh-course-1-mangroves/Marine-Environment.pdf>.

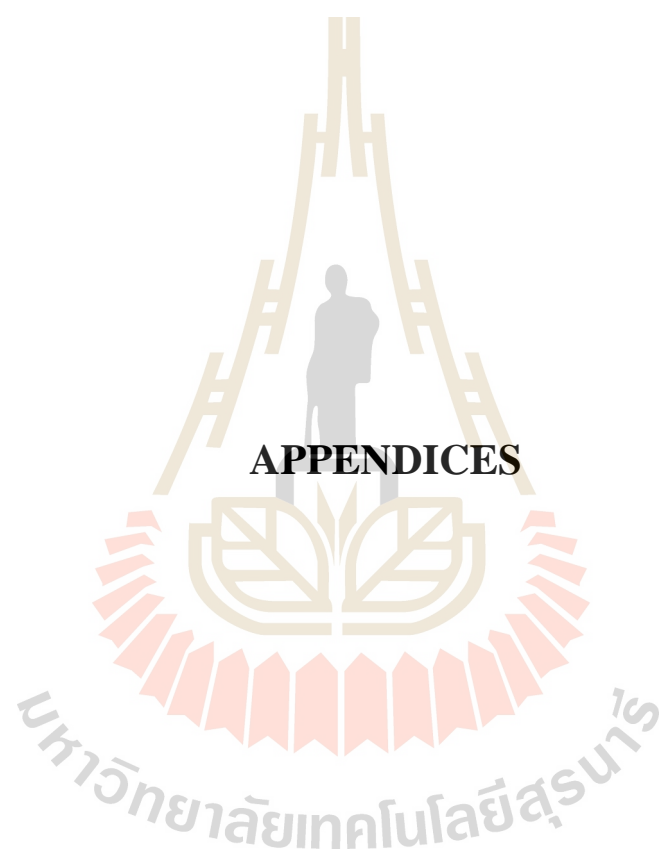
Tassan, S. (1994). Local algorithms using SeaWiFS data for the retrieval of phytoplankton, pigments, suspended sediment, and yellow substance in coastal waters. **Applied optics**. 33(12): 2369-78. doi:10.1364/AO.33.002369.

Thaipichitburapa, P. (2013). **Pesticide dynamic model for aquatic ecosystem of Tha-Chin River, Thailand**. Doctoral Dissertation. Kasetsart University. Thailand.

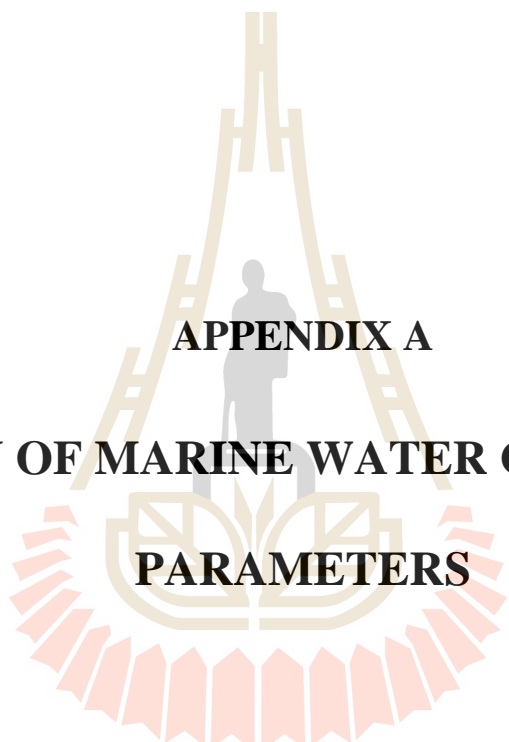
Thirakultomorn, T. (2010). **Forest cover assessment in Thailand using NOAA-AVHRR data**. Master Science Dissertation in Geoinformatics of Suranaree University of Technology. Thailand.

Vasinamakin, V., Kladkleeb, A., Torwinyu, P., and Kosaphol, W. (2008). Red tide phenomena at Tha-Chin River mouth, Samut Sakorn province. **Proceeding of Marine Science Conference. Department of Marine and Coastal Resources**. 25-27 August 2008, Phuket, Thailand.

- Wada, Y., and Ohira, W. (2004). **Reconstructing cloud free spot/vegetation using harmonic analysis with local maximum fitting**. 25th ACRS 2004 Chiang Mai, Thailand.
- Wang, F., Zhou, B., Xu, J., Song, L., and Wang, X. (2009). Application of neural network and MODIS 250 m imagery for estimating suspended sediments concentration in Hangzhou Bay, China. **Environmental Geology**. 56: 1093-1101. doi:10.1007/s00254-008-1209-0.
- Wattayakorn, G., and Jaiboon, P. (2014). An assessment of biogeochemical cycles of nutrients in the inner gulf of Thailand. **European Chemical Bulletin**. 3(1): 50-54.
- Wongsupap, C. (2008). **Eutrophication modelling in the Upper Gulf of Thailand**. Doctoral dissertation of school of engineering and technology, Asian Institute of Technology, Thailand.
- Xu, F. L., Tao, S., Dawson, R. W., and Li, B. G. (2001). A GIS-based method of lake eutrophication assessment. **Ecological Modelling**, 144: 231-244.
- Yilmaz, I. (2009). Landslide susceptibility mapping using frequency ratio, logistic regression, artificial neural networks and their comparison: A case study from Kat landslides (Tokat-Turkey). **Computers and Geosciences**. 35: 1125-1138. doi:10.1016/j.cageo.2008.08.007.



APPENDICES



APPENDIX A

**THE MAIN OF MARINE WATER CONSTITUENT
PARAMETERS**

มหาวิทยาลัยเทคโนโลยีสุรนารี

Table A Data collection of three water constituents in UGoT.

Cruise No.	Station	Chlorophyll-a (mg/m ³)	Suspended sediment (g/m ³)	Color dissolved organic matter-412 (m ⁻¹)
1	1	1.26168	1.40	0.17706
1	2	3.74131	2.45	0.33498
1	3	0.97853	1.50	0.44125
1	4	6.89890	3.00	0.64797
1	5	9.18562	5.00	0.70773
1	6	0.73632	2.65	0.42205
1	7	0.96209	1.57	0.46888
1	8	0.13819	1.13	0.27378
1	9	0.12298	1.10	0.09952
1	10	0.05779	0.65	0.06607
1	11	0.17091	0.80	0.15107
1	12	0.08134	0.72	0.09086
1	13	0.04903	0.55	0.07704
1	14	0.19379	0.98	0.24088
1	15	0.12017	0.66	0.07781
1	16	0.42719	0.77	0.15885
1	17	0.63773	1.95	0.16784
2	1	2.07691	3.40	0.06813
2	2	0.67793	2.80	0.04357
2	3	0.97689	3.25	0.01725
2	4	8.28520	2.85	0.19079
2	5	11.25607	2.40	0.12746
2	6	7.32733	3.65	0.33071
2	7	1.93440	2.90	0.12126
2	8	3.56079	3.10	0.07806
2	9	0.05370	2.63	0.03748
2	10	0.07008	1.25	0.04559
2	11	0.36981	1.08	0.04071
2	12	0.21318	0.90	0.03814
2	13	0.06156	0.63	0.07652
2	14	0.25486	1.67	0.02393
2	15	0.30144	1.90	0.01746
2	16	0.75725	1.20	0.02591
2	17	0.63787	2.20	0.01725
3	1	1.56795	5.00	0.09152
3	2	0.65472	2.80	0.07501
3	3	1.59538	3.70	0.08938
3	4	1.88600	5.70	0.12052
3	5	1.23071	0.95	0.14301
3	6	4.92623	3.70	0.14832
3	7	0.46402	0.72	0.06542
3	8	0.85557	1.53	0.06388
3	9	0.63113	3.00	0.01988
3	10	0.78903	1.10	0.02372
3	11	1.01900	0.90	0.03553
3	12	0.84573	1.08	0.01201
3	13	2.38954	1.50	0.01250
3	14	0.44224	1.20	0.01703
3	15	0.45434	1.15	0.02114
3	16	0.55674	1.40	0.02783
3	17	1.09075	2.40	0.02602

Table A Data collection of three water constituents in UGoT (Continued).

Cruise No.	Station	Chlorophyll-a (mg/m ³)	Suspended sediment (g/m ³)	Color dissolved organic matter-412 (m ⁻¹)
4	1	5.96816	8.97	0.37788
4	2	1.53776	0.84	0.39439
4	3	7.63525	0.81	0.53668
4	4	1.68111	0.78	0.34482
4	5	3.03195	0.77	0.25253
4	6	6.40284	1.50	0.27085
4	7	3.47810	2.32	0.23532
4	8	1.69350	0.61	0.19200
4	9	0.96232	1.56	0.21843
4	10	Na	Na	Na
4	11	1.09595	0.57	0.20708
4	12	1.06015	0.87	0.15965
4	13	1.53384	0.31	0.15998
4	14	3.82510	1.61	0.21190
4	15	Na	Na	Na
4	16	0.70268	0.23	0.26164
4	17	7.48517	1.16	0.37032
5	1	0.77142	3.30	0.22112
5	2a	0.48774	3.85	0.67086
5	2b	0.15846	2.15	0.32184
5	3	0.66308	1.50	0.70825
5	4	1.87266	3.60	0.80794
5	5	0.39489	2.20	0.63779
5	6	0.90302	4.97	0.71549
5	7	0.25424	2.13	0.65545
5	8	0.10675	1.17	0.32387
5	9	0.07779	0.80	0.13196
5	10	0.07309	0.70	0.14287
5	11	0.04166	0.88	0.16091
5	12	0.03849	1.02	0.14413
5	13	0.05716	0.73	0.16996
5	14	0.07616	0.99	0.16239
5	15	0.10884	1.10	0.18295
5	16	0.09937	1.25	0.11732
5	17	0.53970	5.15	0.18399

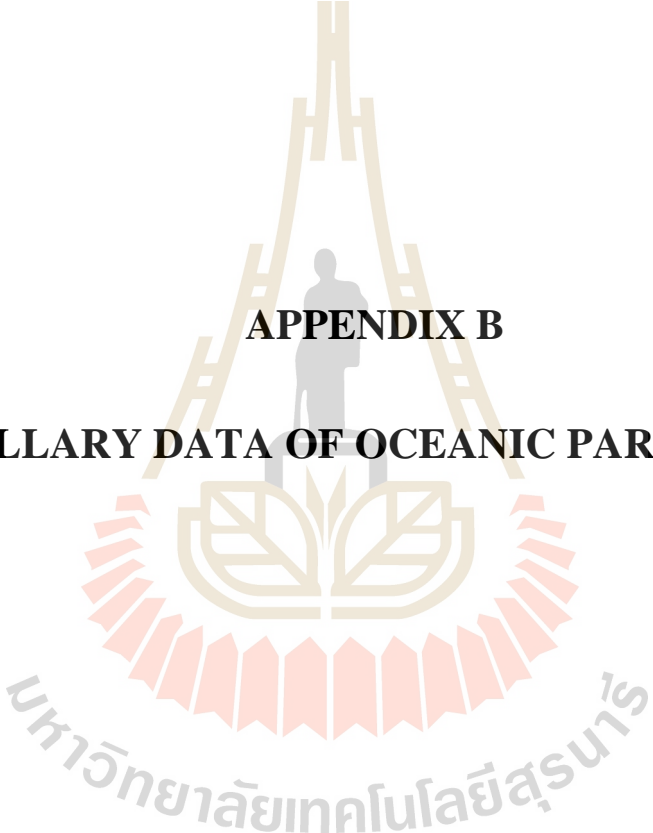
Cruise 1: data was collected from 9 to 11 October 2003.

Cruise 2: data was collected from 4 to 6 December 2003.

Cruise 3: data was collected from 13 to 15 January 2004.

Cruise 4: data was collected from 12 to 15 May 2004.

Cruise 5: data was collected from 7 to 10 October 2004



APPENDIX B

ANCILLARY DATA OF OCEANIC PARAMETERS

มหาวิทยาลัยเทคโนโลยีสุรนารี

Table B.1 Oceanic parameters from field surveys.

Cruise No.	Station	Date	Bottom depth (m)	Wind speed (m/sec)	Wind direction	Transparency (m)
1	1	9 Oct 03	13.0	4.0	180	5.80
1	2	9 Oct 03	15.7	4.5	180	4.40
1	3	9 Oct 03	10.6	3.0	180	5.80
1	4	9 Oct 03	9.0	5.0	180	3.70
1	5	9 Oct 03	16.8	4.0	180	2.80
1	6	9 Oct 03	17.8	4.0	180	4.00
1	7	10 Oct 03	18.8	1.0	225	6.00
1	8	10 Oct 03	24.9	2.0	225	9.00
1	9	11 Oct 03	22.1	3.0	180	12.38
1	10	10 Oct 03	28.2	2.0	180	10.50
1	11	10 Oct 03	27.7	3.0	200	11.70
1	12	10 Oct 03	24.6	3.0	180	12.00
1	13	10 Oct 03	37.2	3.0	180	9.10
1	14	11 Oct 03	19.7	3.0	180	10.62
1	15	11 Oct 03	16.0	5.0	180	10.20
1	16	11 Oct 03	20.5	2.0	180	7.10
1	17	11 Oct 03	27.0	4.5	180	4.80
2	1	4 Dec 03	13.5	9.0	45	4.0
2	2	4 Dec 03	17.0	9.0	45	6.0
2	3	4 Dec 03	12.0	5.0	45	4.0
2	4	4 Dec 03	10.2	1.0	45	4.0
2	5	4 Dec 03	17.0	1.5	45	6.0
2	6	4 Dec 03	17.2	3.0	45	4.0
2	7	5 Dec 03	19.5	8.0	0	6.0
2	8	5 Dec 03	25.3	7.0	0	6.0
2	9	6 Dec 03	22.7	6.0	0	10.0
2	10	5 Dec 03	27.6	5.0	338	9.0
2	11	5 Dec 03	28.9	8.0	0	7.0
2	12	5 Dec 03	25.5	7.0	0	10.0
2	13	5 Dec 03	36.3	6.0	0	16.0
2	14	6 Dec 03	21.0	9.0	0	6.0
2	15	6 Dec 03	17.2	6.0	22	7.0
2	16	6 Dec 03	21.4	5.0	0	8.0
2	17	6 Dec 03	13.0	6.0	0	5.5
3	1	13 Jan 04	14.1	5.0	0	2.00
3	2	13 Jan 04	17.9	3.0	0	6.50
3	3	13 Jan 04	12.5	3.0	0 - 22.5	4.43
3	4	13 Jan 04	10.0	0.0	nd	3.00
3	5	13 Jan 04	nd	0.0	nd	7.52
3	6	14 Jan 04	16.2	2.5	0	2.81
3	7	14 Jan 04	20.2	5.0	0	8.00
3	8	14 Jan 04	26.4	5.0	0	7.88
3	9	15 Jan 04	22.8	3.0	135	9.39
3	10	14 Jan 04	28.0	4.0	22.5	8.21
3	11	14 Jan 04	29.0	5.0	22.5	4.83
3	12	14 Jan 04	25.4	5.0	22.5	7.88
3	13	14 Jan 04	37.8	0.0	nd	11.00
3	14	15 Jan 04	20.7	4.0	180	7.50
3	15	15 Jan 04	17.5	3.0	180	nd
3	16	15 Jan 04	21.6	3.0	180	7.00
3	17	15 Jan 04	12.6	5.0	225	nd

Table B.1 Oceanic parameters from field surveys (Continued).

Cruise No.	Station	Date	Bottom depth (m)	Wind speed (m/sec)	Wind direction	Transparency (m)
	1	12 May 04	12.40	5	225	3.50
4	2	13 May 04	16.80	6	180	6.40
4	3	13 May 04	11.50	6	180	5.31
4	4	13 May 04	9.00	3	202.5	5.40
4	5	13 May 04	15.30	8	180	4.20
4	6	13 May 04	15.40	8	225	3.50
4	7	14 May 04	19.00	8	225	3.00
4	8	14 May 04	24.50	8	202.5	5.89
4	9	15 May 04	22.30	6	202.5	5.50
4	10	Na	Na	Na	Na	Na
4	11	14 May 04	27.80	7	202.5	7.60
4	12	14 May 04	24.60	6	202.5	4.70
4	13	14 May 04	37.70	6	180	9.87
4	14	15 May 04	19.00	6	202.5	5.00
4	15	Na	Na	Na	Na	Na
4	16	15 May 04	19.50	6	225	12.07
4	17	15 May 04	12.10	5	202.5	4.70
5	1	7 Oct 04	14.50	5	110	4.00
5	2a	8 Oct/04	16.50	4	120	4.00
5	2b	8 Oct 04	16.80	4	120	8.50
5	3	8 Oct 04	12.40	1	165	5.00
5	4	8 Oct 04	10.00	1	100	3.50
5	5	8 Oct 04	17.00	2	70	3.00
5	6	8 Oct 04	17.40	2	70	3.00
5	7	9 Oct 04	19.20	4	160	4.00
5	8	9 Oct 04	24.60	5	95	11.00
5	9	10 Oct 04	21.50	4	120	12.00
5	10	9 Oct 04	28.00	2	320	13.00
5	11	9 Oct 04	28.50	1	0	14.00
5	12	9 Oct 04	25.60	2	310	12.00
5	13	9 Oct 04	37.00	2	330	12.00
5	14	10 Oct 04	19.00	4	90	12.00
5	15	10 Oct 04	17.00	2	130	10.00
5	16	7 Oct 04	21.00	5	40	6.50
5	17	7 Oct 04	30.00	4	70	3.50

Table B.2 Water quality parameters from field surveys.

Cruise No.	Station	Ammonia (μM)	Nitrite (μM)	Nitrate (μM)	Phosphate (μM)	Silicate (μM)	Temperature ($^{\circ}\text{C}$)	Salinity (psu)	DO (ml/l)	pH
1	1	11.39	0.41	0.09	0.59	15.61	29.46	29.99	5.33	8.16
1	2	11.19	0.08	0.06	0.74	15.61	29.49	27.85	6.03	8.19
1	3	9.60	0.08	0.00	0.60	12.45	30.42	27.45	6.86	8.40
1	4	9.20	0.04	0.17	1.37	10.87	31.20	22.19	7.50	8.59
1	5	7.00	0.06	0.00	1.35	18.06	31.28	20.15	9.96	8.65
1	6	7.60	0.06	0.00	0.88	18.59	31.00	22.92	5.35	8.47
1	7	6.80	0.04	0.00	0.64	16.83	30.05	24.01	4.70	8.57
1	8	10.40	0.08	0.00	0.49	13.15	29.53	28.06	4.26	8.46
1	9	10.40	0.04	0.03	0.20	6.14	29.65	29.11	1.45	8.41
1	10	8.00	0.04	0.03	0.12	4.56	30.50	31.55	4.39	8.29
1	11	9.60	0.04	0.00	0.21	9.29	29.54	30.17	3.11	8.37
1	12	10.00	0.04	0.00	0.16	4.91	30.28	32.26	2.66	8.30
1	13	8.00	0.04	0.00	0.12	4.38	30.41	31.34	2.52	8.30
1	14	9.60	0.06	0.08	0.41	15.43	29.95	28.36	1.17	8.38
1	15	11.79	0.06	0.15	0.14	7.54	30.14	31.24	1.39	8.31
1	16	9.00	0.04	0.03	0.29	13.85	30.75	28.95	0.41	8.25
1	17	8.00	0.04	0.00	0.16	9.12	30.14	28.15	5.32	8.27
2	1	9.00	0.04	0.17	0.20	5.61	27.55	31.34	8.12	8.37
2	2	10.60	0.08	0.06	0.20	7.19	27.87	31.30	8.37	8.40
2	3	9.20	0.04	0.00	0.18	7.37	27.71	31.36	4.10	8.39
2	4	10.00	0.04	0.17	0.20	9.47	27.60	30.61	10.58	8.45
2	5	9.00	0.06	0.00	0.39	15.61	27.99	30.00	9.62	8.45
2	6	9.20	0.04	0.00	0.64	20.69	28.04	29.05	9.60	8.42
2	7	9.60	0.04	0.07	0.21	11.40	27.86	31.17	8.32	8.40
2	8	10.60	0.08	0.03	0.20	5.09	28.01	31.30	8.57	8.43
2	9	9.00	0.04	0.00	0.16	7.19	28.22	31.24	8.09	8.29
2	10	10.00	0.04	0.00	0.16	7.89	28.65	31.26	8.23	8.40
2	11	10.99	0.02	0.00	0.14	7.72	28.41	31.25	8.34	8.41
2	12	9.80	0.04	0.00	0.16	7.72	28.41	31.25	8.34	8.41
2	13	9.00	0.04	0.00	0.16	7.72	28.76	31.19	8.30	8.41
2	14	7.40	0.02	0.02	0.12	6.84	27.98	31.37	8.39	8.40
2	15	10.40	0.04	0.00	0.18	9.12	28.26	31.28	8.38	8.37
2	16	9.00	0.04	0.03	0.16	8.59	28.12	31.41	8.56	8.40
2	17	10.00	0.04	0.00	0.20	7.19	28.22	31.41	8.56	8.38
3	1	9.40	0.04	0.07	0.23	4.91	26.38	31.70	8.60	8.41
3	2	10.00	0.06	0.01	0.18	8.59	26.62	31.79	8.49	8.39
3	3	9.00	0.41	0.37	0.29	9.47	26.56	31.24	2.19	8.40
3	4	10.60	0.08	0.17	0.35	12.28	26.88	30.80	7.12	8.26
3	5	7.00	0.12	0.00	0.29	8.77	26.51	30.24	9.06	8.48
3	6	12.79	0.16	1.12	0.68	22.97	26.47	30.16	8.72	8.40
3	7	8.00	0.16	0.00	0.20	11.05	26.25	31.16	8.75	8.47
3	8	8.00	0.08	0.00	0.16	7.37	26.83	32.01	8.76	8.46
3	9	10.99	0.04	0.10	0.20	6.84	27.08	32.26	8.50	8.42
3	10	10.00	0.04	0.03	0.16	6.66	27.40	32.17	8.53	8.45
3	11	9.80	0.04	0.07	0.16	7.37	27.03	32.14	8.68	8.44
3	12	8.20	0.06	0.00	0.18	6.31	27.19	32.31	8.53	8.46
3	13	9.20	0.08	0.06	0.14	5.44	27.68	32.21	8.57	8.47
3	14	7.20	0.08	0.06	0.16	8.42	26.80	31.92	8.71	8.44
3	15	10.00	0.08	0.00	0.16	8.59	27.47	32.17	8.48	8.43
3	16	8.00	0.04	0.10	0.12	8.59	27.23	31.96	8.60	8.42
3	17	9.20	0.04	0.10	0.16	5.79	27.48	31.90	8.59	8.41

Table B.2 Water quality parameters from field surveys (Continued).

Cruise No.	Station	Ammonia (μM)	Nitrite (μM)	Nitrate (μM)	Phosphate (μM)	Silicate (μM)	Temperature ($^{\circ}\text{C}$)	Salinity (psu)	DO (ml/l)	pH
4	1	10.60	3.91	1.91	1.11	19.29	30.80	31.01	6.52	8.14
4	2	7.40	0.00	0.14	0.23	21.92	30.79	30.60	6.59	8.64
4	3	5.60	0.04	0.14	0.29	25.43	30.66	30.01	6.64	8.60
4	4	8.00	0.04	0.10	0.18	22.45	30.74	30.39	6.88	8.57
4	5	8.80	0.06	0.15	0.18	14.03	30.73	32.25	6.41	8.53
4	6	8.60	0.04	0.24	0.18	12.98	30.72	32.56	6.21	8.55
4	7	6.20	0.04	0.17	0.16	4.21	30.45	32.97	6.04	8.56
4	8	9.00	0.06	0.44	0.18	10.17	30.35	32.91	6.10	8.52
4	9	8.20	0.04	0.17	0.20	8.24	30.26	32.77	6.25	8.55
4	10	Na	Na	Na	Na	Na	30.35	32.67	6.09	8.53
4	11	7.80	0.04	0.24	0.16	10.52	30.25	32.73	6.59	8.53
4	12	6.60	0.04	0.24	0.16	12.63	30.58	32.63	6.68	8.53
4	13	7.40	0.04	0.17	0.16	8.42	30.74	32.74	6.52	8.53
4	14	8.60	0.04	0.31	0.18	10.17	30.33	32.42	6.46	8.54
4	15	Na	Na	Na	Na	Na	Na	Na	Na	Na
4	16	7.40	0.04	0.31	0.20	14.20	30.58	31.80	6.29	8.54
4	17	6.80	0.04	0.39	0.29	13.15	30.86	30.80	7.38	8.60
5	1	10.32	0.48	0.36	0.53	11.94	29.54	32.19	4.86	8.42
5	2a	13.76	2.05	6.93	1.59	43.21	29.19	24.65	5.39	8.62
5	2b	6.31	0.24	0.04	0.27	5.69	29.52	32.35	5.60	8.58
5	3	11.46	1.08	3.12	1.06	21.04	29.86	24.33	6.32	8.63
5	4	8.02	0.18	0.10	0.53	4.55	30.95	23.67	8.09	8.87
5	5	8.60	0.12	0.30	1.19	1.14	30.99	23.75	7.87	8.97
5	6	10.32	0.36	0.76	1.06	3.41	31.70	22.84	7.90	8.86
5	7	6.88	0.12	0.02	0.60	1.14	29.47	24.51	6.59	8.90
5	8	10.89	0.18	0.66	0.60	6.25	29.57	29.56	5.75	8.86
5	9	9.74	0.12	0.16	0.20	5.12	29.41	32.32	5.29	8.66
5	10	8.02	0.12	0.02	0.27	6.25	30.74	32.21	5.69	8.63
5	11	6.88	0.12	0.02	0.20	5.12	29.56	32.67	5.63	8.61
5	12	8.02	0.12	0.16	0.27	6.82	30.93	32.75	5.59	8.61
5	13	7.45	0.12	0.16	0.23	7.39	30.86	31.84	5.66	8.63
5	14	8.60	0.12	0.30	0.33	6.82	29.70	32.55	5.52	8.64
5	15	8.60	0.24	0.04	0.33	4.55	29.81	32.20	5.65	8.56
5	16	8.60	0.18	0.10	0.33	10.80	30.09	32.68	5.13	8.53
5	17	7.45	0.24	0.00	0.30	10.80	29.65	32.43	5.70	8.54

nd = no data

APPENDIX C

SURFACE PROFILING REFLECTANCE RADIOMETER

(PRR) MEASUREMENT

AND

MODIS DATASET FOR MODEL FORMULATION AND

IMPLEMENTATION

มหาวิทยาลัยเทคโนโลยีสุรนารี

Table C.1 Optical reflectance measured by PRR in cruise 1 (9 to 11 October 2003).

Station	PRR Reflectance ($\mu\text{W}/\text{cm}^2/\text{nm}$)					
	412	443	490	520	565	670
1	0.000964	0.001254	0.001822	0.002185	0.002667	0.000998
2	0.001605	0.001948	0.002442	0.002414	0.003160	0.001300
3	0.000825	0.001145	0.001868	0.002181	0.002734	0.000487
4	0.000653	0.000894	0.001737	0.002397	0.003583	0.001235
5	0.000676	0.001305	0.003144	0.004676	0.007221	0.002337
6	0.001963	0.002246	0.003082	0.003831	0.005067	0.001929
7	0.000989	0.001296	0.001906	0.002303	0.002809	0.001071
8	0.000658	0.001289	0.002807	0.002584	0.002127	0.000525
9	0.002005	0.002674	0.003872	0.002657	0.001735	0.000181
10	0.003413	0.003908	0.004916	0.003210	0.001894	0.000258
11	0.001586	0.002372	0.003867	0.003077	0.002202	0.000230
12	0.004380	0.004624	0.005503	0.003605	0.002189	0.000162
13	0.003698	0.004189	0.005115	0.003763	0.002534	0.000213
14	0.001039	0.001816	0.004069	0.003757	0.003105	0.000463
15	0.003405	0.004025	0.005667	0.004264	0.002884	0.000172
16	0.001515	0.001983	0.003416	0.003287	0.002757	0.000404
17	0.003490	0.003801	0.005093	0.004888	0.004260	0.000741

Table C.2 Optical reflectance measured by PRR in cruise 2 (4 to 6 December 2003).

Station	PRR Reflectance ($\mu\text{W}/\text{cm}^2/\text{nm}$)					
	412	443	490	520	565	670
1	0.008325	0.010271	0.015201	0.016084	0.016715	0.004876
2	0.006950	0.008343	0.011612	0.010845	0.009577	0.001784
3	0.007826	0.008666	0.011585	0.011366	0.010497	0.002516
4	0.002315	0.002352	0.003161	0.003685	0.005032	0.001419
5	0.001352	0.001555	0.002137	0.003057	0.003890	0.000925
6	0.000548	0.000703	0.001216	0.002730	0.003792	0.000785
7	0.004306	0.005294	0.007643	0.007812	0.007832	0.001543
8	0.005413	0.006348	0.009266	0.009340	0.009092	0.001547
9	0.004933	0.005729	0.007223	0.004938	0.003288	0.000560
10	0.004983	0.005318	0.006383	0.004708	0.003277	0.000463
11	0.007902	0.009120	0.012136	0.010578	0.008697	0.001260
12	0.005577	0.006081	0.007594	0.005490	0.003678	0.000487
13	0.004573	0.004809	0.005583	0.003796	0.002427	0.000304
14	0.004625	0.005447	0.007782	0.006392	0.004927	0.000566
15	0.005797	0.006440	0.008413	0.006884	0.005198	0.000734
16	0.006704	0.007540	0.010005	0.008375	0.006466	0.000917
17	0.005970	0.006975	0.010029	0.008564	0.006687	0.000871

Table C.3 Optical reflectance measured by PRR in cruise 3 (13 to 15 January 2004).

Station	PRR Reflectance ($\mu\text{W}/\text{cm}^2/\text{nm}$)					
	412	443	490	520	565	670
1	0.010765	0.013475	0.019007	0.019468	0.019395	0.006452
2	0.007362	0.008634	0.011250	0.010327	0.009076	0.001718
3	0.011385	0.013431	0.018251	0.019665	0.019973	0.005926
4	0.020853	0.022304	0.027402	0.028750	0.028616	0.010173
5	0.001252	0.001406	0.002264	0.002503	0.002419	0.000371
6	0.002855	0.003274	0.004798	0.005119	0.004759	0.001339
7	0.002697	0.003505	0.005618	0.004804	0.003692	0.000458
8	0.006234	0.007250	0.009815	0.008551	0.007125	0.001138
9	0.004045	0.004616	0.005982	0.004479	0.003160	0.000229
10	0.004022	0.004178	0.005289	0.004284	0.003149	0.000489
11	0.006859	0.007988	0.010468	0.009213	0.007560	0.001113
12	0.004780	0.005222	0.006673	0.005537	0.004208	0.000680
13	0.003827	0.003965	0.004889	0.003649	0.002433	0.000269
14	0.005619	0.006666	0.008689	0.006981	0.005316	0.000640
15	0.005182	0.005770	0.007388	0.005813	0.004209	0.000648
16	0.006112	0.006822	0.008766	0.007385	0.005800	0.000902
17	0.007010	0.007971	0.010740	0.010588	0.009575	0.001512

Table C.4 Optical reflectance measured by PRR in cruise 4 (12 to 15 May 2004).

Station	PRR Reflectance ($\mu\text{W}/\text{cm}^2/\text{nm}$)					
	412	443	490	520	565	670
1	0.002669	0.003968	0.007465	0.009425	0.011471	0.001878
2	0.001573	0.002174	0.003535	0.004041	0.004404	0.000686
3	0.000925	0.001193	0.002159	0.003832	0.004957	0.000705
4	0.002012	0.003184	0.006787	0.008857	0.009933	0.000662
5	0.004520	0.005481	0.009027	0.010672	0.010844	0.001206
6	0.004553	0.005281	0.008268	0.010967	0.012200	0.001640
7	0.007835	0.009417	0.014673	0.015984	0.017400	0.002955
8	0.007658	0.009313	0.013282	0.011435	0.009539	0.001162
9	0.008370	0.009755	0.013981	0.013334	0.012372	0.001741
10	Na	Na	Na	Na	Na	Na
11	0.007756	0.008766	0.011477	0.009321	0.007346	0.000644
12	0.009999	0.010980	0.014160	0.012257	0.009911	0.001212
13	0.006279	0.006666	0.008132	0.006412	0.004814	0.000445
14	0.006556	0.007979	0.012032	0.012608	0.012536	0.001763
15	Na	Na	Na	Na	Na	Na
16	0.002473	0.003166	0.005231	0.005040	0.004044	0.000332
17	0.001546	0.002091	0.003630	0.004466	0.005699	0.000847

Table C.5 Optical reflectance measured by PRR in cruise 5 (7 to 10 October 2004).

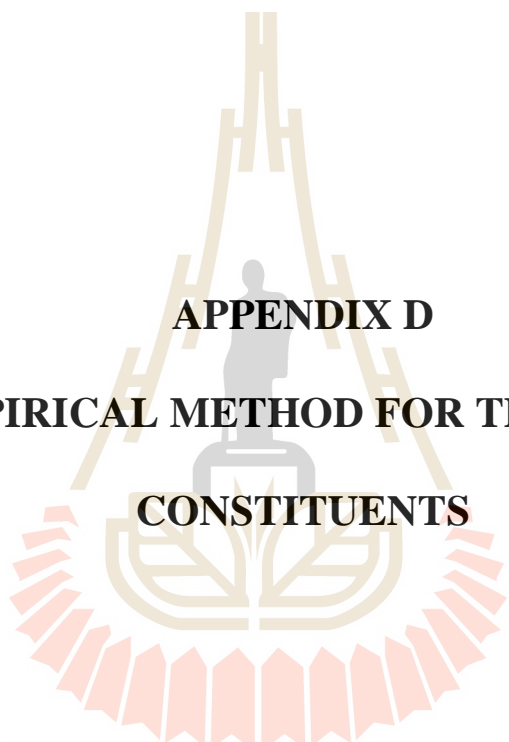
Station	PRR Reflectance ($\mu\text{W}/\text{cm}^2/\text{nm}$)					
	412	443	490	520	565	670
1	0.002927	0.003161	0.004751	0.005824	0.006980	0.001116
2a	0.003210	0.004792	0.008187	0.009142	0.009658	0.002139
2b	0.004257	0.005266	0.008355	0.007866	0.006850	0.000918
3	0.001199	0.001766	0.003257	0.004458	0.006325	0.001424
4	0.000884	0.001250	0.002780	0.004082	0.006005	0.001460
5	0.000659	0.000957	0.001971	0.003197	0.006322	0.001826
6	0.001425	0.002140	0.003889	0.005443	0.008892	0.002570
7	0.001788	0.003549	0.005872	0.006418	0.006848	0.001319
8	0.002928	0.004047	0.006202	0.005184	0.004062	0.000471
9	0.008580	0.008836	0.010668	0.007414	0.004928	0.000489
10	0.008735	0.008696	0.009992	0.006656	0.004116	0.000350
11	0.009067	0.009118	0.009978	0.006988	0.004599	0.000364
12	0.009264	0.009360	0.010805	0.007976	0.005321	0.000307
13	0.007931	0.008070	0.009315	0.006793	0.004594	0.000464
14	0.006243	0.006817	0.008877	0.006820	0.004811	0.000367
15	0.008181	0.008418	0.011216	0.009241	0.006926	0.000547
16	0.006485	0.007571	0.010498	0.009735	0.008191	0.000759
17	0.008872	0.010199	0.015744	0.017045	0.018372	0.003321

Table C.6 The MODIS satellite data based (level-2) for model formulation.

Cruise no.	Date	MODIS L2 Imageries		Remark
		Date	Image name	
Cr1	9-11 Oct 2003	10 Oct 2003	A2003283	Wet season
		28 Oct 2003	A2003301	
		28 Oct 2003	T2003301	
Cr2	4-6 Dec 2003	4 Dec 2003	A2003338	Dry season
		4 Dec 2003	T2003338	
		6 Dec 2003	A2003340	
		6 Dec 2003	T2003340	
Cr3	13-15 Jan 2004	7 Jan 2004	A2004007	Dry season
		7 Jan 2004	T2004007	
		16 Jan 2004	A2004016	
		16 Jan 2004	T2004016	
Cr4	12-15 May 2004	26 Apr 2004	A2004117	Dry season
		30 May 2004	A2004151	
Cr5	7-10 Oct 2004	15 Oct 2004	T2004288	Wet season
		31 Oct 2004	A2004304	
		31 Oct 2004	T2004304	

Table C.7 The MODIS satellite data based (level-2) using for UGoT implementation in years 2010 to 2012.

| Image code |
|----------------|----------------|----------------|----------------|----------------|----------------|
| A2010005070500 | T2010119034500 | A2011001065500 | T2011106034500 | A2012004065500 | A2012196065500 |
| A2010009064000 | T2010009033500 | A2011003064500 | T2011010034500 | A2012006064500 | A2012360063000 |
| A2010011063000 | T2010014035500 | A2011008070500 | T2011021033000 | A2012008063000 | A2012362062000 |
| A2010023065500 | T2010018033000 | A2011009061000 | T2011026034500 | A2012009071500 | A2012363070500 |
| A2010025064000 | T2010041033500 | A2011010065000 | T2011049035500 | A2012010062000 | A2012364061000 |
| A2010036062000 | T2010046035500 | A2011026065000 | T2011079040500 | A2012018071000 | A2012141065000 |
| A2010039065500 | T2010057033500 | A2011039062000 | T2011108033500 | A2012020065500 | T2012008033000 |
| A2010046070000 | T2010062035500 | A2011040070500 | T2011122034500 | A2012022064500 | T2012009041000 |
| A2010053070500 | T2010064034000 | A2011042065000 | | A2012024063000 | T2012020035500 |
| A2010057064000 | T2010073033500 | A2011049065500 | | A2012026062000 | T2012022034000 |
| A2010062070000 | T2010096034000 | A2011079071000 | | A2012038064500 | T2012038034000 |
| A2010064064500 | T2010098033000 | A2011106065000 | | A2012052065500 | T2012022034000 |
| A2010067071500 | T2010103034500 | A2011111071000 | | A2012059070500 | T2012038034000 |
| A2010083071500 | T2010112034000 | A2011120070500 | | A2012061065000 | T2012061034500 |
| A2010094070000 | T2010128034000 | A2011122065000 | | A2012066071000 | T2012077034500 |
| A2010096064500 | T2010130033000 | A2011160061500 | | A2012067061500 | T2012102034000 |
| A2010103065000 | T2010151034500 | A2011186065000 | | A2012077065000 | T2012109034500 |
| A2010110070000 | T2010152043000 | A2011192061500 | | A2012080072000 | T2012125034500 |
| A2010119065000 | T2010163041000 | A2011209065500 | | A2012081062500 | T2012135042500 |
| A2010126070000 | T2010167034500 | A2011216070000 | | A2012082071000 | T2012136033000 |
| A2010128064500 | T2010169033500 | A2011217060500 | | A2012099061500 | T2012141034500 |
| A2010151065000 | T2010176034000 | A2011218065000 | | A2012100065500 | T2012166034000 |
| A2010163071500 | T2010193042500 | A2011225065500 | | A2012102064500 | T2012198034000 |
| A2010167065000 | T2010263034500 | A2011234065000 | | A2012105071500 | T2012237034500 |
| A2010171062500 | T2010296043000 | A2011234065000 | | A2012107070500 | A2013001064000 |
| A2010213070500 | T2010318035500 | A2011298065000 | | A2012109065000 | A2013002072000 |
| A2010238065500 | T2010325040000 | A2011303071000 | | A2012116065500 | A2013003062500 |
| A2010263065000 | T2010327034500 | A2011305065500 | | A2012118064500 | A2013006065500 |
| A2010268071000 | T2010332040500 | A2011307064500 | | A2012125065000 | A2013008064500 |
| A2010286065500 | T2010336034000 | A2011314065000 | | A2012131061500 | A2013010063000 |
| A2010297064000 | T2010343034500 | A2011316064000 | | A2012132065500 | A2013011071500 |
| A2010302065500 | T2010352034000 | A2011321065500 | | A2012134064500 | A2013012062000 |
| A2010318065500 | T2010359034500 | A2011323064500 | | A2012157065000 | A2013013070500 |
| A2010320064500 | T2010361033500 | A2011326071500 | | A2012166064500 | A2013014061000 |
| A2010325070500 | | A2011330065000 | | A2012203070500 | A2013015065000 |
| A2010327065000 | | A2011332064000 | | A2012269065000 | A2013017064000 |
| A2010329064000 | | A2011334062500 | | A2012278064500 | A2013018072000 |
| A2010343065000 | | A2011335071000 | | A2012285065000 | |
| A2010352064500 | | A2011336061500 | | A2012292065500 | |
| A2010359065000 | | A2011337065500 | | A2012294064500 | |
| A2010361064000 | | A2011341063000 | | A2012301065000 | |
| | | A2011344070000 | | A2012303064000 | |
| | | A2011346065000 | | A2012308065500 | |
| | | A2011352061500 | | A2012310064500 | |
| | | A2011353065500 | | A2012313071500 | |
| | | A2011357063000 | | A2012315070000 | |
| | | A2011362065000 | | A2012353062500 | |
| | | A2011364064000 | | A2012354071000 | |
| | | A2011365072000 | | A2012356065500 | |



APPENDIX D
THE EMPIRICAL METHOD FOR THREE WATER
CONSTITUENTS

มหาวิทยาลัยเทคโนโลยีสุรนารี

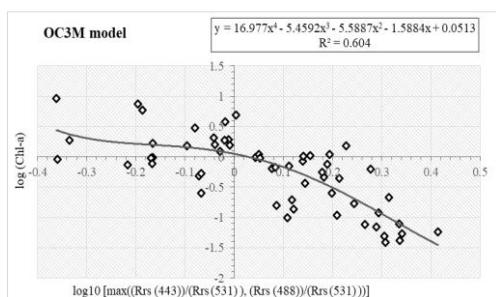


Figure D.1 Chl-a by OC3M model based on in situ and PRR data.

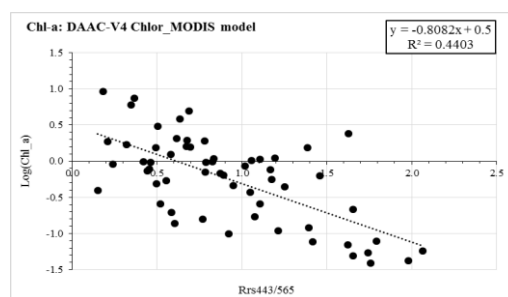


Figure D.2 Chl-a by DAAC-V4 Chlor_MODIS model based on in situ and PRR data.

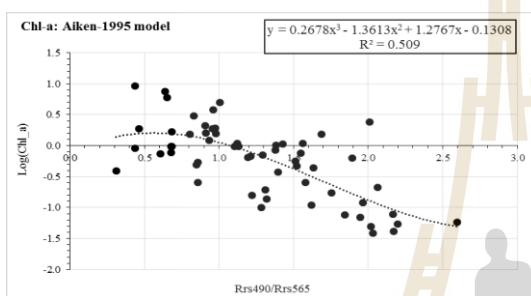


Figure D.3 Chl-a by Aiken-1995 model based on in situ and PRR data.

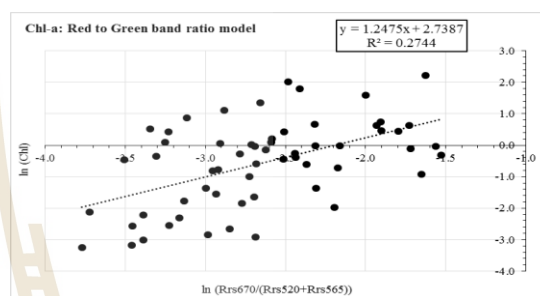


Figure D.4 Chl-a by Red to Green band ratio model based on in situ and PRR data.

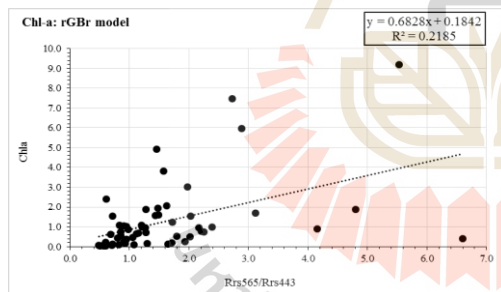


Figure D.5 Chl-a by rGBr model based on in situ and PRR data.

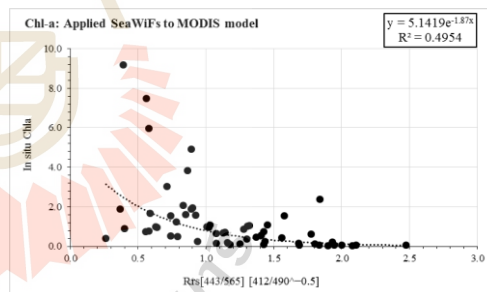


Figure D.6 Chl-a by Applied SeaWiFs to MODIS model based on in situ and PRR data.

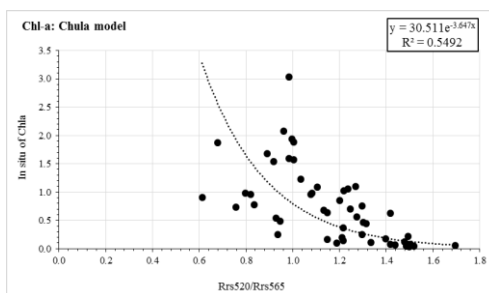


Figure D.7 Chl-a by Chula model based on in situ and PRR data.

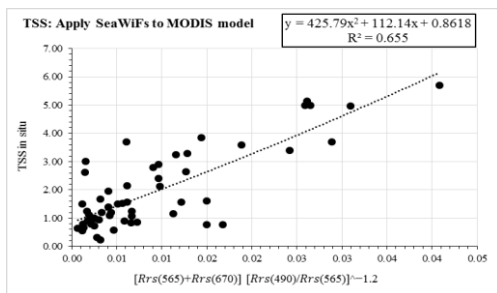


Figure D.8 TSS by Applied SeaWiFs to MODIS model based on in situ and PRR data.

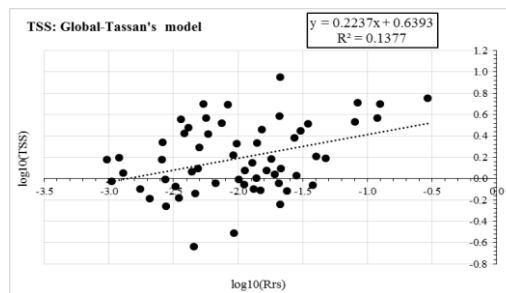


Figure D.9 TSS computed by Global-Tassan's model based on in situ and PRR data.

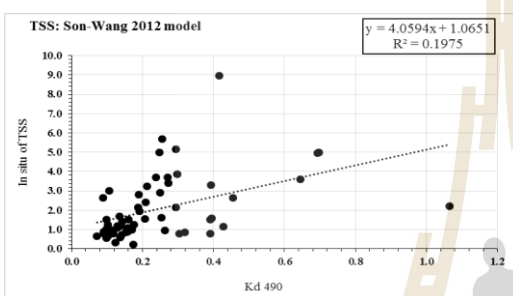


Figure D.10 TSS by Son-Wang 2012 model based on in situ and PRR data.

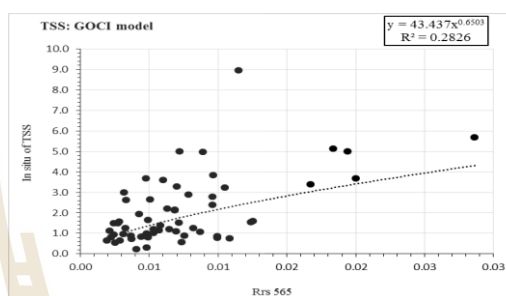


Figure D.11 TSS by GOCI model based on in situ and PRR data.

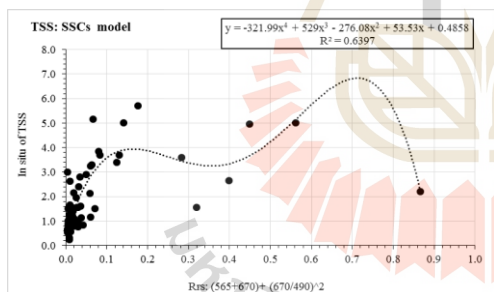


Figure D.12 TSS by SSCs model based on in situ and PRR data.

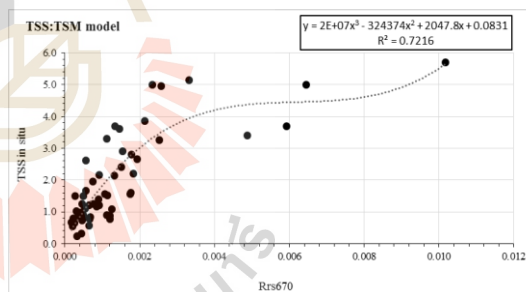


Figure D.13 TSS computed by TSM model based on in situ and PRR data.

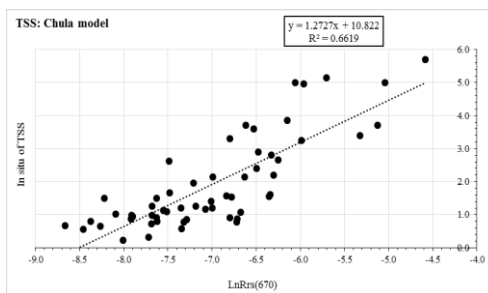


Figure D.14 TSS by Chula model based on in situ and PRR data.

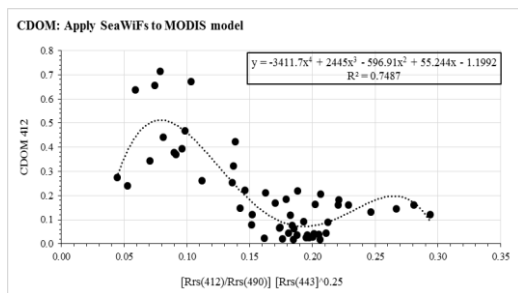


Figure D.15 CDOM by Apply SeaWiFs to MODIS model based on in situ and PRR data.

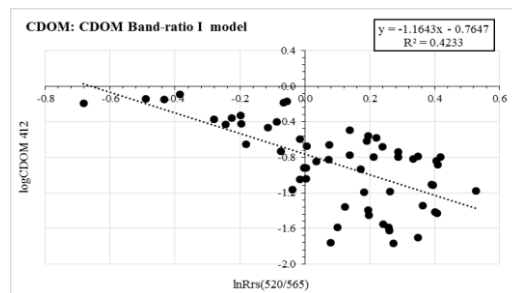


Figure D.16 CDOM by CDOM Band ratio I model based on in situ and PRR data.

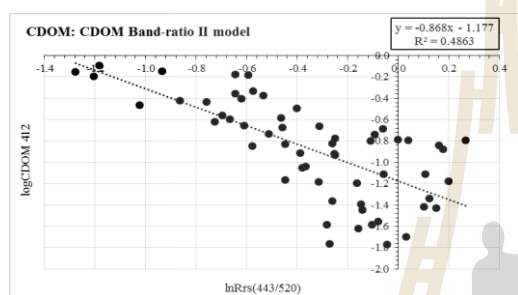


Figure D.17 CDOM by CDOM Band ratio II model based on in situ and PRR data.

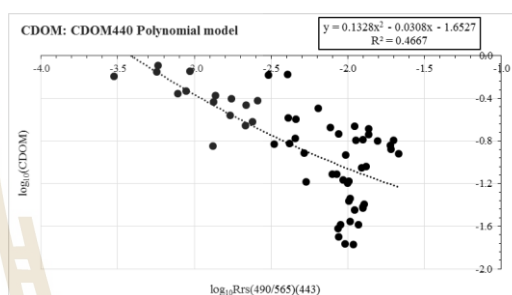


Figure D.18 CDOM by CDOM440 Polynomial model based on in situ and PRR data.

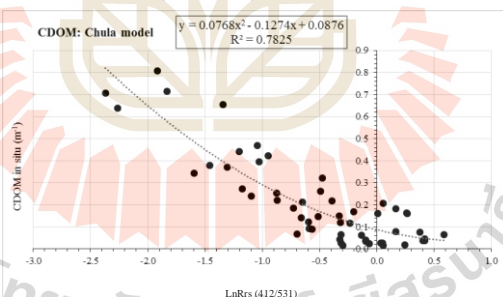
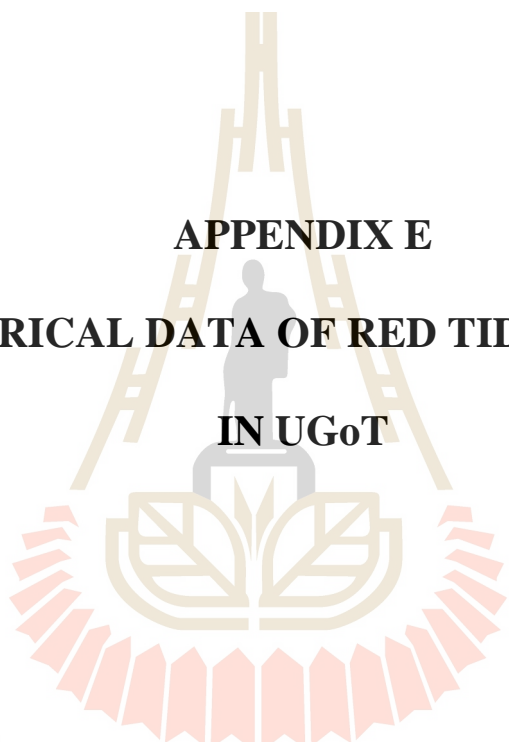


Figure D.19 CDOM by Chula model based on in situ and PRR data.



APPENDIX E
THE HISTORICAL DATA OF RED TIDE PHENOMENA
IN UGoT

มหาวิทยาลัยเทคโนโลยีสุรนารี

Table E The historical data of red tide event that occurred in UGoT area.

NO.	Date	Month	Year	Location Event	Province	Plankton Type	Remark	Reference
1	24	June	2004	Vornnapa beach, Saensuk	Chonburi	Noctiluca scintillans		DMCR-Eastern Center
2	9-21	February	2005	Bang Pakong river mouth		Noctiluca scintillans	Occur in many days	IMS-BUU
3	8	March	2005	Bang Saen beach	Chonburi	Noctiluca scintillans		IMS-BUU
4	8	March	2005	Sri Racha	Chonburi	Noctiluca scintillans		IMS-BUU
5	5	April	2005	Bang Pakong river mouth	Chonburi	Skeletonema costatum		IMS-BUU
6	16	June	2005	Bang Pakong river mouth	Chachoengsao	Noctiluca scintillans		IMS-BUU
7	16	June	2005	Ang Sila	Chonburi	Skeletonema costatum	Not extreme	IMS-BUU
8	16	June	2005	Sri Racha	Chonburi	Skeletonema costatum	Not extreme	IMS-BUU
9	16	June	2005	Ko Si Chang	Chonburi	Skeletonema costatum	Not extreme	IMS-BUU
10	1-4	July	2005	Bang Pakong river mouth	Chachoengsao	Noctiluca scintillans	Extreme event that appear from Angsila to Vonnapa beach and some of aquatic animal died at the 4 day.	IMS-BUU
11	1-4	July	2005	Ko Si Chang	Chonburi	Noctiluca scintillans	Extreme event that appear from Angsila to Vonnapa beach and some of aquatic animal died at the 4 day.	IMS-BUU
12	7	July	2005	Bang Pakong River mouth	Chachoengsao	Chaetoceros spp.		IMS-BUU
13	7	July	2005	Ang Sila	Chonburi	Noctiluca scintilis	Not extreme, more concentration at Ansila and Bang Saen	IMS-BUU
14	7	July	2005	Sri Racha	Chonburi	Noctiluca scintilis	Not extreme, more concentration at Ansila and Bang Saen	IMS-BUU

Table E The historical data of red tide event that occurred in UGoT area (Continued).

NO.	Date	Month	Year	Location Event	Province	Plankton Type	Remark	Reference
15	15-19	August	2005	Vornnapasub	Chonburi	Noctiluca scintilis		DMCR-Eastern Center
16	15-19	August	2005	Laem Taen	Chonburi	Noctiluca scintilis		DMCR-Eastern Center
17	15-19	August	2005	Bang Saen	Chonburi	Noctiluca scintilis		DMCR-Eastern enter
18	1 - 31	August	2005	Bang Pakong River mouth	Chachoengsao	Noctiluca spp. Cerratium spp. Skeletonema spp. Chaetoceros spp.	Occurs all month, Extreme on date of 15 to 25. Aquatic animal was died.	IMS-BUU
19	1 - 31	August	2005	Sri Racha	Chachoengsao	Noctiluca spp. Cerratium spp. Skeletonema spp. Chaetoceros spp.	Occurs all month, Extreme on date of 15 to 25. Aquatic animal was died.	IMS-BUU
20	1 - 6	September	2005	Bang Saen	Chonburi	Noctiluca scintilis		IMS-BUU
21	1 - 6	September	2005	Si Chang	Chonburi	Noctiluca scintilis		IMS-BUU
22	1 - 6	September	2005	Si Racha	Chonburi	Noctiluca scintilis, Cerratium spp.		IMS-BUU
23	22	September	2005	Ao Chonburi	Chonburi	Noctiluca spp. Cerratium spp. Skeletonema spp.		IMS-BUU
24	29	September	2005	Ao Chonburi	Chonburi	Skeletonema costatum.		IMS-BUU
25	29	September	2005	Ang Sila	Chonburi	Noctiluca spp. Cerratium spp.		IMS-BUU
26	29	September	2005	Si Racha	Chonburi	Noctiluca spp. Cerratium spp.		IMS-BUU

Table E The historical data of red tide event that occurred in UGoT area (Continued).

NO.	Date	Month	Year	Location Event	Province	Plankton Type	Remark	Reference
27	6	October	2005	Bang Pakong River mouth	Chachoengsao	Skeletonema costatum.		IMS-BUU
28	6	October	2005	Ang Sila	Chonburi	Skeletonema costatum.		IMS-BUU
29	20	October	2005	Bang Pakong River mouth	Chachoengsao	Noctiluca spp. Cerratium spp.		IMS-BUU
30	20	October	2005	Bang Pakong River mouth	Chachoengsao	Noctiluca spp.		IMS-BUU
31	27–31	March	2006	Ang Sila	Chonburi	Noctiluca spp.	More benthic aquatic animals were died	IMS-BUU
32	27–31	March	2006	Vornnapasub	Chonburi	Noctiluca spp.	More benthic aquatic animals were died	IMS-BUU
33	4	April	2006	Bang Pakong River mouth to Ao Chonburi	Chonburi	Skeletonema costatum, Noctiluca spp.		IMS-BUU
34	4	April	2006	Ang Sila	Chonburi	Noctiluca spp.		IMS-BUU
35	4	April	2006	Si Racha	Chonburi	Noctiluca spp.		IMS-BUU
36	14	July	2006	Ao Chonburi	Chonburi	Chaetoceros spp		IMS-BUU
37	14	July	2006	Ang Sila	Chonburi	Chaetoceros spp		IMS-BUU
38	14	July	2006	Bang Saen	Chonburi	Chaetoceros spp		IMS-BUU
39	9	October	2006	Bang Pakong River mouth to Ao Chonburi	Chonburi	Skeletonema costatum, Noctiluca spp		IMS-BUU
40	-	July	2007	Coastal of Kok Kham	Samut Sakorn	Chaetoceros spp, Ceratium furca , Noctiluca scintillans		DMCR-Upper Center
41	-	October	2007	Laem Pak Beer	Petcha Buri	Noctiluca scintillans		DMCR-Upper Center

Table E The historical data of red tide event that occurred in UGoT area (Continued).

NO.	Date	Month	Year	Location Event	Province	Plankton Type	Remark	Reference
42	28	October	2007	Kok Kham and Pantay Norasing	Samut Sakorn	Noctiluca spp. Cerratium spp. Chaetoceros spp		DMCR-Upper Center
43	5	November	2007	Tachin River mouth	Samut Sakorn	Ceratium furca., Pseudo-nitzschia spp.		DMCR-Upper Center
44	13	November	2007	3 km far from Chao Praya River mouth	Samut Sakorn	Noctiluca spp. Chaetoceros spp		DMCR-Upper Center
45	27	November	2007	Bang Kun Tien	Bangkok	Noctiluca spp. Cerratium spp. Chaetoceros spp Pseudo-nitzschia spp.		DMCR-Upper Center
46	-	November	2007	Tachin River mouth	Samut Sakorn	Ceratium furca, Pseudo-nitzschia spp.		DMCR-Upper Center
47	-	November	2007	Chao Praya River mouth	Samut Prakarn	Noctiluca scintillans		DMCR-Upper Center
48	-	November	2007	Coastal of Bang Kun Tien	Bangkok	Chaetoceros spp., Noctiluca scintillans, Pseudo-nitzschia spp., Ceratium furca, Dinophysis caudata		DMCR-Upper Center
49	-	December	2007	Tachin River mouth	Samut Sakorn	Noctiluca scintillans, Ceratium furca		DMCR-Upper Center
50	-	December	2007	Coastal of Bang Kun Tien	Bangkok	Noctiluca scintillans,		DMCR-Upper Center

Table E The historical data of red tide event that occurred in UGoT area (Continued).

NO.	Date	Month	Year	Location Event	Province	Plankton Type	Remark	Reference
51	3	December	2007	Tachin River mouth	Samut Sakorn	Noctiluca spp. Cerratium spp.		DMCR-Upper Center
52	4	December	2007	Kok Kham	Samut Sakorn	Noctiluca spp. Cerratium spp.		DMCR-Upper Center
53	-	January	2008	Coastal of Bang Kun Tien	Bangkok	Noctiluca scintillans. Dinophysis caudata., Chaetoceros spp.		DMCR-Upper Center
54	-	January	2008	Tachin River mouth	Samut Sakorn	Noctiluca scintillans. Dinophysis caudata., Ciliate protozoa.		DMCR-Upper Center
55	10	January	2008	Tachin River mouth and along coastal	Samut Sakorn	Mesodinium rubrum		DMCR-Upper Center
56	-	February	2008	Tachin River mouth	Samut Sakorn	Noctiluca scintillans. Ceratium furca		DMCR-Upper Center
57	-	February	2008	Tachin River mouth	Samut Sakorn	Noctiluca scintillans.		DMCR-Upper Center
58	-	February	2008	Coastal of Bang Kun Tien	Bangkok	Noctiluca scintillans., Chaetoceros spp.		DMCR-Upper Center
59	-	March	2008	Tachin River mouth	Samut Sakorn	Chaetoceros spp.		DMCR-Upper Center
60	-	March	2008	Coastal of Bang Kun Tien	Bangkok	Noctiluca scintillans.,		DMCR-Upper Center
61	-	April	2008	Tachin River mouth	Samut Sakorn	Chaetoceros spp.		DMCR-Upper Center
62	-	April	2008	Chao Praya River mouth	Samut Prakarn	Skeletonema spp., Thalassiosira spp.		DMCR-Upper Center

Table E The historical data of red tide event that occurred in UGoT area (Continued).

NO.	Date	Month	Year	Location Event	Province	Plankton Type	Remark	Reference
63	-	May	2008	Tachin River mouth	Samut Sakorn	Skeletonema spp., Chaetoceros spp.		DMCR-Upper Center
64	-	May	2008	Coastal of Bang Kun Tien	Bangkok	Noctiluca scintillans.,		DMCR-Upper Center
65	-	June	2008	Tachin River mouth	Samut Sakorn	Skeletonema spp.,		DMCR-Upper Center
66	-	July	2008	Tachin River mouth	Samut Sakorn	Skeletonema spp.,		DMCR-Upper Center
67	-	September	2008	Coastal of Kok Kham	Samut Sakorn	Noctiluca scintillans, Ceratum furca		DMCR-Upper Center
68	-	September	2008	Tachin River mouth	Samut Sakorn	Skeletonema spp., Chaetoceros spp. Noctiluca scintillans		DMCR-Upper Center
69	-	October	2008	Tachin River mouth	Samut Sakorn	Skeletonema spp., Chaetoceros spp.		DMCR-Upper Center
70	-	October	2008	Bang Pakong River mouth	Chachoengsao	Peridinium spp.		DMCR-Upper Center
71	-	October	2008	Ang Sila	Chonburi	Chaetoceros spp.		DMCR-Upper Center
72	-	November	2008	Bang Pakong River mouth	Chachoengsao	Ceratum furca		DMCR-Upper Center
73	-	November	2008	Chao Praya River mouth	Samut Prakarn	Noctiluca scintillans, Ceratum furca		DMCR-Upper Center
74	-	December	2008	Chao Praya River mouth	Samut Prakarn	Noctiluca scintillans., Ceratum furca		DMCR-Upper Center
75	-	December	2008	Tachin River mouth	Samut Sakorn	Noctiluca scintillans., Ceratum furca., Chaetoceros spp.		DMCR-Upper Center

Table E The historical data of red tide event that occurred in UGoT area (Continued).

NO.	Date	Month	Year	Location Event	Province	Plankton Type	Remark	Reference
76	-	December	2008	Pan Tay Norasing	Samut Sakorn	Noctiluca scintillans, Dinophysis caudate, Pseudo-nitzschia spp., Rhizosolenia spp.		DMCR-Upper Center
77	-	January	2009	Chao Praya River mouth	Samut Prakarn	Noctiluca cintillans., Ceratum furca		DMCR-Upper Center
78	-	January	2009	Tachin River mouth	Samut Sakorn	Noctiluca scintillans, Dinophysis caudata		DMCR-Upper Center
79	-	January	2009	Chao Praya River mouth	Samut Prakarn	Noctiluca scintillans., Dinophysis caudata		DMCR-Upper Center
80	-	January	2009	Chao Praya River mouth	Samut Prakarn	Noctiluca scintillans., Dinophysis caudata		DMCR-Upper Center
81	-	February	2009	Tachin River mouth	Samut Sakorn	Noctiluca scintillans., Skeletonema spp.		DMCR-Upper Center
82	-	February	2009	Bang Pakong River mouth	Chachoengsao	Skeletonema spp.		DMCR-Upper Center
83	-	February	2009	Klong Sahakorn	Samut Sakorn	Noctiluca scintillans.,		DMCR-Upper Center
84	-	February	2009	Cha Am beach	Petchaburi	Noctiluca scintillans.,		DMCR-Upper Center
85	-	February	2009	Chao Praya River mouth	Samut Prakarn	Noctiluca scintillans.,		DMCR-Upper Center
86	-	February	2009	Chao Praya River mouth	Samut Prakarn	Noctiluca scintillans.,		DMCR-Upper Center
87	-	March	2009	Tachin River mouth	Samut Sakorn	Noctiluca scintillans.,		DMCR-Upper Center
88	-	April	2009	Tachin River mouth	Samut Sakorn	Cahetoceros spp. Skeletonema spp.		DMCR-Upper Center

Table E The historical data of red tide event that occurred in UGoT area (Continued).

NO.	Date	Month	Year	Location Event	Province	Plankton Type	Remark	Reference
89	-	August	2009	Coastal of Kok Kham	Samut Sakorn	Ceratium furca., Skeletonema spp., Noctiluca scintillans		DMCR-Upper Center
90	-	August	2009	Coastal of Bang Kra Joa	Samut Sakorn	Ceratium furca., Skeletonema spp., Noctiluca scintillans		DMCR-Upper Center
91	-	November	2009	Coastal of Bang Kra Joa	Samut Sakorn	Pseudo-nitzschia spp.		DMCR-Upper Center
92	-	November	2009	Coastal of Bang Kun Tien	Bangkok	Pseudo-nitzschia spp.		DMCR-Upper Center
93	-	November	2009	Tachin River mouth	Samut Sakorn	Caetoceros spp., Peridinium spp..		DMCR-Upper Center
94	-	November	2009	Cha Am	Petchaburi	Rhizosolenia spp., Noctiluca scintillans		DMCR-Upper Center
95	-	December	2009	Chao Praya River mouth	Samut Prakarn	Ceratium furca, Dinophysis caudata,		DMCR-Upper Center
96	-	December	2009	Klong Ka Long	Samut Sakorn	Skeletonema costatum, Thalassiosira spp., Rhizosolenia spp.		DMCR-Upper Center
97	-	March	2010	Tachin River Mouth	Samut Sakorn	Noctiluca scintillans, Skeletonema costatum		DMCR-Upper Center
98	-	July	2010	Tachin River Mouth	Samut Sakorn	Ceratium furca, Skeletonema costatum, Noctiluca scintillans		DMCR-Upper Center

Table E The historical data of red tide event that occurred in UGoT area (Continued).

NO.	Date	Month	Year	Location Event	Province	Plankton Type	Remark	Reference
99	-	July	2010	Bang Kun Tien	Bangkok	Ceratium furca, Noctiluca scintillans		DMCR-Upper Center
100	-	August	2010	Kok Kham	Samut Sakorn	Noctiluca scintillans		DMCR-Upper Center
101	-	August	2010	Cha Am	Prtchaburi	Noctiluca scintillans		DMCR-Upper Center
102	-	October	2010	Klong Ta Boon	Petchaburi	Ceratium furca		DMCR-Upper Center
103	-	October	2010	Bang Ka Jao	Samut Sakorn	Ceratium furca		DMCR-Upper Center
104	-	October	2010	Tachin River Mouth	Samut Sakorn	Skeletonema costatum		DMCR-Upper Center
105	-	November	2010	Tachin River Mouth	Samut Sakorn	Ceratium furca, Noctiluca scintillans, Chaetoceros spp.		DMCR-Upper Center
106	-	December	2010	Kok Kham	Samut Sakorn	Ceratium furca,		DMCR-Upper Center
107	-	December	2010	Kok Kham	Samut Sakorn	Ceratium furca		DMCR-Upper Center
108	-	December	2010	Bang Kun Tien	Bangkok	Ceratium furca	Appear aquatic animal died	DMCR-Upper Center
109	-	December	2010	Bang Pakong River mouth	Chachoengsao	Ceratium furca		DMCR-Upper Center
110	-	December	2010	Bang Pakong River mouth	Chachoengsao	Ceratium furca, Protoperdinium spp., Prorocentrum micans		DMCR-Upper Center
111	-	January	2011	Tachin River mouth	Samut Sakorn	Ceratium furca, Noctiluca scintillans		DMCR-Upper Center
112	-	January	2011	Coastal of Samut Sakorn	Samut Sakorn	Ceratium furca , Dinophysis caudata		DMCR-Upper Center
113		May	2011	Coastal of Samut Sakorn	Samut Sakorn	Ceratium furca , Dinophysis caudata		DMCR-Upper Center

Table E The historical data of red tide event that occurred in UGoT area (Continued).

NO.	Date	Month	Year	Location Event	Province	Plankton Type	Remark	Reference
114	-	July	2011	Klong Long	Samut Sakorn	Ceratium furca, Noctiluca scintillans		DMCR-Upper Center
115	-	August	2011	Coastal of Samut Sakorn	Samut Sakorn	Ceratium furca, Skeletonema costatum		DMCR-Upper Center
116	4	September	2014	Vornnapasub, Bangsaen	Chonburi	Noctiluca spp		Personal record
117	20	March	2014	Chao Pray River mouth, Bang Poo	Samut Prakarn	Noctiluca spp		Personal record
118	11	September	2014	Pattaya to Laem Chabang	Chonburi	Noctiluca spp		Personal record
119	22 – 24	September	2014	Chao Praya to Tachin River mouth	Samut Prakarn	Noctiluca spp		Personal record
120	20 – 25	April	2015	Hat Jao Samran	Petchaburi	Noctiluca spp		Personal record
121	20 – 25	April	2015	Na kok	Samut Sakorn	Noctiluca spp		Personal record
122	20 – 25	April	2015	Pattaya Beach	Chonburi	Noctiluca spp		Personal record
123	3 – 6	July	2015	Ko Si Chang	Chonburi	Noctiluca spp	Aquatic animals died	Personal record
124	3 – 6	July	2015	Bang Saen Beach	Chonburi	Noctiluca spp	Aquatic animals died	Personal record
125	7 – 9	August	2015	Bang Saen Beach	Chonburi	Noctiluca spp	Not extreme	Personal record
126	11	August	2015	Ko Si Chang	Chonburi	Noctiluca spp		Personal record
127	27 – 28	August	2015	Ko Si Chang, Laem Chabang to Bang Saen Beach	Chonburi	Noctiluca spp		Personal record
128	2	September	2015	Bang Saen Beach	Chonburi	Noctiluca spp	Aquatic animals died	Personal record
129	26	June	2016	Bang Saen Beach	Chonburi	Noctiluca spp		Personal record

Table E The historical data of red tide event that occurred in UGoT area (Continued).

NO.	Date	Month	Year	Location Event	Province	Plankton Type	Remark	Reference
130	30	June	2016	Ko Si Chang,	Chonburi	Noctiluca spp		Personal record
131	5	July	2016	Chao Pray River mouth	Samut Prakarn	Noctiluca spp		Personal record
132	11	July	2016	Bang Saen Beach	Chonburi	Noctiluca spp		Personal record

Marine and coastal resources research and development center – Eastern Center.(DMCR-Eastern Center), Rayong Province.

Marine and coastal resources research and development center – Upper Gulf Center.(DMCR-Upper Center), Samut Sakorn Province.

Institute of Marine Science (IMS), Burapha University, Chonburi Province.



APPENDIX F

SAW-QUESTIONNAIRE



QUESTIONNAIRE

This research questionnaire is consist of 4 parts:

- Part I Personal expert description
- Part II About the research explanation
- Part III Expert decision the factor weights
- Part IV Expert recommendation

Remark: This questionnaire is important process for doctoral research to apply in spatial analysis base on GIS techniques. All of your answer and recommendation are not disclose and apply to analysis as only this research.

Part I Personal expert description

Name


Position

Education

Under Graduate Master Degree Doctoral Degree

Work experience

Email address:

Phone number

Part II About the research explanation

2.1 This topic research: Geoinformatics applications to marine water quality and red tide phenomenon assessment in the upper gulf of Thailand.

2.2 An importance of this questionnaire

The expert decision weight and score results are concerning to spatial analysis of red tide phenomena in the Upper Gulf of Thailand. Simple Additive Weight (SAW) is used to analysis for relating the red tide susceptibility area.

2.3 Guideline to assigning the factor weights and scoring weights

Weight linear combination (WLC) method is one of the expert will decide to giving how of importance factor that is concerning to the red tide occurrence from lowest to highest score. The score is 1 that be concern the lowest factor affect to the red tide occurrence while score is 5 that be concern the highest factor affect to the red tide occurrence. The expert can be assign as equal or difference of score in each factor. The scoring in each class is also giving same as the factor weight as well. In process, the factor and class weights are multiply together and become to total score. Consequently, total scores are categorized by lowest to highest based on probability of the red tide occurrence.

Five factors are selected as namely: 1) Total suspended solids (TSS) 2) Color dissolved organic matter (CDOM) 3) Depth 4) Distance from river mouth and 5) Current-velocity. TSS and CDOM can be extract from MODIS satellite data at the red tide occurrence, depth and distance from river mouths are static value that be modify from GIS database while current velocity is become from simulation by expert in oceanography.

Part III Factor and class weights are decide by expert.

Example. The factor and class weights.

Input the sign of \checkmark into the box of factor weight and class score by your opinion. The factor weight have score from 1 to 5 and class score have value from 2, 4, 6, 8 and 10 score, respectively.

Factor	Factor weight					Class	Class score				
	1	2	3	4	5		2	4	6	8	10
Color Dissolved Organic Matter (CDOM) (Unit = m^{-1})					\checkmark	< 0.5	\checkmark				
						0.5 – 1.0			\checkmark		
						1.0 – 1.5			\checkmark		
						1.5 – 2.0				\checkmark	
						> 2.0					\checkmark

Notice: The CDOM is always relating to the soluble of organic substance in water that can be indicates the nutrients richness in coastal water. Thus it be supporting the growth rate of phytoplankton and it be chance to red tide occurrence.

Question for expert:

Input the sign of ✓ into the box of factor weight and class score by your opinion. The factor weight have score from 1 to 5 and class score have value from 2, 4, 6, 8 and 10 score, respectively.

Factors	Factor weight					Class	Class score				
	1	2	3	4	5		2	4	6	8	10
1) Total suspended solids (mg/l)						< 5					
						5 – 10					
						10 - 20					
						20 – 40					
						> 40					
2) Color Dissolved Organic Matter (m ⁻¹)						< 0.5					
						0.5 – 1.0					
						1.0 – 1.5					
						1.5 – 2.0					
						> 2.0					
3) Depth (m)						>20					
						15 – 20					
						10 – 15					
						5 – 10					
						<5					
4) Distance from River Mouths (km)						> 30					
						20 – 30					
						10 – 20					
						5 – 10					
						< 5					
5) Current (velocity) (m/sec)						> 1.0					
						0.5 – 1.0					
						0.1 – 0.5					
						0.05 – 0.1					
						< 0.05					

Part IV Recommendations

4.1 Are you agree with factors that using to red tide susceptibility index map?

Yes

No

Suggestion

.....

.....

.....

.....

.....

.....

4.2 Are you agree with categorizes of classes to red tide susceptibility index map?

Yes

No

Suggestion

.....

.....

.....

.....

.....

.....

4.3 Additional other suggestion

.....

.....

.....

.....

.....

.....

.....

.....

=====

Remark: If you have the suggestion, please contact to researcher as allow:

Mr. Prasarn Intacharoen

Tel: 095-918-9941

E-mail: prasarni@buu.ac.th

===== I would like to thank so much with to help this information =====

Table F List of marine experts.

No.	Name	Position	Office
1	Dr.Vichaya Gunbua	Lecturer	Faculty of Science, Burapha University
2	Dr.Patrawut Taipichitburapha	Lecturer	Faculty of Science, Burapha University
3	Dr.Jariyavadee Suriyapan	Lecturer	Faculty of Science, Burapha University
4	Dr.Wirote La-ongmanee	Lecturer	Faculty of Marine Technology, Burapha University
5	Dr.Waewta Tongra-ar	Scientist	Institute of Marine Science, Burapha University
6	Dr.Thidarat noiraksa	Scientist	Institute of Marine Science, Burapha University
7	Dr.Jitra Teeramatee	Scientist	Institute of Marine Science, Burapha University
8	Dr.Amornrat Kanokrung	Scientist	Institute of Marine Science, Burapha University
9	Dr.Paitoon Makkongphai	Scientist	Institute of Marine Science, Burapha University
10	Ms.Chaluay Musika	Scientist	Institute of Marine Science, Burapha University
11	Mr.Wanchai Wongsudawan	Scientist	Institute of Marine Science, Burapha University
12	Mr.Arwt Munhaphon	Scientist	Institute of Marine Science, Burapha University
13	Dr.Sompob Rungsupha	Scientist	Aquatic Resources Research Institute Chulalongkorn University
14	Dr.Nissara Thavornsod	Researcher	Faculty of Fishery, Kasetsart University
15	Dr.Chakrit Ruengsorn	Researcher	Faculty of Fishery, Kasetsart University
16	Dr.Boontarika Thongdonphum	Researcher	Faculty of Fishery, Kasetsart University
17	Miss.Kanittha Buakaew	Researcher	Faculty of Fishery, Kasetsart University
18	Asst.Prof.Dr.Chanyut Sodtongkong	Lecturer	Faculty of Science and FisheriesTechnology
19	Assc.Prof.Dr.Suwat Tanyaros	Lecturer	Faculty of Science and FisheriesTechnology

CURRICULUM VITAE

Name Prasarn Intacharoen

Date of Birth 19 November 1968

Place of Birth Singhanakorn District, Songkhla Province, Thailand

Education

2006 M.Sc. (Geography Technology) from Burapha University,
Chonburi, Thailand.

1996 B.Sc. (Fishery) from the Rajamangala Institute of Technology,
Bangpra Agriculture Campus, Chonburi, Thailand

1990 Vocational Diploma of Fishery from the Tinsulanonda
Songkhla Fishery College, Songkhla, Thailand.

Position and Place of Work

Lecturer at Department of Aquatic Science, Faculty of Science

Burapha University, Chonburi, Thailand